UNIVERSITY OF LIVERPOOL

INSTITUTE OF AGEING AND CHRONIC DISEASE

MicroRNAs as mediators of neuromuscular development following a low-protein diet pre- and postnatally

Ifigeneia Giakoumaki

Thesis submitted in accordance with the requirements of the University of Liverpool for the degree of Doctor in Philosophy

Liverpool, August 2019

Abstract

Age-related muscle loss is characterised by reduction in the number of myofibres and motor neurons and an additional weakening of the remaining fibres, causing reduction in muscle mass and function. Studies associate premature muscle wasting with influences during early stages of development, including maternal malnutrition. The aim of this study was to examine whether protein-deficient females produce offspring with a reduced number of muscle fibres and altered neuromuscular homeostasis and whether this can be rescued by optimisation of the nutrition in early postnatal stages of development. Female *Thy1-YFP16* mice, expressing yellow fluorescent protein (YFP) only in neuronal cells, were fed either a normal (20%) or a low-protein (5%) diet. Newborn pups were then cross-fostered to different lactating dams (maintained on either a normal or a low-protein diet), within 24 h after birth and maintained on those diets at post-weaning stages until 3 months of age.

Mice born from dams on 20% diet but introduced to a 5% diet (NLL) postnatally show significant reduction in muscle function (strength). Muscle fibre size and number was not affected by dietary reduction of protein, but protein restriction postnatally resulted in reduced muscle function. Mice on a low protein diet postnatally displayed structural abnormalities at neuromuscular junction. To examine how the changes in both muscle force and NMJ morphology may be controlled, specific microRNA expression levels were investigated in muscle and nerve from offspring. Two candidate microRNAs, miR-128 and miR-133a were selected for further investigation due to their reduced expression levels in mice on a low protein diet postnatally and their involvement in skeletal muscle and motoneuron cells. Bioinformatic analysis for miR-128 and miR-133a indicated several predicted target genes involved in key metabolic pathways in skeletal muscle and neuron cell function and maintenance.

Gain- and loss-of-function of miR-128 was performed *in vitro*, using C2C12 as a model of skeletal muscle cells and NSC-34 cells as a model of α-motoneuron cells. Both inhibition and overexpression of miR-128 in C2C12 cells resulted in reduced proliferation and increased cell death, and increased mitochondrial toxicity, while in NSC-34 cells only cell death was increased but proliferation remained unaffected. Overexpression of miR-128 resulted in no phenotypic changes in C2C12 myotubes but reduced the length of axonal outgrowth in NSC-34 cells. MiR-133a overexpression increased proliferation and reduced cell death. Inhibition of miR-133a had the most profound effect on C2C12 myotube phenotype and axonal length of NSC-34 cells. Quantitative PCR analysis of miR-128 predicted target genes of interest revealed changes in gene expression of Nrf-1, Pdgfrα, Cox-I, Cox-IV, Grb-2 and Park-2 genes following transfections with miR-128 in C2C12 and NSC-34 cells. Western blot analysis, however, showed that changes in these predicted target genes on a protein level in both C2C12 and NSC-34 cells were not significant. Analysis of Nrf-1 and Cox-IV in TA muscle of

mice from the NLL group showed no differences in the expression levels of these transcripts. However, Nrf-1 and Grb-2 were significantly upregulated in the sciatic nerve of mice from the NLL group.

To summarise, our data show that maternal protein restriction plays a crucial role in neuromuscular development of the offspring. This could be regulated through microRNA-128 and -133a. *In vitro*, miR-133a and miR-128 affected muscle and nerve cell phenotype. These gene expression changes were similar to those observed *in vivo*. These data indicate the potential role of microRNAs as a novel mechanism of neuromuscular development and potentially maintenance, following dietary alterations in early stages of development.

Doctor of Philosophy Declaration

I hereby declare that this dissertation is a record of work carried out in the Institute of Ageing and Chronic Disease at the University of Liverpool during the period from October 2015 to August 2019. The dissertation is original in content except where otherwise indicated.

Experimental design, execution and analysis of skeletal muscle force measurements presented in Chapter 3 were conducted by Dr Katarzyna Goljanek-Whysall and Dr Aphrodite Vasilaki.

August, 2019

……..

(Ifigeneia Giakoumaki)

Acknowledgments

I would like to thank Prof. Malcolm Jackson and Prof. Anne McArdle for the invaluable opportunity to join the Department of Musculoskeletal Biology II as a summer student and continue my MRes and PhD research in the field of neuromuscular ageing. I would like to extend my thanks to Prof. Graham Kemp and Prof Peter Clegg for the help and support I received during my PhD studies.

I would like to express the uttermost gratitude and appreciation to my supervisors and especially Dr Kasia Goljanek-Whysall and Dr Aphrodite Vasilaki for all the support during my postgraduate studies. Their sheer talent, thoughtfulness and support are admirable. They stood by my side during times of need and extended their help beyond their normal supervisor duties. Without their contribution, completion of this work would not have been possible, I am extremely grateful to have had them as my supervisors, Furthermore, I would like to thank my funders, BBSRC-DTP for the funding, training and support throughout my studies.

A big thank you to all the friends I made during my studies in IACD, to Natalie for all the training and support with experiments on neuromuscular junctions, to Caroline Staunton for the endless coffees and advice, to Antonia, Becky, (Dr Dr!) Caroline Cotton, Neil, Panos, Euan, Adam, Lorenzo and Barbara for caring about me as friends and keeping me motivated and focused until the end. Special thanks go to Alessandro and Rachel, for the endless hours of listening to my complaints and putting up with my frustration, but for always being kind and sympathetic despite the challenges they faced, and for including me in the happiest moments of your life. I would like to thank my dearest friends and colleagues, Francesca (from Portugal), Ana (from Spain) and Mikele (from Italy), who I also consider as sisters and brother, for giving me strength, shoulder to cry on, putting a smile on my face and helping me become a better person every day. Many thanks to the ladies in the PhD write-up room, Rhiannon and Jess, for keeping me motivated during thesis writing. Many thanks to George Sakellariou, Gareth Nye and Adam Lightfoot for the guidance and support during my studies, for all the opportunities and help in my career progression during the last 6 years. Special thanks to my managers and friends at QIAGEN, for giving me the opportunity to be part of their community and for the amazing experience I had during my placement at their site in Manchester.

I would like to thank my friends and fellow dance partners/teachers, Lizzy, Lauren and Amiee for their understanding during the challenging times of my postgraduate studies and for getting my mind out of science and into the creative world of dancing when I mostly needed it. My gratitude and sincere thank you to Rodina, one of the most inspirational people I have had the privilege of knowing, who showed me that no matter how challenging and overwhelming life and work can be, there is always room for a smile on our face.

I cannot thank enough my true friend/neighbour/dance mate/guardian angel, Katherine, without whom I would never have achieved getting this far. For all the

tears you saw me shedding and all the times you saw me struggling mentally and physically, this thesis belongs to you too, I truly owe you.

Special thanks go to my Greek friends Spyridoula, Eleni, Marieta, Eleana and Sofia who I have known for years and they supported me since I first set the goal of pursuing a PhD. Big thank you to my friend Eleni Dimitriadi, for all the great moments we shared in Greece and UK and for reminding me to stay strong during tough times.

Last but not least, I would like to thank my family, especially my parents and brother for being supportive and understanding during my student years in the UK. Thank you for your patience and love, for putting up with my very long-term absence and most importantly for believing in me, for being by my side all the way and for being proud for everything I have achieved so far.

Dedication

To all those I never had the chance to say goodbye.

To my friends Vaggelis Desikos and Dimitra Bairami

R.I.P.

Abbreviations

3'UTR	3'-untranslated region
AChR	acetylcholine receptor
ADP	adenosine diphosphate
AGO	Argonaute
AKT	Protein Kinase B
ALS	Amyotrophic lateral sclerosis
AMPK	5' AMP-activated protein kinase
ANOVA	Analysis of variance
APS	Ammonium Persulfate
ATP	adenosine triphosphate
BCA	Bicinchoninic acid
BCL2	B-cell lymphoma 2
BrdU	Bromodeoxyuridine / 5-bromo-2'-deoxyuridine
BSA	Bovine Serum Albumin
CuZnSOD/SOD1	Copper Zinc Superoxide Dismutase
COX	Cytochrome c oxidase
CO_2	Carbon dioxide
DAPI	4',6-diamidino-2-phenylindole
DMEM	Dulbecco's Modified Eagle's Medium
DMSO	Dimethyl sulfoxide
DPBS	Dulbecco's phosphate-buffered saline
ECM	extracellular matrix
EDL	Extensor Digitorum Longus
ERK	Extracellular signal-regulated kinase
ETC	Electron Transport Chain
F-12 media	Ham's F-12 Nutrient Mix

F-actin	Fibrous actin
FAD	flavin adenine dinucleotide (oxidized form)
FADH2	flavin adenine dinucleotide (reduced form)
FGF	fibroblast growth factor
FoxO	forkhead box O
GM	Growth Medium
GO	Gene Ontology
GTN	Gastrocnemius
H_2O_2	hydrogen peroxide
HS	Horse Serum
IGF	insulin-like growth factor
LDH	Lactate dehydrogenase
MAFbx	Muscle Atrophy F-Box
MAPK	mitogen-activated protein kinases
DMD	Duchene Muscle Dystrophy
miRNAs/miRs	microRNAs
MnSOD/SOD2	Manganese Superoxide Dismutase
mRNA	messenger RNA
MRF	Muscle Regulatory Factor
mRNA	messenger RNA
mtDNA	mitochondrial DNA
mTOR	mammalian target of rapamycin
mTORC1	rapamycin complex 1
MyHC	myosin heavy chain
Murf1	Muscle RING-finger protein-1
Myf-5	Myogenic Factor 5
MyoD	Myogenic Differentiation 1
NAD+	Nicotinamide adenine dinucleotide

NADH	nicotinamide adenine dinucleotide (reduced)
NMJ	Neuromuscular junction
NPC	Neuronal progenitor cells
NRF1	Nuclear Respiratory Factor 1
NRF2	Nuclear Respiratory Factor 2
OXPHOS	oxydative phosphorilation
P/S	Penicillin-Streptomycin
Pax3	paired box 3
Pax7	paired box 7
PBS	Phosphate buffered solution
PDGFRα	platelet-derived growth factor receptor A
PGC-1α	peroxisome proliferator-activated receptor gamma coactivator 1-alpha
PI3K	Phosphoinositide 3-Kinase
pre-miRNA	precursor miRNA
pri-miRNA	primary miRNA
qPCR	Quantitative Polymerase Chain Reaction
RISC	RNA-induced silencing complex
RNA-seq	RNA-sequencing
ROS	reactive oxygen species
RTK	Receptor tyrosine kinase
SDS	Sodium Dodecyl Sulfate
SEM	Standard Error of the Mean
Sirt1	Sirtuin 1
SMA	Spinal muscular atrophy
SN	Sciatic nerve
SOL	Soleus

SP	Side population
TA	Tibialis anterior
TEMED	Tetramethylethylenediamine
Tn	Troponin
TRIM32	Tripartite motif-containing protein 32
UCPs	uncoupling proteins
VEGF	vascular endothelial growth factor
WGA	Wheat germ agglutinin
Wnt	Wingless-type MMTV integration site

Contents

List of Figures

List of Tables

Chapter 1

Introduction

1 Introduction

Ageing is characterised by frailty due to increased muscle wasting and reduced muscle function (Faulkner *et al.* 2007). Age-related decline in muscle mass and function, known as sarcopenia, occurs progressively between the ages of 50-80 years in humans, and it is accompanied by a loss of muscle fibre and motor unit number and additional weakening of the remaining ones (Lexell *et al.* 1988; Marzetti *et al.* 2009). A number of studies have focused on influences that occur at early stages of development and their effect on skeletal muscle development and function. Such influences can be genetic/biochemical or environmental/dietary.

1.1 Skeletal muscle physiology and function

Skeletal muscle comprises approximately 40% of the total body mass and up to date there are 640 named skeletal muscles in the adult human body (Marieb and Hoehn, 2010). Skeletal muscles are attached to the bones directly or indirectly (*via* tendons) and control human body movement (Martini, 2006). The main functions of skeletal muscles are the generation of body movement, the maintenance of body position and posture, the support of soft tissues, the safeguarding of entrances and exits in the body, the maintenance of body temperature, regulation of metabolism and the storage of nutrients (Martini, 2006).

1.1.1 Skeletal muscle structure and organisation

Skeletal muscle consists of 3 types of connective tissue, the epimysium surrounding the entire muscle and separating from surrounding tissues; the perimysium, which divides the muscle into compartments called fascicles; the endomysium, a delicate layer of connective tissue that surrounds the individual muscle cells, called muscle fibres and hosts a network of capillaries, satellite cells and nerve fibres (**Figure 1.1.1**) (Martini, 2006).

Skeletal muscle fibres are multinucleated, post-mitotic cylindrical cells and a characteristic striated morphology (reviewed in Frontera and Ochala, 2015). Striations have a dark zone (A band) and a lighter zone (I band). Striations are formed when the A bands of each myofibril within a single fibre is aligned with the A bands of neighbouring myofibrils (Martini, 2006). Each muscle fibre comprises of hundreds of myofibrils, which are mainly composed of myosin and actin filaments. Myosin filaments (or thick filaments) and actin filaments (or thin filaments) are organised into bundles within the myofibrils, called myofilaments (reviewed in Frontera and Ochala, 2015). Myofilaments are subsequently organised into repeating functional units known as sarcomeres, which are approximately 2 μm in length. Interactions between the thin and thick filaments in each sarcomere are responsible for skeletal muscle contractions (Martini, 2006). Between the sarcolemma and the basal lamina of the skeletal muscle fibre a population of muscle stem cells, known as satellite cells in a quiescent state in mature myofibres (Mauro, 1961). Following muscle injury, satellite cells become activated and re-enter the cell cycle and give rise to a myogenic progeny of muscle-progenitor cells known as myoblasts, which later differentiate into mature muscle fibres (Olguín and Pisconti, 2012). A small number of satellite cells do not undergo differentiation but remains in a stem cell state, in order to maintain the pool of satellite cells on myofibres (Olguín and Pisconti, 2012). Activation and proliferation of satellite cells depends on the expression of muscle regulatory transcription factors (MRFs), including MyoD and Myf-5, which are not expressed when satellite cells are in their quiescent state, while terminal differentiation into myofibres is achieved by expression of myogenin (Olguín and Pisconti, 2012).

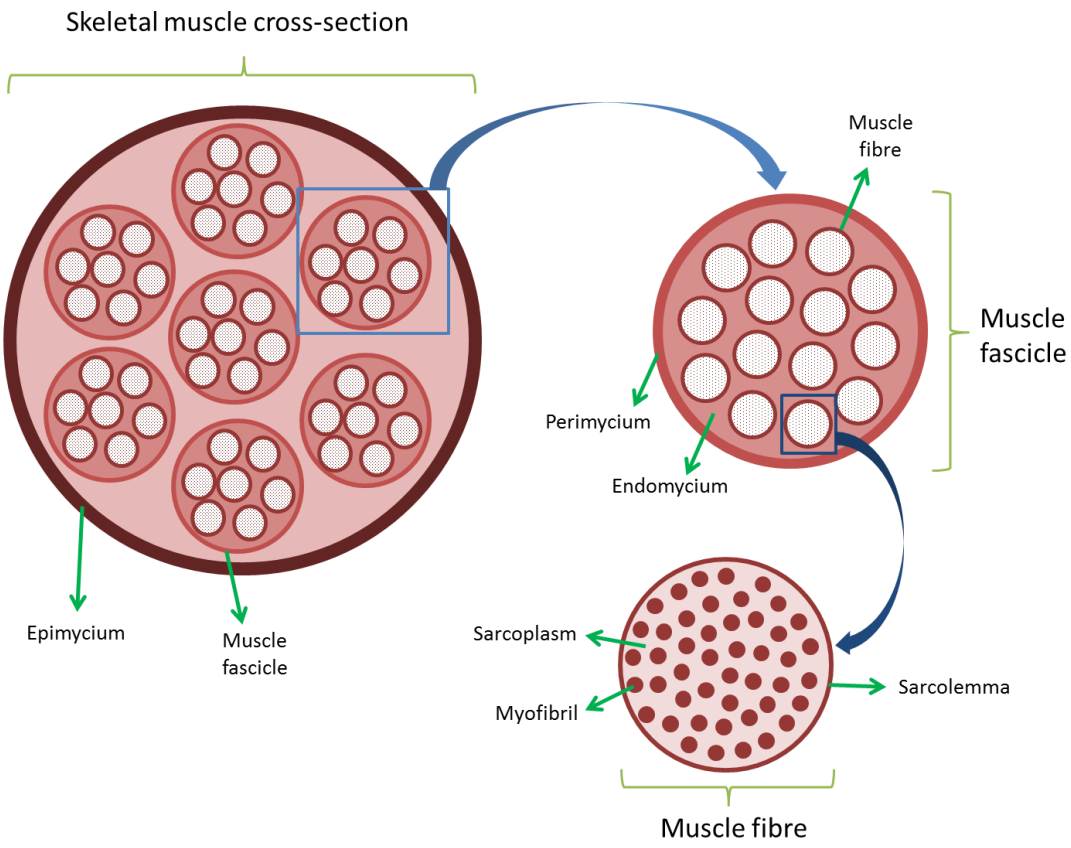

Figure 1.1.1 Schematic representation of the skeletal muscle structure and organisation

1.1.1.1 Skeletal muscle fibre composition

Skeletal muscle function is closely associated with the fibre type composition within the muscle. Skeletal muscle fibres in mammalian adult skeletal muscle are separated into 3 categories depending on the myosin ATPase activity and myosin heavy chain composition: type I fibres (or MyHC I), type IIa fibres (or MyHC IIa), type IIb fibre (or MyHC IIb) and type IIx fibre (or MyHC IIx) (Schiaffino *et al.* 1989). MyHC IIb is found only in small mammals, but this isoform is not seen in human skeletal muscle (reviewed in Choi, 2014). Classification of the different fibre isoforms depends also on the speed of shortening following contraction, the contractile characteristics and force production following stimulation from

the motoneuron, degree of fatigability and metabolic pathways being prevalent (oxitative or glycolytic) (reviewed in Frontera and Ochala, 2015).

Type I fibres or slow-twitch fibres have a smaller diameter than the type II fibres, with the speed of contraction and force generation being much slower than type II fibres (hence slow-twitch) but they are able to maintain contraction much longer, making them fatigue-resistant (Martini, 2006). Type I fibres have a high network of capillaries and high concentration of myoglobin and mitochondria, providing them a high supply of oxygen which is utilised for aerobic metabolism and increased ATP production (hence they are also known as oxidative fibres) (Martini, 2006).

Type II fibres or fast-twitch fibres have a larger diameter than the type I fibres and they respond very quickly to neuronal stimulation in order to contract (hence called fast-twitch). They have relatively small number of mitochondria therefore, the amount of ATP production is limited (Martini, 2006). Because type II fibres generate very powerful contractions very quickly and due to the mitochondria and the ATP produced are limited, type II fibres are susceptible to fatigue. These fibres use glycogen for energy source for force production hence they are known as glycolytic fibres (Martini, 2006). In rodents, type II fibres are separated into type IIa, type IIb and type IIx/d. In humans, type IIa and type IIx, but not type IIb isoform, are expressed in skeletal muscle (Smerdu *et al*. 1994). Interestingly, type IIa fibres, present features of both type I and type IIb fibres, as they use both oxygen and glycogen for their metabolism and force generation, and they seem less susceptible to fatigue than type IIb fibres (Burke *et al.* 1971; Peter *et al.* 1972). Type IIx/d was discovered later by Schiaffino *et al.* and they resembled similar contractile properties with type IIa and type IIb fibres but their resistance to fatigue was intermediate of that seen in type IIa and type IIb (Schiaffino *et al.* 1989; Larsson *et al.* 1991). Force generation by different fibre types follows the pattern: type I < type IIa < type IIx < type IIb, with type IIb fibres being the strongest (Martini, 2006).

In rodents, muscles are classified into slow- or fast-twitch muscles according to their fibre type composition. *Soleus* (SOL) has a high percentage of type I fibres and it is easily noticeable from its red colour. *Extensor digitorum longus* (EDL) *anterior tibialis* (TA) muscle are composed almost exclusively of type II fibres (**Figure 1.1.1.1**) (reviewed in Schiaffino and Reggiani, 2010; Augusto *et al.* 2014).

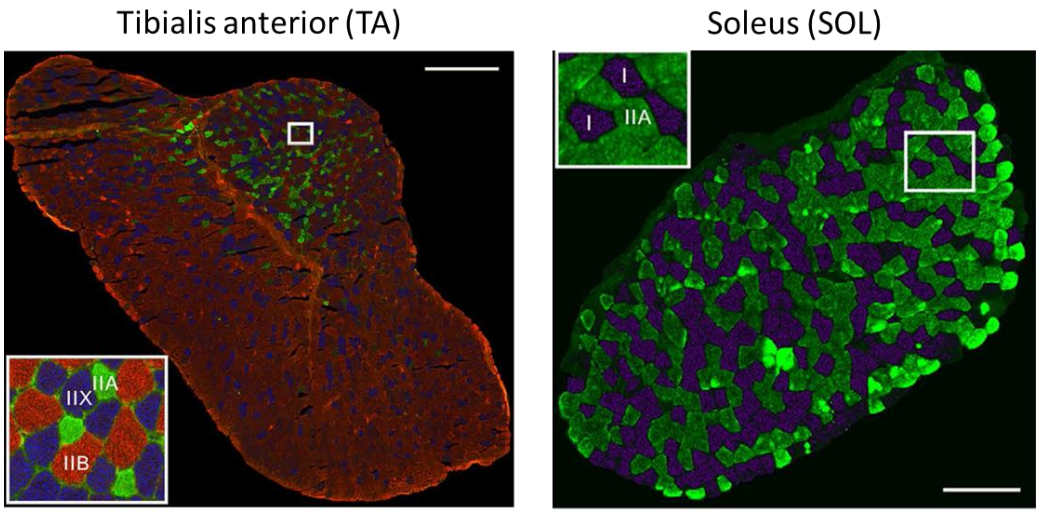

Figure 1.1.1.1 Fibre type distribution in TA and SOL muscles of adult mice following immunofluorescent staining for myosin heavy chain (MyHC) isoforms (from Sakellariou *et al.* 2016).

1.1.1.1.1 Skeletal muscle fibre composition during development

Fibre type composition in skeletal muscles during development is fluid and varies between different muscles. In developing skeletal muscles two more isoforms of MyHC are evident, the neonatal (NN) and the embryonic (EMB) isoforms, which are predominant during early days of development (Pette and Staron, 2000). Moreover, in all muscles a small amount of type I fibre has been recorded in all muscles (Agbulut *et al.* 2003). In EDL muscles fibre type isoforms start shifting mainly at postnatal day 7 (P7), with type II isoforms (IIa, IIb and IIx/d) slowly replacing the embryonic and neonatal isoforms. By P49, EDL muscle is composed almost exclusively of type II fibres (Agbulut *et al.* 2003). For SOL,

gastrocnemius (GTN) and *plantaris* muscles, fibre type shift is mainly observed at P14. Like in EDL, GTN and *plantaris* muscles is only composed of type II isoforms at P49, while SOL muscle is composed of type I fibres and type IIa and IIx fibres (Agbulut *et al.* 2003).

1.1.1.2 Skeletal muscle physiology: The neuromuscular junction (NMJ)

Muscle contraction depends on the communication between the skeletal muscle fibre and the nervous system, which occurs at the neuromuscular junction site (NMJ). The neuromuscular junction is the synaptic connection between the axon of a motoneuron and a skeletal muscle fibre (Levitan and Kaczmarek, 2015). The neuromuscular junction comprises of three main components: the pre-synaptic motor nerve terminal, the synaptic space, known as synaptic cleft and post-synaptic muscle membrane or motor end plate (Verschuuren *et al.* 2016). In humans and rodents, a neuromuscular junction is formed when an α-motoneuron from the lumbar region of the spinal cord extends its axon through the peripheral nerve, innervating a muscle fibre. All the axons branching from a single α-motoneuron and the skeletal muscle fibres they innervate comprise a single motor unit (Fox, 2001). The organisation of a motor unit and the morphology of the neuromuscular junction in rodents are shown in **Figure 1.1.1.2**.

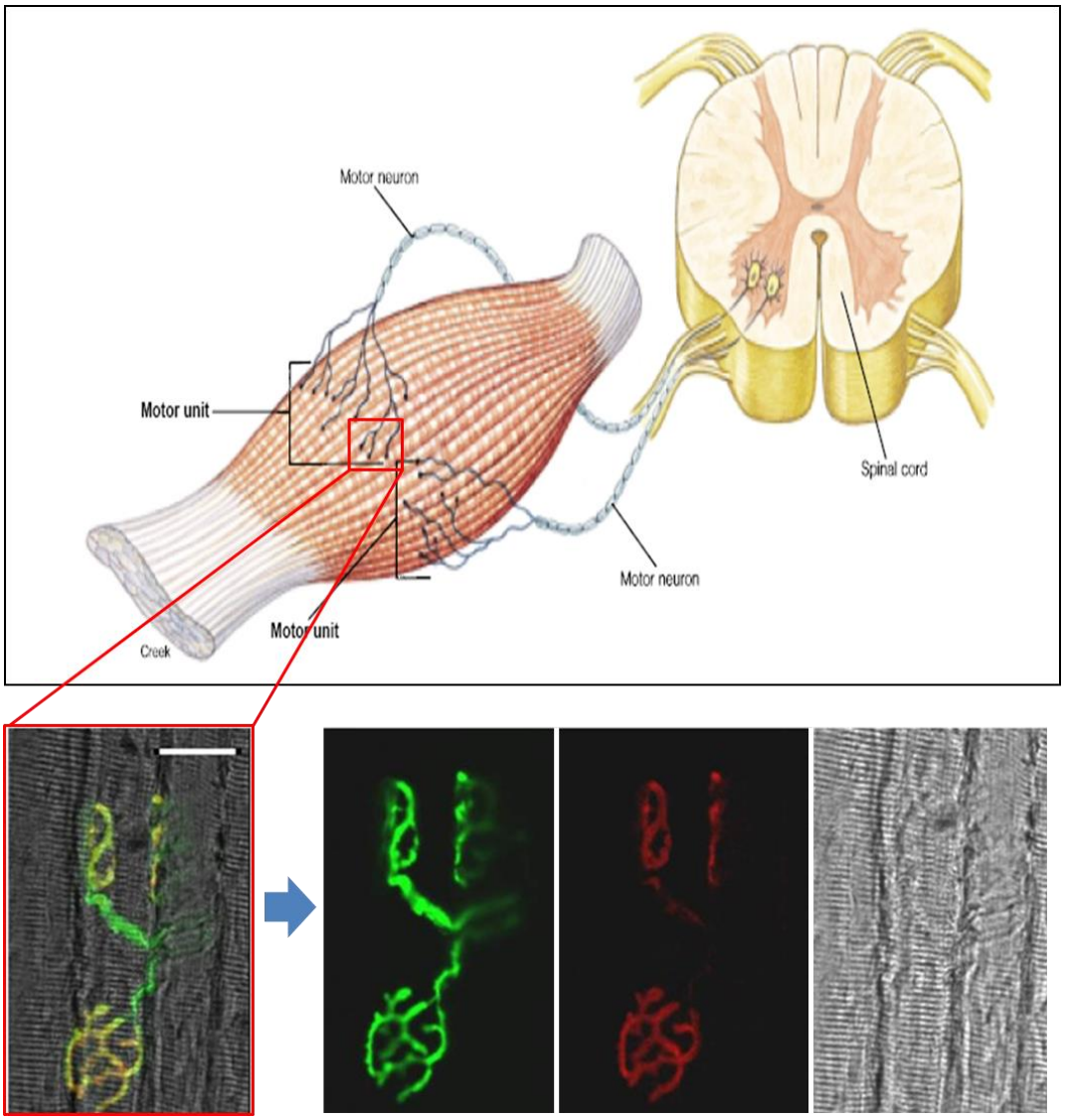

Figure 1.1.1.2 Innervation of the skeletal muscle and the organisation of a motor unit. Schematic (top) from Fox (2001). Images of neuromuscular junction from Vasilaki *et al.* (2016). Neuromuscular junction morphology on individual skeletal muscle fibres, presynaptic motor nerve terminal (green), motor end plate (red) and skeletal muscle fibres (contrast) observed using a confocal microscope.

1.1.1.2.1 Development of NMJ

NMJ development is a multistep process that in rodents it starts during embryonic development until the NMJ structure matures fully during late post-

natal/early adulthood stage of development. In rodents, NMJ formation starts with the formation of aneural AChR clusters across the length of the muscle fibre prior to the arrival of the nerve terminal of the motoneuron, at day E11-12 (reviewed in Li *et al.* 2012). At day E13-14, motoneuron axons innervate the muscle fibres, inducing the formation of new AChR clusters, leading to dispersion of the non-innervated sites (reviewed in Li *et al.* 2012). This redistribution of AChR clusters does not require synaptic or contractile activity (Anderson and Cohen, 1997). Newly AChR clusters formed from day E16 are firstly seen as plaques with an oval shape that are innervated by more than one axon (multiple innervation) (Marques *et al.* 2000). From day E16 until late postnatal stages (P21), the AChR plaques become perforated and gradually from branches, adopting a more complex "pretzel"-like morphology, while they are innervated only by one axon (reviewed in Li *et al.* 2012). The maturation of the morphology for each NMJ varies temporally, as during early postnatal period there is a variation in the shape of NMJs, with some still having the appearance of the embryonic plaque shape while others have visible signs of perforation (Marquez *et al.* 2000). Maturation of the synaptic area was also accompanied by an increase in its overall size, which was visible during the second postnatal week (Balice-Gordon and Lichtman, 1993). AChR-rich areas enlarged along with expansion of space between those areas, but no increase in AChR-rich areas was noted. This observation suggests the increase in the overall synaptic territory from the compact plaque-shape sites seen during embryonic development, where AChR clusters were more distributed more densely (Balice-Gordon and Lichtman, 1993).

AChRs also undergo changes during development. AChR is a transmembrane nicotinic receptor that acts as an ion channel, mediating neuromuscular signal transmission (Missias *et al.* 1996). AChR are comprised of five homologous subunits, giving the receptor a barrel-like shape (Lindstrom, 1997). In mammalian skeletal muscle during development, AChR pentamer consist of four different type of subunits with the following stoichiometry: $\alpha_2\beta\gamma\delta$ (Missias *et al.* 1996). There are two sites for ACh binding located between α1-γ and α1-δ

subunits (**Figure 1.1.1.2.1**) (Lindstrom, 1997). Following postnatal development, foetal γ subunit substituted by ε subunit, resulting in the following AChR stoichiometry: $\alpha_2\beta\varepsilon\delta$ (Missias *et al.* 1996). Although subunits α β δ are present in AChR throughout mammalian development, in rodents, subunit γ is present only during early stages of development and during denervation while subunit ε is evident late in development and only at the synaptic AChRs (Lindstrom, 1997). In humans, subunit γ expression is downregulated but not completely abolished, from 31 weeks of gestation and it is maintained at low levels through adulthood (reviewed in Webster, 2014).

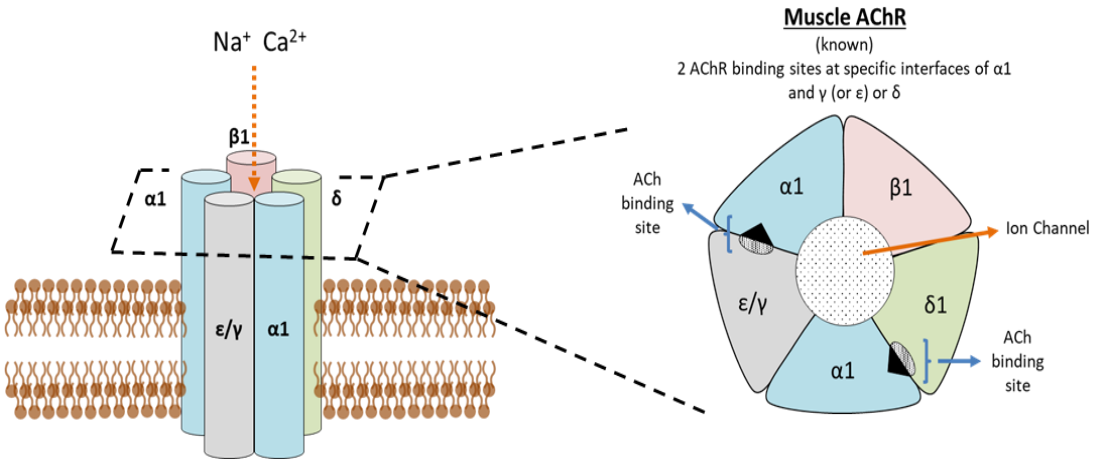

Figure 1.1.1.2.1 The organisation of muscle acetylcholine receptor (AChR). Subunit γ is replaced by subunit ε following postnatal development (redrawn/adapted from Lindstrom, 1997).

1.1.1.2.2 The neuromuscular junction (NMJ): α-motoneurons

Motoneuron cells on the spinal cord are organised into longitudinal columns across the rostrocaudal axis (Landmesser, 1978). Specifically, α-motoneurons are located on the ventral horn of the spinal cord, and they belong to the class of lower motoneuron in the central nervous system (CNS) (reviewed in Stifani, 2014). α-motoneurons have a large cell body and a characteristic neuromuscular

ending (pretzel shape) (reviewed in Stifani, 2014). These motoneurons serve a key role in muscle force generation, as they are excited monosynaptically, and therefore responding quicker to stimuli (Eccles *et al.* 1960). α-motoneurons are divided into three categories, based on the type of muscle fibre they innervate: i) Slow-twitch, fatigue-resistant (SFR), ii) Fast-twitch, fatigue-resistant (FFR) and iii) fast-twitch, fatigable (FF) (Burke *et al.* 1973). SFR α-motoneurons innervate slow-twitch (type I) muscle fibres, they have a significantly lower conduction velocity compared to FF and FFR α-motoneurons and they process the smallest cell body and the lowest degree of complexity in relation to FF and FFR α-motoneurons (reviewed in Kanning *et al.* 2010). FFR α-motoneurons innervate fast-twitch, fatigue-resistant (type IIa) muscle fibres and their characteristics are between the FF and SFR α-motoneurons, in terms of body size, complexity and conduction velocity (reviewed in Stifani, 2014). Finally, FF α-motoneurons innervate fast-twitch-fatigable (type IIb/x) muscle fibres and have the highest conduction velocity and degree of complexity, as well as largest cell body (reviewed in Kanning *et al.* 2010).

1.1.1.2.3 The neuromuscular junction (NMJ): the synaptic site

Skeletal muscle contraction can only occur following successful neuronal signal transmission from the α-motoneuron to the skeletal muscle fibre at the neuromuscular junction (Martini, 2006). In rodents, the neuromuscular junction has a characteristic “pretzel”-like shape, with multiple branching points (**Figure 1.1.1.2.3**). However, the morphology of the neuromuscular junction can vary between vertebrate species (Fox, 2009). A recent study from Jones *et al.* (2017) provided extensive evidence on the morphological differences of the NMJ between mice and humans across their lifespan. Variations in NMJ morphology can also be evident between different muscle groups and different species of the same animal group (i.e. *Drosophila melanogaster*) (Jones *et al.* 2017; Campbell and Ganetzky, 2012).

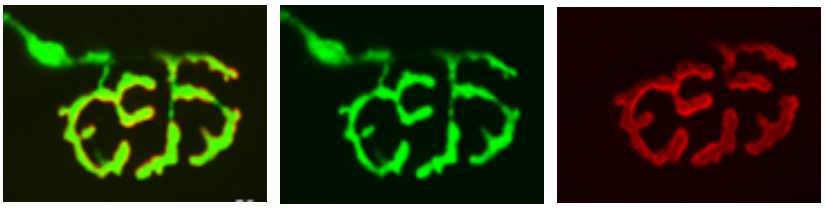

NMJ | Pre-synaptic nerve terminal | Post-synaptic motor end plate

Figure 1.1.1.2.3 The neuromuscular junction (NMJ) on the EDL muscle of an adult mouse (3 months old). The pre-synaptic nerve terminal and post-synaptic motor end plate overlap perfectly for efficient signal transmission, giving the NMJ this "pretzel"-like shape (further details provided in Chapter 3, Section 3.3.4).

Despite the morphological variations, NMJs have three distinct components: i) the pre-synaptic nerve terminal, ii) the synaptic space and iii) the motor end plate (Verschuuren *et al.* 2016).

The presynaptic nerve terminal comprises of the unmyelinated axonal cone of an α-motoneuron, whose myelinated axon is extended through the peripheral nerve (Fox, 2009). The unmyelinated axonal cone of the motoneuron is divided into branches, which reside in close proximity with the skeletal muscle fibre membrane (Fox, 2009). The pre-synaptic nerve terminal is separated from the motor end plate by synaptic cleft, a 12-20 nm space that accommodates the neurotransmitters for a short period after their release from the nerve terminal (Savtchenko and Rusakov, 2007). The postsynaptic membrane is folded into junctional folds that can be up to 1 µm in depth (reviewed in Sanes and Lichtman, 1999). AChR clusters are located at the shoulders of the junctional fold crests, at a density of 10,000/µm^2 or higher, and this concentration of AChR falls 1000-fold in extrasynaptic sites (Salpeter *et al.* 1988). At the deepest end of the junctional folds are the sodium channels and the neuronal cell-adhesion molecule (N-CAM) (reviewed in Sanes and Lichtman, 1999). Formation of AChR clusters depends heavily on two key molecules, agrin and muscle-specific kinase (MuSK). Agrin secreted by motoneuron cells triggers the activation of MuSK, *via*

binding to its receptor, low-density lipoprotein (LDL) receptor–related protein 4 or Lrp4 (reviewed in Li *et al.* 2017). Activation of the agrin-Lrp4-MuSK complex causes AChR cluster formation *via* recruitment of rapsyn and activation of downstream signalling pathways (Verschuuren *et al.* 2016).

1.1.2 Skeletal muscle contraction

1.1.2.1 Pre-synaptic signal transmission for muscle contraction

When the pre-synaptic plasma membrane depolarises following an action potential, voltage-gated calcium channels (VGCCs) open up and Ca^{2+} flows into the nerve terminal (Verschuuren *et al.* 2016). There, Ca^{2+} binds to synaptotagmin located on the synaptic vesicles and triggers the release of the neurotransmitters they carry, including acetylcholine (ACh), *via* exocytosis (Südhof and Rizo, 2011). When the exocytosis is complete, the synaptic vesicles are recycled and refilled with neurotransmitters, ready to be released. Exosome recycling is regulated *via* multiple pathways (Südhof and Rizo, 2011).

Upon release from exosomes, ACh (and other neurotransmitters) diffuse across the synaptic cleft and are then bound to the ACh receptors (AChR), which are tightly clustered on the post-synaptic folds of the motor end plate of the muscle fibre (Verschuuren *et al.* 2016). Following binding, AChR ion channel opens up causing local depolarisation, known as the end plate potential. When the end plate potential reaches a certain threshold, the voltage-gated sodium channels open up sending this action potential across the muscle fibre triggering its contraction (Verschuuren *et al.* 2016).

1.1.2.2 Skeletal muscle fibre activation and contraction

The theory of skeletal muscle force generation was first described by Huxley and Niedergerke, 1954. According to this theory, also known as the sliding filament theory, the sarcomere length shortens disproportionally when the

muscle contracts, with the I band and H zone of the sarcomere being subjected to shortening of their length. However, the length of the A band of the sarcomere does not change, but what changes is the degree of overlap between the thick (myosin) and thin (actin) filament. Hence, sarcomere contraction does not depend on changes in A band length but on the level of sliding between the thin and thick filaments, an observation that gave the name to this theory (Huxley and Niedergerke, 1954).

Force generation depends on a number of factors including muscle size and architecture, innervation, the space between myofilaments and the number of formed myosin-actin cross bridges (reviewed in Frontera and Ochala, 2015). Muscle force is normalised to muscle size is called specific force and it is used as an indicator of muscle quality. During ageing and disease, as well as during denervation, muscle force appears to decline (reviewed in Frontera and Ochala, 2015).

Muscle force generation involves the two major proteins, myosin and actin. Myosin is the major components of the thick filaments combined with titin, which is responsible for the maintenance of the alignment between thick and thin filaments (Martini, 2006). Thin filaments are mainly composed of actin along with tropomyosin and troponin. Actin in thin filaments is in the form of F actin, which consists of molecules of G actin and has a twisted conformation (Martini, 2006). G actin molecules contain active sites for binding of myosin, which under resting conditions is inhibited by the tropomyosin-troponin complex (Martini, 2006). Upon muscle contraction, Ca^{2+} is released and binds to troponin receptors, triggering a conformational change of the troponin-tropomyosin complex and releasing the actin receptors, allowing binding with myosin molecules. This interaction between myosin and actin filaments during muscle contraction is known as cross-bridges (Martini, 2006). When ATP is available, it binds to the active site of the myosin head and it is hydrolysed by the local ATPases into ADP+Pi. The Pi molecule forces myosin to pass the actin filament following the generation of a power stroke, which results in force generation (reviewed in Frontera and Ochala, 2015). The rate of ATP consumption by

ATPases in the myosin heads determines the speed of contraction (Bárány 1967). When ATP is no longer available, the troponin-tropomyosin complex interaction with actin filaments is restored and the muscle stops contracting (**Figure 1.2.2.2**).

Consumption of ATP depends on various factors including the number of myosin heads and the number of cross-bridges formed between myosin and actin filaments. The rate at which ATP is consumed reflects the myosin heavy chain isoform expression (reviewed in Frontera and Ochala, 2015). Muscle contraction occurs only under the control of the nervous system, when the action potential arriving at the neuromuscular junction (NMJ) of each skeletal muscle fibre causes release of Ca^{2+} (Ashley and Ridgwey, 1968).

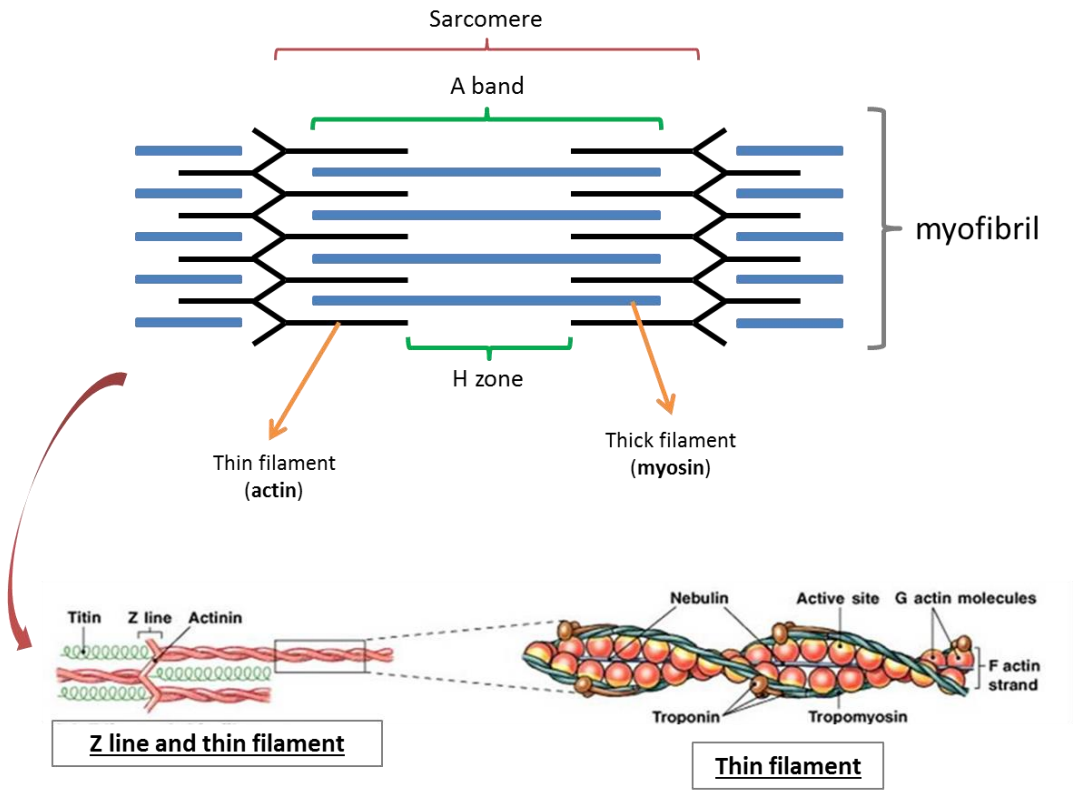

Figure 1.1.2.2 Schematic representation of the sarcomere structure and organisation (adapted/redrawn from Martini, 2006).

1.2 Regulation of neuromuscular physiology and function in development and ageing or disease

1.2.1 Lifestyle and dietary influences on neuromuscular physiology

Epidemiological studies suggest that environmental influences such as nutrition during perinatal life may result in detrimental and long-lasting effects. Restriction of maternal food intake (50% of daily food intake) during gestation and lactation period resulted in 54% reduction in the body weight of the offspring in rats (Beermann, 1983). Later studies revealed similar effect of maternal nutrition in the birth weight and postnatal muscle growth of the mammalian offspring. A study by Bee (2004) demonstrates how fibre type distribution in skeletal muscle is influenced by different maternal feeding regimen in pigs, whereas muscle fibre area is directly influenced by birth weight. Maternal undernutrition in beef has been linked to growth and productivity of the offspring, which develop metabolic syndromes later in life (Funston *et al.* 2010). In sheep, maternal undernutrition contributes to the rise of metabolic diseases later in life, such as glucose intolerance and insulin insensitivity (Costello *et al.* 2008, 2013). On a cellular level, maternal suboptimal nutrition pre- and postnatally reduce myogenic frequency and function in muscle stem cells, leading to impairment in repair mechanisms and reduction in skeletal muscle mass (Woo *et al.* 2011). Furthermore, substantial maternal undernutrition during gestation and insufficient maternal nutrient supply can impair myogenesis due to impairmed growth hormone-insulin-like growth factor (GH-IGF) axis, subsequently affecting the growth of mammalian skeletal muscle fibres (Rehfeldt *et al.* 2011).

A high-saturated fat diet during early developmental stages has been linked to development of type II diabetes, obesity and other metabolic disorders later in life mammals (Yang *et al.* 2012). Early exposure to a high-saturated-fat diet in rats inhibits the development of skeletal muscle by repression of the expression of myogenic genes *via* Wnt/β-catenin signalling, leading to aberrant muscle development (Yang *et al.* 2012).

In terms of protein, maternal high-protein diet has been linked with the regulation of offspring's transcriptome, with long-lasting effect. A study by Oster *et al.* (2012) in pigs showed short- and long-term effects of a high-protein diet on transcriptional regulation of genes involved in cell cycle regulation, energy and nucleic acid metabolism and growth factor signalling pathways in the offspring. Their findings show that maternal protein supply regulates programming of the offspring's genome; while piglets under a high-protein diet during early postnatal stages showed signs of growth retardation obvious at birth and permanently altered development and responsiveness to the common environment of the transcriptome (Oster *et al.* 2012).

Maternal protein-deficient diet can lead to the development of metabolic diseases during adulthood. Results from a study from da Silva Aragão *et al.* (2014) show that maternal malnutrition can alter metabolic flexibility long-term in skeletal muscle of the offspring of rats born from normal or protein-restricted dams, throughout pregnancy and lactation. Their data further suggest that metabolic inflexibility can lead to the development of metabolic disorders associated with malnutrition in early life (da Silva Aragão *et al.* 2014). Another study from Toscano *et al.* highlighted the effects of a protein-deficient diet during gestation on the biomechanical properties of skeletal muscle of offspring. Rats born from a dam fed a low-protein diet demonstrated muscle wasting and diminution of maximum twitch and tetanic tension on the EDL and SOL muscle. Additionally, muscle fibre type proportions were altered in EDL and SOL muscle of 25- and 90-days old pups (Toscano *et al.* 2008). These data demonstrated the effect of low-protein intake in the structure and function of skeletal muscle, which could significantly compromise posture and locomotion of the offspring (Toscano *et al.* 2008).

Exposure to a low-protein diet pre-natally has been shown to have detrimental effects in the development of cognition and memory. Rats exposed to a protein-deficient diet at neonatal stages demonstrated reduced expression of brain-derived growth factor (BDNF) mRNA, a key neurotrophin necessary for neurogenesis, synaptic plasticity and cell survival (Marwarha *et al.* 2017). A study

from Gallagher *et al.* revealed reduction in mitochondrial complex IV activity of rats subjected to a low-protein diet during gestation (Gallagher *et al.* 2005). Low-protein diet during gestation and at early postnatal stages has been associated with reduction neuronal stem cell number in the brain of mice, with concomitant uncontrollable upregulation of stem cell differentiation, resulting in memory deficits (Gould *et al.* 2018). A study from Chen *et al.* (2009) showed that low-protein diet pre-natally followed by normal-protein diet postnatally resulted in shortened lifespan of the offspring. Interestingly, mice born from a mother on a normal diet pre-natally but subjected to a protein-deficient diet postnatally demonstrated slow growth but had an extended lifespan (Chen *et al.* 2009). Furthermore, protein-deficient diet at early stages of development had an impact on key metabolic pathways regulating lifespan, such as IGF-1 signalling (Chen *et al.* 2009). Additionally, a study by Sharma *et al.* 2015 provides evidence of the regulation of small RNA biogenesis by low-protein diet and their influence in embryonic gene expression.

Although several studies have focused on the effect of a low-protein diet on muscle mass and function, there is no study up-to-date focusing on the effects of a protein-deficient diet immediately after birth, during lactation and later on in life, in both the muscle fibres and motoneurons.

1.2.1.1 Skeletal muscle fibre regulation during exercise

Exercise training can influence fibre type transition in skeletal muscle, as a mechanism of adaptation to the energy requirements during different types of exercise. Resistance training caused an increase in type IIa fibres with a parallel decrease in type IIb fibres in skeletal muscle (Staron *et al.* 1990; Heather *et al.* 1991). High-intensity endurance exercise increased type I and type IIa fibres and decreased type IIb fibres in *plantaris* and EDL muscle of rats (Green *et al.* 1984). Similar results were also recorded in previous studies in human skeletal muscle following endurance training (Baumann *et al.* 1987). This transition in fibre types

in skeletal muscle following different exercise regimes highlights the adaptability of skeletal muscle in conditions of different metabolic and energy demands.

1.2.1.2 Dietary influences regulating skeletal muscle fibre composition

Nutrient availability has a key role in fibre type determination in skeletal muscle. Diets high in fat and sugar content caused the greatest shift of slow-to-fast fibre types in SOL while resveratrol treatment had the opposite effect in *plantaris* muscle (Hyatt *et al.* 2016). This great effect of high fat/high sugar diet on SOL is supported by previous studies showing the increased sensitivity of oxidative muscles to insulin resistance (Koerker *et al.* 1990). Interestingly, a long-term high-fat diet increases type IIx fibres in EDL muscle but the same is not observed with short-term high-fat diet (Eshima *et al.* 2017).

Caloric restriction has been shown to attenuate the effects of ageing on fibre type composition in slow and fast muscles (Faitg *et al.* 2019). A reduction of 40% on caloric intake in adult rats was shown to preserve fibre type composition (Joseph *et al.* 2013). A short-term 20% caloric restriction in rats had no positive effect in age-related atrophy of type IIb fibres (Mckiernan *et al.* 2004).

Supplementation or restriction of protein has been associated with changes in mammalian skeletal muscle morphology. Moderate protein restriction upregulates the expression of MyHC I and IIa in skeletal muscles of mammals but such change is not observed with a low-protein diet or in MyHC IIb and IIx/d expression levels (Li *et al.* 2016a). High-protein diet has been associated with fast-to-slow fibre transformation in rats, due to increased oxidative properties of skeletal muscle induced by high-protein dietary content (Nakazato and Song, 2008).

1.2.2 Genetic/biochemical influences of neuromuscular physiology and function

Genetic factors that can affect neuromuscular development and ageing include genetic diseases such as spinal muscular atrophy (SMA). SMA is an autosomal recessive disease that is associated with loss of motoneurons, leading to skeletal muscle denervation and subsequent muscle weakness (Pearn, 1978). A study from Martínez-Hernández *et al.* (2014) showed differences in the percentage of fast and slow myosin in foetal skeletal muscle samples of SMA patients compared to the control samples. Moreover, their findings showed an increase in satellite cell number in postnatal atrophic fibres of SMA patients, indicating abnormal myogenesis (Martínez-Hernández *et al.* 2014).

Biochemical factors include but are not limited to hormonal signalling such as growth and thyroid hormone signalling. Hormonal signalling has a key role in proper neuromuscular development. Hormonal deficiencies during pre-natal stages of development can result in abnormalities of foetal tissues, including skeletal muscles (Fowden *et al.* 1998, 2006). Glucocorticoids are also central mediators of skeletal muscle tissue programming and development during pre-natal stages of development, due to their responsiveness to environmental cues that affect skeletal muscle cell differentiation *in utero,* with consequences later in life (reviewed in Fowden and Forhead, 2009). Furthermore, experiments undertaken in pigs showed that the expression patterns of growth hormone receptor (GHR) during foetal development along with the percentage of GHR in skeletal muscle during gestation suggest the involvement of the growth hormone (GH) in foetal muscle growth (Schnoebelen-Combes *et al.* 1996). Thyroid hormone has the potential to regulate muscle fibre type specification in skeletal muscle during early postnatal development (Russell *et al.* 1988). Imbalances in thyroid hormone levels result in muscle weakness and a myopathic phenotype (Lee *et al.* 2014).

1.2.2.1 Pathophysiological conditions regulating skeletal muscle fibre switch

Fibre type isoforms in skeletal muscles can shift to different types or form hybrid isoforms under certain physiological conditions. Examples of such conditions include ageing, pathophysiological conditions and exercise. Fibre type transition tends to follow a fast-to-slow or slow-to-fast transition, which is reversible and sequential: MyHC I ↔ MyHC IIa ↔ MyHC IIx/d ↔ MyHC IIb (Pette and Staron, 2000). During this transition, hybrid fibres with a combination of MyHC isoforms may form, due to slow protein turnover of MyHC (reviewed in Schiaffino and Reggiani, 2011).

Fibre type transitions have been widely observed in certain pathophysiological conditions. A well-studied example includes conditions characterised by imbalances in thyroid hormone. Thyroid hormone regulates the transition of muscle fibre isoforms from neonatal to adult fast MyHC independently of innervation (Russell *et al.* 1988). This transition is delayed during hypothyroidism but accelerated during hyperthyroidism (d'Albis *et al.* 1990). In adult skeletal muscle, thyroid hormone overexpression during hyperthyroidism induces a slow-to-fast type transition in the direction of MyHC I ↔ MyHC IIa ↔ MyHC IIx/d ↔ MyHC IIb. The opposite direction is observed under hypothyroidism conditions were absence of thyroid hormone drives a fast-to-slow fibre type transition (reviewed in Schiaffino and Reggiani, 2011). Recent studies have shown that thyroid hormone regulation of fibre type isoforms is achieved *via* control of muscle-specific microRNA expression (Zhang *et al.* 2014).

Neurological conditions can also influence fibre type shifting in skeletal muscles. One such example is Huntington's disease, which seems to induce a reduction in type IIb isoform with a concomitant increase in type IIx in EDL muscle of mice. Transition of type IIa to type I fibres was also observed in the SOL muscle of those mice, highlighting the effect of the neurodegenerative disease in both fast and slow muscles (Hering *et al.* 2016). Fibre type switching has also been recorded during ALS disease with muscle fibre transitioning from

fast to slow. Moreover, hybrid fibres have been observed in muscles of ALS (Baloh *et al.* 2007).

1.2.3 Neuromuscular morphology and function during ageing

1.2.3.1 Skeletal muscle fibre switch during ageing

Fibre type changes occur in skeletal muscles during ageing. In fast muscles, such as EDL and TA, a transition of type IIb fibres to type IIx is observed (Larsson *et al.* 1993). In slow muscles such as SOL, type IIa fibres switch to type I during ageing (Larsson *et al.* 1995). Muscle fibre atrophy in fast muscles during ageing is observed in all type II fibre types, while type IIb fibres appeared to be more preferentially lost during ageing (Lexell *et al.* 1988; Sakellariou *et al.* 2016). This susceptibility of type IIb fibres with ageing might be due to neuronal changes resulting in specific denervation of those fibres (Suzuki *et al.* 2009). Loss of type IIb fibres with ageing results in reduction of type II fibre proportion in aged muscles (reviewed in Schiaffino and Riggani, 2011). However, the arrangement of the different fibre types changes during ageing in humans and rodents, with different fibre types tending to group together, as a potential result of denervation-reinnervation process (Kanda and Hashizume, 1989; Lexell and Downham, 1991).

1.2.3.2 Morphological and functional regulation of NMJs during ageing and disease

NMJs can exhibit morphological and structural alterations during ageing or disease. Several changes at the NMJ were characterised by Valdez *et al.* (2010) in ageing mice. These changes include partial or complete denervation of the post-synaptic site, multiple innervation, fragmentation of the AChR areas, axonal swelling, innervation beyond the receptor area and thin axons at the pre-synaptic site (Valdez *et al.* 2010). Moreover, NMJ synaptic area enlargement and

increased complexity and fragmentation have been recorded in old mice (Rudolf *et al.* 2014).

Fragmentation of the synaptic site has been observed in ageing mice and in adult animal models of muscle disorders, including the *mdx* mice, which develop the characteristics of muscular dystrophy (Pratt *et al.* 2015). Similar findings on NMJ fragmentation on ageing and *mdx* mice were also reported from other groups (Lyons and Slater, 1991; Rudolf *et al.* 2014). Fragmentation was also evident at NMJs of mice following tourniquet-induced injury (Tu *et al.* 2017). Fragmentation of NMJs may also occur following damage in the soma of the neuron, injury of the peripheral nerve and during ageing (Kuromi and Kidokoro, 1984; Apel *et al.* 2009; Valdez *et al.* 2010). This morphological change in NMJ could be due to muscle fibre degeneration and regeneration; however, the exact impact of fragmentation on neuromuscular transmission is not clear yet (Pratt *et al.* 2015).

NMJ denervation (partial or complete) has been widely studied both in ageing animals and during musculoskeletal defects. Similar to fragmentation, denervation of the synaptic site may occur as a result of muscle fibre degeneration-regeneration cycle (Pratt *et al.* 2015). However, denervation may result in muscle fibre atrophy and motoneuron cell death in ageing mice and mice with amyotrophic lateral sclerosis (ALS). In these conditions, the affected motoneuron cells do not have the capacity to quickly regenerate their axons and re-innervate the muscle fibre (Valdez *et al.* 2014). Similar results are seen in $SOD1^{-/-}$ mice, which have been widely used as a model or accelerated muscle ageing (Fisher *et al.* 2011). Interestingly, a study from Chai *et al.* (2011) provides evidence that NMJ denervation may be independent of motoneuron defects in geriatric mice.

Under certain conditions, NMJ morphology might adopt a plaque-shaped conformation, similar to that seen during early stages of NMJ maturation. Such conditions include spinal muscular atrophy (SMA). In a study by Kong *et al.* (2009), mice with SMA exhibited delayed maturation of NMJs, which presented

the characteristic plaque formation, in comparison with the control mice. SMA mice also showed abnormal neurotransmission due to impairments in synaptic vesicle release and therefore release of neurotransmitters (Kong *et al.* 2009).

Apart from morphological abnormalities, NMJ function and motor unit potential may also be impaired during ageing and disease, including SMA, ALS and Duchene muscular dystrophy (DMD) and myasthenia Gravis (MG). Although these conditions may have different underlying mechanisms, they might share some common factors. In humans, lowest motor unit potential is recorded in older men with sarcopenia, compared to healthy young men (Piasecki *et al.* 2018). Smaller size of motor unit potential has also been associated with increased possibility of frailty in humans, independently of age or body mass index (Swiecicka *et al.* 2019). Impaired NMJ function is usually attributed to mutations of genes expressing key proteins for AChR clustering. Agrin proteolysis has been shown to destabilise NMJs resulting in a sarcopenia-like phenotype in mice (Bütikofer *et al.* 2011). Inhibition of MuSK, agrin and Lrp4 signalling from has also been observed in patients with MG, who presented increased level of antibodies against these proteins in their plasma (reviewed in Li *et al.* 2017). Interestingly, overexpression of these proteins can prove beneficial in mice expressing these diseases (reviewed in Li *et al.* 2017). Improvement of NMJ function and morphology in mice has been evident following exercise and caloric restriction (Rudolf *et al.* 2014; Valdez *et al.* 2010).

1.3 Key signalling pathways controlling cell function and survival in skeletal muscle and neurons

Skeletal muscle and neuronal function and survival are regulated by key signalling pathways, whose dysregulation may be accounted for cell dysfunction during ageing or disease. Such pathways include: i) IGF-1/AKT/PI3K/mTOR pathway, ii) FoxO signalling, iii) autophagy/mitophagy pathway and iv) neurotrophin pathway.

IGF-1/AKT/PI3K/mTOR pathway has the capacity to control protein synthesis and reduce protein degradation in skeletal muscle. Inhibition of this pathway has been associated with muscle wasting, as IGF-1 declines with age but counteracts the characteristics of sarcopenia when reactivated (reviewed in Larsson *et al.* 2018). Recent studies focus on IGF-1's role in ameliorating progression of neurodegenerative diseases such as ALS, when injected into the muscle of mice (Dodge *et al.* 2008). Another important player regulating protein synthesis and protein breakdown is the mammalian target of rapamycin (mTOR), which is activated by Akt long with other downstream factors (Schiaffino *et al.* 2013). mTOR binds with other proteins to form two distinct complexes, mTORC1 and mTORC2 (Schiaffino *et al.* 2013). mTORC1 has been identified as a key regulator of the autophagy process *via* phosphorylation of the mammalian autophagy-initiating kinase Ulk1 in a nutrient-dependent manner (Hosokawa *et al.* 2009; Kim *et al*. 2011). mTORC1 also controls protein synthesis *via* phosphorylation of key substrates including S6-kinase (S6K) (reviewed in Yang and Guan, 2007). In addition to protein synthesis and degradation, mTOR has been shown to control mitochondrial respiration and gene expression through YY1-PGC1α complex, *via* direct interaction of transcription factor Yin Yang 1 (YY1) with mTORC1 complex in mice (Cunningham *et al.* 2007). Whole-body knockout of mTOR in mice is lethal while muscle-specific knockout of mTOR results in severe myopathy and metabolic abnormalities, including impaired mitochondrial respiration, resulting in premature death at postnatal stages (Risson *et al.* 2009).

FoxO acts downstream of the AKT/PI3K signalling and as a family of transcription factors it controls expression of genes involved in cell proliferation, survival, differentiation, oxidative stress (Paik *et al.* 2009). FoxO family comprises of four members: FoxO1, FoxO3, FoxO4 and FoxO6 and in muscle they regulate muscle atrophy and fibre type specification (reviewed in Xu *et al.* 2016). FoxO3 in particular, is involved in activation of muscle atrophy genes, including atrogin-1, and in the regulation of autophagy process (reviewed in Schiaffino and Reggiani, 2011). FoxO signalling is also involved in the regulation of neurogenesis and neuronal stem cell proliferation and renewal (Paik *et al.* 2009).

Mitophagy is a quality control system for mitochondrial maintenance and function. Dysfunctioning mitochondria are targeted by autophagosomes and delivered to the lysosomes for degradation (reviewed in Yoo and Jung, 2018). Autophagy-related protein LC3 and mitophagy-related proteins PINK1 and Parkin are critical for selected removal of damaged mitochondria (reviewed in Larsson *et al.* 2018). Dysfunction of autophagy/mitophagy process has been associated with ageing phenotype in skeletal muscle due to inability of the cells to discard damaged mitochondria. Mice with muscle-specific deficiency in autophagy present all normal characteristics of sarcopenia including increased muscle wasting, NMJ fragmentation and muscle fibre denervation, leading eventually to premature death (reviewed in Larsson *et al.* 2018).

Neurotrophin signalling has been widely studied on its role in regulating neuronal survival and function, but an increasing number of studies highlight the role of neurotrophins in skeletal muscle development and function (reviewed in Sakuma and Yamaguchi, 2011). The most studied neurotrophins in skeletal muscle include the brain-derived growth factor (BDNF), glial-derived growth factor (GDNF), nerve growth factor (NGF) and neurotrophins-3 and -4/5 (NT-3, NT-4/5). The expression of BDNF in skeletal muscle of rodents varies between different cell types and at different developmental stages (Mousavi and Jasmine, 2006). BDNF expression levels are highly dependent on physiological and pathological conditions, such as exercise in healthy humans and patients with multiple sclerosis (Gold *et al.* 2003). BDNF, along with NT-4, has been shown to inhibit agrin-induced AChR clustering on myotubes *in vitro* (Wells *et al.* 1999). Recent studies have shown a decrease in BDNF levels in the brains of neonatal rat offspring following maternal low-protein diet (Marwarha *et al.* 2017). GDNF expression levels have been detected in both motoneuron cells and skeletal muscle of humans and rodents (Suzuki *et al.* 1998; Nguyen *et al.* 1998). Overexpression of GDNF has been associated with hyperinnervation of skeletal muscle fibres of mice during neonatal stages of development (Nguyen *et al.* 1998). GDNF has also been shown to cause enhanced neurotransmitter release from motoneuron to skeletal muscle fibres through NMJs in neonatal mice,

highlighting its structural and functional role in maintaining NMJ plasticity in neonatal mice (Ribchester *et al.* 1998). The role of NT-4/5 is diverse and depends on the organism species and the stage of postnatal growth; however, studies have associated NT-4/5 expression with fibre type conversion, motoneuron survival, NMJ formation and neurotransmitter release *via* binding to tyrosine kinase receptors TrkB and $p75^{NTR}$ (also known as NGFR) (reviewed in Sakuma and Yamaguchi, 2011). Interestingly, NT-3 has not been associated with regulation of skeletal muscle morphology in chickens (Wells *et al.* 1999). However, NT-3 has been associated with improved skeletal muscle reinnervation, following peripheral nerve injury in rats (Simon *et al.* 2001). NGF has been associated with improved skeletal muscle regeneration of *mdx* mice (Lavasani *et al.* 2006). Phenotypic knockout of NFG in mice leads to skeletal muscle atrophy and a dystrophic phenotype in adult mice (Ruberti *et al.* 2000). Additionally, increased levels of NGF were recorded in muscle biopsies of patients with ALS, but such increase was not observed in skeletal muscle of old rats (reviewed in Sakuma and Yamaguchi, 2011).

1.3.1 Mitochondrial bioenergetics

Mitochondria are the "powerhouses" of the cells, providing the necessary energy for the cell's metabolic activities to occur. Mitochondria regulate cell processes including apoptosis, signal transduction, energy production and metabolism (Li *et al.* 2013). Energy production is mainly achieved by oxidative phosphorylation (OXPHOS), which is the primary function of the mitochondria (Li *et al.* 2013). The term "oxidative phosphorylation" refers to the process by which mitochondria utilise electrons released following oxidation of substrates, which are transported through enzymes in the mitochondrial inner membrane to drive phosphorylation of ADP to ATP (**Figure 1.3.1**) (reviewed in Chaba *et al.* 2014).

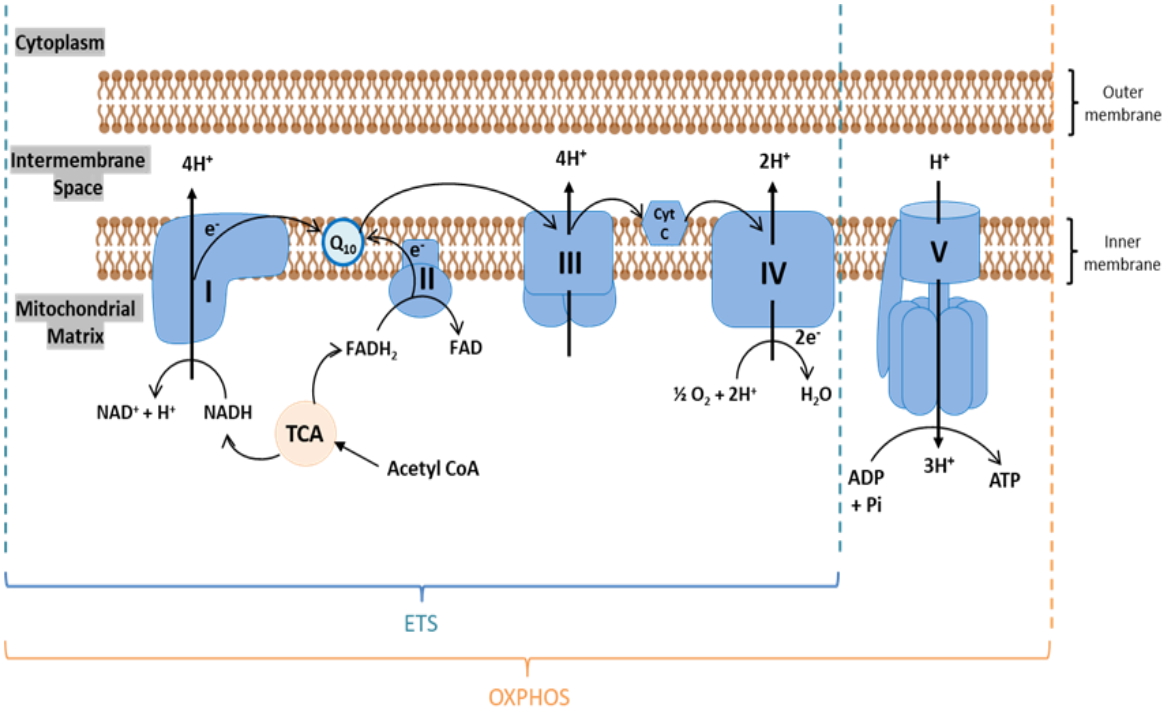

Figure 1.3.1 Mitochondrial oxidative phosphorylation (OXPHOS) electron transport system (ETS) (adapted/redrawn from Matroeni *et al.* 2017).

Electrons are transported through the inner mitochondrial membrane *via* four enzyme complexes (complex I, II, III and IV), three of which pump H^+ to the intermembrane space (complexes I, III and IV). This system is known as the electron transport system (ETS) or electron transport chain (ETC) (reviewed in Gnaiger, 2009). Substrates from nutrient metabolism, such as malate and pyruvate, enter the tricarboxylic acid (TCA) cycle, where NADH is produced and subsequently reduced to NAD^+ by Complex I, which pumps H^+ generated from this reaction into the intermembrane space of the mitochondria (reviewed in Chaba *et al.* 2014). Complex II or succinate dehydrogenase (SDH) is the only enzyme that participates in both the TCA cycle and in ETS. Within the TCA cycle, complex II converts succinate to fumarate with subsequent release of electrons. These electrons are used by complex II within the ETS to reduce $FADH_2$ to FAD, with further release of electrons into the ETS. Complex II is not a proton pump, and it is the second entry point (after complex I) to the ETS (Rutter *et al.* 2010).

Complex III converts ubiquinone to ubiquinol *via* oxidation, pumping generated H^+ into the mitochondrial intermembrane space, while the electrons enter the cytochrome C carrier (reviewed in Chaba *et al.* 2014). Finally, complex IV, the largest enzyme of the ETS, known as cytochrome C oxidase (COX) received electrons from cytochrome C and uses them for the conversion of O_2 to H_2O, using H^+ present in mitochondrial cytosol (reviewed in Chaba *et al.* 2014). The OXPHOS system contains the enzymes of the ETS plus Complex V or ATPase synthase, which uses the H^+ dispensed in the intermembrane space to convert ADP to ATP (reviewed in Jonckheere *et al.* 2012).

The enzymes of the electron transport chain are often seen in the form of large complexes, known as supercomplexes. Three main supercomplexes have been observed between complex I, III and IV: i) Complexes I + III + IV (known as the respirasome), complexes I + III and complexes III + IV (Lapuente-Brun *et al.* 2013). The respirasome (Complex I + III + IV) is most abundant in mammals; however complex IV is found mostly a monomer and not part of a supercomplex, while complex II is the only enzyme that does not form supercomplexes (reviewed in Chaba *et al.* 2014).

Each enzyme of the respiratory chain is comprised of different subunits, which are encoded by both nuclear and mitochondrial genes. Specifically, complex IV is comprised of 13 subunits, 3 of which are encoded by genes in the mitochondrial DNA (mt DNA) (subunits I, II, II) and the rest 10, including subunit IV, is encoded by genes located in the nuclear DNA (Dhar *et al.* 2008). The expression of those genes is regulated by two transcription factors, nuclear respiratory factor 1 (NRF-1) and nuclear respiratory factor 2 (NRF-2) in both rats, mice and humans (Dhar *et al.* 2008).

1.3.1.1 Mitochondrial dysfunction during ageing and disease

Mitochondrial dysfunction can have a detrimental effect on cell function and survival. During ageing, mitochondrial function and mitochondrial enzyme activity decline. This is also accompanied by an accumulation of mutations in

mtDNA (Short *et al.* 2005). Accumulation of mitochondrial mutation has been linked to increase in reactive oxygen species (ROS) production, leading to reduction in OXPHOS (reviewed in Wallace, 1999). Mitochondrial mutation number in neurons is elevated in patients with neurodegenerative disorders, including Alzheimer's and Huntington's disease and these mutations are accompanies by an increase in oxidative damage (reviewed in Wallace, 1999). Mitochondrial dysfunction and decline in ATP production have been associated with reduction in mtDNA copy number with age (Short *et al.* 2005).

Mutation or inhibition of genes encoding mitochondrial proteins has also been responsible for mitochondrial dysfunction during ageing and disease. Deficiency of MnSOD, a mitochondrial protein with antioxidant properties, causes substantial reduction in complexes II and III activity in skeletal muscle of mice, inhibiting the ETS (reviewed in Wallace, 1999). Age-related decline in complexes I, III and IV during ageing in skeletal muscle and brain of mice is believed to be associated with mutations in the mtDNA gene transcripts encoding subunits of these complexes (Feuers, 1998). These results are supported further by the absence of age-related decline in complex II activity, whose subunits are all encoded by genes in nuclear DNA (reviewed in van Remmen and Richardson, 2000). Specifically, decline in complex IV activity with ageing has been observed in the brain, the synaptic mitochondria and skeletal muscle (reviewed in van Remmen and Richardson, 2000). Complex IV is believed to be a key player in cell metabolic control, signalling and survival due to its position as the terminal enzyme in the ETS (reviewed in Arnold 2012). Complex IV defects may be attributed to inhibition of genes encoding its subunits, due to silencing of the transcription factors, such as NRF-1, controlling their expression (Dhar *et al.* 2008). Increased mitochondrial stress and damage beyond protein level can trigger several pathways including mitochondrial degradation *via* mitochondrial autophagy (mitophagy) (reviewed in Yoo and Jung, 2018).

Regulation of molecular mechanisms can be tissue-specific, but it may also occur simultaneously and in multiple tissues. Factors that have the capacity to control

multiple signalling pathways concomitantly in different tissues include small, non-coding RNA molecules, such as microRNAs.

1.4 Control of gene expression by microRNAs

1.4.1 MicroRNA biogenesis, processing and port-transcriptional control of gene expression

MicroRNAs (miRNAs) are small, single-stranded non-coding RNA molecules of approximately 20-22 nucleotides in length, that have the ability to control gene expression mainly by direct binding to the 3'-untranslated region (UTR) region of their mRNA transcript (Ambros, 2001; Lagos-Quintana *et al.* 2002). The first miRNAs, *lin-4* and *let-7*, were discovered in *Caenorhabditis elegans* (*C. elegans*), where mutants of these two miRNAs caused temporal deregulation of lavae development (Lee *et al.* 1993, Reinhart *et al.* 2000). *Lin-4* and *let-7* did not encode for any proteins and produced very small transcripts in length from precursor RNA molecules with a distinguished hairpin structure (Ambros, 2001). A later study on *let-7* revealed the conservation of this miRNA, both in length and sequence between species (Pasquinelli *et al.* 2000).

MicroRNA genes are distributed across the genome and are found either as clusters (polycistronic) or as independent units on intergenic regions, intronic sequences of transcriptional units or exonic sequences of non-coding genes (**Figure 1.4.1**; reviewed in Fazi and Nervi, 2008). Polycistronic miRNA genes generate pri-miRNA transcript processed by endonuclease RNase III Drosha, forming a complex with DiGeorge Syndrome Critical Region 8 (DGCR8) protein (Drosha/DGCR8 complex), producing multiple pre-miRNAs with a characteristic 70-90 nt hairpin-shaped stem-loop structure (Lee *et al.* 2003). Pri-miRNA transcripts generated by independent units (intergenic, intronic/exonic) are also processed by Drosha/DGCR8, generating a 70-90 hairpin-shaped pre-miRNA transcript, which is then exported from the nucleus (Fazi and Nervi, 2008). Certain intronic miRNAs are processed in a Drosha-independent manner, escaping the canonical pathway of pre-miRNA biogenesis and producing pre-

miRNA transcripts known as miRtrons (reviewed in Westholm and Lai, 2011). miRtrons are shorter in length than the canonical pri-miRNAs and are generated by intron splicing and debranching by lariat debranching enzyme (Ldbr), before they enter the canonical pathway of pre-mRNA processing (Ruby *et al.* 2007).

Pre-miRNAs are actively exported from the nucleus into the cytosol by exporting-5 (Yi *et al.* 2003). There, pre-miRNA is recognised by enzyme Dicer and its partner TAR (HIV) RNA binding protein (TRBP) (Dicer/TRBP complex) and cleaved near the terminal loop, producing a miRNA/miRNA* duplex with 2 nt overhand at both 3'-ends (Bernstein *et al.* 2001; Hutvagner *et al.* 2001; reviewed in Starega-Roslan *et al.* 2011). miRNA/miRNA* duplex is loaded onto the Argonaute (Ago) protein of the miRNA-induced silencing complex (RISC) complex, where the least thermodynamically stable strand at the 5' end is retained by the RISK complex ("guide" strand) while the other strand ("passenger" strand) is usually degraded, although in some cases it is functional (Schwarz *et al.* 2003). The "guide" strand bound to the RISC complex (mature miRNA) binds to the 3'UTR region of the target mRNA transcripts *via* a complementary sequence known as the "seed" region (2-7 nucleotides in length at the 5' end of the miRNA) and represses their expression or inhibits their translation (or both) (Doench *et al.* 2004).

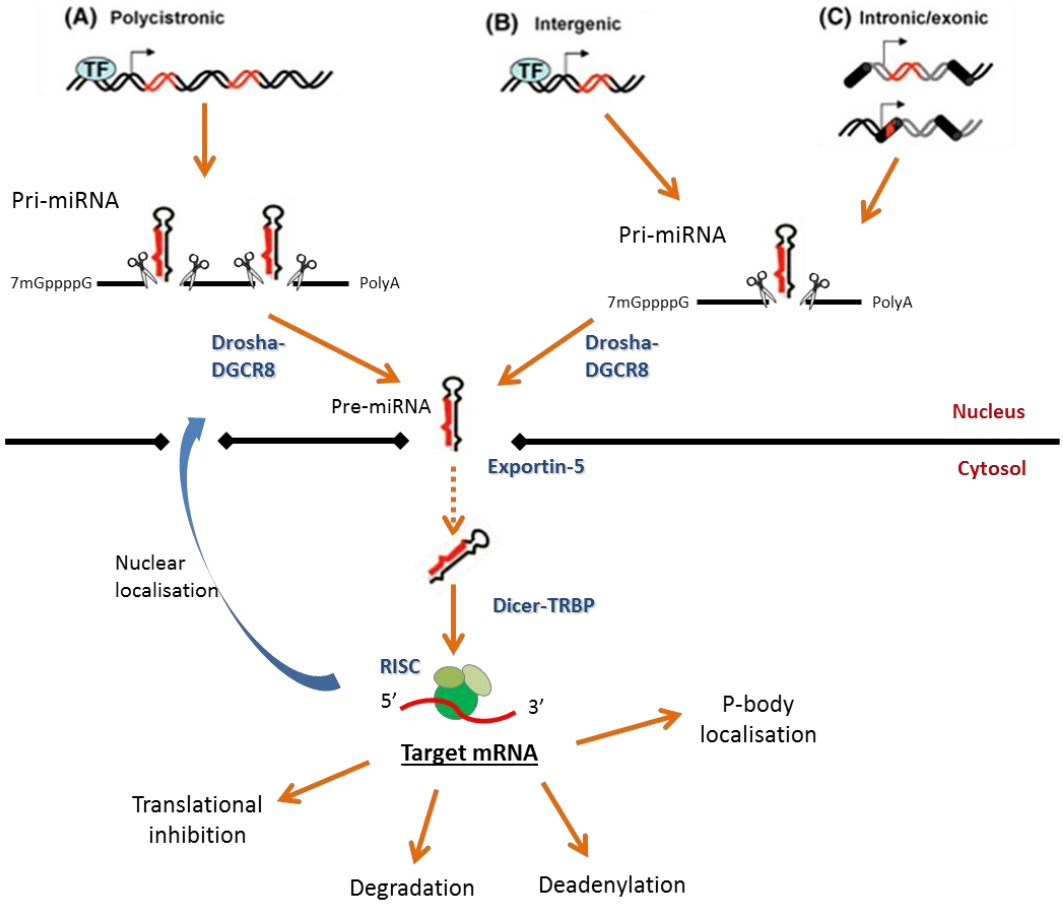

Figure 1.4.1 The canonical pathway of microRNA biogenesis and processing (redrawn from Fazi and Nervi, 2008).

Post-transcriptional gene repression (or in some cases activation) by miRNAs occurs mainly by deadenylation and subsequent degradation or translational repression of the target mRNA as seen in **Figure 1.4.2** (reviewed in Filipowicz *et al.* 2008). mRNA degradation occurs by rapid removal of the poly-(A) tail causing destabilisation of the mRNA transcript and decapping, which then leads to mRNA decay occurring in the P-bodies (Wu *et al.* 2006; Eulalio *et al.* 2007). Degradation of target mRNA is also seen of miRNA-AGO2 to the mRNA target site, where AGO2 acts as an endonuclease, cleaving the mRNA at the centre (Meister *et al.* 2004). Translational repression of the target mRNA can occur *via* three different mechanisms: repression of translation initiation or repression of post-initiation

steps (reviewed in Filipowicz *et al.* 2008). Translational repression at the initiation step is observed when miRNA binds to the m^7G cap in the 3'UTR, preventing the binding of transcription factors such as eIF4E (Humphreys *et al.* 2005; Pillai *et al.* 2005). Translational repression at the initiation step can also take place by eLF6 recruitment to the RISC complex, which binds to the 60S ribosomal subunit, preventing it from joining the 40S subunit and therefore stalling the translation process (Chendrimada *et al.* 2007). Post-initiation translational repression occurs when the ribosomes "drop off" prematurely, terminating the translation process prematurely and leaving the nascent polypeptide incomplete (Petersen *et al.* 2005).

Under certain conditions and in specific tissues or cell types, miRNAs have the potential to induce upregulation of post-transcriptional regulation. A study from Vasudevan *et al.* (2007) provides evidence on how a well study microRNA, let-7, can induce increased translation of its mRNA targets during cell cycle arrest but repress the translation of those mRNA targets during cell proliferation. Based on this evidence, they propose a novel role of microRNA function which oscillates between repression and activation of the targeted mRNAs during difference stages of cell cycle (Vasudevan *et al.* 2007).

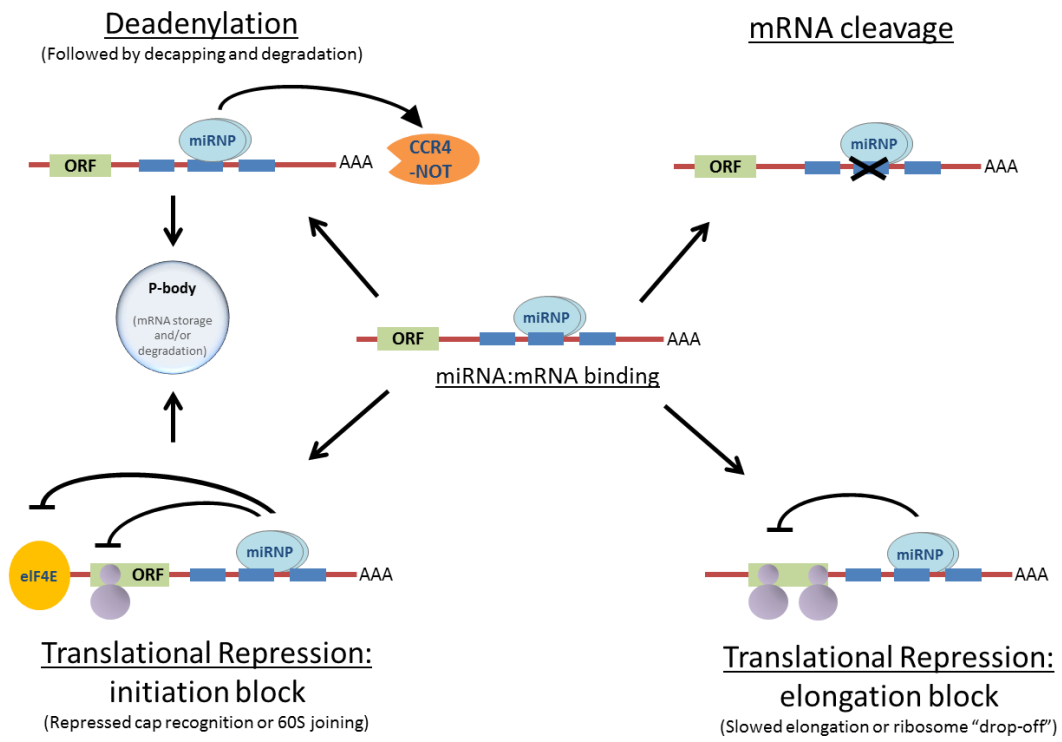

Figure 1.4.2 Mechanisms of miRNA-mediated post-transcriptional gene repression (redrawn from Filipowicz *et al.* 2008).

1.4.2 MicroRNA-128: regulation of key mechanisms in skeletal muscle and neurons

MicroRNA-128 (miR-128) is an intronic miRNA encoded by miR-128-1 and miR-128-2 genes located on the introns of R3HDM1 gene (chromosome 2q21.3) and RCS gene (chromosome 3p22.3) respectively (Bruno *et al.* 2011). These genes are conserved among human, mouse and rat genome (Megraw *et al.* 2010). Following processing, both miR-128-1 and miR-128-2 yield a mature microRNA identical in the sequence, called miR-128 (reviewed in Li *et al.* 2013).

miR-128 is a brain-enriched microRNA that plays a key role in neuronal development and maintenance (reviewed in Ching and Ahmad-Annuar, 2015). miR-128 has also been studied extensively in relation to cancer and tumorigenesis. Increased levels of miR-128 were found in patients with acute

leukaemia and have been considered as a biomarker for prognosis and diagnosis of this type of cancer (Zhu *et al.* 2011). Despite its abundance in the brain and in various types of cancer, miR-128 was also found to be highly expressed in skeletal muscle tissue (Motohashi *et al.* 2013).

1.4.2.1 Role of miR-128 in skeletal muscle

Increased levels of miR-128 expression were recorded in brain and TA muscle in adult mice (Motohashi *et al.* 2013). miR-128 has also been shown to regulate the proliferation and differentiation of muscle side population (SP) cells, a distinct population of muscle stem cells with multipotent characteristics, which do not express the muscle satellite cell marker, Pax7 (Motohashi *et al.* 2012). In their study in 2013, Motohashi *et al.* demonstrated the regulation of insulin signalling pathway by miR-128, through direct targeting of Insr (insulin receptor), Isr-1 (insulin receptor substrate-1) and Pi3kr1 (phosphatidylinositol 3-kinases regulatory 1) mRNA, inhibiting their expression. Inhibition of miR-128 *in vitro*, resulted in hypertrophy of the cultured myotubes and increase of IRS-1 and AKT proteins, while administration of antisense miR-128 *in vivo* resulted in increased skeletal muscle mass in 4 weeks old mice (Motohasi *et al.* 2013). Results from this study show that miR-128 is capable of promoting skeletal muscle hypertrophy *in vivo* and *in vitro*, following inhibition of its expression levels.

Further studies have shown miR-128 directly targeting myostatin (*Mstn*) gene transcript in C2C12 cells, while stalling their proliferation and promote their differentiation into myotubes (Shi *et al.* 2015). *In vivo* experiments showed increased expression of miR-128 accompanied by a significant decrease in MSTN protein levels in the skeletal muscle of 8-weeks old mice (Shi *et al.* 2015). Another study has shown correlation of miR-128 with ATP levels during myoblast differentiation. Specifically, increased levels of miR-128 were in agreement with increased ATP levels at Day 4-8 post-differentiation of C2C12 cells (Siengdee *et al.* 2015). Furthermore, miR-128 increased levels in C2C12 myotubes were accompanied by up-regulation of the expression levels of genes involved in

mitochondrial energy metabolism, including *Cox6a2* (Seingdee *et al.* 2015). *Cox6a2* gene encodes one of the subunits of Complex IV of the mitochondrial respiratory chain and inhibition of this gene has been shown to decrease mitochondrial activity and promote muscle-fibre type switching, protecting mice against high-fat diet-induced obesity (Quintens *et al.* 2013). miR-128 has also been implicated in skeletal muscle stress response by directly targeting the v-Maf avian musculoaponeurotic fibrosarcoma oncogene homolog G (MAFG) gene transcript and therefore controlling biochemical pathways associated with oxidative stress (Caggiano *et al.* 2017). In line with previous studies, Dai *et al.* (2016) demonstrate the ability of miR-128 to regulate bovine satellite cell proliferation and differentiation in skeletal muscle *via* direct targeting and inhibition of Sp1 transcript. Similar results were obtained from studies in cardiomyocytes, where inhibition of miR-128 resulted in increased proliferation of postnatal cardiomyocytes cells; the opposite results were seen with tissue-specific overexpression of miR-128 in neo-natal mice (Huang *et al.* 2018).

1.4.2.2 Role of miR-128 in neuronal cells

The abundance of miR-128 expression in the brain and central nervous system (CNS) has made it an ideal candidate for investigation of the mechanisms it regulates. miR-128 has the capacity to determine neuronal progenitor cell fate *in vivo* and *in vitro* by directly targeting Pcm1, which controls proliferation and neurogenesis of NPC cells in the developing cortex of mice (Zhang *et al.* 2016). Overexpression of miR-128 *in vitro* and *in utero* enhanced neuronal differentiation of NPC cells but inhibited their proliferation, by supressing the translation of Pcm1 mRNA (Zhang *et al.* 2016). Spatial as well as temporal regulation of miR-128 expression is important for the regulation of neuronal development in the cortex of mouse embryo (Franzoni *et al.* 2015). In their study, Franzoni *et al.* (2015) have demonstrated how inhibition of miR-128 caused excessive migration of neuronal cells in the upper layer of the cortex. Two more studies have demonstrated the role of miR-128 in neuronal excitability

in mice. The first study from Tan *et al.* (2013) highlighted the modulation of motor behaviour by miR-128 through regulation of neuronal signalling pathways and neuron excitability. Specifically, they demonstrated the effect of miR-128 inhibition on neuronal motor hyperactivity in adult neurons, resulting in seizure and a Parkinson's-like phenotype in mice (Tan *et al.* 2013). An inverse relationship was observed between neurons overexpressing miR-128 and motor activity, which appeared decreased and was accompanied by a reduction in ERK2 activation (Tan *et al.* 2013). Similar data were shown in a later study from McSweeney *et al.* (2016), where inhibition of miR-128 in neuronal cells *in vitro* caused increased neuronal hyperactivity.

Apart from direct targeting of specific mRNAs, miR-128 has been shown to control gene expression in developing neurons by controlling nonsense-mediated decay (NMD) process. NMD mediates degradation of mRNA transcripts and inhibition of this process has been associated with impaired neurotransmitter signalling and synaptic vesicle cycling at the neuromuscular site (Long *et al.* 2010). miR-128 disrupts NMD by direct targeting of one of its genes, Upf1, causing disruption in NMD pathways and subsequent upregulation of the mRNA transcripts regulated by NMD for degradation (Bruno *et al.* 2011).

Several studies have focused on the association of miR-128 with neuropsychiatric disorders, due to its ability to regulate neuronal cell behaviour and fate. Of particular interest is the interaction of miR-128 with Arpp21, as miR-128 gene is located within an intron of the longest isoform of Arpp21 gene, which it also targets (Megraw *et al.* 2010). Deregulation of Arpp21 expression has been associated with several neurological syndromes, including but not limited to Alzheimer's, epilepsy and anxiety (reviewed Ching and Ahmad-Annuar, 2015).

1.4.2.3 Role of miR-128 in cell senescence, metabolism and cancer

Aside from its role in skeletal muscle and CNS, miR-128 has been shown to be involved in regulating cell senescence, cholesterol metabolism and various forms of cancer biology. miR-128 promotes cell senescence by direct targeting of Bmi-1, which results in inhibition of cancer cell growth by increased intracellular ROS levels (Venkataraman *et al.* 2010). Several studies have reported miR-128 as a tumour suppressive microRNA, as downregulation of its expression levels is seen in various types of cancer, such as glioblastoma, medulloblastoma and acute myeloid leukaemia (reviewed in Feliciano *et al.* 2010). A study from Papagianakopoulos *et al.* (2012) highlighted miR-128 tumour suppressive properties by targeting and repression of Egfr and Pdgfrα genes, involved in the receptor tyrosine kinase (RTK) signalling. Cell apoptosis in embryonic kidney stem cells was induced by repression of Bcl-2-associated X protein (Bax) gene through direct targeting by miR-128 (Adlakha and Saini, 2011). BAX, a member of the Bcl-2 family, is translocated under stress conditions from the cytosol to the outer membrane of the mitochondria, creating pores and impairing mitochondria respiration, leading the cells to apoptosis (Adlakha and Saini, 2011). Findings from the study by Lian *et al.* (2018) are also in line with these findings. Specifically, Lian *et al.* have demonstrated the regulation of colorectal cancer cell apoptosis during overexpression of miR-128, which supresses the expression of its direct target sirtuin-1 (Sirt-1), leading to accumulation of intracellular ROS (Lian *et al.* 2018). Apart from its pro-apoptotic properties, miR-128 has also been associated with the regulation of cholesterol homeostasis. Upregulation of miR-128 was associated with decreased expression of genes involved in cholesterol metabolism by repression of genes involved in cholesterol efflux (Aldakha *et al.* 2013). Whether miR-128 retains similar properties under the effect of dietary protocols altering cholesterol balance, remains to be investigated.

1.4.3 MicroRNA-133a: regulation of key mechanisms in skeletal muscle and neurons

MicroRNA-133a belongs to a family of microRNAs expressed specifically in muscle tissue and are therefore known as “myomiRs” (reviewed in van Rooij *et al.* 2008). miR-133a gene is clustered with miR-1 gene on chromosome 2 (seprated by 9.3 kb) and on chromosome 18 (separated by 2.5 kb) in mice (Chen *et al.* 2005). Both miR-1 and miR-133a are expressed as a bicistronic transcript specifically in cardiac and skeletal muscle tissue (Chen *et al.* 2005). miR-133a-1 and miR-133a-2 (chromosomes 18 and 2 respectively) have an identical sequence which only differs in the last 2 nucleotides at the 3’ end of miR-miR-133b (reviewed in van Rooij *et al.* 2008). This similarity in miR-133 sequences can prove challenging in functional studies.

1.4.3.1 Role of miR-133a in cardiac and skeletal muscle

The role of microRNA-133a (miR-133a) in muscle development and function has been extensively studied, since its tissue-specific expression was reported by Lagos-Quintana *et al.* (2002). miR-133a has been identified as a key regulator of skeletal muscle and cardiac muscle cell proliferation and differentiation *in vitro* and *in vivo*. In their study, Chen *et al.* (2005) identified miR-133a as an inducer of myoblast proliferation in C2C12 cells. Temporal regulation and level of miR-133a expression was also proven essential, as increased miR-133a levels in malformations of cardiac tissue during development (Chen *et al.* 2005). Furthermore, Chen *et al.* (2005) identified serum response factor (Srf) gene, a key player in proliferation and differentiation of skeletal muscle, as a direct target of miR-133a. Expression levels of miR-133a are higher during differentiation of C2C12 myotubes but levels are not detectable in C2C12 myoblasts, implying that its expression is induced during differentiation *in vitro* (Rao *et al.* 2006). Furthermore, findings from Rao *et al.* (2006) demonstrated the regulation of miR-133a expression by MyoD and myogenin in C2C12 myotubes, which is in line with findings from previous findings from Chen *et al.* (2006).

Inhibition of miR-133a in C2C12 myotubes appeared affect myotube elongation and morphology rather than differentiation process, as seen with other myomiRs (Kim *et al.* 2006). Expression of miR-133a in C2C12 myotubes was suppressed with addition of FGF which is a key component of ERK/MAPK pathway (Sweeetman *et al.* 2008). During early development, miR-133a expression is also regulated by MEF-2 enhancer on a transcriptional and post-transcriptional level in skeletal and cardiac muscle of mice (Liu *et al.* 2007). Regulation of myogenesis *in vitro* also occurs through repression of uncoupling protein -2 (UPC-2) gene, which is a direct target of miR-133a (Chen *et al.* 2009b). Repression of Upc-2 expression in C2C12 cells resulted in attenuated proliferation and enhanced myoblast differentiation, highlighting further the key role of miR-133a in the regulation of myogenesis (Chen *et al.* 2009b).

Three studies focused on the effect of gain- and loss-of function of miR-133a in skeletal muscle fate and disease. A study from Huang *et al.* (2011) revealed direct targeting of Igf1r transcript by miR-133a. Gain- and loss-of-function experiments showed suppression of Igf1r expression in C2C12 myotubes following overexpression of miR-133a; however supplementation of IGF-1 (ligand of IGF-1R) in C2C12 cells resulted in upregulation of miR-133a expression (Huang *et al.* 2011). The findings from this study indicate regulation of miR-133a expression *via* IGF-1 mediated feedback loop in modulation of myogenesis, suggesting that miR-133a could be a promising therapeutic target for skeletal muscle diseases (Huang *et al.* 2011). A second study from Deng *et al.* (2011) investigated the effect of miR-133a overexpression in *mdx* mice, a model of Duchene muscular dystrophy. miR-133a expression levels were significantly increased in the skeletal muscle of those mice; however, transgenic mice overexpressing miR-133a in skeletal muscle demonstrated normal muscle development and function (Deng *et al.* 2011). Interestingly, a third study from Liu *et al.* (2011) demonstrated the effect of miR-133a deletion *in vivo,* adult-onset centronuclear myopathy in fast-twitch muscle fibres, impaired mitochondrial function and fibre type switching in mouse skeletal muscle. miR-133a was also

implicated in the regulation of fibre type conversion through modulation of thyroid hormone action in skeletal muscle (Zhang *et al.* 2013).

Further studies have focused on the role of miR-133a in the regulation of myogenesis *via* modulation of different pathways. In their study, Zhang *et al.* (2012) indicated Sp-1 transcript as a direct target of miR-133a, inducing mitotic arrest in C2C12 myoblasts and inhibiting proliferation. Moreover, miR-133a was identified as a repressor of ERK1/2 signalling pathway activity, by directly targeting two components of this signalling pathway, Fgfr1 and Ppp2ac transcripts (Feng *et al.* 2013). Repression of ERK1/2 signalling resulted in repressed cell proliferation and promotion of cell differentiation (Feng *et al.* 2013). Inhibition of miR-133a in chick embryos led to an increase in the expression levels of the target genes BAF60a and BAF60b transcripts, impairing the timing of myogenic differentiation (Goljanek-Whysall *et al.* 2014). Foxl2 transcript was also identified as a direct target of miR-133a, regulating skeletal muscle differentiation *in vitro* through a different mechanism than the ones previously described (Luo *et al.* 2015). A recent study from Mok *et al.* (2018), also implicated Hedgehog pathway modulation *via* miR-133a in the regulation of myogenesis at embryonic stages.

1.4.3.2 Role of miR-133a in neuron cells

Despite its specific expression in skeletal and cardiac muscle, recent studies have associated changes in miR-133a expression following neuronal alterations and injury. Expression levels of known target genes of miR-133a were significantly altered in rats 7 days following traumatic spinal cord injury (SCI), suggesting a possible relationship between miR-133a and injury responses at the spinal cord (Yunta *et al.* 2012). These findings are in line with previous evidence from Nakanishi *et al.* (2009) showing an upregulation of miR-133a expression levels just 24 hours after spinal cord injury in mice. Interestingly, during early embryonic development, miR-133a appears to have an inhibitory role in stem cell differentiation to neuron cells, by suppression of neuronal genes involved in

neuronal cell fate specification *in vitro* (Ivey *et al.* 2008; Izarra *et al.* 2017). Recent study by Hoye *et al.* (2017) has shown the potential role of miR-133a in motoneuron cells, with a number of its target genes showing increased expression levels in those cells during postnatal growth. In the context of neuromuscular junctions, expression of miR-133a does not seem to be significantly altered after 10 days of denervation in TA muscle of ALS mouse model (Williams *et al.* 2009).

In recent years, microRNAs have been of particular interest due to their potential of controlling multiple signalling pathways in many different tissues simultaneously, making them a high-throughput mechanism of gene expression. This is of particular importance in the field of skeletal muscle development and ageing where multiple events occur simultaneously.

1.5 Hypothesis

Pre- and/or early postnatal protein restriction adversely affects the homeostasis of muscle fibres and/or neuromuscular junctions and this is, at least partially, regulated by modified microRNA-target interactions in muscles and nerves of the offspring. Therefore, manipulation of microRNA expression may serve as a tool for restoration of neuromuscular morphology and function during dietary protein restriction.

1.6 Aims

The aims of this study were to:

i) Determine the effects of protein-deficient diet during pre- and postnatal stages of development in skeletal muscle and neuromuscular junctions of 12-week old mice (**Chapter 3**)

ii) Identify changes in expression levels of microRNAs, selected based on their function, in skeletal muscle and peripheral nerve of 12-week old mice on a protein-deficient diet pre- or postnatally (**Chapter 4**)

iii) Identify predicted target genes of microRNAs with potential role in regulating neuromuscular homeostasis and differentially expressed in muscle and/or nerve of 12-week old mice on a protein-deficient diet pre- or postnatally using *in silico* analysis (**Chapter 4**)

iv) Investigate the effect of gain- and loss-of-function of miR-128 and miR-133a in skeletal muscle cell phenotype *in vitro* (**Chapter 5**)

v) Investigate the effect of gain- and loss-of-function of miR-128 and miR-133a in motoneuron cell phenotype *in vitro* (**Chapter 6**)

vi) Investigate the expression levels of miR-128 predicted target genes and their protein content in skeletal muscle and motoneuron cells *in vivo* and *in vitro* (**Chapter 7**)

Chapter 2

Methods

2 Materials and Methods

2.1 Animals

In this study female and male C57BL/6 *Thy1-YFP16* transgenic mice were used (The Jackson Laboratory; Thy-1 YFP-16, Stock# 003709). These mice express yellow fluorescent protein (YFP) in the motor neurons and sensory neurons at high levels (with no expression in non-neuronal cells and no apparent toxic effects) allowing the visualisation of motor neurons and muscle innervation from mid-gestational stages without the use of antibody staining (Vasilaki *et al*. 2016). This provides a novel approach in the assessment of structural alterations in motor neurons and neuromuscular junctions (NMJs) in muscle using fluorescent microscopy.

All experiments were performed in 12-week old mice, allowing the examination of the effect of a protein-deficient diet until the end of postnatal period. All mice were housed in the Biomedical Services Unit at the University of Liverpool under a control environment and subjected to 12 h light-12 h dark cycle.

Two weeks prior mating, nulliparous female mice where introduced to either a control diet (20% Crude Protein W/W ISO' (P), Code 829206, Special Diet Services, Essex, UK) or a low protein diet (5% Crude Protein W/W ISO' (P), Code 829202; Special Diet Services, Essex, UK) and maintained in those diets throughout the study. Both diets will be isocaloric but differ in the amount of casein as previously described (Chen *et al*. 2009; **Appendix, Table A6**). After acclimation to the chow, breeders were placed together and maintained in those diets throughout the study.

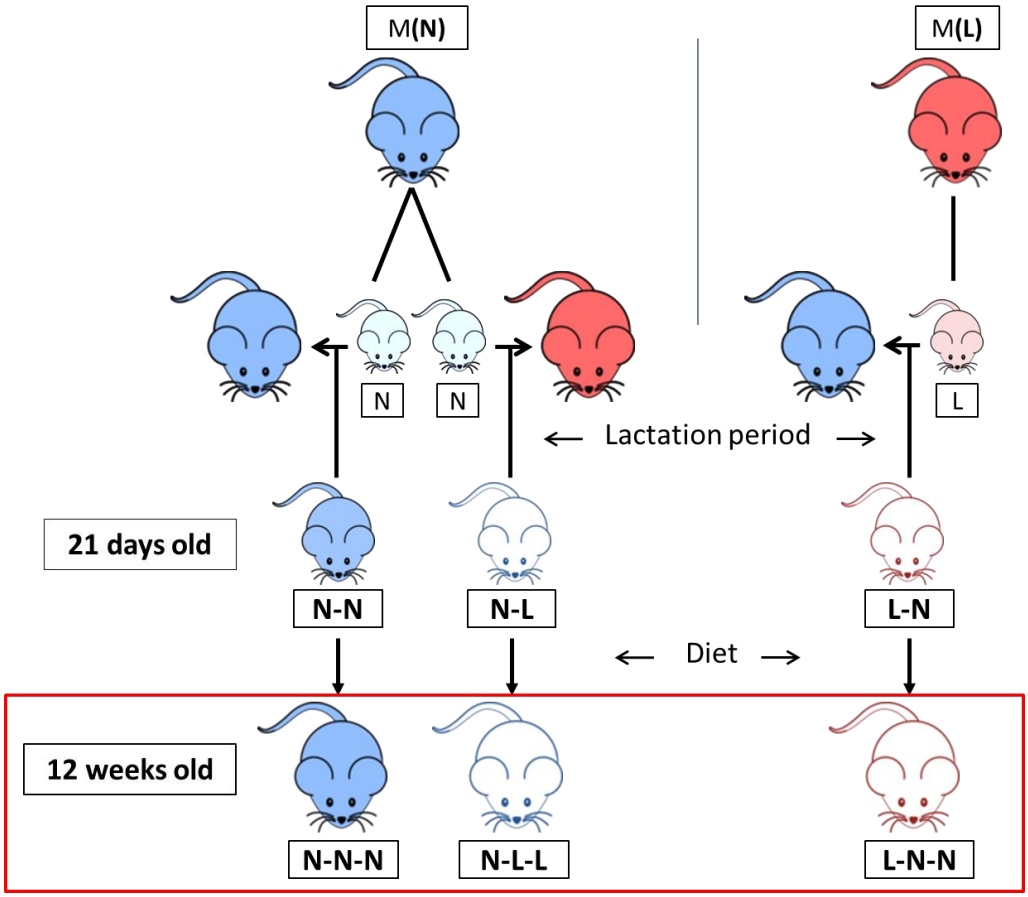

Figure 2.1.1 Experimental design (N) 20% diet (L) 5% diet. **Group N**: Control mice produced from dams fed on normal chow. **Group L**: Mice produced from dams maintained on a low protein diet. **Group N-N**: Mice produced from dams maintained on a normal protein diet and fed postnatally by a dam maintained on a normal diet. Culled and analysed at weaning (21 days). **Group N-L**: Mice produced from dams maintained on a normal protein diet but fed postnatally by a dam maintained on a low diet. Culled and analysed at weaning (21 days). **Group L-N**: Mice produced from dams maintained on a low protein diet but fed postnatally by a dam maintained on a normal diet. Culled and analysed at weaning (21 days). **Group N-N-N**: Control mice produced from dams fed on normal protein chow, fed postnatally by a dam maintained on a normal diet until weaning and maintained on a normal diet until 3 months of age. **Group N-L-L**: Control mice produced from dams fed on normal protein chow, fed postnatally by a dam maintained on a low diet until weaning and maintained on a low diet until 3 months of age. **Group L-N-N**: Mice produced from dams fed on low

protein chow, fed postnatally by a dam maintained on a normal diet until weaning and maintained on a normal diet until 3 months of age.

Newborn pups born from either a mother on a normal protein diet **(M(N))** or a protein-deficient diet **(M(L))** were cross-fostered to a different lactating dam maintained either on a normal or a low-protein diet, within 24 hours after birth, generating the following 3 groups: NN, NL, LN. **(Figure 2.1.1).** Pups were culled either at weaning (21 days) by cervical dislocation or were weaned onto either the deficient or the control diet until 12 weeks of age, generating 3 groups: NNN, NLL, LNN. Group N-N-N represents the control group with mice produced from dams fed on normal protein chow, lactated postnatally by a dam maintained on a normal diet until weaning and maintained on a normal diet until 12 weeks of age. Group N-L-L represents mice produced from dams fed on normal protein chow, fed postnatally by a dam maintained on a low-protein diet until weaning and maintained on a low-protein diet until 12 weeks of age. Group L-N-N represents mice produced from dams fed on low-protein chow, fed postnatally by a dam maintained on a normal diet until weaning and maintained on a normal diet until 3 months of age.

A more detailed explanation for the keys of each group is shown in **Figure 2.1.2** using "NLL" as an example key.

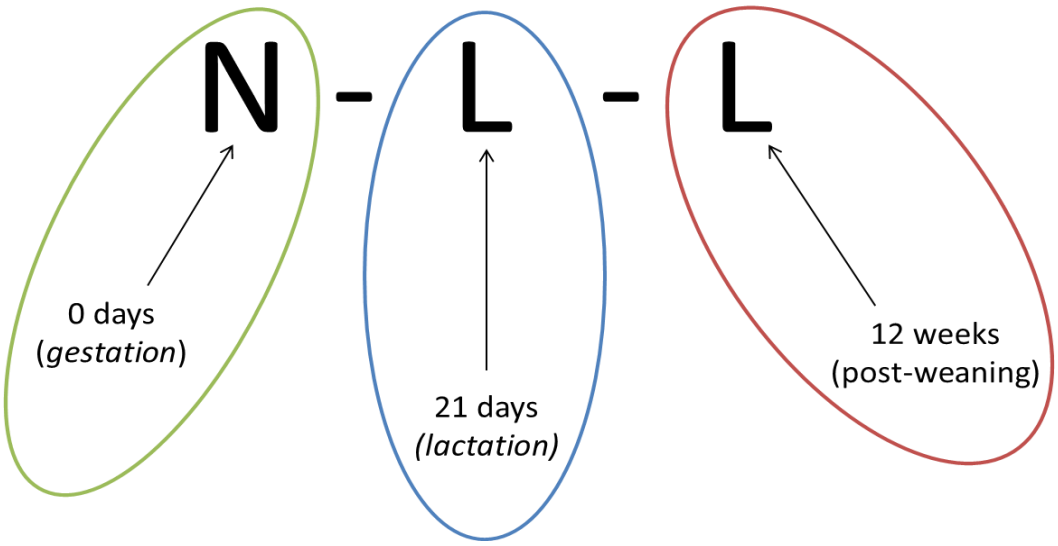

Figure 2.1.2 Schematic illustration of the key name that has been used to distinct separate mice in the different experimental groups based on their protein diet they were under at different time points and up until 12 weeks of age.

2.2 EDL muscle force measurements

At 12 weeks of age, mice were collected and anaesthetised *via* intraperitoneal (IP) injections of ketamine hydrochloride (66 mg/kg) and medatomidine hydrochloride (0.55 mg/kg).

Following successful anaesthesia of the mouse, the distal level of the tendon of the EDL muscle was exposed and secured to the lever arm of a servomotor (Aurora Scientific). The knee of the hindlimb was fixed and bipolar platinum wire electrodes were placed across the exposed peroneal nerve. Optimal length (Lo) of the EDL muscle was recorded using serial increments of 1 Hz stimulation and set at the length that generates the maximal force. To determine the Po, EDL muscle was electrically stimulated to contract at Lo with optimal stimulation voltage (8–10 V) every 2 min for 300 ms with 0.2 ms pulse width. The frequency of stimulation was then increased from 10 to 50 Hz and followed by 50 Hz increments to a maximum of 300 Hz. When the maximum force of the EDL muscle reached a plateau, despite the increase of the stimulation frequency, Po was recorded.

2.3 Tissue collection and preparation

Reagents:

- 10% neutral-buffered formalin (NBF) (Cat# HT501128; Sigma Aldrich, Dorset, UK)
- Tissue preservative solution:
    - 0.01 M phosphate buffered saline buffer solution (PBS) (Cat# P4417; Sigma Aldrich, Dorset, UK)

- 0.1% w/v NaN_3 (Cat# S2002; Sigma Aldrich, Dorset, UK)

Protocol:

Mice were sacrificed by cervical dislocation. Body weight of the mice was recorded immediately following culling and muscle from both lower hindlimbs and both sciatic nerves were isolated and their weight was recorded. Following dissection, tissues were processed accordingly. Samples were then stored at -80°C or 4°C until used. The fur of the mouse was removed from the rest of the body which was then fixed with 10% NBF for 24 h before stored in 0.1% PBS-NaN_3.

2.4 Neuromuscular junction (NMJ) staining

Reagents:

- α-bungarotoxin Alexa Fluor™ 594 Conjugate (Cat# B13423; Molecular Probes, Life Technologies Ltd, UK)
- 0.01 M phosphate buffered saline buffer solution (PBS) (Cat# P4417; Sigma Aldrich, Dorset, UK)
- 0.1% w/v NaN_3 (Cat# S2002; Sigma Aldrich, Dorset, UK)
- 0.1% v/v Triton X-100 (Cat# X100; Sigma Aldrich, Dorset, UK)
- 0.04% v/v Tween-20 (Cat# P1379; Sigma Aldrich, Dorset, UK)

Protocol:

To visualise acetylcholine receptors (AChRs) in *Thy1-YFP16* mice, EDL muscles were stained as described previously (Valdez *et al*. 2010). Fixed EDL muscles were immersed into 0.1% PBS-Triton X-100 solution for 30 min, for permeabilisation of the tissue. Muscles were then stained 1:500 Alexa 594-conjugated α-bungarotoxin (α-BTX) for 30 min in the dark at room temperature (RT). Finally, the muscles were washed once in 0.04% PBS-Tween-20 solution for 30 min in the dark at RT, before placed into 0.1% PBS-NaN_3 for long term preservation.

2.5 Visualisation and analysis of NMJs

To perform NMJ structural analysis, maximum intensity multichannel images were generated from confocal z-stacks using Nikon Ni-E Elements software (Nikon, Tokyo, Japan). Merged images from each muscle were then montaged into a single image file using ImageJ software (Image Processing and Analysis in Java; National Institutes of Health, Bethesda, MD, USA). AChR innervation (motor end plate) was defined as co-localisation of the presynaptic terminal (green) with fluorescently labelled AChRs (red). NMJ structural changes were scored and divided into 3 main groups: Normal, partially or completely denervated and morphologically abnormal NMJs. NMJs classified as normal when presenting a "pretzel"-like morphology and full colocalisation between the presynaptic terminal (nerve; green) and the AChR clusters (red). Partially denervated NMJs were defined as those with the motor end plate not completely apposed by the nerve (pre-synaptic end) terminal. Fully denervated NMJs were those with no presence of presynaptic terminal in the junction leaving all motor end plate unoccupied. Morphologically abnormal NMJs were considered those with full colocalisation but were presenting morphological characteristic outside of the "pretzel-like" shape of the NMJs. Morphologically abnormal NMJs were divided into 3 subgroups: limited branching; limited folds or "branches" of the receptor area, fragmentation; irregularly formed NMJ sites with "open" formation, discontinuous to the oval "pretzel-like" shape, small size; NMJs with considerably smaller size compared to normal neighbouring ones. Examples of such NMJs are shown in **Figure 2.5**. Criteria for structural classifications of NMJs were adjusted from Valdez *et al*. 2010.

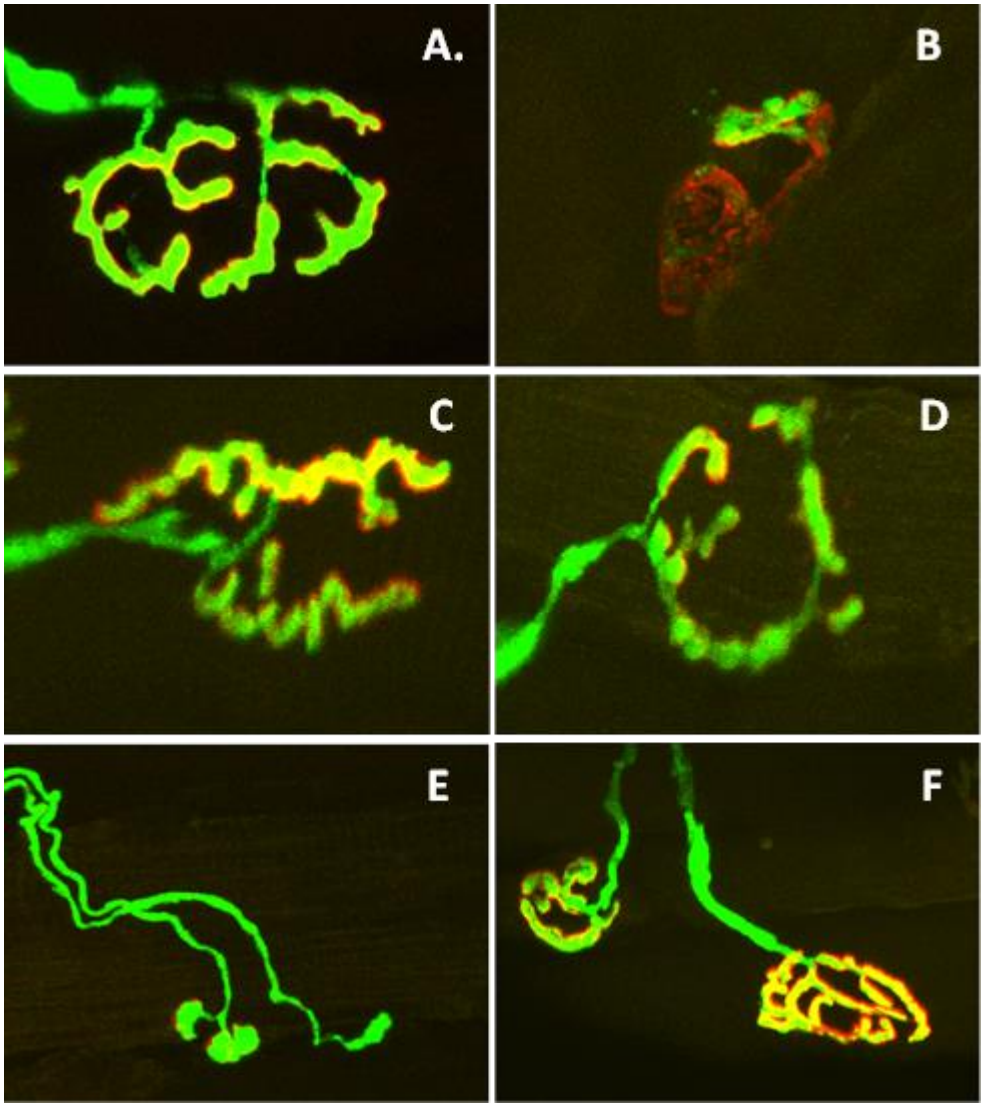

Figure 2.5 Structure of NMJs in mouse EDL muscle. **A)** Normal "pretzel-like" NMJ structure, branching and co-localisation of motor end plate (AChRs; red) and pre-synaptic end terminal (nerve; green) being evident, **B)** Partially denervated NMJ, motor end plate not apposed by a pre-synaptic end terminal in the majority of the junction, **C)** Fragmented NMJ, lack of "pretzel-like" shape, structure appears "broken" in two separate parts, **D)** Limited/defective branching, periphery of NMJ is present but branching in the centre is very limited, **E)** Limited branching/small size NMJ, pre- and post-synaptic terminals are present but structure is not fully formed, **F)** Small size of NMJ in comparison with a neighbouring normal size NMJ.

2.6 Histology and gelatine embedding

Reagents:

- Sucrose solution:
    - 0.01 M phosphate buffered saline buffer solution (PBS) (Cat# P4417; Sigma Aldrich, Dorset, UK)
    - 30% w/v sucrose (Cat# S9378; Sigma Aldrich, Dorset, UK)
- Gelatine solution:
    - 0.01 M phosphate buffered saline buffer solution (PBS) (Cat# P4417; Sigma Aldrich, Dorset, UK)
    - 7.5% (w/v) porcine-derived gelatine solution (Cat# G1890; Sigma Aldrich, Dorset, UK)
    - 15% (w/v) sucrose (Cat# S9378; Sigma Aldrich, Dorset, UK)
    - 0.1% (w/v) NaN_3 (Cat# S2002; Sigma Aldrich, Dorset, UK)
- Optimal Cutting Temperature (O.C.T.) compound (Cat# KMA-0100-00A; CellPath, Powys, UK)
- Isopentane (Cat# 15711819; Fisher Scientific, Loughborough, UK)
- Liquid Nitrogen (LN_2)

Protocol:

Gelatine embedding is a method commonly used to provide rigidity to fragile tissues and preserve their structure during preparation and cryosectioning (Gill *et al.* 2016). It is also used as a method of preservation of samples but also serves as a mold for sample positioning prior to sectioning (Fan *et al*. 2015). Sucrose incubation of fixed tissues ensures dehydration of tissues, forcing H_2O molecules out of the tissue, preventing crystal formation and cryo-damage of the tissue. Gelatine embedding provided a stable structure for whole muscle tissue to be positioned transversely on the cork before snap-freezing.

Tissues embedded in gelatin were then vertically aligned on cork disks, were covered in O.C.T mounting medium and frozen in isopentane cooled in LN_2.

Samples remained immersed in ice-cold isopentane for a minimum of 30 sec before covered with foil and stored at -80^{o}C until cryosectioning.

Prior to sectioning, tissues were placed inside the cryostat chamber for 30 min to allow acclimatisation of tissue samples to the cryostat temperature. Cryostat (Leica 1890) was set to -22^{o}C and sectioning thickness was set at 12 µm. Sections were collected on gelatine coated slides and left to air-dry overnight before stained the following day.

2.7 Gelatine-coating of glass slides for tissue sections

Reagents:

- 1 g porcine-derived gelatine (Cat# G1890; Sigma Aldrich, Dorset, UK)
- 0.19 g Chromium (III) Potassium Sulfate ($KCr(SO_4)_2$) (Cat# 1010360250; Merck, Dorset, UK)
- 0.5 g NaN_3 (Cat# S2002; Sigma Aldrich, Dorset, UK)
- dH_2O

Protocol:

Gelatine powder was dissolved in 200 mL of dH_2O at 45^{o}C on a heating magnetic stirrer. When fully dissolved, chromium (III) potassium sulfate and NaN_3 were added. Solution was stirred at 45^{o}C until all the components were homogenised in the solution. Gelatine solution was then filtered in a clean glass baker using a filter paper and poured into a histo-staining glass pot and covered to avoid dust accumulation in the solution. Microscopy slides were immersed into the solution for 3-5 sec and were positioned vertically and let to dry overnight at RT and covered to protect from dust attaching on them. Slides were stored into a slides' box until used. The remaining gelatine solution was transferred back in the bottle and stored at 4^{o}C until future use.

2.8 Transverse muscle sections staining

Reagents:

- Wheat germ agglutinin (WGA) – fluorescein (5 µg/mL) (Cat# FL-1021-5; Vector Laboratories Ltd., Peterborough, UK)
- 4',6-diamidino-2-phenylindole (DAPI) – hard set (Cat# H-1500; Vector Laboratories Ltd., Peterborough, UK)
- Ice-cold methanol (MetOH) (Cat# 34860; Sigma Aldrich, Dorset, UK)
- 0.01 M phosphate buffered saline buffer solution (PBS) (Cat# P4417; Sigma Aldrich, Dorset, UK)
- 0.04% v/v Tween-20 (Cat# P1379; Sigma Aldrich, Dorset, UK)

Protocol:

Muscle sections were retrieved from -20^{o}C and left to air-dry at RT for aprox. 10 min. Sections were fixed with ice-cold MetOH for 10 min at RT before washed 2x 5 min with PBS-Tween-20 (0.04%). Muscle sections were incubated in 300 µL of 1:1000 WGA diluted in 0.01M PBS solution for 10 min in the dark at RT. Following staining slides were washed 2x 5 min with PBS-Tween-20 (0.04%) before mounted with hard-set DAPI. The slides were left to set overnight in the dark at RT before being imaged.

2.9 Confocal microscopy

Fluorescence images were obtained using a C1 Nikon Eclipse Ti confocal laser scanning microscope (Nikon, Tokyo, Japan) equipped with a 405 nm excitation diode laser, a 488 nm excitation argon laser, and a 543 nm excitation helium–neon laser. Slides were kept in the dark at all times. Consecutive images were acquired using 20x objective and were stitched into a single high-resolution image using Adobe Photoshop CS6.

2.10 Image analysis of EDL and TA muscle sections

Image analysis of EDL and TA transverse muscle sections was performed using ImageJ software ((Image Processing and Analysis in Java; National Institutes of Health, Bethesda, MD, USA). All analyses were performed semi-automatically, using the "Tissue Cell Geometry Stats" macro created by the Institute for Research in Biomedicine, University of Barcelona (Barcelona, Spain) (http://adm.irbbarcelona.org/image-j-fiji#TOC-Automated-Multicellular-Tissue-Analysis).

Individual images acquired from different areas of the muscles were stitched together to create a montaged multichannel image of the whole muscle section using Adobe Photoshop. Images were imported into ImageJ software, split into individual channels and only the channel with the muscle fibre membrane stain (green) was used for the analysis. Image was converted to 8-bit file and "Tissue Cell Geometry Stats" plugin was selected for the analysis of the muscle fibres. Parameters were set as follows: default parameters were selected, "Light background" was deselected, "Noise tolerance" was set between 10-23, depending on the quality of each section, output type as "Segment particles" and "Preview point selection" was maintained. Following merging/segmentation of the muscle fibres and calculation of the number and size of the fibres in the image, further processing was performed to exclude any selections that were not fibres (vessels, gaps etc.). All files generated from the image analyses were saved accordingly.

2.11 *In silico* analysis of predicted gene targets of miR-128 and miR-133a

Bioinformatic analysis of the predicted target genes of miR-128 and miR-133a was performed using three databases: TargetScanMouse7.1, STRING and KEGG database.

*TargetScanMouse7.1 (*http://www.targetscan.org/mmu_71/)

In order to investigate the predicted target genes for miR-128 and miR-133a, TargetScanMouse7.1 database was used. MiR-128 and miR-133a were selected from the list of broadly conserved microRNA families and a full list of predicted target genes was obtained. For certain gene targets, the name was imported in the appropriate section of the home page. A list of all the microRNAs and their equivalent target sites (conserved and/or poorly conserved) were obtained. A number of predicted target genes of interest was selected for further analysis.

*STRING (*Version 10.5; https://string-db.org/)

The full list of predicted target genes of each microRNA as obtained from TargetScanMouse7.1 was imported into STRING database (Version 10.5), in order to investigate the interactions between the predicted target genes on a protein level. Each protein (derived from a gene transcript) was depicted as a node, which was connected to neighbouring nodes. Disconnected or individual nodes were excluded from the network analysis. Interactions between the nodes were assessed based on degree of confidence (low=0.150, medium=0.400, high=0.700, highest=0.900). Information obtained was used for illustration of the network using CytoScape software.

*KEGG (*https://www.genome.jp/kegg/)

Following network analysis on a protein level, selected predicted target genes, which demonstrated strong interactions on a protein level (degree of confidence set to "highest" (0.900)), were imported into KEGG Pathway database in order to investigate the signalling pathways they are involved in and/or share. KEGG Reference number (KO number) was imported into KEGG Mapper tool, and "Search&Color Pathway" was selected. The KO number was imported in the box followed by background (bg) colour and foreground (fg) colour. An example of such import is: "K15290 brown,yellow". When all proteins have been imported,

“uncoloured diagrams were selected in order to obtain coloured items only for the proteins of interests in the pathways. Pathways of interests were selected from the list of all the pathways were one or more of the proteins of the list are involved in. Proteins encoded from predicted target genes were coloured in cyan (miR-128) or orange (miR-133a), depending on the microRNA by which they were targeted.

2.12 RNA isolation from tissue and cell samples

Reagents:

- TRIzol reagent (Cat# 15596026; Invitrogen, Paisley, UK)
- Liquid Nitrogen (LN_2)
- Nuclease-free H_2O (Part of Cat# 218073; QIAGEN, Manchester, UK)
- Iso-amyl alcohol:chloroform 25:1 (Cat# 25666; Sigma Aldrich, Dorset, UK)
- Isopropanol (Cat# 59304; Sigma Aldrich, Dorset, UK)
- Ethanol (EtOH) (Cat# 51976; Sigma Aldrich, Dorset, UK)

Protocol:

Muscles and nerves were ground in LN_2 in pestle and mortar and transferred into 1 mL of TRIzol. Prior to RNA isolation, TRIzoL samples were allowed to stand at RT for 5 min before addition of 200 µL of chloroform. Samples were shaken vigorously for 20-30 sec and let to stand at RT for 5 min. Samples were centrifuged at 12,000 x g for 10 min at 4^{o}C and incubated for 5 min at RT. Following incubation, approximately 250 µL of aqueous phase containing the RNA were collected and transferred into a new Eppendorf tube. To achieve RNA precipitation, the aqueous phase collected was mixed with 500 µL of 100% isopropanol and mixed by manual inversion of the tubes for 10-15 sec. Samples were incubated at RT for 25-30 min and then centrifuged at 21,100 x g for 30 min at 4^{o}C. Following centrifugation, the supernatant was discarded and pellet was left to dry for 5 min before washed in 250 µL of 70% EtOH. Samples were incubated for 30 min at RT before centrifuged at 21,100 x g for 5 min at 4^{o}C.

Supernatant was discarded and samples were centrifuged again at 21,100 x g for 5 min at 4°C for the remaining EtOH residues to be collected at the bottom of the tubes and be discarded. Any excess EtOH was left to evaporate at RT for a maximum of 5 min. Finally, RNA pellet was resuspended in 10 µL RNase-free H_2O and placed immediately on ice to avoid degradation. RNA concentration and purity were estimated according to the 260/280 and 260/230 ratio recorded using Nanodrop2000 (ThermoFisher).

2.13 First strand cDNA synthesis

Reagents:

For microRNA cDNA synthesis:

- miScript HiSpec Buffer (5x) (Part of Cat# 218161; QIAGEN, Manchester, UK)
- miScript Nucleics Mix (10x) (Part of Cat# 218161; QIAGEN, Manchester, UK)
- miScript Reverse Transcriptase mix (Part of Cat# 218161; QIAGEN, Manchester, UK)
- RNase-free H_2O (Part of Cat# 218161; QIAGEN, Manchester, UK)

For mRNA cDNA synthesis:

- SuperScript™ II Reverse Transcriptase kit (Cat# 18064014; Invitrogen, Paisley, UK)
    - 200 U/mL Superscript II reverse transcriptase
    - 5x First-strand Buffer
    - 100 mM Dithiothreitol (DTT)
- 50 µM Random hexamers (Cat# N8080127; Invitrogen, Paisley, UK)
- 10 mM Deoxynucleotides (dNTP's) mix:
    - 100 mM Deoxynucleotide Set (Cat# DNTP100; Sigma Aldrich, Dorset, UK)
    - RNase-free water (Part of Cat# 218161; QIAGEN, Manchester, UK)

- 40 units/µL RiboLock RNase inhibitor (Cat# EO0381; Invitrogen, Paisley, UK)
- RNase-free water (Part of Cat# 218161; QIAGEN, Manchester, UK)

Protocol:

cDNA synthesis for microRNA and mRNA was performed using 100-200 ng RNA from tissues or cells using the T100 Thermocycler (BioRAD, Hertfordshire, UK). Each cDNA required a different RT reaction mix, using the reagents and volumes as shown in the table below:

Table 2.13 Reagents used for cDNA synthesis of microRNAs and mRNAs.

	microRNA	mRNA
miScript HiSpec Buffer (5x)	4 µL	-
miScript Nucleics Mix (10x)	2 µL	-
miScript Reverse Transcriptase Mix	1 µL	-
Random Hexamers	-	1 µL
First Strand Buffer (5x)	-	4 µL
DTT	-	2 µL
dNTP	-	1 µL
Superscript II	-	0.5 µL
RNase Inhibitor	-	1 µL
RNase-Free H_2O + RNA template	13 µL	9.5 µL
Total reaction volume	20 µL	20 µL

For microRNAs, one-step cDNA synthesis was performed using RTscript enzyme according to the diagram bellow:

Figure 2.13.1 cDNA synthesis protocol for microRNAs. Each reaction containing RNA template, RNAse-free H_2O and RT reaction mix was placed in the Thermocycler and cDNA synthesis was performed according to the steps shown.

For gene transcripts, two-step cDNA synthesis was performed using Superscript II enzyme, according to the following protocol:

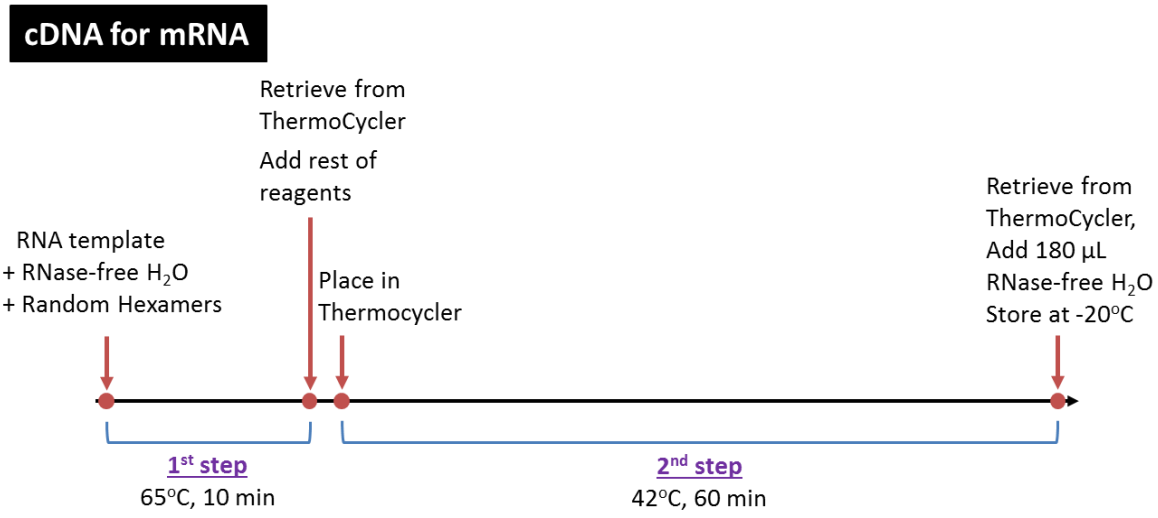

Figure 2.13.2 cDNA synthesis for gene transcripts (mRNA), in a two-step protocol. Addition of RT mix occurs between 1st and 2nd step of cDNA synthesis, before samples are placed back in the Thermocycler.

Following cDNA synthesis, all sample were diluted 1:10 with 180 µL of RNase-free H_2O and stored at -20°C until used for quantitative PCR (qPCR).

2.14 Primer design

Primers for qPCR on mRNA transcripts were designed using the NCBI primer blast tools.

For target genes from miR-128 and -133a, the following parameters were used during primer design:

Table 2.14 Parameters used for primer design.

Primer design parameters	
Organism	*Mus musculus*
Exon junction span	Span exon-exon junction
Amplicon size (bp)	50-100
Primer Tm (°C)	57-63 *(Opt.: 60)*

From the list of candidate primer pairs, those with repeated base a T as an ultimate base or with 3 or more G/C bases at 3' end were disregarded. Primer pairs with low self-complementarity, Tm difference less than 1°C were preferred and no non-specific binding to other target sequences were preferred.

2.15 Quantitative Polymerase Chain Reaction (qPCR)

Reagents:

For microRNA expression analysis:

- cDNA (microRNA, 10x diluted)

- SsoAdvanced Universal SYBRGreen Supermix (Cat# 1725271; BioRAD, Hertfordshire, UK)
- microRNA primers (QIAGEN, Manchester, UK)
- Universal primers (Part of Cat# 218073; QIAGEN, Manchester, UK)

For mRNA expression analysis:

- cDNA (mRNA, 10x diluted)
- SsoAdvanced Universal SYBRGreen Supermix (Cat# 1725271; BioRAD, Hertfordshire, UK)
- mRNA primers (Sigma Aldrich, Dorset, UK)

Protocol:

Primers, cDNA and SsoAdvanced SybrGreen Supermix were added in each well of a 96-well plate (BioRAD Hertfordshire, UK), according to the following table:

Table 2.15.1 Volumes of reagents per reaction in a qPCR run for microRNA and mRNA.

	microRNA	mRNA
Universal primers	0.7 µL	-
microRNA-specific primer	0.7 µL	-
Forward primer (10 µM)	-	1 µL
Reverse primer (10 µM)	-	1 µL
BioRAD SybrGreen Mastermix	5 µL	5 µL
cDNA template	5 µL	5 µL
Total reaction volume	11.4 µL	12 µL

Each cDNA sample was loaded 3 times to create technical replicates. Each plate contained a no-template control (NTC) triplicate, containing all the components of a reaction (**Table 2.15.1**), but lacking the cDNA template. NTCs served as a negative control to assess genomic contamination, secondary structures of primers or primer dimers. Following loading of reagents and template, plates were sealed, centrifuged for 5 sec and placed into the BioRAD CFX Connect™ Real-Time PCR Detection System (BioRAD Hertfordshire, UK). Expression relative to SNORD-61 or RNU-6 for microRNAs and 18S or β2-microglobulin for mRNA transcripts was calculated using the delta delta C_t (ddC_t) method. The qPCR conditions for each run are shown on the table below:

Table 2.15.2 qPCR conditions for microRNAs and mRNAs.

qPCR conditions		Pre-heating	Denaturation	Annealing	Extension	Cycles
microRNA	Temperature	95°C	95°C	55°C	72°C	40
	Time	3 min	30 sec	30 sec	30 sec	
mRNA	Temperature	95°C	95°C	58°C	72°C	40
	Time	3 min	30 sec	30 sec	30 sec	

All qPCR runs were assessed using a melt curve to ensure detection of a single product and assess formation of primer dimers and/or contamination. Melt curves were generated following the end of the 40th cycle of the qPCR run. Melt curve conditions for both microRNA and mRNA qPCR runs were: 95°C for 10 sec, 65-95°C, with 0.5°C increments for 5 sec each and plate read at 95°C for 50 sec.

2.16 Cell culture of muscle and nerve cells

Reagents:

For C2C12:

- Growth Media (**GM_{C2C12}**):

    - Dulbecco's Modified Eagle's Medium with high glucose (Cat# D5671; Sigma Aldrich, Dorset, UK)
    - 10% v/v foetal bovine serum (FBS) (Cat# 10100147; Sigma Aldrich, Dorset, UK)
    - 1% v/v GlutaMax (Cat# 35050061; Gibco, Paisley, UK)
    - 1% v/v penicillin–streptomycin (Cat# P4333; Sigma Aldrich, Dorset, UK)
- Differentiation Media (**DM_{C2C12}**):
    - Dulbecco's Modified Eagle's Medium with high glucose (Cat# D5671; Sigma Aldrich, Dorset, UK)
    - 2% v/v horse serum (HS) (Cat# 26050-070; Sigma Aldrich, Dorset, UK)
    - 1% v/v GlutaMax (Cat# 35050061; Gibco, Paisley, UK)
    - 1% v/v penicillin–streptomycin (Cat# P4333; Sigma Aldrich, Dorset, UK)
- Growth Media (**$GM_{NSC\text{-}34}$**):
    - 1:1 mixture of Dulbecco's Modified Eagle's Medium/Nutrient Mixture F-12 Ham with L-Glutamine (Cat# D8437; Sigma Aldrich, Dorset, UK)
    - 10% v/v foetal bovine serum (FBS) (Cat# 10100147; Sigma Aldrich, Dorset, UK)
    - 1% v/v penicillin–streptomycin (Cat# P4333; Sigma Aldrich, Dorset, UK)
- Differentiation Media (**$DM_{NSC\text{-}34}$**):
    - 1:1 mixture of Dulbecco's Modified Eagle's Medium/Nutrient Mixture F-12 Ham with L-Glutamine (Cat# D8437; Sigma Aldrich, Dorset, UK)
    - 3% v/v foetal bovine serum (FBS) (Cat# 10100147; Sigma Aldrich, Dorset, UK)
    - 1% v/v penicillin–streptomycin (Cat# P4333; Sigma Aldrich, Dorset, UK)

Protocol:

In vitro experiments were performed using C2C12 myotubes as a model of myofibres and NSC-34 cells as a model of motoneuron cells.

C2C12 cell line is a subclone cell line of skeletal muscle cells originally derived from the C2 cell line isolated from *mdx* mice (Yaffe and Saxel, 1977). NSC-34 is a hybrid cell line created by fusion of neuroblastoma mouse cells and motoneuron-enriched embryonic mouse spinal cord cells (Egget *et al.* 2000).

Prior to plating, cells were centrifuged at 1,500 rpm for 5 min to discard freezing media containing DMSO, and cell pellet was resuspended in pre-warmed 20% FBS growth media (GM_{C2C12}, GM_{NSC-34}) for 24 h to aid attachment of the cells. Following 24 h, media was replaced with 10% FBS growth media (GM_{C2C12}, GM_{NSC-34}) and was renewed every 48 h. All cells were cultured in T75 cell culture flask and differentiated in 6- and 12-well flat-bottom plates (Costar), in a humidified incubator at 37^{o}C with 5% CO_2.

Differentiation of C2C12 cells was induced when cells reached 90% confluency. Confluent cells were cultured in differentiation media (DM_{C2C12}) for 7-10 days before staining. Fusion of cells and formation of myotubes was visible from Day 2 post differentiation.

For cell differentiation, NSC-34 cells were cultured in differentiating media (DM_{NSC34}), as described by Egget *et al.* 2000. To successfully induce differentiation and allow development of axonal projections, cells were introduced to differentiation media when they reached a confluency of 60-80%.

2.17 Cell passaging

Reagents:

- Dulbecco's Phosphate Buffered Saline (DPBS) (Cat# D8537; Sigma Aldrich, Dorset, UK)
- TrypLE Express (Cat# 12604013; Gibco, Paisley, UK)

Protocol:

For cell dissociation from a T75 flask, media was discarded and cells were washed 1-2 times for 10 sec each with 3mL of DPBS followed by incubation with

2 mL TrypLE for 20 sec. TrypLE was discarded and flasks were incubated at 37°C for 3 min. Following incubation, cells were immediately collected from the flasks using growth media and the flask was washed several times to ensure collection of maximum number of cells. Cells were transferred to a sterile falcon tube and diluted accordingly before being plated into a new flask or plate.

2.18 Preparation of tissue culture plates for cell imaging

Reagents:

- Laminin, 1 mg/mL (Cat# 114956-81-9; Sigma Aldrich, Dorset, UK)
- Dulbecco's Phosphate Buffered Saline (DPBS) (Cat# D8537; Sigma Aldrich, Dorset, UK)

Protocol:

Cells to be stained and imaged were plated in 12-well plates coated with laminin according to a standard protocol (Soriano-Arroquia *et al*. 2017). Laminin working solution was prepared in 1x DPBS in 5 µg/mL concentration. In each well, 500 µL of laminin solution were added and plate was incubated in a humidified incubator at 37°C with 5% CO_2 for 30-60 min. Following incubation, laminin solution was removed from the wells carefully to avoid contact with the bottom of the well. All wells were washed with DPBS and cells were immediately seeded onto the plate, to prevent laminin from drying out.

2.19 Seeding of C2C12 and NSC-34 cells

Reagents:

- Dulbecco's Phosphate Buffered Saline (DPBS) (Cat# D8537; Sigma Aldrich, Dorset, UK)
- TrypLE Express (Cat# 12604013; Gibco, Paisley, UK)
- Growth medium (GM_{C2C12}, GM_{NSC34})
- 0.4% Trypan Blue (Cat# T8154; Sigma Aldrich, Dorset, UK)

Protocol:

Cells were dissociated from the T75 flasks using TryPLE enzyme (Section 2.17). Following incubation, TryPLE was inactivated with growth medium and cells were centrifuged at 1,500 rpm for 5 min. Following centrifugation, the supernatant was discarded and the cell pellet was resuspended in 10 mL growth medium. Immediately after resuspension, 10 µL of cell suspension was mixed 1:1 with trypan blue stain and 10 µL of the mixture were placed in a Neubaeur haemocytometer. When observed under a microscope, dead cells appear blue (stained with Trypan Blue) whilst live cells appear unstained. Live cell number was recorded from each of the 4 corner squares (**Figure 2.19**). Following counts, cells per volume unit was calculated and an appropriate amount of cell suspension was diluted in growth media ($GM_{C2C12,}$ GM_{NSC34}) before being added to flat-bottom plates (Costar). For cell imaging, cells were plated in 12-well plates pre-coated with laminin (Section 2.18). For C2C12, 1 mL of cell suspension was plated in each well of a 12-well plate to achieve confluency before inducing differentiation. For NSC-4 cells, 10,000 cells/well (2,632 cells/cm^2) were plated to achieve optimum confluency for neuronal differentiation.

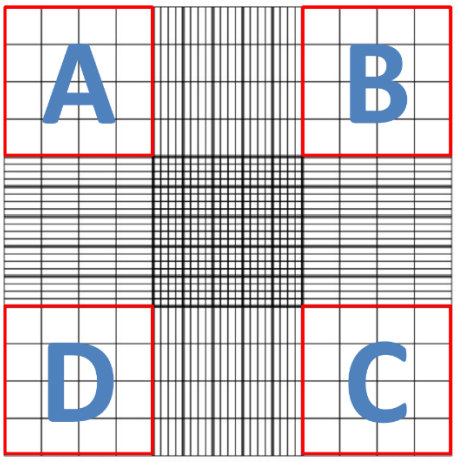

Figure 2.19 Standard gridline of an Improved Neubaeur haemocytometer. A-D squares represent the areas where cell number was recorded.

2.20 Cell harvesting for RNA and protein isolation

Reagents:

- Dulbecco's Phosphate Buffered Saline (DPBS) (Cat# D8537; Sigma Aldrich, Dorset, UK)
- TrypLE Express (Cat# 12604013; Gibco, Paisley, UK)
- TRIzol reagent (Cat# 15596026; Invitrogen, Paisley, UK)

Protocol:

Cells plated on a 6-well plate were rinsed once with pre-warmed PBS and were incubated with 300 µL of TryPLE for 3 min in a humidified incubator at 37^{o}C with 5% CO_2. TryPLE was inactivated by dilution with 600 µL of PBS and cells from each well were collected into a separate pre-chilled Eppendorf tube. The wells were washed with additional 600 µL of PBS to collect remaining cells and added to the respective tubes, which were immediately placed on ice. Following collection of all samples, cells were centrifuged at 21,100 x g for 5 min in a pre-cooled centrifuge at 4^{o}C. For RNA samples, supernatant was discarded and cell pellet was resuspended in 1mL TRIzoL reagent. Protein samples were frozen without further processing. All samples were stored at -20^{o}C until used for RNA isolation or protein extraction. For each transfection condition, 6 wells were used for either RNA or protein expression analysis, whilst each well represents a biological replicate (n number).

2.21 Cell transfections with miR-128 and miR-133a

Reagents:

For miR-128:

- Lipofectamine 2000 (Cat# 11668027 ; Invitrogen, Paisley, UK)
- 5 nmol miScript miR-128-3p mimic (Cat# MSY0000140; QIAGEN, Manchester, UK)

- 5 nmol miScript miR-128-3p inhibitor (Cat# MIN0000140; QIAGEN, Manchester, UK)
- 5 nmol miScript Inhibitor Negative Control (Cat# 1027271; QIAGEN, Manchester, UK)
- Dulbecco's Modified Eagle's Medium with high glucose (Cat# D5671; Sigma Aldrich, Dorset, UK)
- Differentiation Media (DM_{C2C12}, DM_{NSC34})

For miR-133a:

- microRNA inhibitor negative control (Scr) (100 µM; Dharmacon, Colorado, USA)
    - Sequence:
        - Antisense: 5'-Fl-mA*mC*mUmCmAmCmCmGmAmCmAmGmCmGmUmUmGmAmA*mU*mG*mU*mU-Cholesterol-3'
        - Sense: 5'mC(*)mA(*)mGmUmAmCmUmUmUmUmGmUmGmUmAmGmUmA(*)mC(*)mA(*)mA-Cholesterol-3'
- microRNA-133a mimic (miR) (100 µM; Dharmacon, Colorado, USA)
    - Sequence:
        - Antisense: 5'-UUUGGUCCCCUUCAACCAGCUG-3'FITC
        - Sense: 5'-Chol-GCUGGUAAAAUGGAACCAAAU-3'
- microRNA-133a inhibitor (AM) (100 µM; Dharmacon, Colorado, USA)
    - Sequence: 5'-Fluorescein-mC*mA*mGmCmUmGmGmUmUmGmAmAmGmGmGmAmCmC*mA*mA-mA*-3'Chol
    - - phsophorthioate bonds
    - m - 2'-O-methyl bonds

Protocol:

Transfections of miR-128 mimic and antagomir were performed using Lipofectamine 2000. 24 h following seeding, plates were retrieved from the incubator and the media was discarded. For each well of a 6-well plate 1 mL of pre-warmed DMEM media was added and for each well of a 12-well plate 500 µL of DMEM was added. DMEM media containing no additives was used to avoid

interference of additive solutions with the transfection reagents. Cells were incubated for 40-50 min with DMEM media in a humidified incubator at 37°C with 5% CO_2. In the meantime, lipofectamine working solution was prepared for each of the negative control (Scr; scrambled), miR mimic (miR) and miR inhibitor (AM; antagomiR) (**Table 2.21.1**). Lipofectamine was added to DMEM media with no FBS or Pen/Strep and left to incubate for 5 min. Following incubation, lipofectamine solution was added drop-by-drop to each working solution of Scr, miR and AM in 1:1 volume, to a final of 500 µL/well for a 12-well plate and a 1 mL/well for a 6-well plate.

Table 2.21.1 Reagents used for miR-128 mimic and antagomir transfections. Same concentrations and volumes were used for both C2C12 and NSC-34 cells.

For miR-128:		
	6-well plate (µL per well)	12-well plate (µL per well)
For Scr/miR (100 nM):	5 µL	2.5 µL
For AM (200 nM):	10 µL	5 µL
For Lipofectamine:	8 µL	4 µL

Lipofectamine 2000 was incubated with Scr/miR/AM for 30 min at RT. Next, plates were retrieved from the incubator, media was discarded and 1 mL of transfections solution was added in each well of a 6-well plate and 500 µL of the transfection solution was added in each well of a 12-well plate. For control cells, DMEM was added in the same volume as the transfection solutions. Cells were incubated with the transfection solution for 5-6 h in a humidified incubator at 37°C with 5% CO_2 before media was replaced with differentiation media (DM_{C2C12}, DM_{NSC34}). For C2C12 cells, transfection protocol was repeated on Day 3

and Day 5 post-seeding, to enhance efficiency of transfection in myotubes. NSC-34 cells were transfected 24 h following seeding of the cells.

For miR-133a, transfection protocol did not require Lipofectamine, as the Scr, miR and AM reagents were cholesterol conjugated. For cells to be transfected with miR-133a, differentiation media (DM_{C2C12}, DM_{NSC34}) was added to the wells 24 h following cell seeding for NSC-34 cells and 3 days following seeding for C2C12 (signs of myotube formation). Transfection reagents were added directly on the wells according to **Table 2.21.2:**

Table 2.21.2 Reagents used for miR-133a mimic and antagomir transfections. Same concentrations and volumes were used for both C2C12 and NSC-34 cells.

For miR-133a:		
	6-well plate (µL per well)	12-well plate (µL per well)
For Scr/miR (100 **n**M):	2 µL	1 µL
For AM (200 **n**M):	4 µL	2 µL

Cells were collected for RNA and protein isolation 48 h post transfections. For imaging, C2C12 cells were stained 7 post transfections while NSC-34 were stained 10 days following transfections.

2.22 Immunostaining of C2C12 and NSC-34 cells

Reagents:

- Dulbecco's Phosphate Buffered Saline (DPBS) (Cat# D8537; Sigma Aldrich, Dorset, UK)
- Block 1 solution:

    - 0.1% v/v Triton-X100 (Cat# X100; Sigma Aldrich, Dorset, UK)
    - 10% horse serum (HS) (Cat# 26050-070; Sigma Aldrich, Dorset, UK)
    - DPBS (Cat# D8537; Sigma Aldrich, Dorset, UK)
- Block 2 solution:
    - 0.05% v/v Triton-X100 (Cat# X100; Sigma Aldrich, Dorset, UK)
    - 10% horse serum (HS) (Cat# 26050-070; Sigma Aldrich, Dorset, UK)
    - DPBS (Cat# D8537; Sigma Aldrich, Dorset, UK)
- Methanol (MetOH) (Cat# 34860; Sigma Aldrich, Dorset, UK)
- DAPI (Cat# MBD0015; Sigma Aldrich, Dorset, UK)

For C2C12:

- Anti-MyHC 1^{ry} Ab (Cat# MF20-c 2ea; Developmental Studies Hybridoma Bank)
- Goat Anti-Mouse Alexa Fluor 488 Conjugate, 2^{ry} Ab (Cat# A-10680; Invitrogen, Paisley, UK)

For NSC-34:

- Anti Beta-III Tubulin, Alexa Fluor 488 Conjugate (Cat# AB15708A4; Millipore, Middlesex, UK)

Protocol:

Cells were retrieved from the incubator and the media was aspirated. Wells were rinsed 1-2 times with DPBS and cells were then fixed with MetOH for 10-15 min. For C2C12, cold MetOH was used for 10 min while for NSC-34 cells MetOH at RT was used for 15 min for cell fixation, to prevent cell detachment during fixation. Following fixation, 500 µL of DPBS was added to the wells containing MetOH and then the solution was discarded. Mixing of MetOH with DPBS prior to removing it from the wells prevents cells from drying out quickly. Cells were rinsed 1-2 times with PBS followed by addition of 500 µL of Block 1 solution for 1-2 h at RT. Following blocking, cells were washed once with PBS for 5 min followed by incubation with Block 2 solution containing the primary antibody (Ab) (MF-20, 1:1000, β-III Tubulin, 1:400). Cells were covered in foil and allowed

to incubate at 4^{o}C overnight. Following incubation with primary Ab, cells were retrieved from 4^{o}C and left at RT for approximately 1 h. Staining solution was removed from wells and stored at 4^{o}C until future use. Cells were washed 2-3 times for 5 min with DPBS.

For C2C12, 500 µL of anti-mouse Alexa Fluor - 488 2^{ry} Ab solution (1:1000 in Block 2) was added to each well and left to incubated in the dark at RT for 1-2 h on a rocker at low speed.

Cells were washed 1-2 times with DPBS for 5 min before 500 µL of DAPI stain (1:1000 in PBS) was added to each well and left to incubate for 15 min. DAPI staining solution was removed from wells and stored at 4^{o}C until future use and cells were washed 1 time with DPBS. Finally, 1 mL of DPBS was added to each well and plate was sealed with Parafilm to avoid evaporation. Imaging of cells took place the following day.

C2C12 cells were placed on a rocker at low speed during staining while NSC-34 cells were left on a flat surface as rocking would cause detachment of cells.

2.23 Image analysis of C2C12 and NSC-34 cells

For C2C12:

Following immunostaining, cells were imaged under the Nikon Ti Live Cell imaging microscope under x20 magnification. Images were analysed using ImageJ Software (Image Processing and Analysis in Java; National Institutes of Health, Bethesda, MD, USA). The diameter of each myotube was measured from three different points across the length of the myotube (each end and the centre of myotube). The average value of the three diameter measurements was calculated, in order to determine the diameter of each myotube. Nuclei present in each of the myotubes were counted manually and were recorded in order to determine fusion index. Threshold value expressed as a % was determined using the “threshold” function. Threshold value determined the % of “empty area”

over the “green area” on each field of view, providing an indication of how much area is occupied by MF20+ stained (green) cells (myotubes).

For NSC-34:

Immunostained NSC-34 cells were imaged using the Nikon Ti Live cell imaging microscope under x20 magnification. Z-stack images were acquired and analysed using ImageJ Software (Image Processing and Analysis in Java; National Institutes of Health, Bethesda, MD, USA). Z-stack images were segmented into single channels and the “green” channel (B-III tubulin+) was used for axonal tracing of NSC-34 cells. Images were then converted to 8-bit image files and the “simple Neurite Tracer” plugin was used from “Plugins” > “Segmentation” drop down menu. Axonal length, branching point were recorded. For NSC-34 cells to be considered as differentiated, axonal length should be equal or longer than 2x the diameter of the cell body of the neuron (Chai *et al*. 2011).

2.24 Sample preparation for protein extraction

Reagents:

- Dulbecco’s Phosphate Buffered Saline (DPBS) (Cat# D8537; Sigma Aldrich, Dorset, UK)
- 1% SDS (Cat# L3771; Sigma Aldrich, Dorset, UK)
- Protease inhibitors (Cat# A32955; ThermoFisher, Paisley, UK)

Protocol:

Cell pellets were obtained from -20^{o}C and left to thaw on ice. Cell pellets were centrifuged at 21,100 x g for 5 min in a pre-cooled centrifuge at 4^{o}C and the supernatant was discarded. Cell pellet was resuspended in 50 µL of 1% SDS containing protease inhibitors Cells were sonicated on ice for 3x 5 sec and centrifuged briefly before used for bicinchoninic acid assay (BCA).

2.25 Determination of protein concentration by bicinchoninic acid assay (BCA)

Reagents:

- Bicinchoninic acid (BCA) solution (Part of Cat# BCA1; Sigma Aldrich, Dorset, UK, Dorset UK)
- Copper sulphate (Part of Cat# BCA1;Sigma Aldrich, Dorset, UK, Dorset UK)
- 1 mg/ml protein standard solution (Cat# P0834; Sigma Aldrich, Dorset, UK)
- dH_2O

Protocol:

BCA assay was performed on a 96-well plate. In order to determine protein concentration of the cell samples, a standard curve of known protein concentration samples was generated. Sample concentrations used for the standard curve are shown in **Table 2.25**:

Table 2.25 Concentration of standard curve samples used for protein determination in BCA assay.

BCA Standard sample concentrations (µg/mL)							
500	250	200	150	100	50	25	Blank

Each standard was added in a duplicate in a volume of 20 µL per well. The average value was calculated from the values of the duplicate and was used to plot the standard curve. Protein samples from cells were added on the plate in triplicates, in 1:19 dilution, to a final volume of 20 µL per well. Copper sulphate solution was diluted 50x with BCA solution and a volume of 200 µL from this mixture was added in each well. The plate was incubated at 37^{o}C for 30 min followed by the measurement of the absorbance at 570 nm using a spectrophotometer (BMG laboratories, Buckinghamshire, UK). Protein

concentration for each sample was calculated based on the standard curve values.

2.26 Estimation of the protein content of samples using SDS-PAGE and western blotting techniques

2.26.1 Polyacrylamide gel preparation

Reagents:

- 30% acrylamide solution (Cat# EC-890; Protogel, National Diagnostics, USA)
- ProtoGel Resolving Buffer (4X) (Cat# EC-892; Protogel, National Diagnostics, USA)
- ProtoGel Stacking Buffer solution (Cat# EC-893; Protogel, National Diagnostics, USA)
- 10% ammonium persulphate solution (APS) (Cat# A3678; Sigma Aldrich, Dorset, UK, Dorset UK)
- NNN'N-tetramethylethylene-diamine (TEMED) (Cat# T9281; Sigma Aldrich, Dorset, UK)
- dH_2O
- Ethanol (EtOH) (Cat# 51976; Sigma Aldrich, Dorset, UK)

Protocol:

The polyacrylamide gel was prepared in two stages. First, 12% of acrylamide concentration gel (resolving) was prepared as described in **Table 2.26.1** and poured between 2 gel plates (8 x 10 cm) with 1.5mm spacers at a volume of 8 mL. Approximately 300 µL of EtOH was added at the top of the gel to disrupt any bubbles formed and create an even top surface on the gel. When the resolving gel was set, EtOH was discarded and the top of the gel was washed 3 times with dH_2O to discard any EtOH residues. Excess H_2O was removed using blot papers. Stacking gel at 4% acrylamide concentration was prepared according to instructions in **Table 2.26.1**. Stacking gel was added until the top edge of the

glass plates and 1.5 mm-thick 12-well comb was secured at the top of the plates, to allow sample loading. Gels were stored at 4°C overnight until used the following day.

Table 2.26.1 Volumes of reagents for resolving and stacking gel preparation.

	12% resolving	4% stacking
Resolving	5 mL	-
Stacking	-	2.5 mL
dH_2O	6.8 mL	6.1 mL
Protogel	8 mL	1.3 mL
APS	200 µL	100 µL
TEMED	20 µL	25 µL
Total volume	**~ 20 mL**	**~ 10 mL**
Volume/Gel	**8 mL**	**4 mL**

2.26.2 SDS-PAGE for protein samples

Reagents:

- Pre-stained protein marker (8-260 kDA) (Cat# 928-60000; Chameleon Duo, LI-COR Biosciences, Ltd., UK)
- Protein Loading Buffer Blue (5x) (Cat# EC-886; National Diagnostics, USA)
- Running buffer (1x):
    - 10x Tris/Glycine/ SDS (w/v) solution (Cat# EC-870; National Diagnostics, Hull, UK)
    - dH_2O

Protocol:

Protein samples were retrieved from -20°C and thawed on ice. Samples were diluted with dH_20 to yield a 20 µg protein sample. Following dilution, 2 µL of 5x protein loading buffer was added to each sample to a final volume of 10 µL.

Samples were heated to 95°C for 10 min and centrifuged at 21,000 x g briefly and kept on ice until loaded on the gel.

Polyacrylamide gels were loaded into a tank and filled with running buffer diluted 1:10 with dH_2O, to produce a 1x running buffer solution. The comps were removed from the gels and 3 µL of protein ladder was loaded followed by 10 µL of protein samples in each neighbouring well. The lid was placed over the tank with the electrodes connected to a gel electrophoresis power supply, and the power was set to 20 mA per gel. Gels were allowed to run until the lowest ladder (8 kDa) reached the bottom of the gel.

2.26.3 Western blotting

Reagents:

- Anode 1 buffer, pH 10.4:
    - 0.3 M Tris (Sigma Aldrich, Dorset, UK)
    - 20% MetOH (Cat# 34860; Sigma Aldrich, Dorset, UK)
- Anode 2 buffer, pH 10.4:
    - 25 mM Tris (Sigma Aldrich, Dorset, UK)
    - 20% MetOH (Cat# 34860; Sigma Aldrich, Dorset, UK)
- Cathode buffer, pH 7.6:
    - 40 mM 6-amino n hexanoic acid (Sigma Aldrich, Dorset, UK)
    - 20% MetOH (Cat# 34860; Sigma Aldrich, Dorset, UK)
- Ponceau S stain (Sigma Aldrich, Dorset, UK)

Protocol:

Proteins were transferred from the acrylamide gel to a nitrocellulose membrane (Cat# 10600002; GE Healthcare Life Sciences, Buckinghamshire, UK) using a semi-dry trans-blot system (Trans-Blot SD Semi-Dry Transfer Cell; BioRAD, Hertfordshire, UK). The acrylamide gel was removed from the glass plates, the stacking gel was discarded and the resolving gel was placed on the nitrocellulose membrane soaked in Anode II buffer, and sandwiched as shown in **Figure 2.26.3**.

The current was set to 100 mA per gel for 1 h to achieve good protein transfer. Following transfer, nitrocellulose membrane was stained with Ponceau S stain to confirm equal loading and transfer of all proteins.

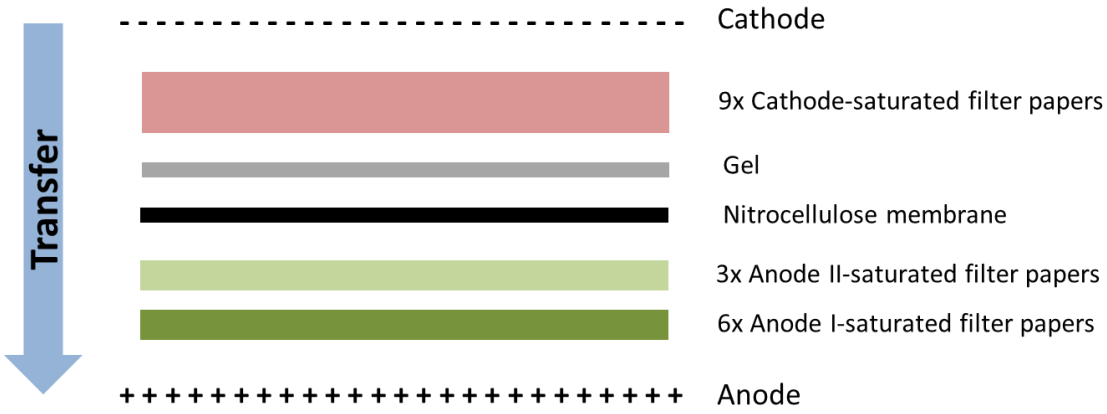

Figure 2.26.3 Schematic showing the semi-dry transfer set-up system for transfer of proteins from the SDS-PAGE gel to the membrane.

2.26.4 Processing of nitrocellulose membrane and protein detection

Reagents:

- 0.005% v/v PBS-Tween-20 (PBS-T) solution
- Blocking solution:
    - 5% milk powder
    - 0.005% PBS-T
- Primary antibody (1^{ry} Ab) solution:
    - 1% milk powder
    - 0.005% PBS-T
- Secondary antibody (2^{ry} Ab) solution:
    - 3% milk powder
    - 0.005% PBS-T
- Antibodies (**Table 2.26.4**)

Protocol:

Following confirmation of protein transfer and amount by Ponceau S, the nitrocellulose membrane was washed with ddH_2O followed by PBS, until Ponceau S was removed from the membrane. The nitrocellulose membrane was then blocked with 10 mL of blocking solution for 1 h at RT. Following blocking, the membrane was washed 3x 5 min with PBS-T before incubated with the appropriate 1^{ry} Ab solution overnight at 4^{o}C. Following overnight incubation, the membrane was left to equilibrate at RT for approximately 15 min and then washed 3x 5 min with PBS-T before incubated with the appropriate 2^{ry} Ab solution for 1 h at RT. The membrane was then washed 3x 5 min with PBS-T and imaged using a LI-COR Odyssey CLx imaging system (LI-COR, Cambridge, UK).

Table 2.26.4 List of antibodies (1^{ries} and 2^{ries}) used for detection of proteins on nitrocellulose membranes.

	Catalogue #	Host	Dilution
LC-3	ab92890	Rb	1:1000
Sirt-1	ab32441	M	1:1000
COX-IV	3E11	M	1:500
NRF-1	ab175932	Rb	1:500
Tomm-20	ab186734	Rb	1:1000
IRDye 800CW	925-32210	Goat (anti-M)	1:1000
IRDye 680RD	925-68071	Goat (anti-Rb)	1:1000

2.26.5 Data analysis of Western blot experiments

Following imaging of the membrane, the intensity of the bands was recorded using ImageJ software (Image Processing and Analysis in Java; National Institutes

of Health, Bethesda, MD, USA). The intensity of the bands was normalised to the intensity of the Ponceau S bands from the entire sample, which has been described as a more reliable method for accurate protein quantification (Aldridge *et al.* 2008; Eaton *et al.* 2013; Li and Shen, 2013; Taylor and Posch, 2014).

2.27 Proliferation assay

Reagents:

- Cell Counting Kit – 8 (CCK-8) solution (Cat# 96992; Sigma Aldrich, Dorset, UK)
- Growth Media (GM_{C2C12}) (Section 2.16)
- Growth Media (GM_{NSC34}) (Section 2.16)
- Transfection reagents (Section 2.21)

Protocol:

C2C12 and NSC-34 cells were plated as previously described into a 96-well plate in 1,000 cells/well (3,125 cells/cm^2) confluency. Cells were incubated in growth media (GM_{C2C12}, GM_{NSC34}) at 37^oC and 5% CO_2 for 24 h to allow proper attachment. The plates were then retrieved from the incubator and transfected with miR-128 (Scr, mimic, AM) or miR-133a (Scr, mimic, AM), according to the protocol in **Section 2.21**. After 6 h of transfection, media was replaced to 3% FBS in both C2C12 and NSC-34 cells to ensure survival and prevent over-proliferation until the assay was performed. The plates were then retrieved from the incubator 48h following transfections and a known number of viable C2C12 or NSC-34 cells were plated (**Table 2.27**) for preparation of a standard curve. Plates were incubated for 4-6 h to allow attachment of newly plated cells. Following incubation, the plates were retrieved from the incubator and 10 µL of CCK-8 reagent were added in each well. The plates were left to incubate for 3 h in the dark at 37^oC and 5% CO_2. Following incubation, the plates were retrieved from the incubator and the absorbance was measured at 450 nm using a microplate

reader. The number of cells following transfections with miR-128 and miR-133a was calculated using the standard curve.

Table 2.27 Known number of viable cells plated in each plate for the generation of a standard curve.

Number of viable cells for st. curve (cells/well)							
32,000	16,000	8,000	4,000	2,000	1,000	500	Blank

2.28 Cytotoxicity assay

Reagents:

- CytoTox 96® Non-Radioactive Cytotoxicity Assay kit (Cat# G1780; Promega, Southampton, UK)
- Passive Lysis 5x Buffer (Cat# E1941; Promega, Southampton, UK)
- 1 M acetic acid (Cat# A6283; Sigma Aldrich, Dorset, UK)
- 100 µM H_2O_2 (Cat# H1009-100mL; Sigma Aldrich, Dorset, UK)
- Growth Media (GM_{C2C12}) (Section 2.16)
- Growth Media (GM_{NSC34}) (Section 2.16)
- Transfection reagents (Section 2.21)

Protocol:

NSC-34 and C2C12 cells were plated as previously described into a 96-well plate at a 2,000 cells/well (6,250 cells/cm^2) confluency and incubated in growth media (GM_{C2C12}, GM_{NSC34}) at 37^oC and 5% CO_2 for 24 h to ensure good attachment. Both C2C12 and NSC-34 cells were then retrieved from the incubator and transfected with miR-128 (Scr, mimic, AM) or miR-133a (Scr, mimic, AM) as previously described (**Section 2.21**). Additionally, 12 wells with cells (C2C12 or NSC-34) in each plate were used for transfections with lipofectamine-conjugated Scr (6 wells) and cholesterol-conjugated Scr (6 wells). These wells were incubated with 100 µM H_2O_2 in 3% FBS media (100 µL/well of

GM_{C2C12} or GM_{NSC34}) following 6 h of transfections, to serve as a positive control for maximum cell cytotoxicity. The rest of the wells were incubated only in 3% FBS media (100 µL/well of GM_{C2C12} or GM_{NSC34}) following 6 h of transfections. Plates were then placed in an incubator for 48 h at 37^{o}C and 5% CO_2. Following incubation, plates were retrieved from the incubator and 50 µL aliquots from all wells were transferred to a new 96-well plate, according to manufacturer's instructions. Each well was then supplemented with 50 µL of CytoTox 96® Reagent and plates were then incubated for 30 min at RT in the dark. Following incubation, 50 µL of 1 M acetic acid was added in each well to stop the reaction and the absorbance was recorded at 490 nm using a microplate reader.

For Maximum lactate dehydrogenase (LDH) Release Control, 6 wells were used per plate for both C2C12 and NSC-34 cells and 20 µL of Passive Lysis 5x Buffer were added to these wells 45 min before transfer of aliquots on to fresh plates.

2.29 Mitotoxicity assay

Reagents:

- Mitochondrial ToxGlo™ Assay (Cat# G8000; Promega, Southampton, UK)
- 20 µM Carbonyl cyanide 3-chlorophenylhydrazone (CCCP) (Cat# C2759; Sigma Aldrich, Dorset, UK):
    - Diluted in 100 mM DMSO to produce a 20 mM stock solution
- Dimethyl sulfoxide (DMSO) (Cat# D4540; Sigma Aldrich, Dorset, UK)
- Growth Media (*GM_{C2C12}) (Section 2.16):
    - DMEM (Cat# D5671) replaced by DMEM/low glucose media (Cat# 31885049; Gibco™, ThermoFisher, Paisley, UK)
- Growth Media (*GM_{NSC34}) (Section 2.16):
    - DMEM (Cat# D5671) replaced by DMEM/low glucose media (Cat# 31885049; Gibco™, ThermoFisher, Paisley, UK)
- Transfection reagents for miR-128 (Section 2.21)

Protocol:

C2C12 and NSC-34 cells were plated as previously described into a 96-well plate (opaque walls/clear flat bottom) at a confluency of 2,000 cells/well (6,250 cells/cm^2) and 3,000 cells/well (9,375 cells/cm^2) respectively. Cells were incubated in growth media (GM_{C2C12}, GM_{NSC34}) at 37°C and 5% CO_2 for 24 h to ensure good attachment. Both C2C12 and NSC-34 cells were then retrieved from the incubator and transfected with miR-128 (12 wells for each: Scr, mimic, AM) as previously described (**Section 2.21**). Extra wells were left untreated in both plates, in order to use as positive and negative control. Following 6 h of transfections, media was replaced to 3% FBS growth media (*GM_{C2C12}, *GM_{NSC34}) and left to incubate for 48 h according to the protocol. From each transfection group (Scr, miR, AM), 6 wells were treated with CCCP in order to induce mitophagy. Control wells were also treated with DMSO, to use as vehicle control for CCCP. Both plates were then retrieved from the incubator following transfections and 20 µL of 5x Cytotoxicity reagent was added to each well. Both plates were allowed to incubate at 37°C for 30 min in the dark before fluorescence was measured using a fluorescence plate reader equipped with a rhodamine 110 filter set. Plates were left to equilibrate for 10 min at RT before the addition of 100 µL of ATP Detection Reagent in each well. Luminescence was then recorded using a microplate luminometer (Promega). Cytotoxicity and mitotoxicity were expressed as fold-change of each well divided by the average absorbance value of the Scr wells.

2.30 Statistical Analysis

All statistical analysis was performed with Graphpad 5 software (San Diego, USA). One-way ANOVA followed by a Dunnett's post-hoc analysis was performed for comparison of groups with the control group (NNN for *in vivo* experiments and Scr-transfected cells for *in vitro* experiments). Chi-squared (χ^2) test was performed for detection of significant changes in data distributions. Data were

represented as mean ± SEM. N number represents animals for *in vivo* studies and wells for *in vitro* studies.

Chapter 3

Effect of low-protein diet pre- and postnatally on the neuromuscular system of 12-week old mice

3.1 Introduction

Age-related sarcopenia is characterised by loss of skeletal muscle mass and function (Faulkner *et al.* 2007). Loss of muscle mass and function is linked to loss of skeletal muscle fibres and motor neurons, with an additional weakening of the remaining muscle fibres (Marzetti *et al.* 2009). These physiological changes during ageing have been associated with influences that occur early in life. Longitudinal studies provide a link between individual birth weight and muscle function later in life, providing evidence that early development may affect muscle mass and function during ageing (Sayer *et al.* 2006).

Maternal nutrition has been strongly associated with pre- and postnatal growth in both rodents and humans. Specifically, suboptimal nutrition during gestation has been linked to reduction in body weight and impaired muscle growth in mice (Beermann, 1983; Rehfeldt *et al.* 2011). Lower birth weight of the offspring has been linked to maternal undernutrition in humans (Victora *et al.* 2008). Maternal low-protein nutrition during gestation and lactation can cause long-term metabolic changes in the skeletal muscle of the offspring (da Silva Aragão *et al.* 2014). Skeletal muscle wasting, reduction in EDL muscle forces and change in muscle fibre type proportion in EDL and SOL muscles has been demonstrated in rats born from dams on a protein-deficient diet (Toscano *et al.* 2008).

Preliminary studies from our laboratory indicate that mice born from dams maintained on a normal protein diet but fed postnatally by a foster dam maintained on a low-protein diet (NL) demonstrated significant reduction in body size, body weight, muscle weight and length and muscle fibre size at 21 days of age days of age when compared with pups from dams maintained on a normal protein diet throughout the *in utero* and postnatal periods (NN) (**Figure 3.1 A-F**). Moreover, mice born from dams maintained on a low-protein diet but fed postnatally by a dam maintained on a normal diet (LN) demonstrated significant reduction only in the EDL muscle length, compared to the control group (NN) (**Figure 3.1 E**).

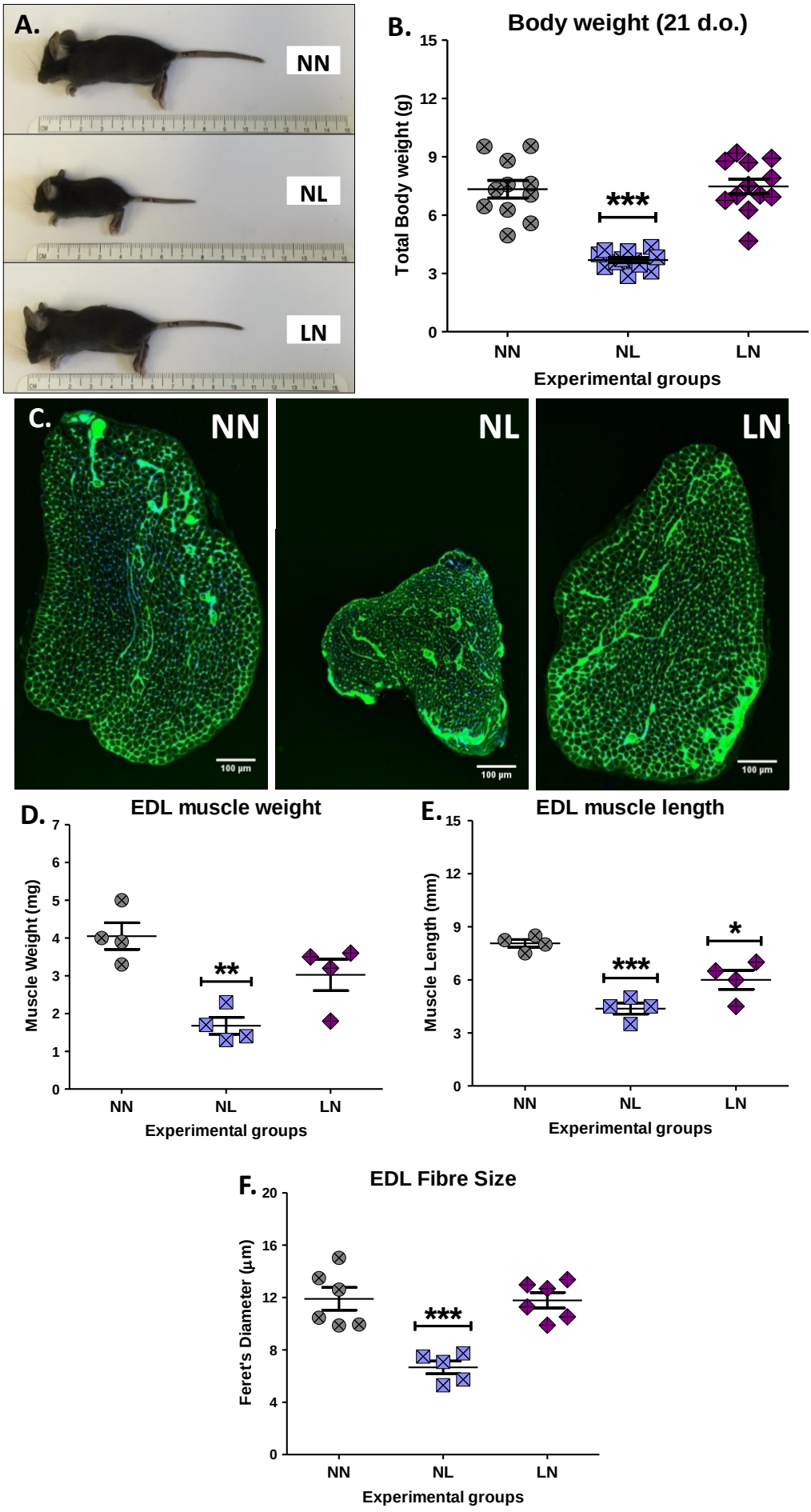
A.
NN
NL
LN
B.
Body weight (21 d.o.)
Total Body weight (g)
15
12
9
6
3
0
***
NN
NL
LN
Experimental groups
C.
NN
NL
LN
100 µm
100 µm
100 µm
D.
EDL muscle weight
Muscle Weight (mg)
7
6
5
4
3
2
1
0
**
NN
NL
LN
Experimental groups
E.
EDL muscle length
Muscle Length (mm)
15
12
9
6
3
0
***
*
NN
NL
LN
Experimental groups
F.
EDL Fibre Size
Feret's Diameter (µm)
20
16
12
8
4
0
***
NN
NL
LN
Experimental groups

Figure 3.1 The effects of reduced protein intake *in utero* or postnatally on **A)** body size and **B)** total body weight (g) of 21-day old mice. *represents significant differences compared with NNN (control) group, ****P ≤0.001* (*mean ± SEM; n*=11-12*, One-Way ANOVA with Dunnett's post-hoc analysis*). **C)** Transverse section of EDL muscle from 21-day old mice (NN, NL, LN) stained with WGA (green) and DAPI (blue) and visualised under a confocal microscope, Scale bar: *100 µm*, Magnification: *x20*, Section thickness: *12 µm,* **D)** EDL muscle weight (mg), **E)** EDL muscle length (mm), **F)** EDL fibre size (expressed as Ferret's diameter) of 21-day old mice (NN, NL, LN). *represents significant differences compared with NNN (control) group **P ≤0.05, **P ≤0.01, ***P ≤0.001* (*mean ± SEM; n*=4-6*, One-Way ANOVA with Dunnett's post-hoc analysis*). Keys for NN, NL and LN explained in detail in Chapter 2, Section 2.1.

The aim of this study was to examine whether these changes associated with low protein intake during gestation or lactation persist during early adulthood and whether these changes affect muscle mass, function and/or motor neuron dysregulation, as well as molecular changes in skeletal muscle.

3.2 Methods

3.2.1 Mice preparation

Groups of mice were weaned at 21 days old onto either the deficient diet or the 20% protein control diet to produce the three following groups: NNN; NLL; LNN (Chapter 2, Section 1). Mice were maintained until 12 weeks of age. Prior to culling, EDL force measurements were conducted as described in Chapter 2, Section 2.2, in order to determine the maximum force generated by the EDL muscle in these mice.

3.2.2 Isolation and preparation of EDL muscles from 12-week old mice for histological analyses and NMJ imaging

EDL muscles from the left limb of 12-week old mice were dissected following culling and processed as described in Chapter 2, Section 2.3. The EDL muscle from the right limb of those mice was dissected, mounted on a silgard-coated dish using surgical pins and fixed with 10% NBF for 1 h at RT (Chapter 2, section 2.3). Following, fixation, EDL muscles were rinsed twice with PBS and stored in 0.1% PBS-NaN_3 until used for staining and imaging of neuromuscular junctions (NMJs) (described in Chapter 2, Sections 2.4, 2.5). For determination of muscle fibre size, EDL muscles were sectioned using a cryotome (Leica 1890) at 12 µm thickness. EDL sections were mounted on Superfrost Plus slides (Thermofisher) and sections allowed to air-dry for a minimum of 1 h at RT prior to staining. EDL muscle sections were stained with WGA and DAPI, according to protocol described in Chapter 2, Section 2.8. Image acquisition was performed using a Nikon Ti Confocal Microscope (Chapter 2, Sections 2.9) and image analysis was performed as described in Chapter 2, Section 2.10. For NMJ visualisation and scoring, pre-fixed EDL muscles were stained with Alexa Fluor-594 α-bungarotoxin, according to protocol described in Chapter 2, Section 2.4. Image acquisition was performed using a Nikon Eclipse Ni-E Intravital confocal microscope (Nikon, Tokyo, Japan) and images were processed and scored as described in Chapter, Section 2.5.

3.2.3 First Strand cDNA synthesis and real-time qPCR analysis of marker genes in TA muscle of 12-week old mice

TA muscles from the right limb of 12-week old mice were dissected following 24 h whole-body fixation and were grounded in a mortar using LN_2. When fully grounded, TA muscles were immersed in TRIzol and were prepared for RNA isolation using phenol-chloroform method, as described in Chapter 2, Section 2.12. RNA concentration and purity were recorded using NanoDrop2000 (Thermofisher Scientific). First Strand cDNA synthesis was performed using

SuperScript™ IV VILO™ Master Mix (Cat# 11756050, Invitrogen, Paisley, UK) according to manufacturers' protocol. In each cDNA reaction, 100 ng of RNA was used (5 ng/µL). cDNA reaction volume was diluted 1:10 to a final volume of 200 µL and stored at -20^{o}C until used for qPCR. Real-time qPCR was performed according to the protocol in Chapter 2 Section 2.15. Gene expression analysis was performed according to the delta-delta Ct method (ddCt), using 18S as the housekeeping gene. Primer sequences are shown in **Table 3.2.3** below:

Table 3.2.3 Primer sequences of the gene transcripts.

Gene name	Primer sequences (5' – 3')	
	Forward	Reverse
Atrogin-1	GCAGAGAGTCGGCAAGTC	CAGGTCGGTGATCGTGAG
FoxO-3	AGTGGATGGTGCGCTGTGT	CTGTGCAGGGACAGGTTGT
MuSK	GCCTTCAGCGGGACTGAG	GAGGCGTGGTGACAGG
MyHC I	TTGTGCCGTAGGAATGTGGG	CCTTTCTCGGAGCCACCTTG
MyHC IIa	CTCCAAGGACCCTCTTATTTCCC	ACTGCTGAACTCACAGACCC
MyHC IIb	GAGGCAATCAGGAACCTTCGG	TGTGTGTCCTTCAGCATTCCC
MyHC IId/x	AAGTTTGGACCCACGGTCG	CAGTGAGAGAGCCTGCCTTTA
18S	CGGCTACCACATCCAAGGAAGG	CCCGCTCCCAAGATCCAACTAC

3.2.4 Statistical Analysis

Statistical analysis was performed using Graphpad 5 (Graphpad Software, San Diego, USA). Statistical comparisons from physiological and histological analyses were performed using One-way ANOVA with Dunnett's post-hoc analysis, using NNN as the control group. Data were represented as mean ± SEM. N number represents animals used in each group.

3.3 Results

3.3.1 The effect of pre- or postnatal protein-deficient diet on body and muscle weight of 12-week old mice

Total body and muscle weights of 12-week old mice subjected to a protein-deficient diet (5% protein) either pre- or postnatally is shown in **Figure 3.3.1.1**. Body weight of mice on a protein-deficient diet postnatally (NLL) was significantly lower compared with mice on a normal diet (NNN) (**Figure 3.3.1.1 A**). Muscle weight of EDL and TA muscle showed no significant changes between the three experimental groups **(Figure 3.3.1.1 B, C),** although the weight of SOL, GTN and Quad muscles was significantly reduced in NLL mice **(Figure 3.3.1.1 D-F)**. No visible difference in the body size was observed upon collection of the animals.

Ratio of skeletal muscle weight in relation to total body weight of NNN, NLL and LNN mice is shown in **Figure 3.3.1.2**. The ratio of EDL, TA, SOL, GTN and Quad muscle weight to total body weight showed no significant changes between the three groups, despite changes of individual muscle weight observed previously.

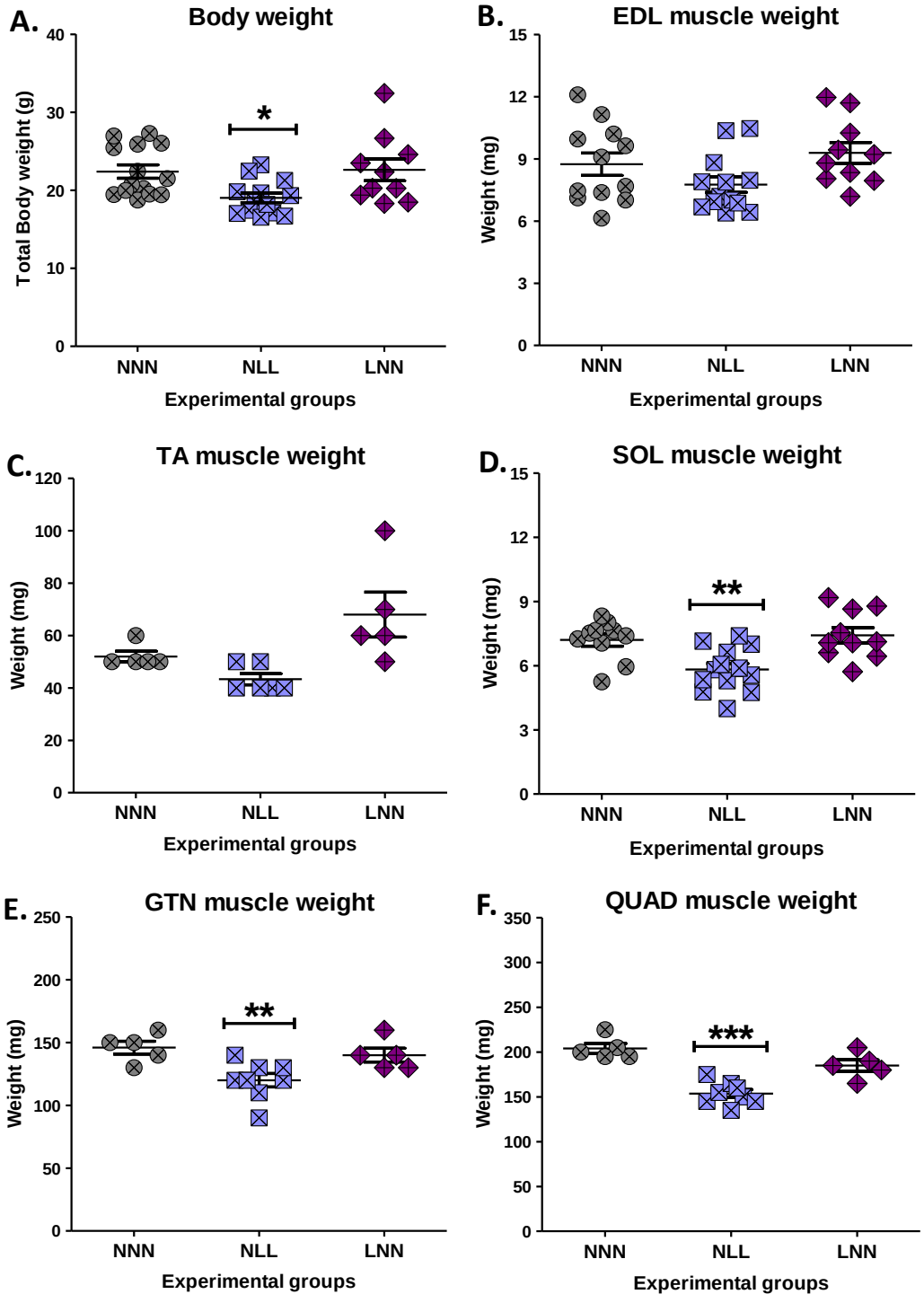

Figure 3.3.1.1 Total body and muscle weight of 12-week old mice. **(A)** Total body weight (g) and **(B-F)** muscle weight of EDL **(B)**, TA **(C)**, SOL **(D)**, GTN **(E)** and Quadriceps **(F)** muscles (mg) isolated from 12-week old mice subjected to a protein-deficient diet (5% protein) pre- or postnatally. *represents significant

differences compared with NNN (control) group, **P ≤0.05, **P ≤0.01, ***P ≤0.001* (*mean ± SEM; n*=5-14*; One-Way ANOVA with Dunnett's post-hoc analysis*).

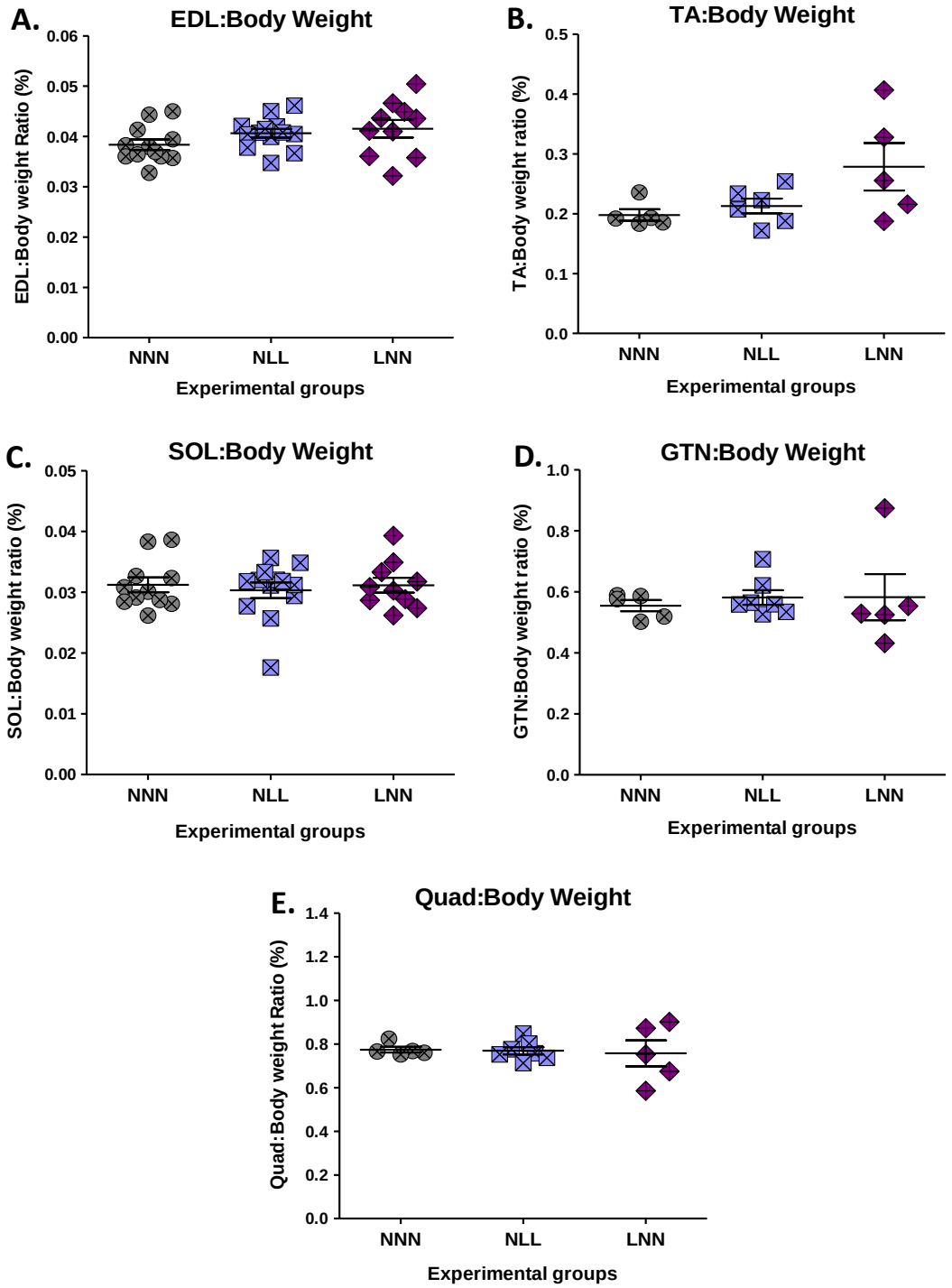

Figure 3.1.1.2 Muscle-to-body weight ratio of 12-week old mice. Ratios body to **A)** EDL, **B)** TA, **C)** SOL, **D)** GTN and **E)** Quad muscles from 12-week old mice

subjected to a protein-deficient diet (5% protein) pre- or postnatally, expressed as a %. NNN was used as the control group for statistical comparisons (*mean ± SEM; n*=5-14*; One-Way ANOVA with Dunnett's post-hoc analysis*).

3.3.2 The impact of protein-deficient diet during pre- or postnatal stages of development on skeletal muscle force generation in 12-week old mice

Maximum force of EDL muscle, correlation between muscle force *versus* EDL muscle weight and body weight of 12-week old mice are shown in **Figure 3.3.2.** Maximum force of EDL muscle was significantly lower only in the NLL group, compared to the control (NNN), but the specific muscle force showed not differences between the groups (**Figure 3.3.2 A, B**). Correlation analysis for maximum force *versus* total body weight indicated a week correlation between the two, with Pearson's coefficient (R) <0.5 **(Figure 3.3.2 B).** However, correlation analysis for maximum force and EDL muscle weight showed a significant but moderate correlation, with Pearson's coefficient (R) just above 0.5 **(Figure 3.3.2 C). (Figure 3.3.2 C).**

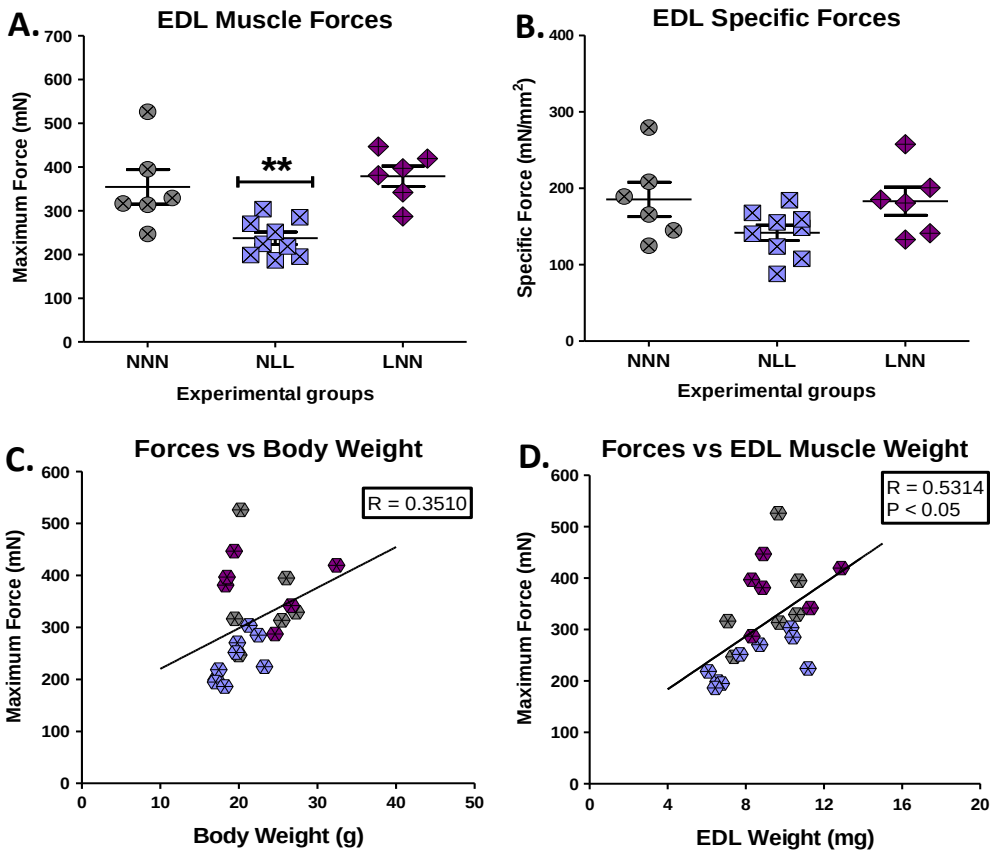

Figure 3.3.2 EDL muscle forces in 12-week old mice. **A)** Maximum force of EDL muscle (mN) of 12-week old mice and **B)** Specific tetanic force of EDL muscle (Specific Force (mN/mm^2)) of 12-week old mice, *represents significant differences compared with NNN (control) group, ***P ≤0.01* (*mean ± SEM; n*=5-14*; One-Way ANOVA with Dunnett's post-hoc analysis*). **C)** Correlation of maximum muscle force (mN) *versus* total body weight (g) and **D)** Correlation of maximum force (mN) *versus* EDL muscle weight (mg) of 12-week old mice, R ≥ 0.25 indicates a week correlation between the two variables, R ≥ 0.50 indicates a moderate correlation between the two variables (*n*=21*; Pearson's correlation analysis*).

3.3.3 Histological examination of the EDL muscle in 12-week old mice following a 5% protein diet pre- or postnatally

Histological analyses of EDL muscle are shown in **Figure 3.3.3.1.** EDL fibre size showed no significant differences between the three groups (**Figure 3.3.3.1 C**). EDL fibre number was significantly lower in both NLL and LNN mice compared to the control group (**Figure 3.3.3.1 B**). Distribution curves for EDL fibre size for all three groups were plotted, in order to assess whether fibre sizes follow similar distribution patterns across all experimental groups. Distribution of the EDL fibre sizes was similar between the three groups, with no significant shift been recorded (**Figure 3.3.3.2**)

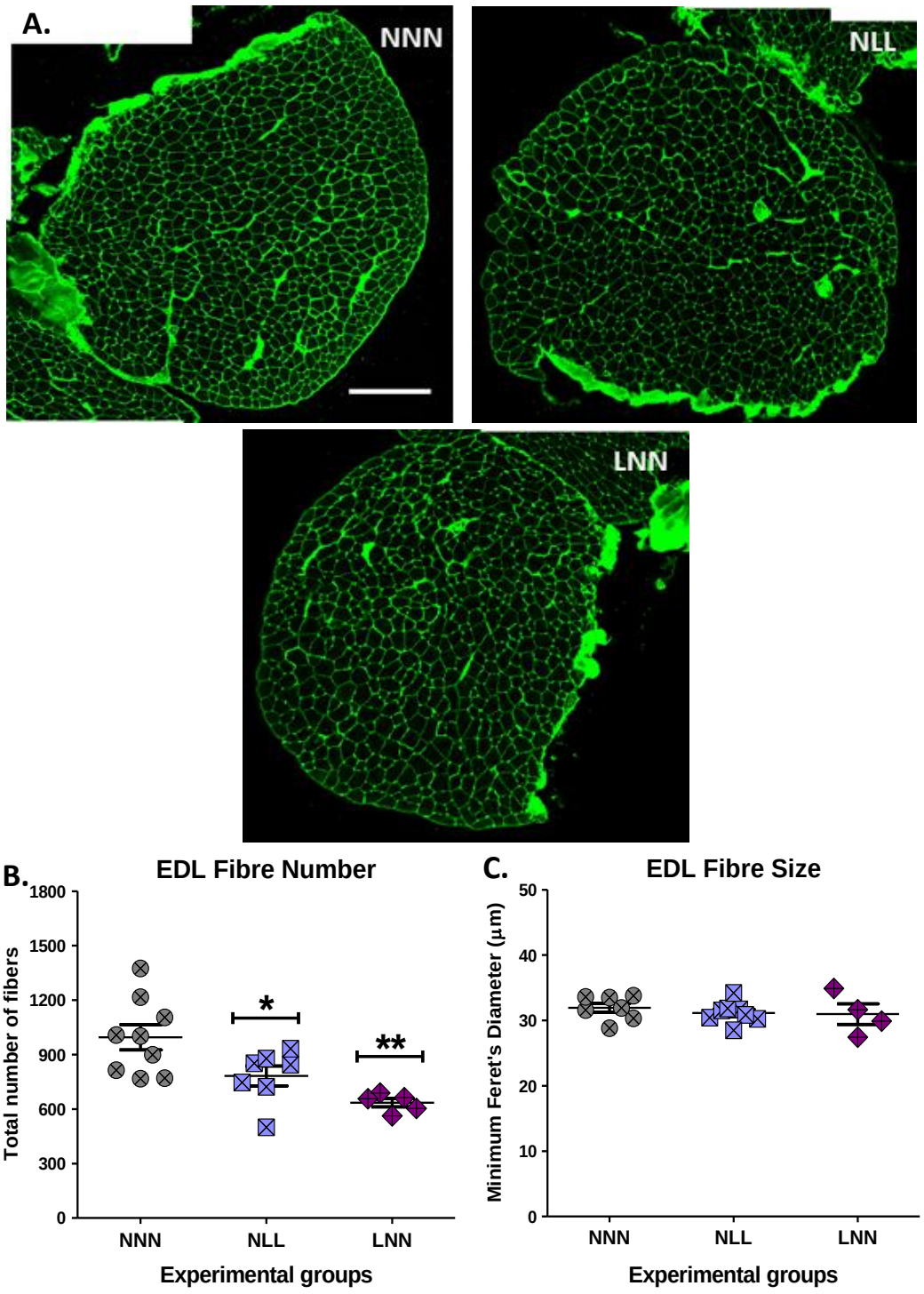

Figure 3.3.3.1 Histological examination of the EDL muscle of 12-week old mice. **A)** Transverse sections of EDL muscle from 12-week old mice stained with WGA (green) and visualised under a confocal microscope. Scale bar: *200 µm*, Magnification: *x20*, Section thickness: *12 µm.* **B)** EDL fibre number and **C)** EDL fibre size in 12-week old mice. *represents significant differences compared with

NNN (control) group, **P ≤0.05, **P ≤0.01* (*mean ± SEM; n*=4-8, *One-Way ANOVA with Dunnett's post-hoc analysis*). Representative images shown.

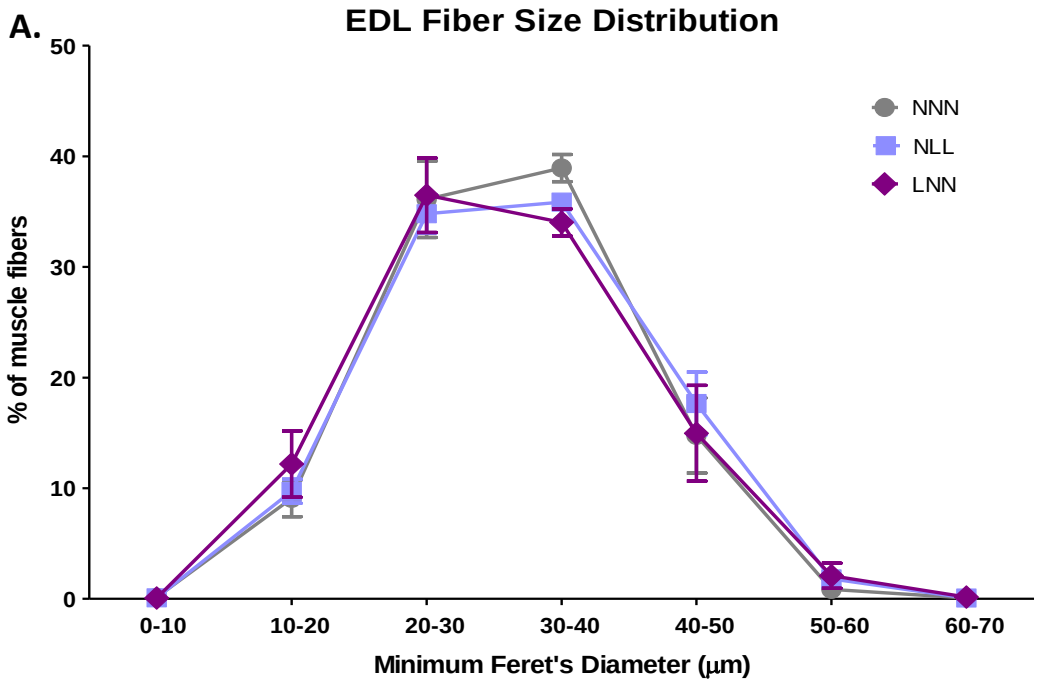

Figure 3.3.3.2 Myofibre distribution analysis of EDL muscle, expressed as a percentage of total muscle fibres analysed in EDL muscle of 12-week old mice (*mean ± SEM*; *n*=4-6*, Chi-square test*).

3.3.4 Assessment of NMJ integrity in 12-week old mice following a low-protein diet pre- and postnatally

Images and analysis of NMJ morphology in EDL muscles of 12-week old mice following a low-protein diet pre-or postnatally is shown in **Figure 3.3.4.1** and **Figure 3.3.4.2**. Analysis of NMJ images revealed the presence of morphological abnormalities in NLL and LNN, rather than denervation (partial or complete) of the synaptic site **(Figure 3.3.4.1)**. Individual NMJs where subsequently scored into normal, morphologically abnormal and denervated in all three groups. Significant differences in the number of NMJs with morphological abnormalities were recorded in NLL compared to the control group (NNN) **(Figure 3.3.4.2 A).**

NMJs with morphological abnormalities in all three groups were then scored and subdivided into fragmented, small in size or with limited/defective branching (Chapter 2, Section 2.5). The proportion of NMJs with small size, fragmented or defective branching was higher in NLL mice compared to the control group (NNN) **(Figure 3.3.4.2 B-D).**

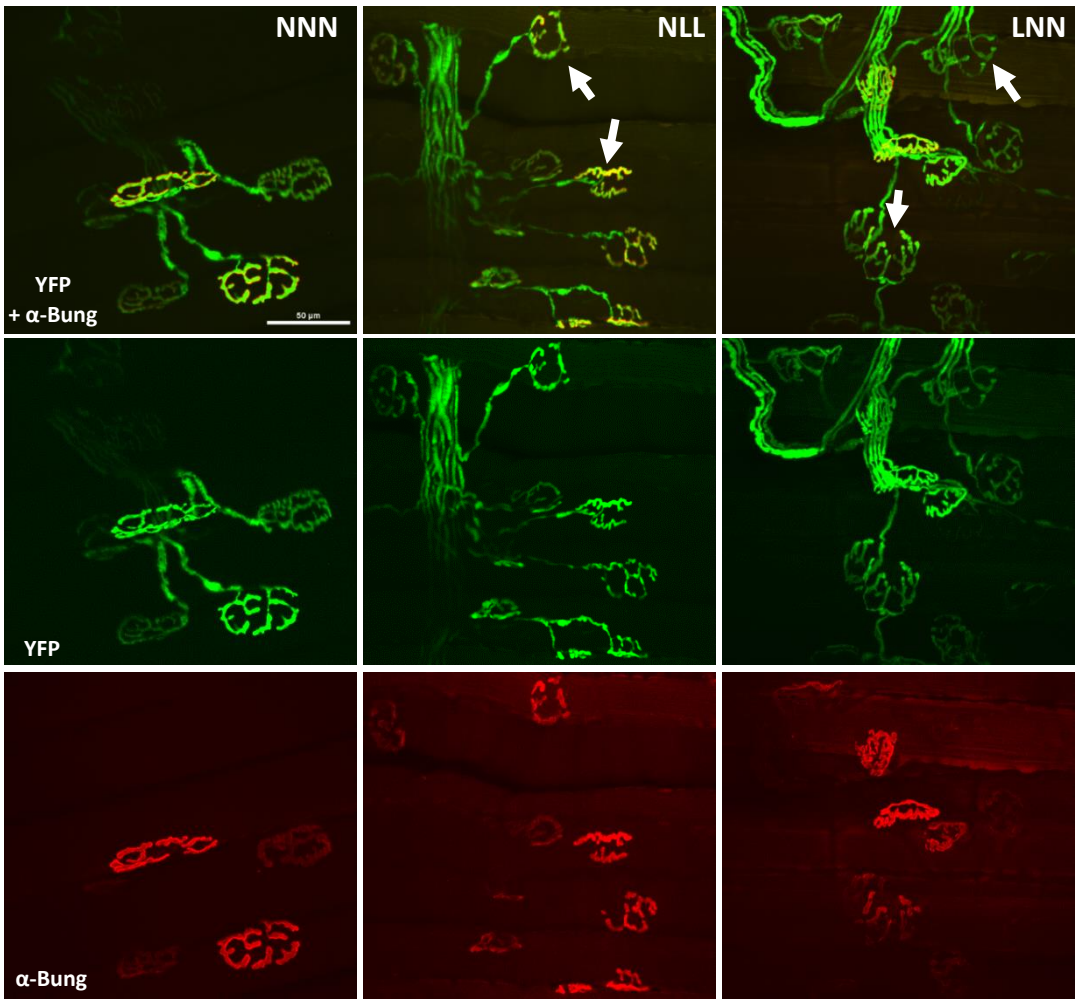

Figure 3.3.4.1 Characterisation of NMJs in EDL muscle of 12-week old mice on a normal or a protein-deficient diet pre- or postnatally. The pre-synaptic terminal expressing YFP (green) and the post-synaptic end plate stained with α-bungarotoxin (red) show perfect overlap. A number of NMJs in NLL and LNN mice show morphological aberrations (arrow) in comparison with the "pretzel" shape seen in the control group. Scale bar: *50 µm*, Magnification: *x60*. Representative images shown.

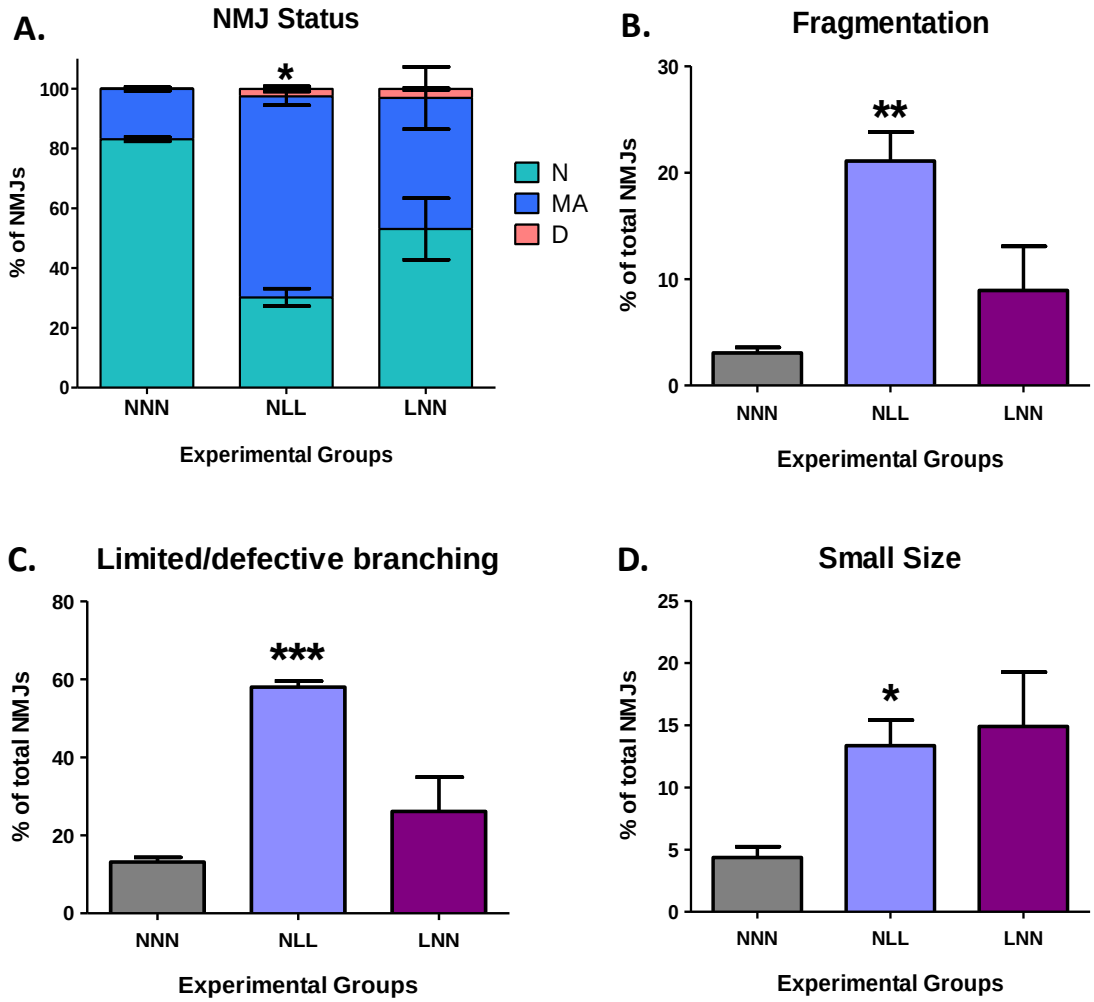

Figure 3.3.4.2 Classification of NMJs changes in EDL muscle of 12-week old mice on a normal or a protein-deficient diet pre- or postnatally. **A)** NMJs were divided into 3 main categories: normal (N), morphologically abnormal (MA) and denervated (partial or complete) (D) and expressed as a percentage of the total number of NMJs scored per muscle. **B-D)** Scoring of NMJs with morphological abnormalities into 3 sub-categories: fragmented **(B)**, with limited/defective branching **(C)** or with small synaptic area **(D)** *represents significant differences compared with NNN (control) group, **P ≤0.05, **P ≤0.01, ***P ≤0.001* (*mean ± SEM; n=3, One-Way ANOVA with Dunnett's post-hoc analysis*).

3.3.5 Gene expression analysis of marker genes for muscle fibre isoforms, muscle atrophy and NMJ formation in TA muscle of 12-week old mice following a low-protein diet pre- and postnatally

Expression analysis of genes involved in determination of myosin heavy chain isoforms in TA muscle of 12-week old mice are shown in **Figure 3.3.5.1**. Expression levels of MyHC-IIa revealed significant increase in gene expression levels in NLL group, compared to the control group (NNN) (**Figure 3.3.5.1 B**). Expression levels of MyHC-I (**Figure 3.3.5.1 A**), MyHC-IIb (**Figure 3.3.5.1 C**) and MyHC-IId/x (**Figure 3.3.5.1 D**) showed no significant differences between the groups. However, the sample variation and the small N number did not allow a definitive conclusion to be drawn.

Expression levels of Atrogin-1, MuSK and FoxO-3 genes are shown in **Figure 3.3.5.2.** Analysis of Atrogin-1 expression levels showed significant increase in expression levels both in NLL mice and LNN, compared to the control group (NNN) (**Figure 3.3.5.2 A**). On the contrary, MuSK and FoxO-3 expression levels revealed no differences between the groups (**Figure 3.3.5.2 B, C**).

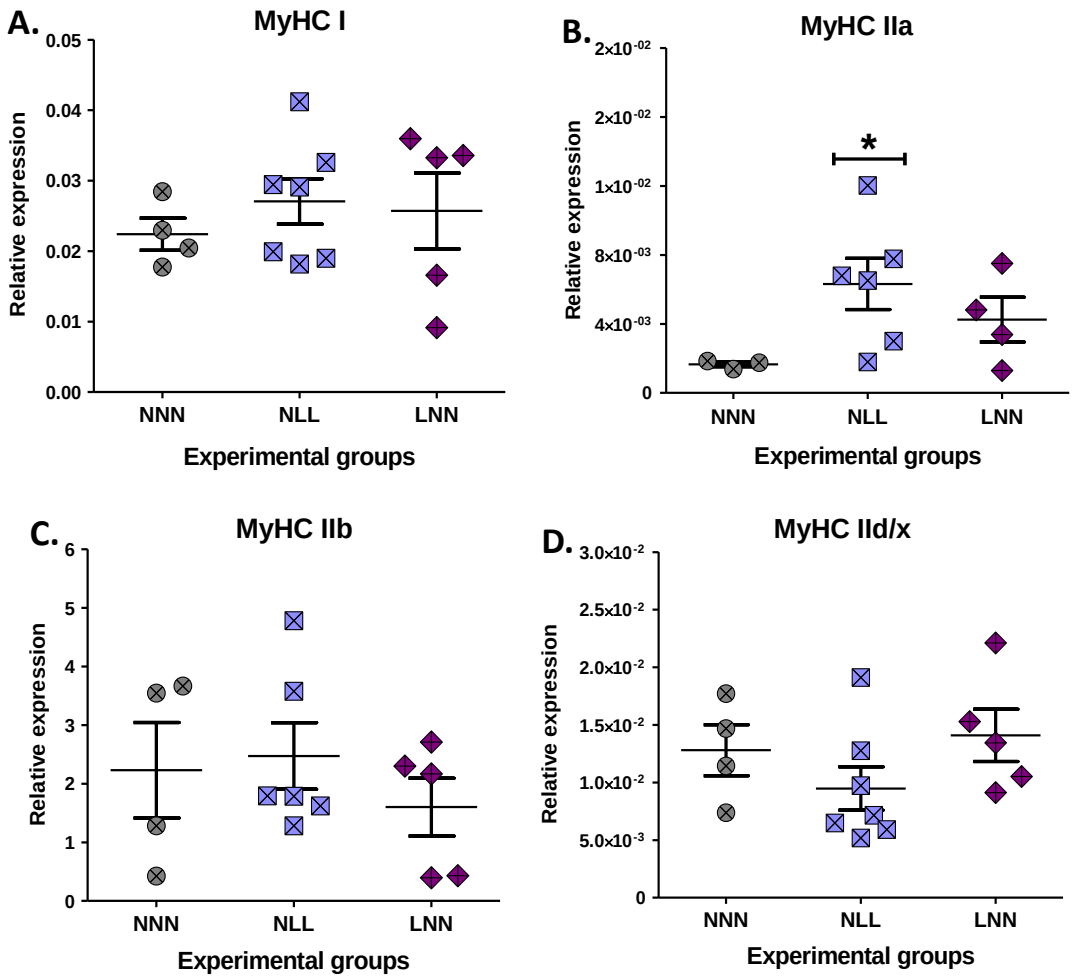

Figure 3.3.5.1 Expression analysis of MyHC isoforms in TA muscle of 12-week old mice following a low-protein diet pre- or postnatally. Relative expression levels of **A)** MyHC-I, **B)** MyHC-IIa, **C)** MyHC-IIb and **D)** MyHC-IId/x. *represents significant differences compared with NNN (control) group, **P≤0.05* (*mean ± SEM; n*=3-7*, One-Way ANOVA with Dunnett's post-hoc analysis*).

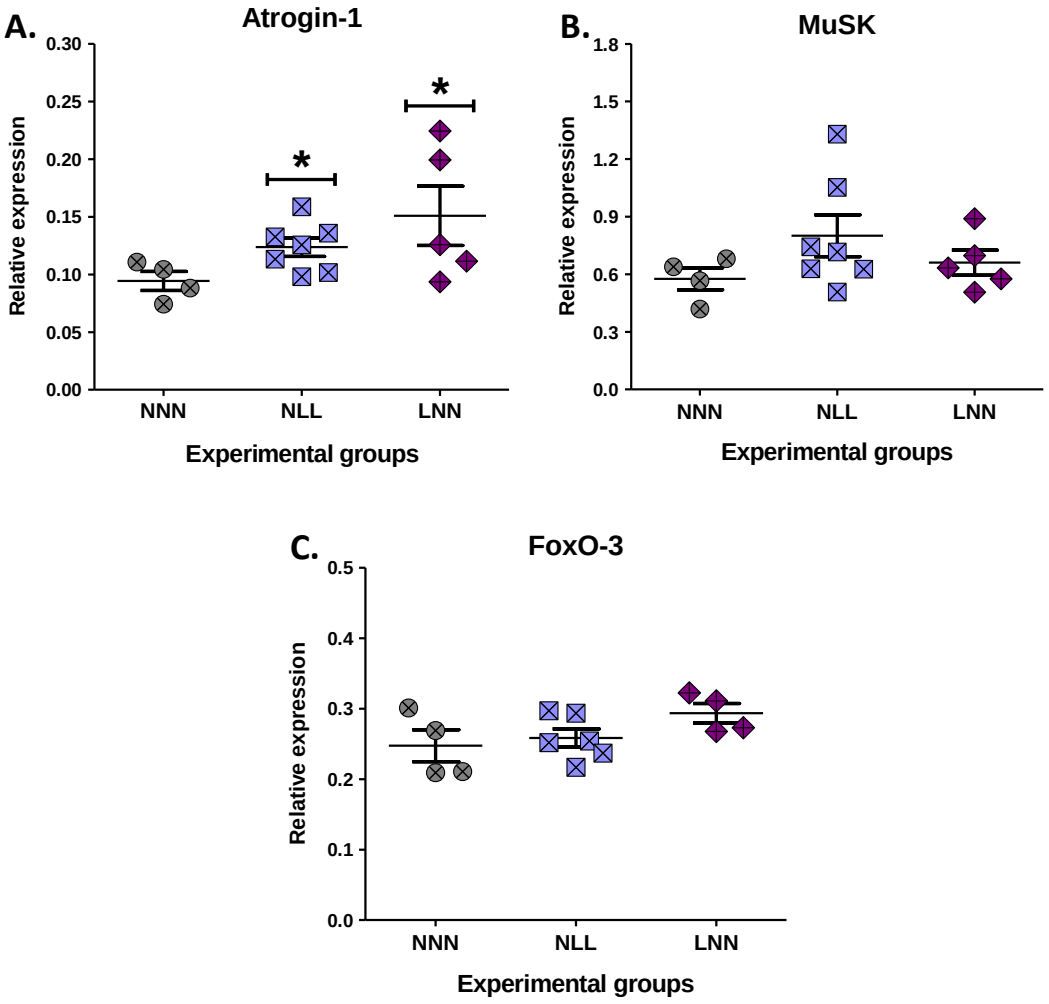

Figure 3.3.5.2 Expression analysis of **A)** Atrogin-1, **B)** MuSK and **C)** FoxO-3 genes in TA muscle of 12-week old mice following a low-protein diet pre- or postnatally. *represents significant differences compared with NNN (control) group, **P≤0.05* (*mean ± SEM; n*=4-7*, One-Way ANOVA with Dunnett's post-hoc analysis*).

3.4 Discussion

The aim of this study was to determine the effect of reduced protein diet pre- or postnatally on NMJ structure, muscle mass and function in mice during adulthood. Mice on a normal or a protein-deficient diet during gestation or

lactation were subjected to a normal or a low-protein diet after weaning, until 12 weeks of age (NNN, NLL, LNN mice; Chapter 2, Section 2.1). Assessment of body and muscle physiology and function in mice subjected to a protein-deficient diet was performed in order to investigate whether changes seen during gestation or lactation stages (21-day old mice) persist until early adulthood (preliminary data, **Figure 3.1**). This assessment would also indicate in which developmental stage dietary modifications play a crucial role in skeletal muscle wasting. Data collected from 12-week old mice showed a reduction in total body weight and muscle strength, accompanied by reduction in the muscle weight of specific skeletal muscles of the lower limbs. However, the reduction in maximum force generation of the EDL muscle was not accompanied by a reduction in its specific force. Therefore, the reduction of the maximum force may be attributed to the morphological alterations seen at the NMJs rather than changes in muscle fibre number. No structural differences were observed in muscle fibre size, but noticeable differences in the morphology of the NMJs and muscle fibre number were recorded. Quantitative expression analysis of marker genes involved in regulation of muscle mass and function revealed changes in the expression levels of those genes in mice on a protein-deficient diet. These changes could indicate the potential impact of dietary protein restriction early in life in the regulation of molecular mechanisms of muscle composition, muscle morphology and function and NMJ maintenance.

3.4.1 The effect of low-protein diet pre- or postnatally on body and muscle mass, muscle size and muscle function of 12-week old mice

Analysis of total body weight and maximum force generation in EDL muscle showed significant decline of both only in mice on a low-protein diet at postnatal stages of development (NLL) (**Figure 3.3.2**). Similar reduction was seen in the weight of SOL, GTN and Quad muscle in NLL mice but no changes were recorded in the weight of EDL and TA muscle of NLL mice, compared to the control group

(NNN) (**Figure 3.3.1.1**). Muscle weight of mice from the LNN group showed no differences, compared to the control group (NNN) (**Figure 3.3.1.1**).

The reduction in body weight in 12-week old mice on 5% protein diet postnatally highlights the systemic effect of dietary interventions and the important role of nutrients during development. Changes in body weight following restriction of nutrients have been previously reported in both mice (Yang *et al.* 2014; Chen *et al.* 2009) and humans (reviewed in Soliman *et al.* 2014). In terms of protein restriction in humans, several cases of malnutrition due to suboptimal protein intake have been recorded in infants even in developed countries with wide range of adverse effects (Tierney *et al.* 2010). Several studies have highlighted the link between body weight and muscle function, where muscle strength was assessed. Specifically, in humans low body weight early in life has been associated with reduced muscle function later in life (Sayer *et al.* 2004). In mice, early life protein restriction has been linked to lower body and organ weight and changes in the expression of key proteins associated with muscle function and maintenance (Chen *et al.* 2009). Data from this study showed significant reduction in the muscle weight in SOL, GTN and Quad muscle (composed of type I and type II muscle fibres) but not in EDL and TA muscles (composed predominantly of type II muscle fibres). However, correlation analysis of EDL muscle weight compared with the maximum force showed a link between lower muscle weight and reduced maximum muscle force (**Figure 3.3.2 D**). Similar results were obtained from correlation analysis between body weight and maximum muscle force. Specific muscle force showed no differences between the three groups, indicating that maximum muscle force generation in NLL mice may be reduced due to morphological alterations seen at the synaptic site rather than intrinsic muscle mechanisms. These data indicate that individual muscle weights may not show significant differences between the groups, but they could be directly associated with lower maximum force generation from the muscle. Absence of significant differences in mice in the LNN group suggests that pre-natal protein restriction does not have a direct impact on skeletal muscle weight and force generation during adulthood.

3.4.2 The effect of maternal protein restriction on muscle physiology

Histological analysis of the EDL muscle was necessary in order to assess any potential effect of maternal protein restriction in skeletal muscles of the offspring. EDL muscle has a high percentage of fast-twitch muscle fibres (MyHC type II isoforms) (Augusto *et al.* 2004), which are preferentially lost during ageing. Therefore, this muscle is ideal for measurement of the contractile properties of skeletal muscle in mice. Morphological analysis of the EDL muscle showed no differences in muscle fibre size. However, significant reduction in EDL fibre number was recorded in NLL and LNN mice (**Figure 3.3.3.1**). This reduction in fibre number of NLL mice at 12 weeks of age may be the result of preferential loss of smaller muscle fibres at earlier stages of development. It is interesting that we did not see a significant reduction in the weight of the EDL muscles in this group given this finding. However, it is possible that the muscles of these mice have gained bulk *via* other sources such as fat infiltration, which was not examined in this thesis. Furthermore, the small size of the EDL muscle makes it technically challenging to detect changes in its weight between the three experimental groups.

Mice from the LNN group also had a significant reduction in myofibres number at 12 weeks of age (**Figure 3.3.3.1**). It is possible that the loss of muscle fibre size in mice from the NLL and LNN group would be due to different mechanism involved, as suggested by qPCR data. Distribution analyses of the fibre size in EDL muscle showed no significant shift in the fibre size distribution (**Figure 3.3.3.2**). Again, the lack of a significant reduction in the weight of the EDL muscles may be due to bulk gained *via* other sources such as fat infiltration. In order to determine whether that is indeed the case, further investigation is required.

Previous studies have demonstrated a strong link between muscle force and muscle physiology in terms of muscle fibre size and number. Weaker muscles have been associated with reduced number of muscle fibre size and/or number, one of the main characteristics of sarcopenia (reviewed in Doherty, 2008).

Recent studies have demonstrated a reduction in muscle strength during early ageing but in the absence of muscle atrophy, suggesting that reduction in the muscle force may be a predecessor of physiological changes seen in the muscle at later stages (Chan *et al.* 2010). Although loss of muscle function without changes in muscle physiology has not been frequently reported, other factors may be equally responsible for a reduction in muscle strength. Examples of such factors include changes in MyHC isoforms, affecting the contractile properties of the muscle (Barany, 1967), innervation and signal transmission at the synaptic site of the muscle (Sheth *et al.* 2018), changes in the levels of ROS (Palomero *et al.* 2013), mitochondrial content (Short *et al.* 2005) and changes in key molecular mechanisms regulating muscle mass and function (reviewed in Jackman and Kandarian, 2004). Molecular changes of critical molecules for skeletal muscle mass and function, the structure and morphology of synaptic sites and mitochondrial homeostasis were further investigated in our study.

3.4.3 Physiological changes at the neuromuscular junction site in 12-week old mice on a protein-deficient diet

To elucidate the mechanisms causing a reduction in muscle force generation in 12-week old mice on a protein-deficient diet postnatally, assessment of the structure of the NMJ was assessed. Firstly, NMJs were categorised into normal, morphologically abnormal or denervated (partial or complete) in order to examine whether changes in structure and morphology would be as severe as those seen in diseases (Lyons and Slater, 1991; Pratt *et al.* 2015) or during ageing (Vasilaki *et al.* 2016). Scoring of NMJs showed a significantly higher proportion of morphologically altered NMJs in the NLL group compared to the control group; although perfect overlap between the pre-and post-synaptic site was evident in the majority of NMJs (**Figure 3.3.4.1**). Moreover, partial denervation in a small number of NMJs in both NLL and LNN groups was noted but their proportion was below 5% of total NMJs scored and presented no significant differences compared to the control group (NNN) (**Figure 3.3.4.2**). This small proportion of

partially denervated NMJs was not surprising, considering that evidence of complete denervation in the muscle is not common in young/adult mice not affected by a severe condition such as muscular dystrophy, in which more striking physiological effects are also noted (Lyons and Slater, 1991).

Since significant differences in the NMJs with morphological abnormalities were recorded in the NLL group, subsequent scoring of those NMJs was performed. Three subcategories of morphological abnormalities were generated based on fragmentation of the synaptic components, limited or defective branching and small synaptic surface area. Similar criteria for NMJ scoring have been used in previous studies (Valdez *et al.* 2010) although the NMJ phenotype was much more severe than the one seen in our study. Data collected showed a significant increase in the proportion of the NMJs in all three subcategories in mice from the NLL group, compared to the control (NNN) group (**Figure 3.3.4.2**).

Collectively, results from the NMJ scoring indicate alterations in the morphology of the NMJ site but very little evidence of partial denervation and no visible impairments in the overlap of the pre- and post-synaptic components were recorded. Although defects in the NMJs have been previously reported to impact skeletal muscle function, such defects are usually quite striking, including partial or fully denervated NMJs or lack of overlapping of the junction components (reviewed in Tintignac *et al.* 2015). These aberrations have been recorded in mice models with severe muscle defects (Lyons and Slater, 1991; Fischer *et al.* 2011) and during ageing (Vasilaki *et al.* 2016). Alterations in the morphology of the NMJs such as the ones seen in this study may be the results of delayed development. Small NMJ size and limited branching in the synaptic site similar to that observed in mice from the NLL group has been recorded in several studies examining the developmental stages and maturation of NMJs in mice (Slater, 1982; reviewed in Shi *et al.* 2012). Assuming that mice from the NLL group exhibit delayed development, this would align with the small proportion of partially denervated NMJs and any fragmentation seen which may be the result of NMJ remodelling rather than a deficit. Indeed NMJ remodelling in mice during postnatal stages of development includes branching elimination, parts of

unoccupied AChR clusters and along with structural other structural changes (Balice-Gordon and Lichtman, 1993; Marques *et al.* 2000). It is noteworthy that recent studies performing functional tests in muscle fibres occupied by an abnormal NMJ (e.g. fragmented) showed that such abnormalities per se do not affect the contractile properties of the skeletal muscle fibre (Willadt *et al.* 2016). However, there are studies showing a close association between NMJ morphology and muscle function in mice following injury (Tu *et al.* 2017). Here, we advocate that the NMJ structural alterations observed in this study may be the result of underlying dysregulation in molecular mechanisms due to maternal protein restriction. This would result in a phenotype agreeing with delayed development in mice from the NLL group. Unlike the NMJ phenotype observed in mice from the NLL group, no significant changes in NMJ structure where seen in 12-week old mice from the LNN group, compared to the control. This is in line with the normal force generation of the EDL muscle of these mice. As such, pre-natal protein restriction does not result in aberrations of NMJ morphology during adulthood.

3.4.4 The impact of protein-deficient diet on molecular mechanisms of skeletal muscle morphology, muscle atrophy and NMJ formation in TA muscle of 12-week old mice

In order to examine the hypothesis that protein restriction could have an effect on molecular mechanisms in the muscle during development, quantitative analysis of gene expression was performed for genes associated with muscle and NMJ physiology and function. Isolated RNA from TA muscle of 12-week old mice was used for cDNA synthesis and qPCR for the following genes: MyHC type I, IIa, IIb and IId/x isoforms, Atrogin-1, FoxO-3 and MuSK.

Relative expression analysis of MyHC type IIa isoform in TA muscle revealed a significant upregulation in gene expression levels in the NLL group compared to the control group. Expression levels of MyHC type I, type IId/x and type b showed no significant differences between the groups. Increased intragroup variability in

gene expression levels along with a low n number for each group were important restrictions for accurate estimation of the gene expression levels of these gene transcripts (**Figure 3.3.5.1**).

Several studies have established the TA muscle as a MyHC type IIb-rich muscle similar to the EDL in adult mice (Augusto *et al.* 2004) with MyHC type IId/x being the second most abundant isoform, followed by type IIa. During development, the composition of a skeletal muscle changes, with some MyHC isoforms being replaced. Specifically, the EDL muscle is predominantly composed by MyHC type IIb fibres at the age of 21 days, when MyHC type IIa is still present. By 90 days of age, the EDL muscle is devoid of the type IIa isoform and is composed almost exclusively of type IIb fibres and in smaller proportion type IId/x (Agbulut *et al.* 2003). Very similar composition has also been observed in TA muscle, with MyHC type IIb being more abundant in adult mice (Augusto *et al*, 2004). Changes in muscle fibre composition in terms of MyHC isoforms can have an impact on the contractile properties of the muscle. Knockout mice for MyHC IIb or IId/x show distinct differences in muscle force generation (Acakpo-Satchivi *et al.* 1997). Other studies have shown that adult mice lacking of MyHC IId expression demonstrated an increase in the expression of MyHC IIa isoform, potentially acting as a compensatory mechanism (Santorius *et al.* 1998). Although MyHC IIa and IId/x fibres generate less force than type IIb fibres, upregulation of MyHC type IIa expression in mice from the NLL group might be a compensatory mechanism or an indicator of developmental defect in the TA muscles of those mice. However, it is possible that this level of overexpression may not be sufficient to recover muscle force in these mice. In order to examine whether this is indeed the case and whether these data are consistent in both EDL and TA muscles, immunofluorescent staining in transverse sections of those muscles would be necessary. Quantification of myofibres of different MyHC isoforms would provide an indication of potential shifts between different isoforms or the presence of hybrid myofibres in these muscles.

In addition to the expression patterns of MyHC isoform genes, differences in the expression levels of genes involved in muscle atrophy and synapse formation

were also investigated (**Figure 3.3.5.2**). Relative gene expression of Atrogin-1 in TA muscle showed a significant increase in the expression levels in mice from both the NLL and LNN group. Atrogin-1 is a muscle-specific gene highly expressed during skeletal muscle atrophy (Gomez *et al.* 2010) but lower expression levels have been reported in aged mice with sarcopenia (Edström *et al.* 2006). Upregulation of this gene in mice of the NLL and LNN groups does agree with the reduction in muscle fibre number in the EDL muscle of these mice, but it may also be an early indicator of the tendency of those muscle fibres to undergo atrophy, a phenotype that could be studied later on in adult life. In terms of synaptic formation, expression levels of MuSK gene showed no significant differences between the groups. During postnatal development in mice, MuSK activation plays a fundamental role in NMJ maintenance and maturation *in vivo* (DeChiara *et al.* 1996; Hesser *et al*, 2006). Taken into account the structural changes seen in NMJ morphology in this study, it is possible that molecular changes in MuSK gene my have not yet been evident. In order to assess the molecular changes underlying the morphological alterations seen in NMJs, it would be important to examine the expression levels of additional genes, including AChR-α, AChR-ε and AChR-γ subunit genes. Upregulation in gene expression of the AChR-γ gene may indicate possible damage at the NMJ site, including denervation (Valdez *et al.* 2014). AChR-γ subunit is gradually substituted by AChR-ε subunit during NMJ maturation at early stages of development (Missias *et al.* 1996). Therefore, analysis of the expression level of the two AChR isoforms would be a useful tool to access whether delayed development or NMJ denervation/remodelling occurs in mice of the NLL group.

All things considered, reduction of EDL muscle force seen only in NLL mice might be the combined result of myofibres loss and defective NMJs. Myofibre loss in LNN mice but normal NMJ structure might be insufficient for reduction in EDL muscle force. Examination of MyHC isoforms and AChR subunits would provide a more collective explanation on the effect of the protein-deficient diet during early life.

Chapter 4

MicroRNA expression and *in silico* analysis of predicted target genes

4.1 Introduction

MicroRNAs are important regulators of gene expression, controlling the expression of multiple transcripts in more than one tissue. Data from our lab show that several microRNAs have been associated with the regulation of skeletal muscle and nerve homeostasis, including miR-181, miR-199 and miR-378. MiR-181 has been identified as a key microRNA for the establishment of skeletal muscle phenotype during muscle development, with expression levels being upregulated in the muscle during differentiation (Naguibneva *et al.* 2006). MiR-181a, a member of miR-181 family, has been shown to regulate Sirt-1 expression on a protein level in skeletal muscle cells regulating myotube size (Soriano-Arroquia *et al.* 2016). MiR-181d, another member of miR-181 family, has been identified as negative regulator of axonal outgrowth and elongation (Wang *et al.* 2015). Studies have shown that miR-378 expression is positively regulated by MyoD during muscle cell differentiation (Gagan *et al.* 2011). Mice lacking of miR-378 expression show resistance to obesity induced by a high-fat diet and enhanced mitochondria metabolism (Carrer *et al.* 2012). MiR-199a expression has been induced in several model organisms of muscular dystrophy, including *mdx* mice (Alexander *et al.* 2013). Moreover, miR-199a was identified as a regulator of myogenesis *via* negative regulation of several factors of the WNT signalling pathway (Alexander *et al.* 2013). Ablation of miR-199a gene has been linked to reduced mTOR activity and induction of neurodevelopmental pathophysiology (Tsujimura *et al.* 2015), while miR-199b has been associated with attenuation of acute spinal cord injury (Zhou *et al.* 2016).

Expression of microRNAs may often be tissue specific with some microRNAs being more abundantly expressed in certain tissues and under certain conditions. Examples of such microRNAs are miR-128 and miR-133a, which are highly expressed in skeletal muscle.

MicroRNA-128 is expressed at high levels in the central nervous system, specifically the brain, and in skeletal muscles (Lee *et al.* 2008). Increased levels of miR-128 have also been reported during development (Franzoni *et al.* 2015). Studies have shown that miR-128 is an important regulator of neurogenesis and

neuronal differentiation (Zhang *et al*. 2016; reviewed in Li *et al.* 2013). Expression levels of miR-128 increase gradually in mice during postnatal development and peak during adulthood (Tan *et al.* 2013). The role of miR-128 appears to be more versatile, as it is has also been described as a tumour suppressor. A study from Papagiannakopoulos *et al.* has demonstrated the tumour suppressive role of miR-128 by direct targeting of EGFR and PDGFRa, both interacting with RTKs (Papagiannakopoulos *et al.* 2012). Another study has identified Irs1, Insr, and Pi3k1r, components of Insulin signalling/Akt pathway as direct target genes of miR-128 (Motohashi *et al.* 2013). These findings are in agreement with studies showing pathways in cancer, neurotrophin signalling, MAPK and insulin signalling pathway as highly enriched pathways with miR-128 target genes (Motohashi *et al.* 2013; Ching and Ahmed-Annuar, 2015).

Unlike miR-128, microRNA-133 belongs to a conserved family of microRNAs known as "myomiRs" and it is specifically and highly expressed in skeletal and cardiac muscle (Chen *et al.* 2006). Expression of miR-133 is closely regulated by myogenic factors MyoD and SRF, which subsequently regulates skeletal muscle cell proliferation and differentiation (Chen *et al.* 2006; Rao *et al.* 2006). Regulation of myoblast proliferation and differentiation by miR-133 has been observed *via* ERK1/2 signalling pathway (Feng *et al.* 2013). Moreover, a study from Deng *et al.* revealed an upregulation in the expression of miR-133a, a member of miR-133 family, in skeletal muscle of *mdx* mice at one month of age (Deng *et al.* 2011). This study also reported that both skeletal and cardiac muscle development in *mdx* mice overexpressing miR-133a was not compromised (Deng *et al.* 2011). Although, miR-133 and specifically miR-133a has been studied extensively on muscle *in vitro* and *in vivo*, there is not much evidence of its involvement in motoneuron cell survival and function. Hoye *et al.* have identified enrichment of miR-133a in motoneurons of mice, similar to that of miR-218, known as "motomiR" (Hoye *et al.* 2017). Moreover, their data supports that miR-133a may play a functional role in the regulation of postnatal motoneuron fate (Hoye *et al.* 2017).

The aim of this chapter was to assess the expression levels of candidate microRNAs in skeletal muscle and peripheral nerve of 12-week old mice that have been subjected to either a normal or a protein-deficient diet pre- or postnatally for functional studies. Data collected from this chapter was used for microRNA gain- or loss-of-function experiments and identification of potential target genes in muscle and nerve *in vitro* (Chapters 5-7).

4.2 Materials and methods

4.2.1 cDNA synthesis and qPCR for microRNAs

Protocols for cDNA synthesis and qPCR for microRNAs have been described in detail in Chapter 2. Briefly, for first strand cDNA synthesis, 100 ng of RNA isolated from TA and SN tissues was used. RNA template, RNase-free H_2O and cDNA reaction mix containing RT enzyme were added to a final volume of 20 µL, as shown in Chapter 2, Section 2.13 (**Table 2.13**). cDNA synthesis protocol for microRNAs is described in Chapter 2, Section 2.13 (**Figure 2.13.1**). Following cDNA synthesis, reaction volume was diluted 1:10 to a final volume of 200 µL and was either used immediately for qPCR or stored at -20^{o}C until future use. For qPCR on microRNAs, each cDNA sample was run in triplicate, with a final reaction volume of 11.4 µL. Reagents for each qPCR reaction sample are shown in Chapter 2, Section 2.15 (**Table 2.15.1**). Protocol for qPCR run on microRNAs is described in Chapter 2, Section 2.15 (**Table 2.15.2**). Quantification of microRNA expression was performed using the delta delta Ct (ddCt) method (Livak and Scmittgen, 2001). Relative expression of microRNAs was normalised to SNORD-61 or RNU-6 housekeeping gene. MicroRNA ID numbers are shown on the table below:

Table 4.2.1 Primer IDs used in qPCR for each microRNA tested in TA and SN of 12-week old mice.

microRNA	ID
miR-128	MIMAT0000140
miR-133a	MIMAT0000145
miR-199a	MIMAT0000230
miR-199b	MIMAT0004667
miR-181a	MIMAT0000660
miR-181d	MIMAT0017264
miR-378a	MIMAT0003151

4.2.2 Identification of miR-128 and miR-133a predicted target genes and investigation of their role in metabolic processes

Predicted target genes of miR-128 and miR-133a were investigated using TargetScanMouse 7.1 (http://www.targetscan.org/mmu_71/). Both miR-128 and miR-133a are within the conserved families of microRNAs among different organisms, with identical mature sequences. The list of predicted target genes was obtained for each microRNA, and a number of predicted target genes of interest associated with skeletal muscle physiology and NMJ formation, morphology and function was selected. The selected predicted target genes were imported into STRING database (Version 10.5; https://string-db.org/). Each gene was illustrated as a node connected with one or more neighbouring nodes. Disconnected nodes were excluded from the network. Interactions between the nodes were assessed based on degree of confidence (low=0.150, medium=0.400, high=0.700, highest=0.900). Network was illustrated using CytoScape Software, based on the information obtained from STRING Database. To evaluate the role of each gene in specific biochemical processes, Kyoto Encyclopaedia of Genes and Genomes (KEGG) Pathway database was used (https://www.genome.jp/kegg/). KEGG Reference number (KO number) for each protein encoded by each predicted target gene of interest was obtained and

imported into KEGG Mapper. Signalling pathways containing all or a number of those target genes were shown. Following selection of signalling pathway of interest, proteins encoded from predicted target genes were coloured in cyan (miR-128) or orange (miR-133a), depending on the microRNA by which they were targeted.

4.2.3 Statistical analysis

Statistical analysis of qPCR results was performed using Graphpad 5 (Graphpad Software, San Diego, USA). Data analysis was performed using One-Way ANOVA with Dunnett's post-hoc analysis, using NNN as the control group. Data are represented as mean ± SEM. N Number represents animals used.

4.3 Results

4.3.1 Expression levels of candidate microRNAs in TA muscle and sciatic nerve of 12-week old mice on a low-protein diet in pre-or postnatal stages of development

Analysis of the expression levels of candidate microRNAs is shown in **Figures 4.3.1.** and **4.3.2**. Expression of miR-199a, -199b, -181a, -181d and -378 appeared upregulated in the TA muscle of NLL mice compared to the rest of the groups, but the P value was 0.2242, 0.1234, 0.0667, 0.0831 and 0.0658 respectively (**Figure 4.3.1**). Analysis of the expression levels of miR-128 in TA muscle revealed a significant reduction of miR-128 levels in both NLL and LNN mice (**Figure 4.3.2 A**). Interestingly, miR-133a levels were significantly lower only in the TA muscle of NLL mice, with the LNN mice recording a P value of 0.051 (**Figure 4.3.2 B**). Despite the significant differences recorded in the TA muscle, miR-128 and -133a levels in the SN showed no differences between the three experimental groups (**Figure 4.3.2 C, D**). Based on this data, miR-128 and miR-133a were selected for further analysis.

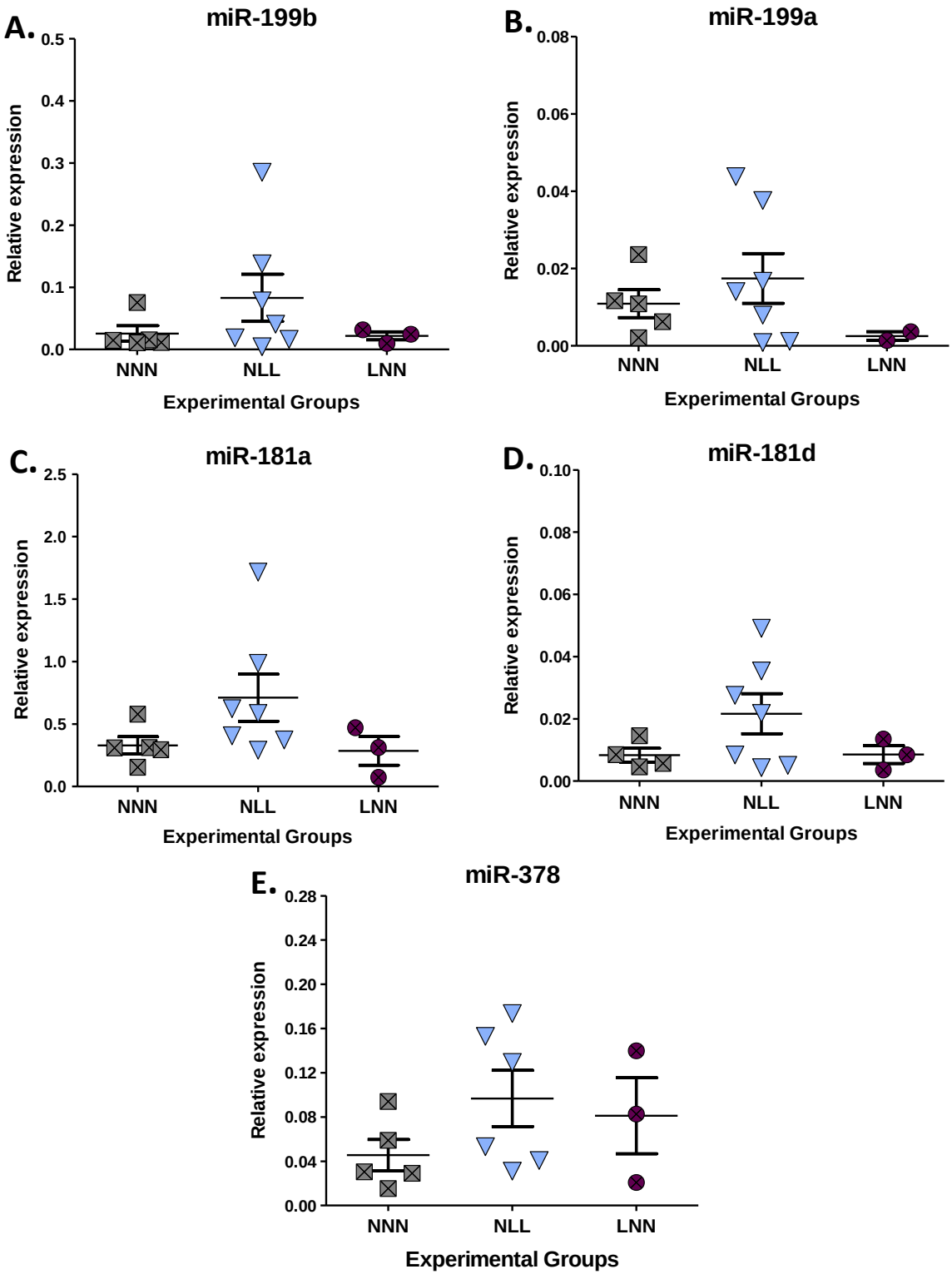

Figure 4.3.1 Expression levels of candidate microRNAs in TA muscle of 12-week old mice subjected to a normal or a low-protein diet pre- or postnatally. Quantitative PCR analysis of microRNA **A)** miR-199b, **B)** miR-199a, **C)** miR-181a, **D)** miR-181d and **E)** miR-378. Expression relative to RNU-6 is shown. NNN serves

as control group for statistical comparison, (*mean ± SEM; n*=3-7*, One-Way ANOVA with Dunett's post-hoc analysis*).

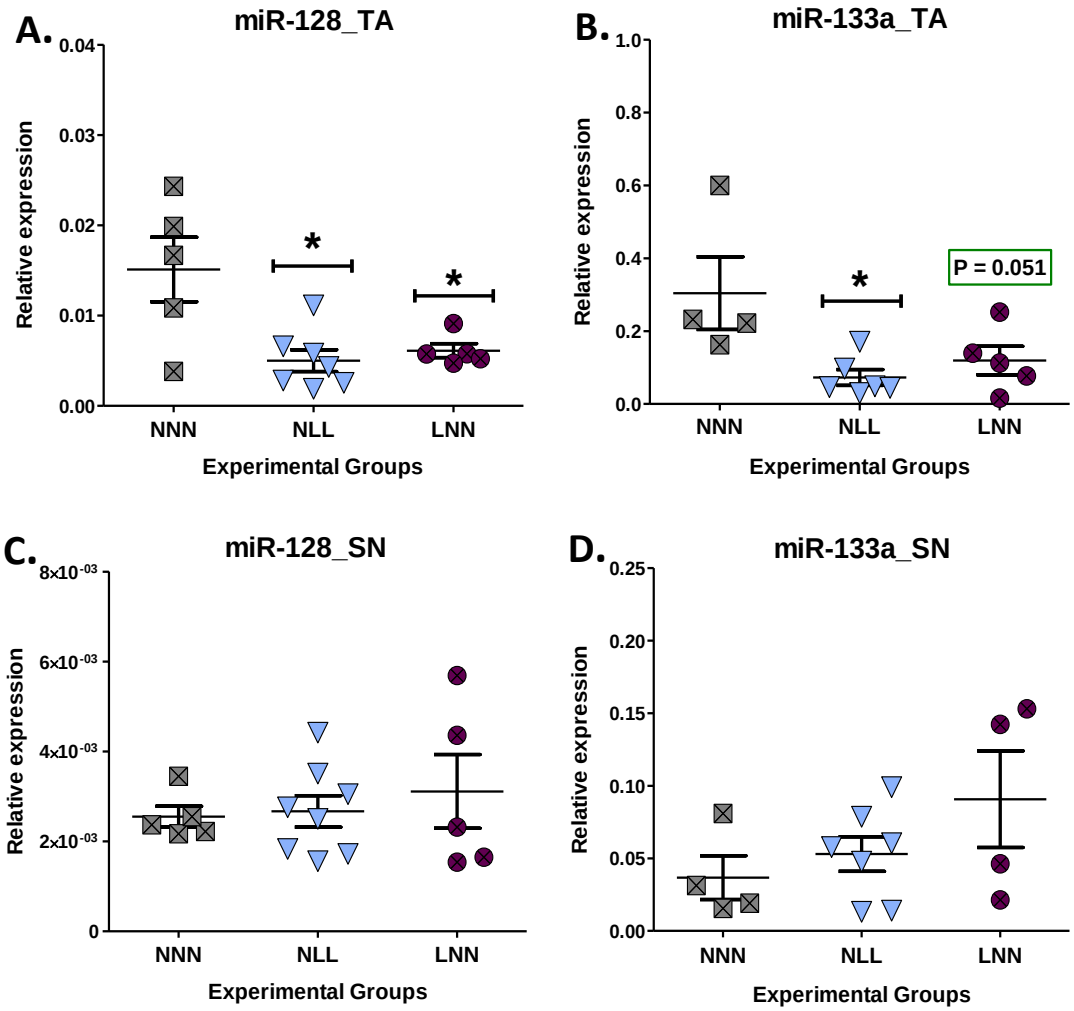

Figure 4.3.2 Expression levels of microRNAs miR-128 and miR-133a in (**A, B**) TA and (**C, D**) SN of 12-week old mice subjected to a normal or a low-protein diet pre- or postnatally. Expression relative to SNORD-61 is shown. *represent significant differences compared with the NNN (control) group, (*mean ± SEM; n*=3-7*, One-Way ANOVA with Dunnett's post-hoc analysis*).

4.3.2 Identification of predicted target genes of miR-128 and miR-133a using TargetScanMouse 7.1 database

The predicted target genes of miR-128 and miR-133a were investigated using TargetScanMouse 7.1 database. From the pool of the predicted target genes (>1000) for miR-128 recorded from TargetScan, only a 19 of those genes were selected to be further investigated (**Table 4.1.2.1**). Similarly, 16 selected predicted target genes for miR-133a are shown in **Table 4.1.2.2**, as selected from a pool of target genes (>600) recorded using TargetScan**.** These genes are involved in key pathways regulating NMJ integrity and signalling as well as muscle mass and function. Seed sequence of the miR-128 in the 3'UTR of the predicted target gene was the following: *5'–CACUGUGA–3'*. Seed sequence for miR-133a in the 3'UTR of the predicted target gene was the following: 5'–GGACCAAA–3'. Each candidate predicted target genes had at least one conserved seed region on the 3'UTR, with some target genes having seed regions, which were poorly conserved across the species. A number of predicted target genes (shown in red) may be targeted by both miR-128 and miR-133a on at least one seed region (often poorly conserved) (**Appendix, Table A1 and A2**).

Table 4.3.2.1 List of the selected miR-128 predicted target genes as recorded using TargetScanMouse 7.1. Ensembl ID and seed region in 3'UTR are shown. Genes marked in red may also be targeted by miR-133a.

miR-128 predicted target genes (TargetScan)				
			Seed region (in the 3'-UTR)	
Name	Gene	Ensembl ID	Conserved	Poorly conserved
nerve growth factor receptor (TNFR superfamily, member 16)	Ngfr	ENSMUST00000000122.6	272-279	N/A
nerve growth factor receptor (TNFRSF16) associated protein 1	Ngfrap1	ENSMUST00000178632.2	28-34	N/A
growth factor receptor bound protein 2	Grb2	ENSMUST00000106497.2	1695-1701	N/A
platelet derived growth factor receptor, alpha polypeptide	Pdgfra	ENSMUST00000000476.9	2852-2858	2398-2404
son of sevenless homolog 1 (Drosophila)	Sos1	ENSMUST00000068714.5	3529-3535	446-452, 1727-1433, 1477-1483
growth factor receptor bound protein 2-associated protein 1	Gab1	ENSMUST00000034150.8	1198-1204	N/A
insulin receptor	Insr	ENSMUST00000091291.4	207-213	3851-2858
insulin receptor substrate 1	Irs1	ENSMUST00000069799.2	230-237	N/A
F-box protein 32 (atrogin-1)	Fbxo32	ENSMUST00000022986.6	4341-4347	N/A
forkhead box O1	Foxo1	ENSMUST00000053764.5	415-421	N/A
forkhead box O4	Foxo4	ENSMUST00000062000.4	228-234	N/A
sirtuin 1	Sirt1	ENSMUST00000120239.2	744-750	N/A
neural cell adhesion molecule 1	Ncam1	ENSMUST00000114476.2	1028-1035	586-592, 612-627, 2169-2175
neurocan	Ncan	ENSMUST00000002412.8	3181-3187	865-871
synaptosomal-associated protein 25	Snap25	ENSMUST00000028727.5	407-713, 1159-1165	N/A
synaptotagmin I	Syt1	ENSMUST00000105276.2	1460-1467, 1692-1698	N/A
nuclear respiratory factor 1	Nrf1	ENSMUST00000115212.2	N/A	1232-1239, 1603-1609
nuclear factor, erythroid derived 2, like 2 (Nrf-2)	Nfe2l2	ENSMUST00000102672.4	60-66	N/A
parkin RBR E3 ubiquitin protein ligase	Park2	ENSMUST00000191124.1	N/A	715-722

Table 4.3.2.2 List of the selected miR-133a predicted target genes as recorded using TargetScanMouse 7.1. Ensembl ID and seed region in 3'UTR are shown. Genes marked in red may also be targeted by miR-128.

miR-133a predicted target genes (TargetScan)				
			Seed region (in the 3'-UTR)	
Name	Gene	Ensembl ID	Conserved	Poorly conserved
clathrin, light polypeptide (Lca)	Clta	ENSMUST00000107846.4	94-101	N/A
synaptotagmin I	Syt1	ENSMUST00000105276.2	1606-1612, 2246-2252	N/A
vesicle-associated membrane protein 2	Vamp2	ENSMUST00000117780.1	1378-1384	N/A
regulating synaptic membrane exocytosis 1	Rims1	ENSMUST00000115273.3	1777-1784	N/A
unc-13 homolog A (C. elegans)	Unc13a	ENSMUST00000030170.9	2204-2211	N/A
adaptor-related protein complex 2, mu 1 subunit	Ap2m1	ENSMUST00000007216.8	254-260	N/A
complexin 2	Cplx2	ENSMUST00000026985.8	4109-4115	N/A
Braf transforming gene	Braf	ENSMUST00000002487.9	5803-5810	N/A
insulin receptor	Insr	ENSMUST00000091291.4	1063-1069	N/A
fibroblast growth factor 1	Fgf1	ENSMUST00000117566.2	353-360	N/A
paired box 7	Pax7	ENSMUST00000030508.8	2128-2134, 3326-3332	1970-1976
GRP1 -associated scaffold protein	Grasp	ENSMUST00000000543.4	275-282	N/A
myosin IXb	Myo9b	ENSMUST00000168839.2	569-576	235-241
myosin, heavy polypeptide 1, skeletal muscle, adult (MHC II d/x)	Myh1	ENSMUST00000124516.2	22-28	N/A
translocase of outer mitochondrial membrane 20	Tomm20	ENSMUSG00000093904	N/A	3889-3896
nuclear respiratory factor 1	Nrf1	ENSMUST00000115212.2	457-463	N/A

4.3.3 Protein interactions of predicted target genes of miR-128 and miR-133a using STRING Database

The interactions between the predicted target genes of miR-128 and miR-133a were examined on a protein level, in order to determine whether they are involved in biological processes associated with skeletal muscle and NMJ formation and function. Interactions were investigated using STRING database (Version 10.5) and were illustrated using CytoScape software. Interactions of predicted target genes of miR-128 shown in **Figure 4.3.3.1** are depicted according to the level of confidence, with the weakest interactions marked with green lines and the strongest with red. Same pattern of interaction is also shown for miR-133a predicted target genes (**Figure 4.3.3.2**). Examination of the interactions between the predicted target genes of both microRNAs indicated strongest relationship between a cluster of target genes, which could potentially be involved in the same metabolic process. For miR-128, the predicted target genes with strongest interactions are: Syt1, Grb2, Gab1, Sos1, Ngfr, Ngfrap1, Pdgfra, Isr1, Insr, Foxo1, Foxo4, Sirt1 and Atrogin1 (**Figure 4.3.3.1**). For miR-133a, strongest interactions were observed between the following target genes: Clta, Ap2m1, Vamp, Syt1, Cplx2, Rims1 and Unc13a (**Figure 4.3.3.2**).

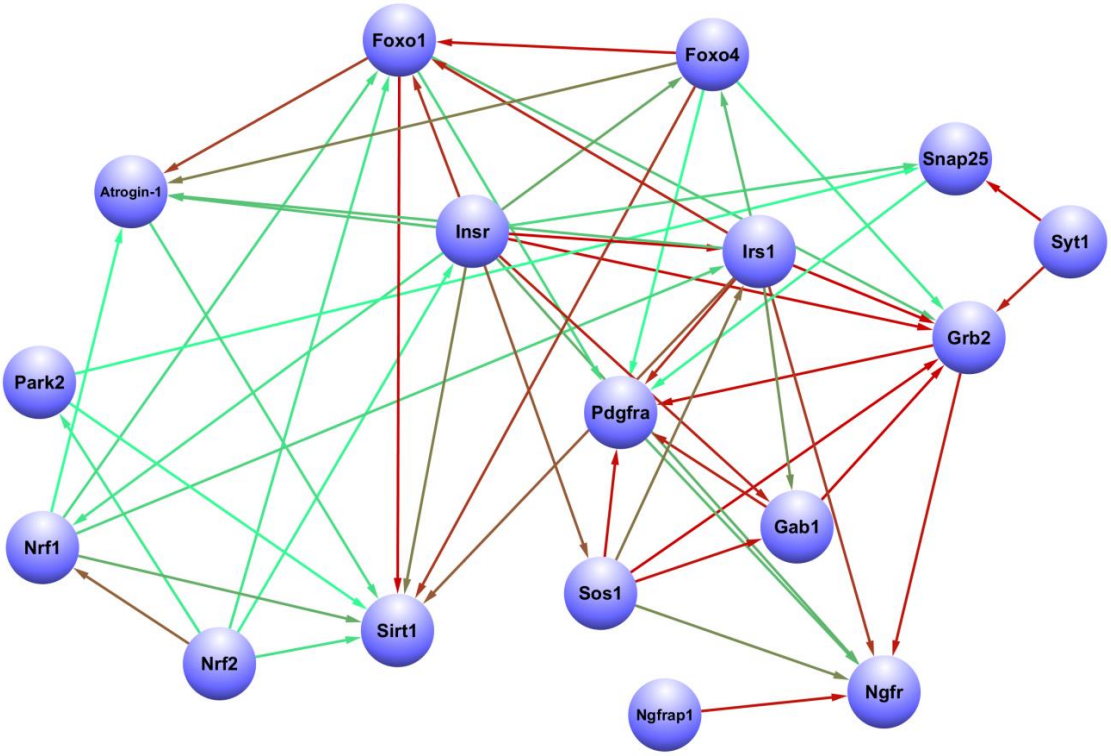

Figure 4.3.3.1 Interactions of predicted target genes of miR-128 using CytoScape software. Green lines indicate the weakest interactions (confidence level <150) and red lines indicate the strongest interactions (confidence level ≥ 0.900). Interactions were drawn based on the combined scored of interactions recorded on STRING database.

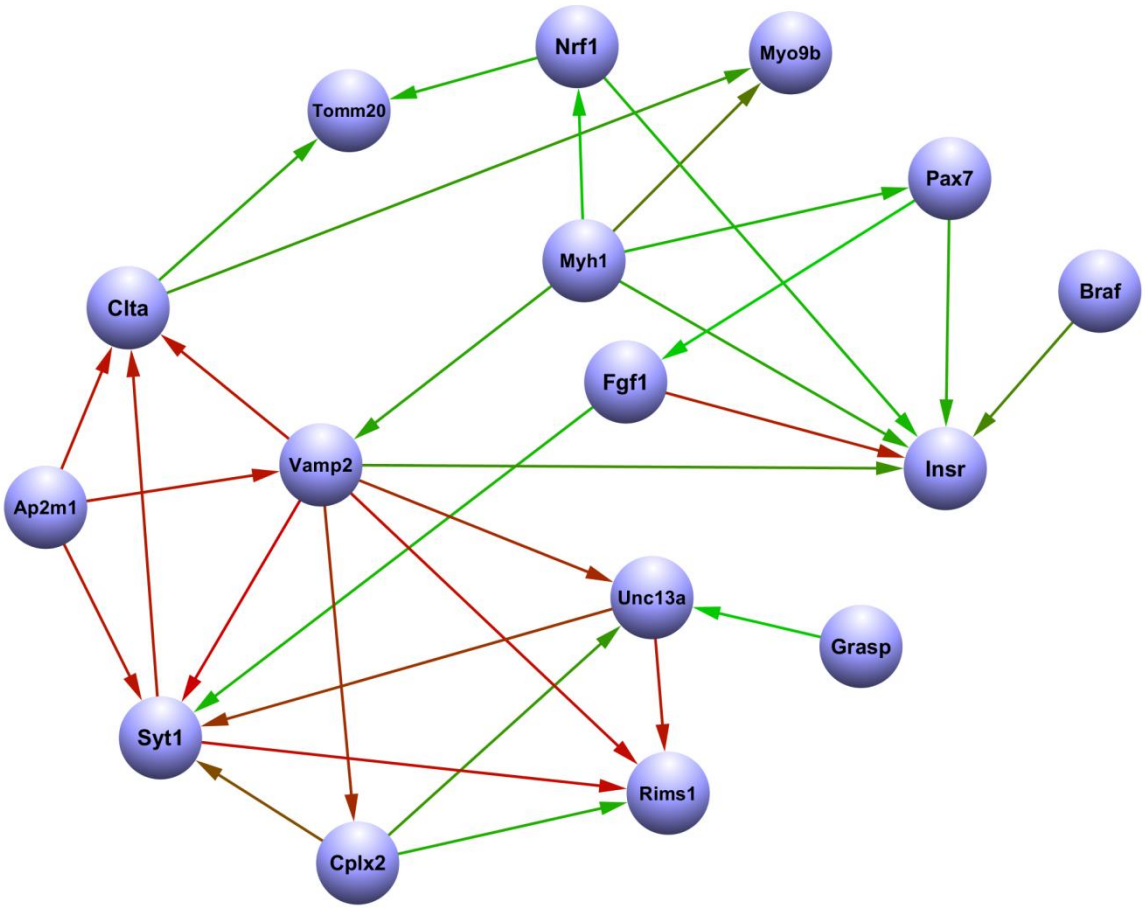

Figure 4.3.3.2 Interactions of predicted target genes of miR-133a using CytoScape software. Green lines indicate the weakest interactions (confidence level <150) and red lines indicate the strongest interactions (confidence level ≥ 0.900). Interactions were drawn based on the combined scored of interactions recorded on STRING database.

4.3.4 Investigation of predicted target gene involvement in signalling pathways using KEGG PATHWAY Database

Involvement of predicted target genes of miR-128 and miR-133a in key signalling pathways was investigated using KEGG PATHWAY Database. Target genes from both microRNAs appear to be involved in 4 signalling pathways: synaptic vesicles cycle, neurotrophin, FOXO and longevity signalling pathway (**Figure 4.3.4 A-D**). Predicted target genes of miR-128 are shown in cyan colour and those of miR-133a are shown in orange. Additional predicted target genes to those described in **Section 4.3.3** are also involved in each of those signalling pathways. One such example is the Cacna1a gene, encoding VGCC protein in the synaptic vesicle cycle, which is a predicted target gene of miR-128 (**Figure 4.3.4 A**). Exclusion of multiple predicted target genes from the analysis performed previously was decided, taking into consideration factors including, but not limited, to strength of interactions with other predicted target genes, relevance to skeletal muscle and/or NMJ physiology and function and novelty of the predicted target (not previously published as a direct target of the miR).

It is noteworthy that miR-133a target genes are mostly involved in the synaptic vesicle cycle, while a group of miR-128 predicted target genes (Grb2, Gab1, Sos1, Insr, Irs1) appear in more than one signalling pathway (**Figure 4.3.4 B-D**). Furthermore, FoxO signalling and longevity regulating pathway are also influenced by dietary restriction (**Figure 4.3.4 C, D**).

A.

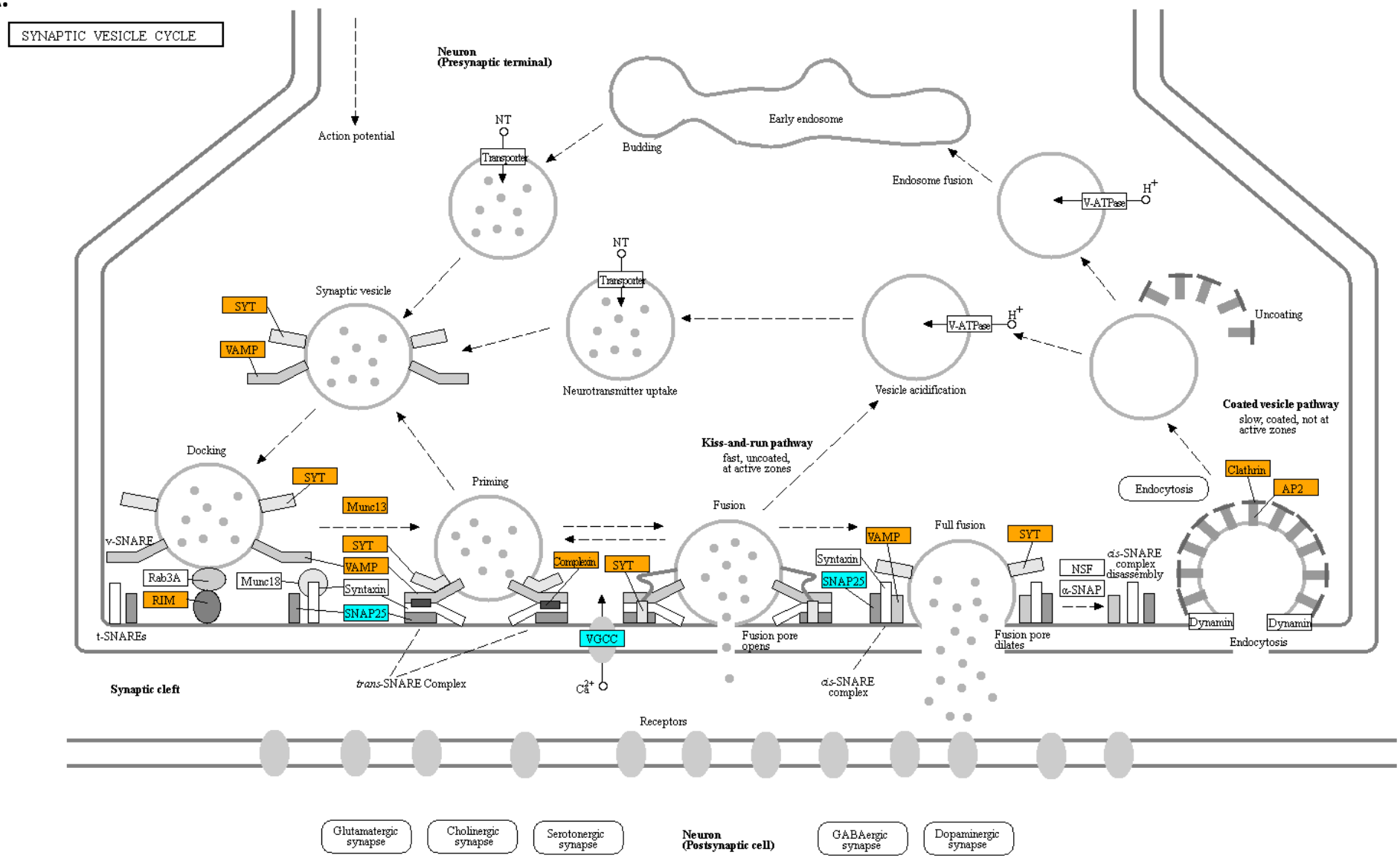

miR-133a

miR-128

Gene	KEGG Name
Syt-1	SYT
Vamp2	VAMP
Unc13a	Munc13
Rims1	RIM
Cplx2	Complexin
Ap2m1	AP-2
Clta	Clathrin
snap25	SNAP25
Cacna1a	VGCC

B.

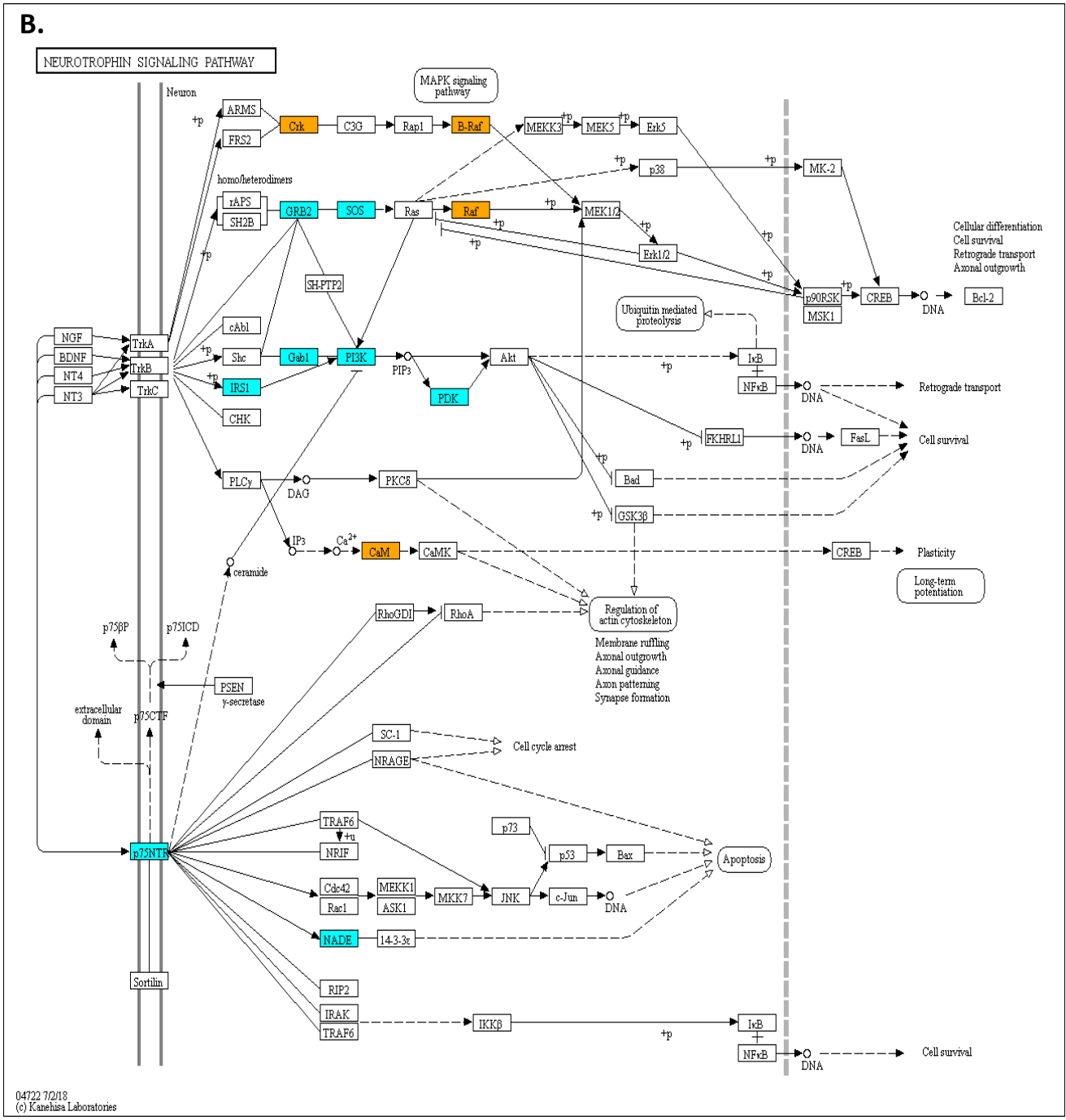

Gene	KEGG Name
Gab-1	Gab1
Grb-2	GRB2
Sos-1	SOS
Irs-1	IRS1
Ngfr	p75NTR
Ngfrap1	NADE
Pik3ca	PI3K
Pdpk1	PDK
Braf	B-raf
Crk	CRK
Calm-1	CaM

miR-133a

miR-128

C.

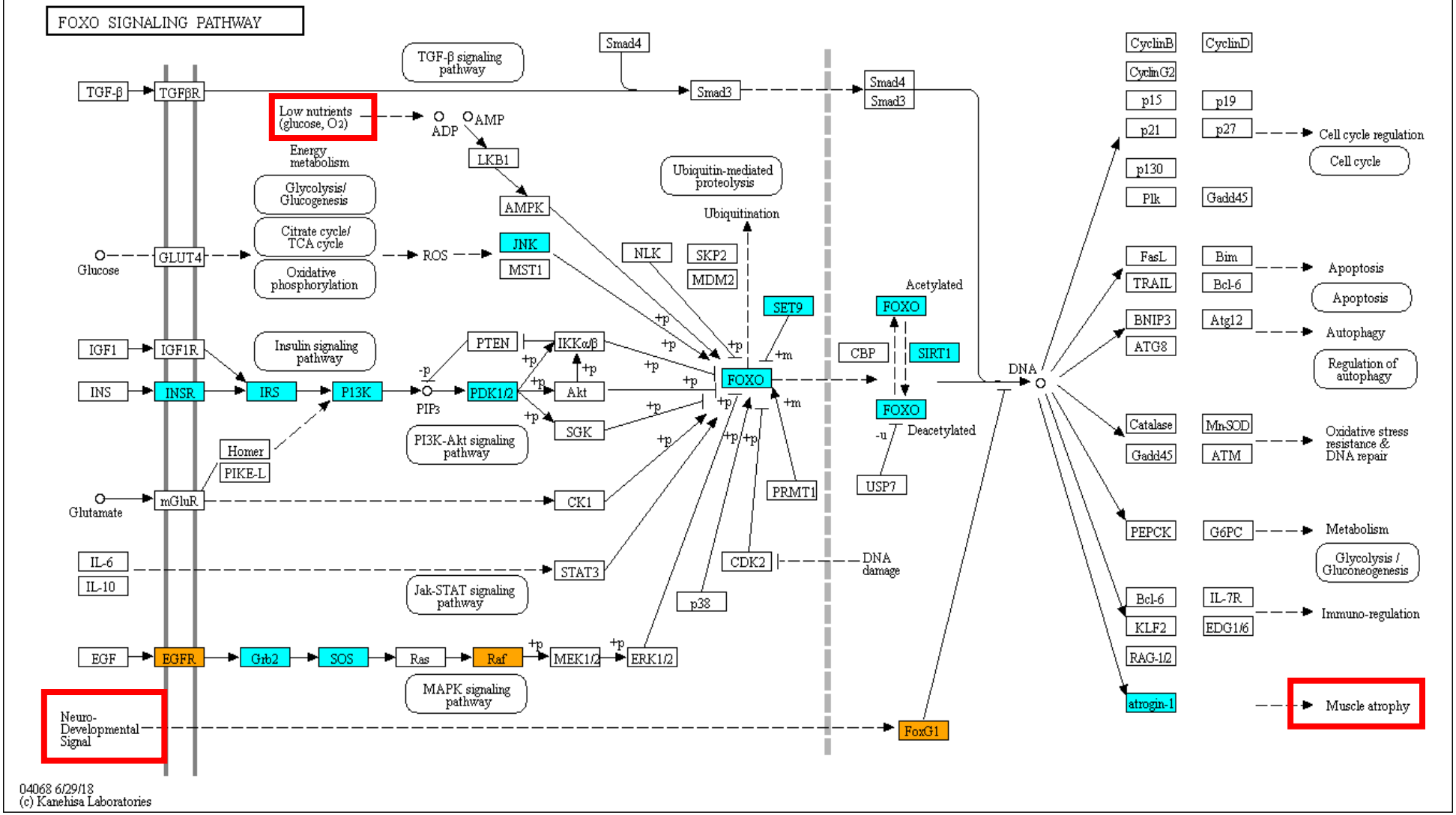

miR-133a

miR-128

Gene	KEGG Name
Grb-2	GRB2
Sos-1	SOS
Irs-1	IRS1
Insr	INSR
Pik3ca	PI3K
Pik3r1	PI3K
Pdpk1	PDK
Mapk10	JNK
Setd7	SET9
Foxo1	FOXO
Foxo4	FOXO
Sirt-1	SIRT1
Mapk10	JNK
Braf	B-raf
Foxg1	FoxG1
Efgr	EGFR

D.

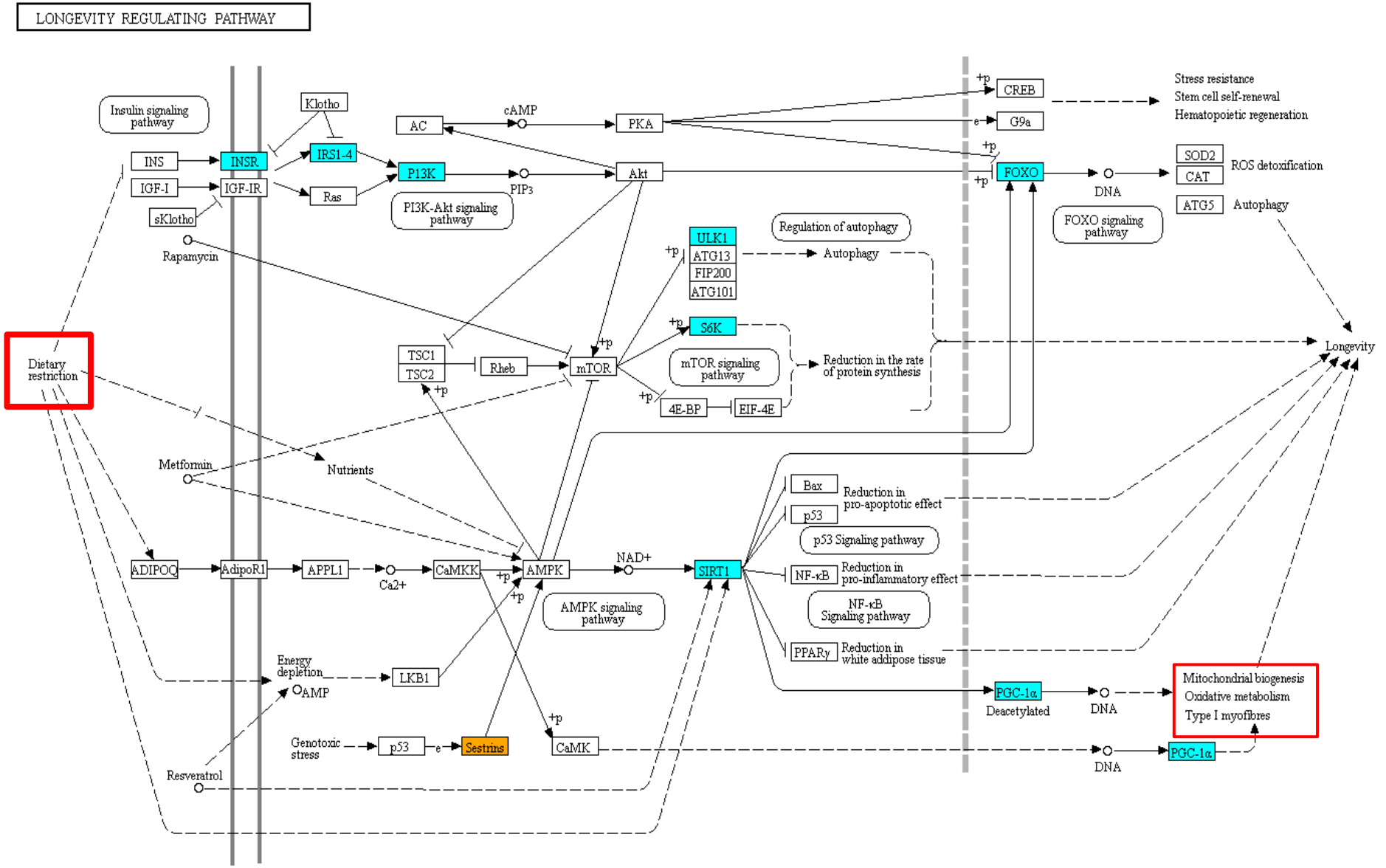

miR-133a

miR-128

Gene	KEGG Name
Ppargc1a	PGC1A
RPS6KB	S6K
Irs-1	IRS1
Insr	INSR
Pik3ca	PI3K
Pik3r1	PI3K
Foxo1	FOXO
Sirt-1	SIRT1
Ulk1	ULK1
Sesn1/3	Sestrin

Figure 4.3.4 Involvement of predicted target genes of miR-128 and miR-133a in signalling pathways. **A)** Synaptic vesicle cycle, **B)** Neurotrophin signalling pathway, **C)** FoxO signalling pathway and **D)** Longevity regulating pathway. Predicted target genes shown on a protein level are highlighted as cyan (miR-128) or orange (miR-133a) depending on the microRNA by which they are targeted. Signalling pathways adapted from KEGG PATHWAY database.

4.4 Discussion

The aim of this Chapter was to examine the expression levels of candidate microRNAs in skeletal muscle and peripheral nerve of 12-week old mice subjected to a normal or a low-protein diet at pre- or postnatal stages of development, for functional studies. Identification of candidate microRNAs with altered expression patterns in muscle and/or nerve may be responsible for changes of signalling molecules on an mRNA level. As such, genes targeted by microRNAs with dysregulated expression pattern, are predicted to have a downstream implication on the regulation of signalling pathways they are involved. Quantitative qPCR analysis from RNA isolated from muscle and nerve of 12 weeks old mice showed differences in the expression of miR-128 and miR-133a. Investigation of predicted target genes for both microRNAs indicated interaction between a group of genes involved in key signalling pathways, which control muscle:nerve cross-talk, muscle physiology and function and lifespan.

4.4.1 Expression of candidate microRNAs in muscle and nerve of 12-week old mice on a normal or protein-deficient diet pre- or postnatally

Quantitative PCR analysis of candidate microRNAs in TA muscle revealed no changes in the expression level of miR-199a, -199b, -181a, -181d and -378 in NLL mice. In contrary, expression analysis of miR-128 showed significant downregulation in the expression levels in TA muscle of both NLL and LNN mice, but no changes in miR-128 expression were observed in SN. Similarly, miR-133a was significantly downregulated in TA muscle of NLL mice, but not LNN mice where P value = 0.051. As seen with miR-128, expression of miR-133a in SN was not significantly different between the three experimental groups.

Data obtain from qPCR analysis suggest that a protein deficient diet at pre- or postnatal stages of development may have the potential to alter molecular mechanisms, such as microRNA expression. Specifically, altered microRNA expression appears to be tissue-specific, as both miR-128 and miR-133a show

significant differences in the expression levels in TA muscle but not in SN, which could indicate muscle-specific changes important for NMJ alterations or other mechanisms.

It is not surprising that miR-133a expression is affected in muscle but not in peripheral nerve, as miR-133 family is widely known as "myomiRs" due to high expression levels in skeletal muscle (reviewed in Horak *et al*. 2016). Involvement of miR-133 isoforms has been widely investigated in muscle *in vivo* (Chen *et al*. 2006; Deng *et al*. 2011; Zhang *et al*. 2014) and *in vitro* (Zhang *et al*. 2012; Feng *et al*. 2013). Studies have also examined the role of this microRNA in NMJ integrity during ageing (Valdez *et al.* 2014). Although there is some evidence of miR-133b involvement in functional recovery and regeneration of axons following peripheral nerve or spinal cord injury (Wu *et al.* 2011; Yu *et al.* 2011), the role of miR-133a in peripheral nerve has not been extensively investigated. Moreover, recent studies have shown increased expression of miR-133a in mouse spinal cord (Bak *et al.* 2008).

In contrast with miR-133a, miR-128 is mostly abundant in the CNS in mice (He at al. 2012). Higher expression of miR-128 has been recorded during development (Franzoni *et al.* 2015) and in cancer (reviewed in Li *et al.* 2013; Yu *et al.* 2017). Although a brain-enriched microRNA, miR-128 expression levels in skeletal muscle are the highest following those observed in CNS (Motohashi *et al.* 2013; Lek Tan *et al.* 2013). Recent studies carried out *in vitro* have highlighted the role of miR-128 in key signalling processes regulating skeletal muscle physiology in primary mouse myoblasts (Motohashi *et al.* 2013) and C2C12 myoblasts (Shi *et al.* 2015). In combination with our qPCR data from TA muscle of NLL and LNN mice showing downregulation of miR-128 expression levels, miR-128 is a promising candidate microRNA to investigate further in this study.

4.4.2 Investigation of miR-128 and miR-133a predicted target genes and their interactions using TargetScanMouse 7.1 and STRING database

Detailed information on miR-128 and miR-133a was obtained from miRBase. Mature microRNAs were identified as mmu-miR-128-3p and mmu-miR-133-3p accordingly. These two mature miRs were used in TargetScanMouse database to identify the list of predicted target genes. In total, 1097 predicted target genes carrying conserved sites for miR-128 binding were identified while 616 predicted target genes carrying conserved sited for miR-133 were identified. For miR-128, 19 predicted target genes were selected, of which 2 genes (Nrf1, Park2) were carrying only poorly conserved sites for miR-128 binding (**Table 4.1.2.1**). The rest 17 genes were carrying either only a conserved site or both conserved and poorly conserved sites. Similarly, for miR-133, 16 predicted target genes were of interest and only 1 of those (Tomm20) was carrying only a poorly conserved site for miR-133 binding (**Table 4.1.2.2**), while the rest were carrying a conserved only or both conserved and a poorly conserved site. Interestingly, miR-128 and miR-133 share 13 of the predicted target genes of interest, with each miR targeting either conserved or poorly conserved sites on the same gene transcript (Appendix**, Table A1 and A2**).

For miR-128, from the 19 predicted target genes only 17 are shown in the network as 2 genes (Ncam1 and Ncan) showed no interactions with the rest of the gene transcripts. Strongest interactions were recorded between the following transcripts: Syt1, Grb2, Gab1, Sos1, Ngfr, Ngfrap1, Pdgfra, Isr1, Insr, Foxo1, Foxo4, Sirt1 and Atrogin1. Gene transcripts Irs1 and Insr have been established as direct targets of miR-128, resulting in alterations in Irs1/Akt insulin signalling during myogenesis (Motohashi *et al.* 2013). Gene transcript Grb2 has been implicated in NMJ homeostasis (Gingras *et al*. 2016) while Sos1 and Pdgfra mutations have been associated with severe embryonic phenotype and skeletal defects (Wang *et al.* 1996; Fantaouzzo and Soriano, 2014). Previous studies have shown that Ngfr (also known as p75NTR) and Ngfrap1 (also known as NADE or Bex3) are able to induce neurotrophin-mediated apoptosis of neuronal cells even during normal development in mice (Mukai *et al.* 2002). However, it has been

suggested that Ngfr may have a more diverse role depending on the interactions with other neurotrophin receptors (reviewed in Chen *et al.* 2009). Atrogin-1 gene transcript (also known as Fbxo31) has been a well-established gene associated with muscle atrophy (Botine *et al.* 2001; Gomes *et al.* 2001; reviewed in Yang *et al.* 2015) and upregulation of this gene has been reported in the cartilage and chondrocytes of osteoarthritic mice (Kim *et al.* 2017). Transcription of Atrogin-1 is closely dependent on activation of FoxO activation (Botine *et al.* 2001; Gomes *et al.* 2001). In contrary, Sirt-1 is capable of blocking FoxO activity leading to inhibition of muscle atrophy (Lee and Goldberg, 2013).

Network analysis for miR-133 predicted target genes revealed strongest interactions between the following genes: Clta, Ap2m1, Vamp2, Syt1, Cplx2, Rims1 and Unc13a. Clta gene transcript encodes protein clathrin and along with AP2 (adaptor protein 2, encoded by Ap2m1) it forms a protein complex coating the outer surface of the vesicles during clathrin-mediated endocytosis (reviewed in Owen *et al.* 2004). Syt1 gene transcript, predicted target of both miR-128 and miR133, encodes synaptotagmin 1 (SYT-1) protein, involved in calcium-dependent neurotransmitter release and synaptic vesicle endocytosis (Poskanzer *et al.* 2003; Yao *et al.* 2011). Interestingly, Syt-1 is highly expressed in the brain during development and mutations in Syt-1 gene have been associated with neurodevelopmental disorders in humans (Baker *et al.* 2018). Another component of Ca^{2+}-dependent exocytosis, complexin 2 protein (encoded by Cplx-2 gene) is essential for normal neurological function. Mice lacking of complexin 2 develop cognitive abnormalities and motor deficits (Glynn *et al.* 2003). Vamp-2 gene (also known as Syb2) is a component of the protein complex SNARE, required for efficient neurotransmission *via* synaptic vesicles (Liu *et al*. 2015). Studies in mice have shown that even moderate alteration on Vamp2 expression could impair neurotransmission (Koo *et al.* 2015). Moreover, Vamp2 homozygous knock-out mice did not survive following birth and they exhibited profound changes in their body shape but no developmental abnormalities (Schoch *et al.* 2001). Release of neurotransmitters through exocytosis also requires the proteins Rims1 and Unc13a (Kaeser *et al.* 2012). Knock-out mice for Rim1α

isoform manifested dysregulated presynaptic plasticity while depletion of both Rim1α and Rim1β isoform in mice resulted in increased lethality in early postnatal life (Kaesar *et al.* 2008). Similarly, deficiency of Unc13 in mice results in immediate paralysis and death at birth. Despite the severe phenotype the NMJ site of these mice display no apparent morphological alterations, however the number of the sites and the motoneurons they originate from are substantially altered (Varoqueaux *et al.* 2005).

Evidence from previous studies suggest that a number of the predicted target genes of interest showing strong interactions may have an impact on metabolic mechanisms and neuromuscular communication. This was further investigated by exploring the metabolic processes those genes are involved at.

4.4.3 Signalling pathway analysis of miR-128 and miR-133 predicted target genes using KEGG PATHAWAY Database

In order to elucidate the impact of altered expression of miR-128 and miR-133a, metabolic pathway analysis was performed using KEGG Pathway Database. Assessment of metabolic pathways was used for the prediction of potential dysregulation of key mechanisms due to imbalances on specific protein molecules, caused by altered levels of their gene transcript in a tissue.

A number of predicted target genes of miR-128 and miR-133 showed strong interactions, as seen in **Figures 4.3.3.1** and **4.3.3.2**. When those predicted target genes were further investigated using KEGG Pathway database, most of them appeared to participate in the same metabolic pathway. Some of those genes were also seen in more than one metabolic pathway. Specifically, for miR-133, all the predicted target genes with strong interactions are involved in the synaptic vesicle cycle, shown in **Figure 4.3.4 A.** Furthermore, 2 more predicted target genes from miR-128 are also seen in the synaptic vesicle cycle, Snap25 and Cacna1a (also known as VGCC). It is noteworthy that Syt1 is a predicted target gene with preferential conserved binding sites for both miR-128 and miR-133a as

seen in TargetScanMouse database. These data suggest that downregulation of the predicted target genes, due to overexpression of miR-133, may impede endocytosis of the vesicles or inhibit the formation of the SNARE complex and therefore the fusion of the vesicles and release of neurotransmitters (reviewed in Jan and Fasshauer, 2012). Downregulation of the proteins in SNARE complex may lead to neurodegeneration similar to that seen during ALS while deletion of these proteins (Liu *et al.* 2015). In contrast, downregulation of miR133 could potentially result in overexpression of these proteins. One example from published data is the overexpression of Munc-18 protein, part of SNARE complex, which has been linked to schizophrenia-related behaviour in mice (Urigüen *et al.* 2013). Although several studies have demonstrated the adverse effects of SNARE proteins downregulation in mice, there is not much evidence for overexpression of those proteins. Therefore, the implications of a potential upregulation in the gene transcript in the case of downregulation of specific microRNAs can only be speculated.

Contrary to miR-133, miR-128 predicted target genes with the strongest interactions in the network are seen in several different metabolic pathways. Previous studies have shown the association of predicted target genes of miR-128 with pathways in cancer, MAPK pathway and neurotrophin pathway among others (Ching and Ahmad-Annuar, 2015). In line with these data, KEGG analysis shows that a number of the target genes of interest were involved in the neurotrophin signalling pathway (**Figure 4.3.4 B**). A study from Motohashi *et al.* has identified Irs1, Insr, and Pi3kr1 (subunit of PI3K) gene transcripts as direct targets of miR-128 (Motohashi *et al.* 2013). Among the predicted target genes seen in the neurotrophin pathway is also Pdpk1 gene encoding PDK, a master kinase responsible for the phosphorylation and therefore activation of AKT. Although complete lack of PDK in mice results in lethality at embryonic stages, lower protein levels have been linked to smaller body size during development (Lawlor *et al.* 2002). Of particular interests were the predicted target genes Ngfr (encoding p75NTR), Ngfrap1 (encoding NADE), Grb-2, Gab-1 and Sos-1. NGFR, predicted target of miR-128 and miR-133, is a lower affinity receptor for binding

of certain neurotrophins and pre-neurotrphins, including NGF and BDNF (reviewed in Chen *et al.* 2009). NGFR expression differs between organisms and increased expression levels have been noted during development or in pathological conditions associated with neural cell death (reviewed in Chao, 2003). Increased levels of expression during development have been associated with regulation of neuronal innervation of target cells and subsequent elimination of neuronal cells that failed to innervate their target (reviewed in Majdan and Miller, 1999). The role of NGFR during development in conjunction with our data of miR-128 downregulation and NMJ morphology observed in Chapter 3 could agree with the hypothesis that NLL mice may exhibit a developmentally delayed NMJ phenotype. NGFR has been previously described to induce cell apoptosis *via* activation of NADE protein (encoded by Ngfrap1) following binding of NGF to the NGFR-NADE complex (Mukai *et al.* 2002). While Ngfr and Ngfrap1 encode proteins involved in cell death, the role of Grb-2, Gab-1 and Sos-1 appear to be different. Gab-1 protein expression in both skeletal muscle and Schwann cells in peripheral nerves has been associated with postnatal NMJ maturation (Young Park *et al.* 2017). Moreover, Grb-2 and Sos-1, involved in Ras signalling, mediate cell survival, proliferation and differentiation (Mazzon *et al.* 2018). Specifically, recent studies show enrichment of Grb-2 at the post-synaptic site of the NMJ, and the importance of Grb-2 in the formation of AChR clusters (Gingras *et al.* 2016). Collectively, miR-128 predicted target genes within the neurotrophin signalling pathway are involved in cell apoptosis or cell survival. In the event of upregulation of those gene transcripts due to downregulation of miR-128, we speculate that the balance between neurotrophin-mediated cell survival/apoptosis could shift, but towards which direction requires further investigation.

Predicted targets Grb-2, SOS-1, Insr, Irs-1, Pdpk1 and Pi3k isoforms (Pik3r1, Pik3ca) are also involved in FOXO signalling pathway, along with some miR-133 target genes (**Figure 4.3.4 C**). Central protein molecules of FOXO signalling pathway, FOXO-1, FOXO-4 and Sirt-1 are also predicted target genes of miR-128. Interestingly, Sirt-1 gene transcript is targeted by both miR-128 and miR-133a,

and carries a conserved seed sequence for preferential binding of miR-133 (as seen in TargetScanMouse). A study from Lee and Goldberg (2013) shows that Sirt-1 levels fall dramatically following food deprivation only in Type II-rich skeletal muscles such as TA and EDL, contributing to increased muscle atrophy. Sirt-1 can promote deacetylation of FOXO proteins and therefore trigger muscle wasting, but overexpression of Sirt-1 has been reported to inhibit FOXO activity and protect the muscle from atrophy. This dual role of Sirt-1 makes it a crucial regulator of skeletal muscle atrophy (Lee and Goldberg, 2013). On the other hand, Atrogin-1 gene transcript itself is amongst the predicted target genes of miR-128. Gomez *et al.* have previously reported a dramatic upregulation of Atrogin-1 mRNA levels in GTN muscle following fasting, when compared to mRNA levels of other tissues such as brain and liver (Gomez *et al.* 2001). Although the selected miR-128 predicted targets appear to be most prevalent in FOXO signalling pathway, a few predicted target genes of miR-133 are also found. FoxG1 gene transcript, encoding FOXG1 protein, is one of the predicted target genes of miR-133, carrying a binding site for preferential binding of miR-133 (as seen in TargetScanMouse). This protein appears to act independently of the rest of FOXO components, as seen in **Figure 4.3.4 C.** FoxG1 acts as a transcription factor crucial to the regional subdivision of the developing brain (Boggio *et al.* 2016). Although complete depletion of FoxG1 is lethal, mutations have been associated with neurodevelopmental disorders (Boggio *et al.* 2016), while overexpression of FOXG1 has been linked to autism (Mariani *et al.* 2015). Apart from its localization to the nucleus, FOXG1 can also translocate to the mitochondria, controlling energy biogenesis and other mitochondrial functions (Pancrazi *et al.* 2015).

Gene transcripts Insr, Irs-1, Pi3k isoforms (Pik3r1, Pik3ca), FoxO-1, FoxO-4 and Sirt-1 appear also appear in Longevity regulation pathway. This is of no surprise considering that major metabolic pathways are involved in the regulation of longevity, including but not limited to insulin pathway, PI3K/AKT, FOXO, mTOR, AMPK and p53 signalling pathways (**Figure 4.3.4 D**). Gene transcripts not seen in the rest of the pathways are Ulk1, Rps6kb (encoding S6K) and Ppargc1a

(encoding PGC-1a). PGC-1a is a transcription factor which may act either antagonistically or in cooperation with FOXO molecules, depending on the tissue and the function it is involved (Lee and Goldberg, 2013). PGC-1a expression appears to be partly regulated by Sirt-1, acting as an inhibitor of muscle atrophy by inhibition of FOXO activity (Sandri *et al.* 2006). Studies have reported involvement of PGC-1a in mitochondria biogenesis and function (reviewed in Fernandez-Marcos and Auwerx, 2011), fatty acid oxidation (Vega *et al*. 2000) and the formation of type-I (or slow-twitch) muscle fibres in skeletal muscle (Lin *et al.* 2002). Thus, PGC-1a has been reported as anti-ageing factor, promoting longevity (Reviewed in Satoh and Imai, 2004). ULK1 protein in its phosphorylated form is involved in the regulation of autophagy in response to starvation (Lee and Tournier, 2011). ULK1 is regulated either by mTOR or by AMPK, depending on the nutrient availability (Kim *et al.* 2011). ULK1 interacts directly with mTOR during in conditions of high-nutrient availability (Hosokawa *et al.* 2009). However, during starvation, Ulk1 is activated *via* phosphorylation by AMPK, activating autophagy process (Kim *et al.* 2011). Activation of autophagy *via* AMPK-mediated phosphorylation and activation of ULK1 is necessary for stem-cell renewal and pluripotency and any disruption to this process may compromise the role of ES cells (Gong *et al.* 2018). Disruption of ULK1 phosphorylation *via* AMPK during starvation conditions may also impair mitochondrial biogenesis and cell survival, thus affecting energy biogenesis (Egan *et al.* 2011). Due to its nutrient-dependent activation, autophagy may be a potential target mechanism in our study, being differentially regulated in mice on a protein-deficient diet at different stages of development. S6K, which is involved in the regulation of protein synthesis, is a kinase also dependent on phosphorylation for its activation, mainly *via* mTOR (Zhang *et al.* 2014). Studies have shown the role of S6K in the regulation of protein synthesis and force generation in skeletal muscles, without causing an increase in skeletal muscle mass (Marabita *et al.* 2016). Interestingly, mice lacking of S6K have lower body weight and smaller size (Shima *et al.* 2016). Moreover, whole body $S6K1^{-/-}$ mice demonstrated increased lifespan, with female mice also showing an increase in the maximum lifespan greater than the male mice (Selman *et al.* 2009).

Overexpression of several proteins involved in the longevity pathway appears to have a beneficial effect on mouse lifespan and act as anti-ageing mechanisms. An example of such proteins is IRS-1, which was elevated in the skeletal muscle of mice following a low-protein diet postnatally, implying improved insulin sensitivity in those mice (Chen *et al*. 2009). Evidence gathered from previously published studies highlighting some protein molecules (e.g. S6K, ULK-1) which could potentially explain the phenotype observed in NLL mice and LNN mice. However, due to sample processing prior to use in experimental analysis it was not possible to investigate the levels of certain molecules any further. Whether alterations in the levels of these proteins and their gene transcripts may occur due to protein-deficient diet and/or dysregulation of miR-128 and miR-133 expression remains unknown and needs to be further investigated.

Chapter 5

Gain- and loss-of-function of miR-128 and miR-133a in C2C12 cells

5.1 Introduction

MicroRNAs often show tissue-specific or tissue-enriched expression. In skeletal muscle tissue, two examples of such microRNAs are miR-128 and miR-133a.

In a study from Lee *et al.* microRNA-128 shows highest expression levels in skeletal muscle tissue (Lee *et al.* 2008). MicroRNA-128 has been described as a regulator of skeletal muscle development *via* targeting of myostatin in C2C12 cells (Shi *et al.* 2015). Direct target genes of miR-128 also regulate myogenesis through insulin signalling/AKT pathway (Motohashi *et al.* 2013). Furthermore, miR-128 has been associated with the maintenance of quiescent state of muscle side population (SP) cells, a distinct type of muscle stem cells, as well as with the regulation of the differentiation of those cells in multiple cell types (Motohashi *et al.* 2012). Although some studies provide strong evidence of miR-128 involvement in skeletal muscle development, the exact role of miR-128 in differentiated skeletal muscle cells has not been described.

MicroRNA-133, also known as one of the "myomiRs" is specifically expressed in skeletal and cardiac muscle (Chen *et al.* 2006). Previous studies have demonstrated the regulation of skeletal muscle cell proliferation and differentiation by miR-133 either regulation of its expression levels from myogenic factors such as MyoD (Chen *et al.* 2006; Rao *et al.* 2006) or *via* regulation of Erk1/2 signalling pathway (Feng *et al.* 2013). *In vivo* studies have shown increased expression levels of miR-133 in the skeletal muscle of *mdx* mice; However, suppression of miR-133 function had no effect on skeletal muscle development and function (Deng *et al.* 2011). A study from Chen *et al.* 2009 demonstrated the regulation of myogenic fate *via* direct targeting of UCP2 by miR-133a, a member of the uncoupling proteins family involved in the inhibition of muscle differentiation and promotion of myoblast proliferation (Chen *et al.* 2009).

Although many studies have investigated the role of miR-128 and miR-133a in skeletal muscle development, the implication of those two microRNAs in

terminal differentiation and maintenance of skeletal muscle cells has not been fully explored. Furthermore, investigation of the role of these two microRNAs in C2C12 myoblast and myotube cell behaviour could provide further understanding on the mechanisms involved in loss of myofibres and reduced muscle force in 12-week old mice on a low-protein diet pre- or postnatally. The aim of this chapter was to investigate the effect of gain- and loss-of-function of miR-128 and miR-133a in C2C12 cell proliferation, viability, mitotoxicity and differentiation. Results of these studies will provide an insight on the impact of imbalances in the expression levels of miR-128 and miR-133a in adult skeletal muscle *in vivo*.

5.2 Methods

5.2.1 Culture and differentiation of C2C12 cells

C2C12 cells were retrieved from LN_2 and thawed in a 37^{o}C water bath until there was no ice present in the vial. Cell suspension from the cryovial was mixed with 3 mL of pre-warmed growth media (Chapter 2, Section 2.16) and centrifuged immediately at 1,500 rpm for 5 min to discard freezing media containing DMSO. The supernatant was discarded and the cell pellet was resuspended in 10 mL of growth media (GM_{C2C12}) and plated into a T75 flask (Corning). The cells were then incubated in a humidified incubator at 37^{o}C with 5% CO_2 until they became confluent. When 70-80% confluency was reached, the cells were passaged 1:10 into fresh T75 flasks as described in Chapter 2, Section 2.17.

For C2C12 cell differentiation, cells were seeded into a 12-well plate at a confluency of 50,000 cells/well (13,158 cells/cm^2), to be used for cell imaging following transfections (Chapter 2, Section 2.19). The remaining cells were seeded into three 6-well plates, to be used for RNA and protein isolation following transfections with scrambled sequence, miR-128 mimic, AM-128, miR-

133a mimic and AM-133a. Plates were incubated in GM_{C2C12} until fusion of myoblasts was evident and first signs of myotube formation were observed. Cells from all plates were then transfected according to the protocol in Chapter 2, Section 2.21. Following 48 h of transfections, C2C12 cells were harvested for RNA and protein isolation, as described in Chapter 2, Section 2.20. C2C12 myotubes at Day 7-11 of differentiation were stained for imaging and determination of their phenotype as described in Chapter 2, Section 2.22.

5.2.2 Image analysis of C2C12 myotubes following transfections with miR-128 and miR-133a

Differentiated C2C12 cells were immunostained with MF20 antibody (myosin heavy chain II) and DAPI following transfections with either miR-128 or miR-133a as described in Chapter 2, Section 2.22. Cells were imaged using a Nikon Ti Live cell imaging microscope under x20 magnification. Myotube diameter, myotube area, nuclei per myotube and fusion index were analysed using ImageJ software (Chapter 2, Section 2.23).

5.2.3 Assays for cell proliferation, viability and mitochondrial toxicity following transfections with miR-128 or miR-133a

C2C12 cells were seeded on 96-well plates for use in proliferation, viability and mitotoxicity assays. For proliferation and viability, C2C12 cells were plated as described in Chapter 2, Section 2.27 (for proliferation assay) and Section 2.28 (for cytotoxicity assay). Cells were allowed to incubate for 24h following plating before they were transfected with scrambled sequence, miR-128 mimic, AM-128 or scrambled sequence (cholesterol conjugated), miR-133a mimic, AM-133a. Both proliferation and cytotoxicity assay were performed 48h following transfections. Experimental protocol and analysis of the data obtained from both assays were performed according to manufacturer's instructions. Mitotoxicity assay was performed as described in Chapter 2, Section 2.19, following

transfection of C2C12 with scrambled, miR-128 mimic and AM-128. Interpretation of data was performed following the manufacturer's instructions. Values recorded following measurement of fluorescence absorbance indicated the potential cytotoxic effect of miR-128 in C2C12 myoblasts, fluorescence measurement was followed by measurement of luminescence, which indicated the potential mitotoxic effect of miR-128 in C2C12 myoblasts. To determine whether miR-128 is a mitotoxic compound, fold-changes in mitotoxicity were assessed in comparison with the cytotoxicity values recorded.

5.2.4 Statistical Analysis

Statistical analysis was performed using Graphpad 5 (Graphpad Software, San Diego, USA). Analysis of the data was performed using One-Way ANOVA, with Dunnett's post-hoc analysis, using scrambled-treated cells as the control group Distribution data were analysed using Chi-square (χ^2) test. Data collected from mitotoxicity assay were analysed using Two-Way ANOVA, with Bonferroni post-hoc analysis. Data from the cytotoxicity and mitotoxicity assays were presented as fold-changes compared to the control (scrambled-treated cells) group. Data were represented as mean ± SEM. N number represents wells used per transfection condition.

5.3 Results

5.3.1 The effect of miR-128 gain- and loss-of-function on C2C12 myotube phenotype

C2C12 myotubes transfected with scrambled sequence (control), miR-128 mimic (miR-128) and miR-128 inhibitor (AM-128) and stained with MF20 and DAPI are shown in **Figure 5.3.1.1 A.** C2C12 myotubes transfected with miR-128 mimic (miR-128 overexpression) showed formation of a network of long and uniform myotubes, with nuclei fused within the myotubes seen spread across

the length of the cells. C2C12 myotubes transfected with AM-128 (miR-128 inhibitor) appeared to be fewer in number and they displayed a circular-like morphology rather than an elongated morphology similar to that seen in miR-128 transfected cells. Several occurrences of C2C12 with spherical appearance (arrows) rather than a long tube-like morphology were observed, which also appeared to have more nuclei/myotube. Analysis of C2C12 myotube diameter revealed no changes in myotube width following miR-128 overexpression or inhibition (**Figure 5.3.1.1 B**). Assessment of myotube area revealed a slight increase in the number of MF20-positive myotubes within each field of view, following overexpression of miR-128 (P=0.058; **Figure 5.3.1.1 C**). Furthermore, C2C12 fusion index is higher following overexpression and inhibition of miR-128, when compared to the control (Scr) group (**Figure 5.3.1.1 D**).

Distribution analyses of C2C12 myotube diameter and number of nuclei present per myotube are shown in **Figure 5.3.1.2**. Myotube diameter analysis indicated that the number of C2C12 myotubes transfected with miR-128 was higher in the diameter range of 20-40 µm, but no significant shift in the size distribution was recorded (**Figure 5.3.1.2 A**). Distribution analysis of the number of nuclei on myotubes of different diameter range revealed a proportional increase in the number of nuclei per myotubes with increase in of their diameter in all groups (**Figure 5.3.1.2 B**).

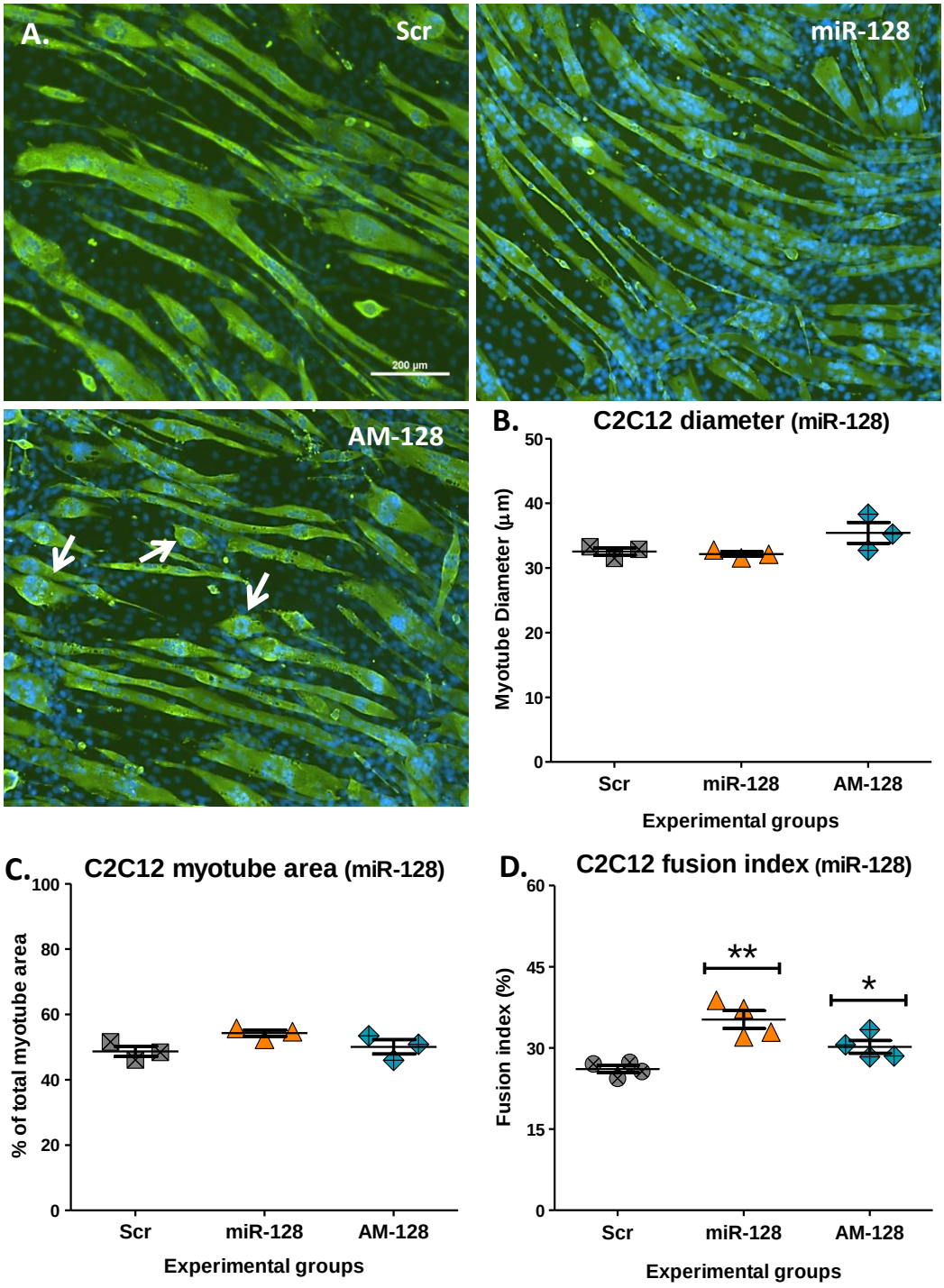

Figure 5.3.1.1 Gain- and loss-of-function of miR-128 in C2C12 myotubes. **A)** C2C12 myotubes transfected with Scr, miR-128 or AM-128 as indicated; myotube formation was established with myosin heavy chain and nuclei immunostaining (MF20=Green; DAPI=Blue). **B)** Myotube diameter of transfected C2C12 myotubes with ≥2 nuclei. **C)** Quantification of total C2C12 myotube area expressed as a percentage of total area per field of view. **D)** Fusion index of C2C12 cells,

expressed as a % of nuclei in within the myotubes to total nuclei counted in each field of view. *represent significant differences compared with the Scr (control) group, *P≤0.05, *** P≤0.001 (*mean ± SEM*; *n*=3-4*; One-Way ANOVA with Dunnett's post-hoc analysis*). Representative images shown.

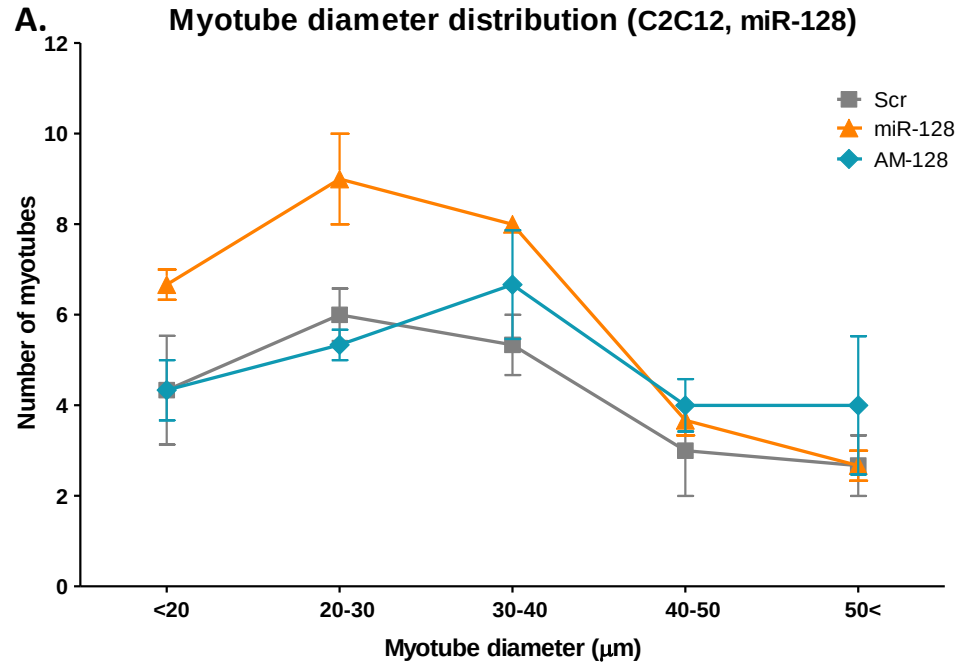

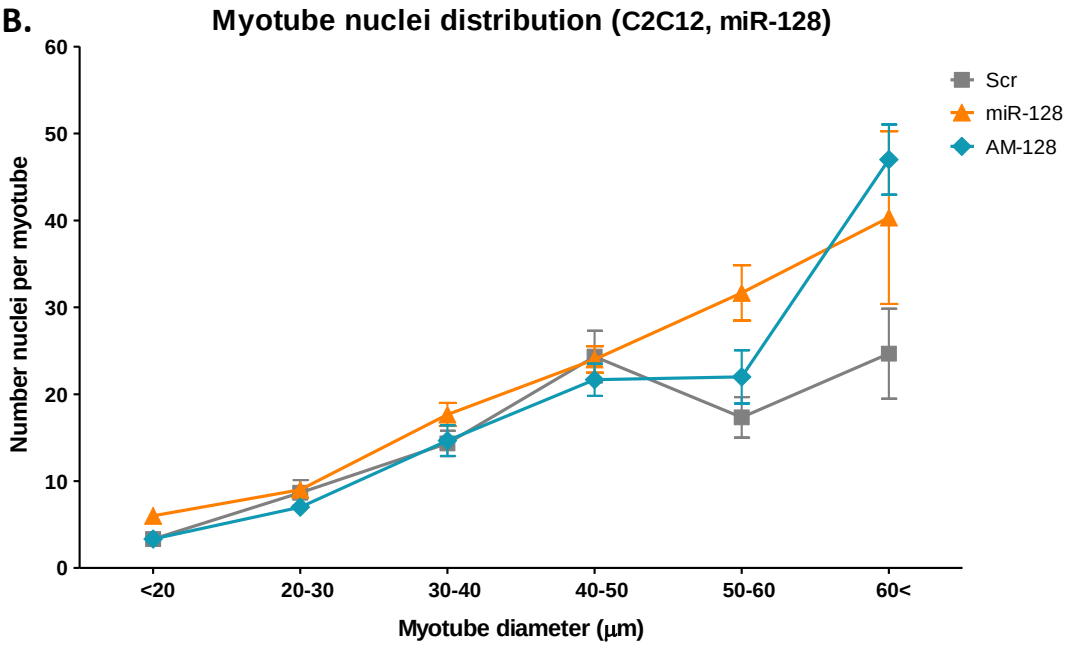

Figure 5.3.1.2 Distribution analysis of **A)** myotube diameter and **B)** number of nuclei in C2C12 myotubes transfected with Scr, miR-128 and AM-128. *represent significant differences compared with the Scr (control) group (*mean ± SEM*; *n*=3*; Chi-square test*).

5.3.2 The effect of miR-133a gain- and loss-of-function on C2C12 myotube phenotype

C2C12 myotubes transfected with miR-133a mimic (miR-133a) and miR-133a inhibitor (AM-133a) are shown in **Figure 5.3.2.1 A.** Myotubes transfected with miR-133a mimic (miR-133a) appeared to be thinner in diameter compared to those transfected with miR-133a inhibitor (AM-133a). Myotube analysis showed a significant increase in the diameter of myotubes (**Figure 5.3.2.1 B**) and a larger area occupied by myotubes per field of view following transfection with AM-133a, in comparison to the control group (Scr) (**Figure 5.3.2.1 C**). Fusion index of C2C12 myotubes transfected with miR-133a or AM-133a revealed no significant difference compared to the control group (Scr) (**Figure 5.3.2.1 D**).

Examination of myotube diameter distribution revealed the prevalence of myotubes with diameter $\leq$30 μm in miR-133a transfected cells compared to the rest of the groups, but no significant shift was observed in diameter distribution between the groups (**Figure 5.3.2.2 A**). Similarly, myotube nuclei distribution showed no differences between the groups, indicating a proportional relationship between number of myotube nuclei number and myotube diameter (**Figure 5.3.2.2 B**).

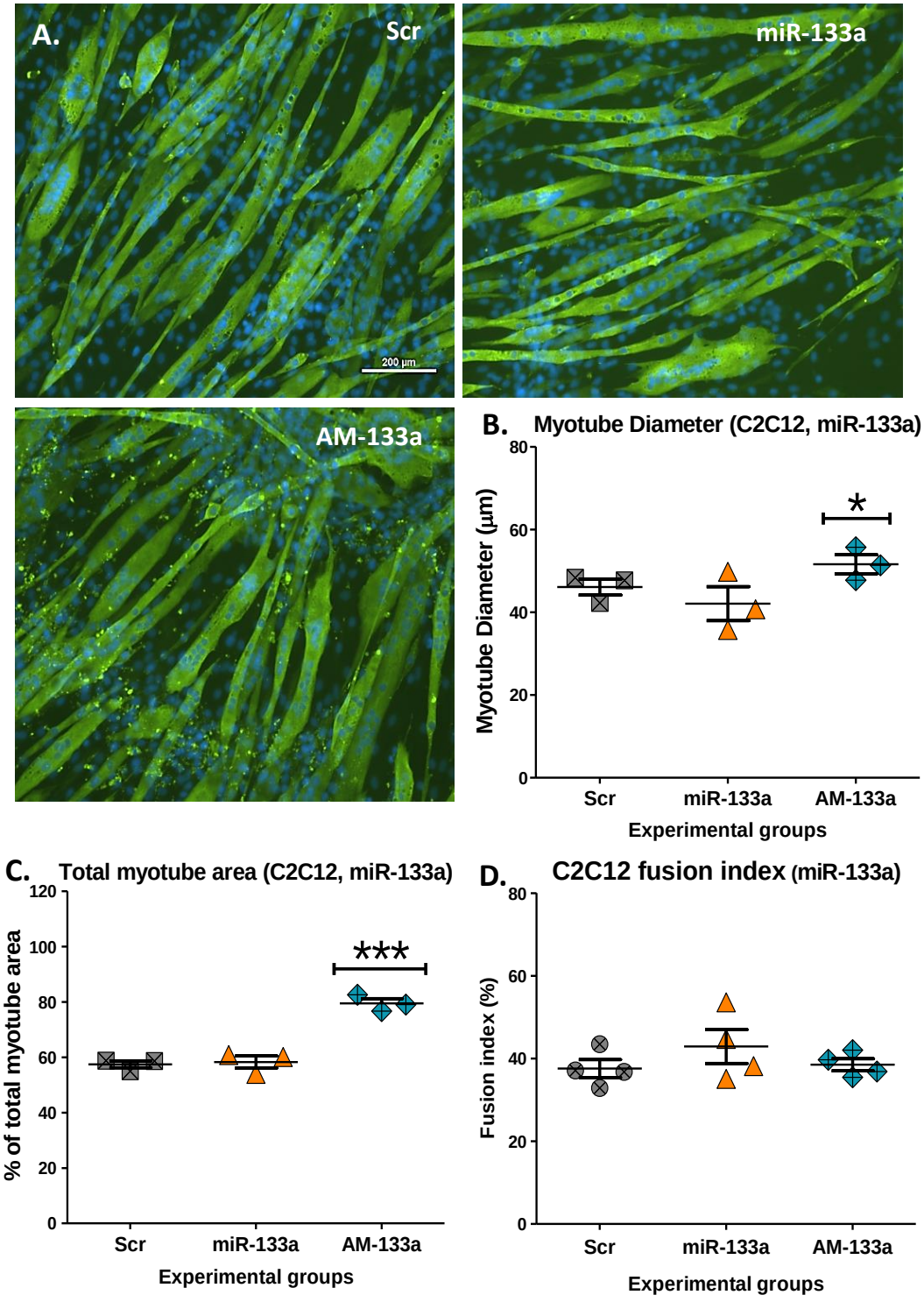

Figure 5.3.2.1 Gain- and loss-of-function of miR-133a in C2C12 myotubes. **A)** C2C12 myotubes transfected with miR-133a or AM-133a as indicated; myotube formation was established with myosin heavy chain and nuclei immunostaining (MF20=Green; DAPI=Blue). **B)** Myotube diameter of transfected C2C12 myotubes with ≥2 nuclei. **C)** Quantification of total C2C12 myotube area expressed as a

percentage of total area per field of view. **D)** Fusion index of C2C12 cells, expressed as a % of nuclei in within the myotubes to total nuclei counted in each field of view. *represent significant differences compared with the Scr (control) group, *P≤0.05, ***P≤0.001 (*mean ± SEM*; *n*=3*; One-Way ANOVA with Dunnett's post-hoc analysis*). Representative images shown.

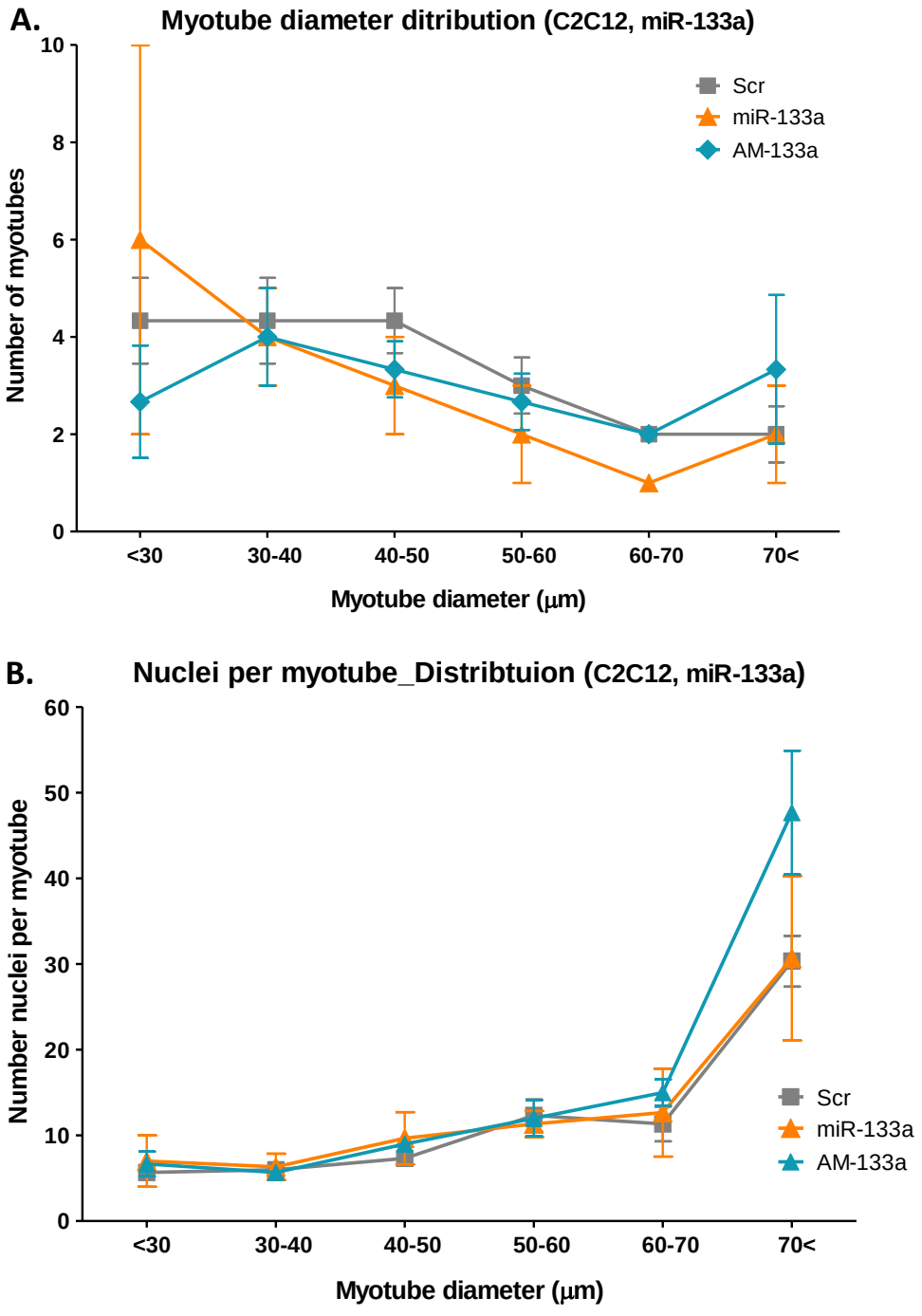

Figure 5.3.2.2 Distribution analysis of **A)** Myotube diameter and **B)** Number of nuclei in C2C12 myotubes transfected with miR-133a and AM-133a. Scr served as control for statistical comparison (*mean ± SEM*; *n*=3*; Chi-square test*).

5.3.3 The effect of gain-of-function and loss-of-function of miR-128 and miR-133a on C2C12 myoblast proliferation

CCK-8 proliferation assay analyses from C2C12 myoblasts following miR-128 and miR-133a transfections are shown in **Figure 5.3.3.** Proliferation rate of C2C12 myoblasts following miR-128 overexpression and inhibition was significantly reduced compared to the control (Scr) group (**Figure 5.3.3 A**). Similarly, both miR-133a and AM-133a transfections appeared to have a positive effect in the proliferation of C2C12 myoblasts, with the number of cells being significantly increased after overexpression and inhibition of miR-133a (**Figure 5.3.3 B**).

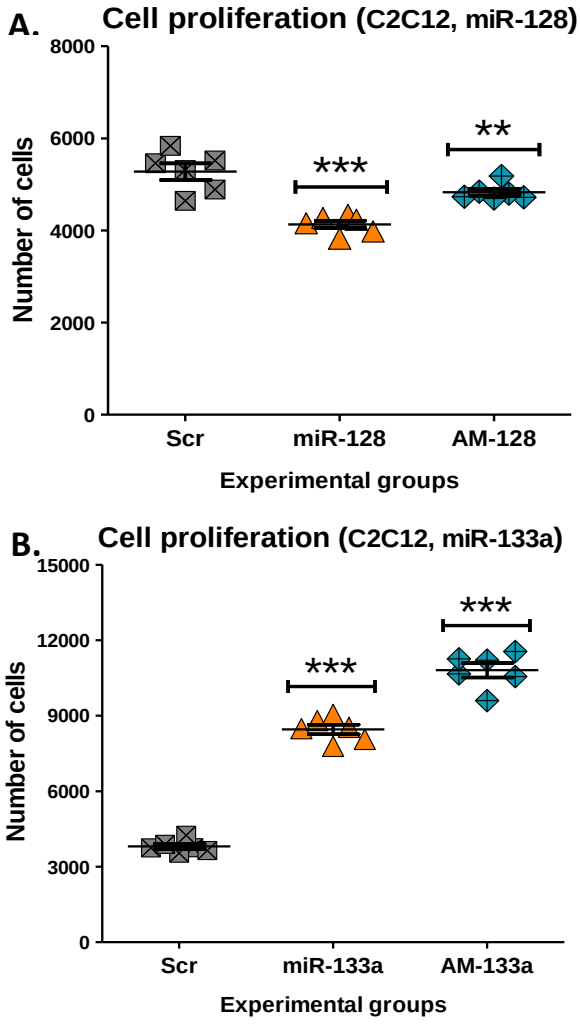

Figure 5.3.3 CCK-8 proliferation assay of C2C12 myoblasts following transfection with miR-128 or miR-133a. **A)** C2C12 myoblast number following transfection with Scr, miR-128 or AM-128. **B)** C2C12 myoblast number following transfection with Scr, miR-133a or AM-133a. *represents significant differences compared with the Scr (control) group, **P≤0.01, ***P≤0.001 (*mean ± SEM*; *n*=6*; One-Way ANOVA with Dunnett's post-hoc analysis*).

5.3.4 The effect of gain-of-function and loss-of-function of miR-128 and miR-133a in C2C12 myoblast viability

Analyses of CytoTox 96 assay on C2C12 myoblast following transfection with miR-128 or miR-133a is shown in **Figure 5.3.4.** C2C12 viability was determined based on cell death (expressed as % cytotoxicity) following transfections with either miR-128 or miR-133a. C2C12 myoblast cell death was significantly higher following both overexpression and inhibition of miR-128 (miR-128, AM-128) compared to the Scr transfected cells (**Figure 5.3.4 A, C**). Cell death in C2C12 myoblasts transfected with miR-133a mimic was significantly lower compared to the rest of the groups (**Figure 5.3.4 B, D**).

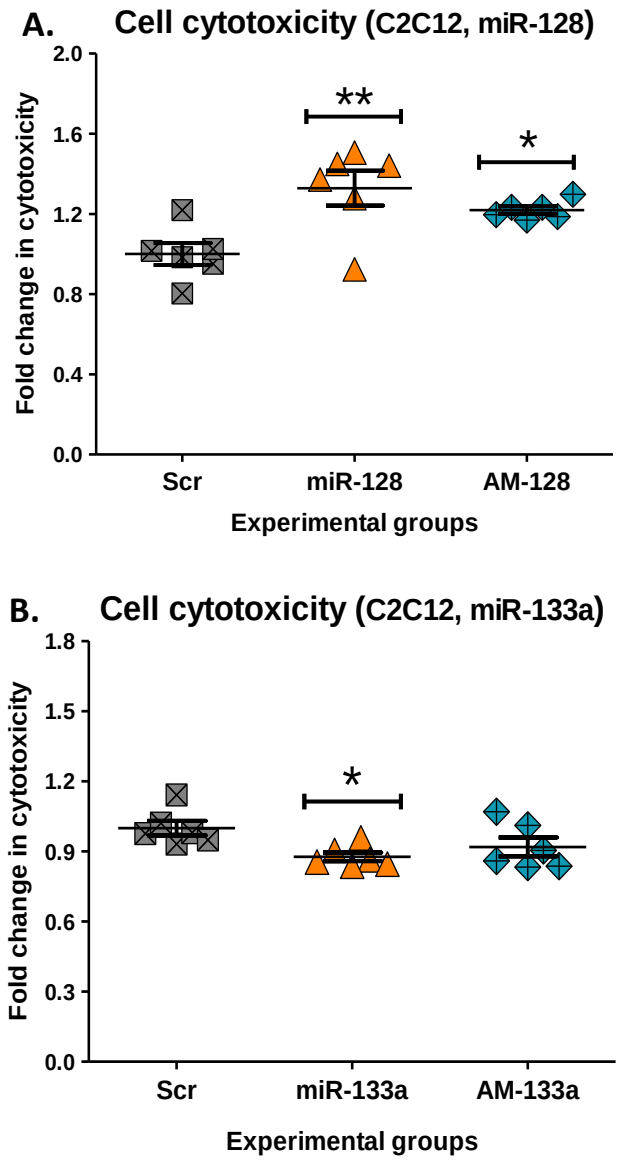

Figure 5.3.4 CytoTox96 cytotoxicity assay of C2C12 myoblasts following transfection with miR-128 or miR-133a. **A)** C2C12 cell death expressed as fold-change in cytotoxicity following transfection with Scr, miR-128 or AM-128, using Scr as the control group. **B)** C2C12 cell death expressed as fold-change in cytotoxicity following transfection with Scr, miR-133a or AM-133a, using Scr as the control group. *represents significant differences compared with the Scr (control) group, *P≤0.05, **P≤0.01, ***P≤0.001 (*mean ± SEM*; *n*=6*; One-Way ANOVA with Dunnett's post-hoc analysis*).

5.3.5 The effect of miR-128 gain-of-function and loss-of-function on C2C12 myoblast mitochondrial toxicity

Data obtained from mitochondrial ToxGlo mitotoxicity assay following transfections of C2C12 cells with miR-128 is shown in **Figure 5.3.5.** Comparison of the fold-change observed in the cytotoxicity of the C2C12 cells showed significant increase following transfection of cells with miR-128 and AM-128. On the contrary, the fold-change of the ATP levels of the C2C12 following transfection with miR-128 and AM-128 was significantly decreased, indicating decreased production of ATP and therefore an increase in mitochondrial toxicity. These data indicate that miR-128 and AM-128 act as mitototoxicant compounds inducing necrosis of C2C12 myoblast.

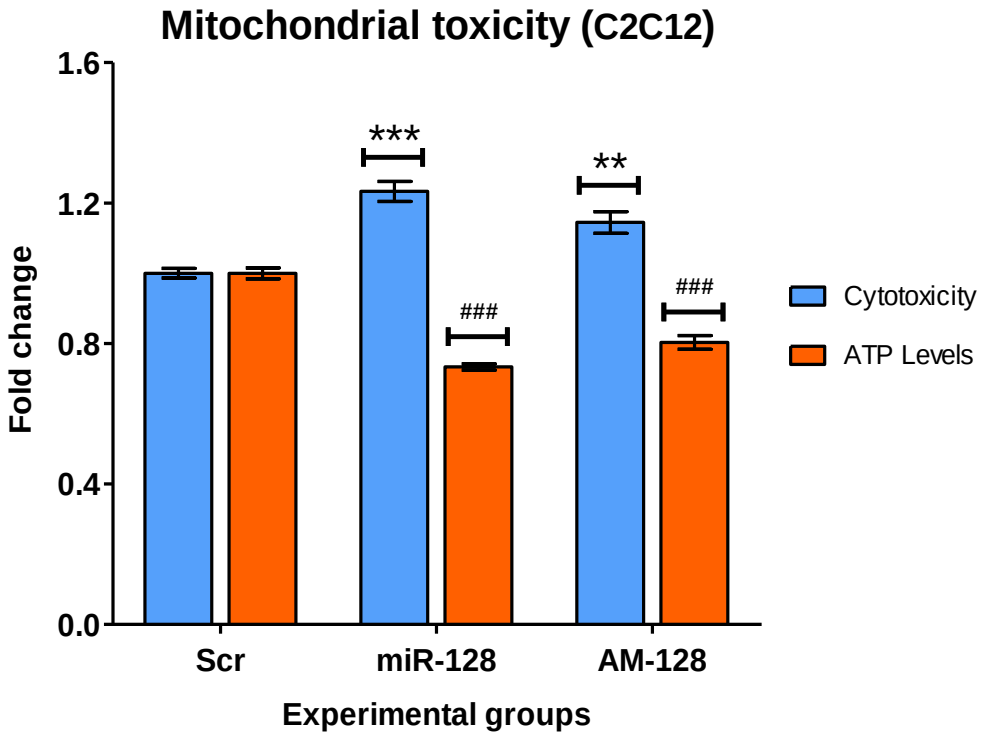

Figure 5.3.5 Mitochondrial ToxGlo two-stage mitotoxicity assay of C2C12 myoblasts following transfections with miR-128. The first step measures dying/dead cells, whilst the second step measures ATP produced. C2C12 cell death expressed as cytotoxicity indicated as fold-change following transfection with Scr, miR-128 or AM-128, using Scr as the control group. C2C12 mitochondrial toxicity following transfection with Scr, miR-133a or AM-133a

expressed as fold-change, using Scr as the control group. Scr served as the control for statistical comparison, *statistical comparison with Scr values in cytotoxicity, #statistical comparison with Scr values in mitotoxicity $^{*,\#}P \leq 0.05$, $^{**,\#\#}P \leq 0.01$, $^{***,\#\#\#}P \leq 0.001$ (*mean ± SEM*; *n*=6*; Two-Way ANOVA with Bonferroni's post-hoc analysis*).

5.4 Discussion

This chapter focused on the effect of gain- and loss-of-function of miR-128 and miR-133a in C2C12 cells. Findings from these experiments could serve as a useful tool to understand the mechanism affected during overexpression or inhibition of these two miRs *in vitro* and *in vivo*. Data collected from image analyses following transfection of C2C12 with either miR-128 or miR-133a appeared to have a different effect on the cell behaviour, suggesting a different mechanism involved during myogenesis and differentiation. The main findings can be summarised in the table below:

Table 5.4 Summary of the main findings following miR-128 and miR-133a overexpression and inhibition in C2C12 myoblasts and myotubes. ↑ indicates increase in the specific phenotype/function, ↓ indicates reduction in the specific phenotype/function, ─ indicates no change in the specific phenotype/function.

	miR-128	AM-128	miR-133a	AM-133a
Proliferation	↓	↓	↑	↑
Cell death	↑	↑	↓	–
Mitochondrial toxicity	↑	↑	N/A	N/A
Myotube diameter	–	–	–	↑
Myotube area	–	–	–	↑
Cell fusion	↑	↑	–	–

5.4.1 Overexpression and inhibition of miR-128 in differentiated C2C12 myotubes

Image analysis of C2C12 myotubes transfected with Scr, miR-128 mimic or AM-128 showed no significant difference in myotube diameter, myotube area or number of nuclei per myotube between the groups. However, differences were observed in the fusion index of the C2C12 myotubes at Day 7 of differentiation. Specifically, cell fusion was increased in C2C12 myotubes transfected with miR-128 and AM-128, compared to the scrambled-treated myotubes (**Figure 5.3.1 D**). Furthermore, it was evident that myotubes overexpressing miR-128 showed a "healthier" phenotype, with their nuclei spread across the length of the myotube as opposed to round cell phenotype with multiple fused nuclei. Unlike miR-128, myotubes transfected with AM-128 as well as those transfected with Scr sequence appeared to have a round shape, with their nuclei concentrated at the ends of the tube or in the centre. The formation of those round-shaped myotubes could be attributed to myotube detachment from the plate's surface due to cell death or due to disruption in their attachment factors. A study from Schoneich *et al.* (2015) shows that Bcl-2 is likely to control myotube apoptosis at early stages but not at late stage of differentiation (Day6). Another explanation would be that inhibition of miR-128 could impact negatively terminal differentiation. Although there is no evidence in current literature of such an effect of miR-128 on terminal differentiation of C2C12, there are studies showing that inhibition of certain microRNAs after the onset of differentiation may affect myogenesis (Goljanek-Whysall *et al.* 2012). A study from Dai *et al.* shows overexpression of miR-128 inhibiting skeletal muscle cell differentiation *via* direct targeting of SP1 gene while the opposite was observed with inhibition of miR-128 (Dai *et al.* 2016). Specifically, in their study Dai *et al.* show the formation of myotubes following overexpression of miR-128 but at a later time-point following transfection (Dai *et al.* 2016). Taken these data into consideration, it is possible that miR-128 overexpression may actually stall or delay the formation of myotubes rather than completely abolishing it. Therefore, the myotubes observed in miR-128 overexpression in **Figure 5.3.1.1 A** could have a "healthier"

phenotype due to their formation later during transfections. In contrary, inhibition of miR-128 could have resulted in formation of myotubes earlier during transfections, resulting in faster utilisation of the growth factors in the media due to increased metabolic rate and therefore myotube apoptosis at an earlier time point. Considering the fusion index data and the time of transfections (Day 3 post-differentiation), it is also possible that miR-128 overexpression may prevent the fusion of more nuclei, while inhibition of miR-128 may promote hyperfusion, resulting in these circular shapes in the myotubes. Similar morphology in C2C12 myotubes as the one observed in AM-128 treated cells has been previously reported following treatment of myotubes with rotenone. Specifically, treatment of myoblasts with rotenone (inhibitor of mitochondrial complex I) did not cause detachment or cell death at Day 3 of differentiation, but a round-shaped morphology of those cells was observed (Grefte *et al.* 2015). Interestingly, increased expression of miR-128 in C2C12 myotubes was detected at Day 4 of differentiation and was positively correlated with increased levels of ATP (Siengdee *et al.* 2015).

Despite the lack of significant differences in the myotube diameter of miR-128 transfected C2C12 myotubes, distribution analysis of myotube diameter was performed. Myotubes were separated in different diameter ranges allowing the estimation of the number of myotubes falling within each diameter range. Although no significant difference was observed in the distribution between the different groups, it was evident that myotubes overexpressing miR-128 were mostly within the 20-30 μm (**Figure 5.3.1.2 A**). Interestingly, miR-128 inhibition caused a slight shift of the distribution, with those myotubes being more abundant in number in the 30-40 μm diameter range. These data collectively suggest that inhibition of miR-128 could cause some hypertrophy in a portion of transfected myotubes, which may not be obvious when the average diameter is taken into consideration. In this case, these data are in agreement with that been previously shown (Motohashi *et al.* 2013).

In order to examine whether these differences in the diameter distribution could be due to hypertrophy of the myotubes independently of the myoblast

fusion, distribution nuclei per myotube size for each myotube counted was plotted (**Figure 5.3.1.2 A)**. Analysis revealed a linear relationship between the number of nuclei and the increase in the size range, suggesting that the number of cells fused to form myotubes was proportional to the diameter of the myotubes.

5.4.2 Overexpression and inhibition of miR-133a in differentiated C2C12 myotubes

Analysis of C2C12 myotube images revealed a significant increase in myotube diameter following inhibition of miR-133a (AM-133a), although the opposite was not observed in cells overexpressing miR-133a (**Figure 5.3.2.1 A, B**). Significant increase following inhibition of miR-133a was also observed in total myotube area but no differences were observed in the fusion index of those cells (**Figure 5.3.2.1 C, D**). These observations suggest that inhibition of miR-133a may cause myotube hypertrophy, however overexpression of miR-133a does not cause atrophy but instead inhibits hypertrophy.

Distribution analysis of myotube diameter showed the highest number of myotubes in miR-133a with a diameter under 30 µm, in comparison with the AM-133a, where the number of myotubes is higher from diameter sizes >60 µm (**Figure 5.3.2.1 A**). Despite those differences in peak numbers, Chi-square test showed no significant differences in the diameter distribution between the groups. Distribution analysis of the number of nuclei per myotube showed a parallel relationship across all groups (**Figure 5.3.2.1 B**). These data reveal that the number of fused cells resulting in mature myotubes was the same across the different diameter ranges in all the groups. Therefore, miR-133a may have a role in hypertrophy of myofibres rather than myogenesis through extra fusion of cell. Moreover, these data on myotube hypertrophy and fusion index indicates that hypertrophy of myotubes may be independent of cell fusion. This is in line with a study from McCarthy *et al.* (2011) showing that satellite cells are not required for muscle fibre hypertrophy in mice. However, the number of myotubes in each

diameter distribution appears to shift slightly, with larger myotubes being present in AM-133a wells in comparison with the rest of the groups. Previous studies have shown that miR-133a expression is downregulated in skeletal muscle showing hypertrophy (Ge and Chen, 2011). Furthermore, a study from Huang *et al.* indicated that miR-133a overexpression can supress IGF-1R post-transcriptionally in C2C12 cells (Huang *et al.* 2011). Suppression of IGF-1R may result in inhibition of IGF-1/Akt pathway, resulting in skeletal muscle atrophy (reviewed in Hitachi and Tochida, 2014). Despite these findings, Boettger *et al.* argue that manipulation of microRNAs in miR-133 family may have a distinctive phenotype in skeletal muscle. They support the notion that lack of miR-133b in a knockout mouse model may be rescued by other microRNAs of miR-133 family such as miR-133a (Boettger *et al.* 2014). In order to support this as the case in our study, further investigation is required including sequencing experiments or qPCR analysis to establish the levels of expression of other miRs of the miR-133 family during inhibition of miR-133a. Although, many studies have described the role of miR-133a in skeletal muscle proliferation and differentiation *in vitro* and *in vivo*, there is not much evidence on the effect of miR-133a inhibition in terminal differentiation of C2C12 myotubes.

5.4.3 The effect of miR-128 overexpression and inhibition on C2C12 cell proliferation, cell death and mitochondrial toxicity

Overexpression and inhibition of miR-128 in C2C12 myoblasts caused significant reduction in the cell number as seen from the proliferation assay, indicating that proliferation rate of C2C12 is impaired (**Figure 5.3.3 A**). Reduction in the cell number seen in the proliferation assay is accompanied by significantly increased rate of cell death, as observed by the increased levels of C2C12 cytotoxicity, compared to the control group (Scr) (**Figure 5.3.4 A**). In order to evaluate whether this increase in the cell death is the results of underlying mitochondrial dysfunction, a mitotoxicity assay was performed in C2C12 myoblasts following transfections with miR-128. Analysis of the mitotoxicity data

showed a significant increase in the cytotoxicity following overexpression and inhibition of miR-128 and a parallel decrease in ATP levels of those two groups compared to the control (**Figure 5.3.5**). Increase in cytotoxicity with parallel decrease in ATP levels indicated that overexpression and inhibition of miR-128 had a mitotoxic effect. Therefore, cell death occurring following transfections of myoblasts with miR-128 or AM-128 might be due to mitophagy.

Overexpression of miR-128 in C2C12 myoblasts has been previously associated with inhibition of cell proliferation rate (Motohashi *et al.* 2013). Overexpression of miR-128 has been associated with reduction in proliferation rate of other cell types including muscle side population (SP) cells and cardiomyocytes (Motohashi *et al.* 2012; Huang *et al.* 2018). There seems to be no study indicating the role of miR-128 in the regulation of cell death. However, the data from the cytotoxicity assay indicate that overexpression of miR-128 is associated with increased cell death. This could be due to impaired cell metabolism, which would also explain the reduction in cell proliferation. Impairment of mitochondrial metabolism could result in mitochondrial dysfunction, leading to cell death *via* necrosis (Lemasters *et al.* 1991). In order to assess whether the increase in the cell death was due to mitochondrial dysfunction, a mitotoxicity assay was performed. Results indicated that miR-128 acts as a mitotoxin, therefore the increased cell death could be due to mitophagy. The same results were recorded following C2C12 myoblast transfections with AM-128, indicating that both overexpression and inhibition of miR-128 could result in mitophagy but possibly *via* different pathways. Similar role of miR-128 in proliferation of satellite cells was recorded in a previous study where both overexpression and inhibition of miR-128 resulted in stalling of cell proliferation, but *via* the regulation of different proteins (Dai *et al.* 2016). Therefore, miR-128 expression could be regulated by a feedback mechanism maintaining its levels for normal cell behaviour. This would be in line with recent findings from Gabisonia *et al.* (2019) showing that miR-199 expression can stimulate cardiac repair in pigs following myocardial infraction, but the levels of miR-199 need to be to be tightly regulated. This study also demonstrates that

uncontrolled levels of miR-199 can result in cardiac arrhythmia and sudden death (Gabisonia *et al.* 2019).

5.4.4 The effect of miR-133a overexpression and inhibition on C2C12 cell proliferation and cell death

Proliferation rate of C2C12 myoblasts following transfections with miR-133a showed a significant increase in the cell number following both overexpression and inhibition for miR-133a (**Figure 5.3.3 B**). C2C12 cell death rate appeared to be significantly reduced only after overexpression of miR-133a, which is in line with the increased proliferation rate (**Figure 5.3.4 B**). Furthermore, inhibition of miR-133a causes no difference in the rate of cell death in C2C12 myoblasts. This could be possible if inhibition of miR-133a could have triggered the endogenous cell overexpression of other miR-133 family members, providing protection against cell death. This could also explain the increase in the cell number observed following treatment of C2C12 myoblasts with AM-133a, which could be the result of activation of different cellular mechanisms by other members of the miR-133 family.

Previous studies on the involvement of miR-133a in myoblast proliferation have been controversial. A study from Chen *et al.* shows the positive regulation of myoblast proliferation by miR-133, and inhibition of proliferation with miR-133 inhibition (Chen *et al.* 2006). More studies support these findings, showing promotion of myoblast proliferation by miR-133 (Kim *et al.* 2006). However, miR-133 has been shown to inhibit myoblast proliferation *via* ERK1/2 pathway (Feng *et al.* 2013). A study from Zhang *et al.* supports the negative role of miR-133 in myoblast proliferation, by inducing G1 phase arrest (Zhang *et al.* 2012). Despite the extensive studies on miR-133 and muscle cell fate, there has been limited evidence on the specific effect of miR-133a in myoblast behaviour, in comparison with other members of the miR-133 family (e.g. miR-133b, miR-133c). A study from Liu *et al.* (2011) shows that deletion of miR-133a *in vivo* does not cause changes in the skeletal muscle of mice until after 4 weeks of age (Liu *et al.* 2011).

However, Liu *et al.* state that the absence of a phenotype with deletion of miR-133a in skeletal muscle might be due to expression of miR-133b, which is not detected in the heart muscle of those mice; hence the phenotype in cardiac muscle is more severe (Liu *et al.* 2011).

Phenotypic analysis of C2C12 myotubes following manipulation of miR-128 and miR-133a expression revealed differences in the effect of miR-128 and miR-133a in C2C12 differentiation, proliferation, survival and mitochondrial function. Therefore, miR-128 and miR-133a have an impact on C2C12 behaviour and differentiation *via* the control of separate mechanisms. Future approaches will involve the assessment of proliferation and viability of C2C12 cells with more sensitive techniques, such as Ki67 or BrdU and acridine orange/ethidium bromide (AO/EB) staining.

Chapter 6

Gain- and loss-of-function of miR-128 and miR-133a in NSC-34 cells

6.1 Introduction

Multiple microRNAs have been shown to be involved in neuronal development and regulation of the central nervous system and have been carefully investigated in several neuronal cell types. One such cell type, the α-motoneurons located in the spinal cord and lower brain stem, are often cultured *in vitro* using spinal cord explants (Nurcombe *et al.* 1984; Arnold *et al.* 2012). Such a technique can often be costly and time-consuming. An alternative *in vitro* model of motoneuron-like cells, known as NSC-34 cells, is a hybrid cell line which has been widely used for neuronal cell-based assays (Cashmann *et al.* 1992; Eggett *et al.* 2000; Matusica *et al.* 2008).

MicroRNA-128 is abundantly expressed in the central nervous system and specifically the brain (Lee *et al.* 2008). During development, miR-128 expression levels control neuronal morphology and excitability (Franzoni *et al.* 2015). Despite being a key regulator of neuronal development, miR-128 levels appear to show the highest expression levels during adulthood (Tan *et al.* 2013). A study from Tan *et al.* has identified miR-128 as a suppressor of ion channel expression as well as signalling molecules involved in the ERK pathway (Tan *et al.* 2013). MicroRNA-128 has also been discussed in studies focusing on cognitive function and neuropsychiatric disorders (reviewed in Ching and Ahmed-Annuar 2015). Specifically, predicted target genes of miR-128 have been shown to be involved in neurotrophin signalling, MAPK and insulin signalling pathway (reviewed in Ching and Ahmed-Annuar, 2015).

Unlike miR-128, miR-133 has not been studied as extensively in neuron cells. Known as a “myomiR”, miR-133 has been investigated in relation to neuromuscular interactions *in vivo* (Valdez *et al.* 2014), however there is limited evidence for its involvement in neuronal cell behaviour and function. Hoye *et al.* have identified increased levels of miR-133a in mouse motoneurons, similar to those of known motomiRs such as miR-218 (Hoye *et al.* 2017). Interestingly, in their study Hoye *et al.* support the possibility that miR-133a may have a functional rather than a morphological role in regulating motoneuron fate postnatally (Hoye *et al.* 2017).

The aim of the work was to assess the effect of gain- and loss-of-function of miR-128 and miR-133a on motoneuron cell function and morphology using NSC-34 cell line. Furthermore, the potency of the two microRNAs in controlling cell proliferation, viability and mitochondrial toxicity specifically in motoneurons was investigated. Results from this study could provide a novel explanation for the involvement of the two microRNAs in regulation of motoneuron cell fate and function.

6.2 Methods

6.2.1 Cell culture and differentiation of NSC-34 cells

NSC-34 cells were recovered from LN_2 and thawed either at RT or in a 37°C water bath until there was no ice visible. Cell suspension was collected from the cryovial, mixed with 3 mL of pre-warmed growth media (GM_{NSC-34}; Chapter 2, Section 2.16) and centrifuged immediately at 1,500 rpm for 5 min to discard freezing media containing DMSO. The cell pellet was then resuspended in 10 mL of growth media (GM_{NSC-34}) and plated into a T75 flask (Corning). Cells were then incubated in a humidified incubator at 37°C with 5% CO_2, and media was replaced every two days until cells reach 70-80% confluency. When 70-80% confluency was reached, cells were passaged 1:4 into fresh T75 flasks in a total volume of 10 mL cell suspension, as described previously in Chapter 2, section 2.17.

For immunostaining and characterisation of the phenotype, NSC-34 cells were seeded into a 12-well plate pre-coated with 5 µg/mL laminin (Chapter 2, Section 2.18), at a confluency of 50,000 cells/well (13,158 cells/cm^2). Cells were left to differentiate for 7-11 days following transfections, in order to develop axonal projections. The remaining cells were plated into three 6-well plates, for use in RNA and protein isolation following transfections. All plates were incubated in GM_{NSC-34} for 24 h to allow appropriate attachment on the cell surface and were

then used for transfections with miR-128 or miR-133a according to the protocols in Chapter 2, Section 2.21). Following 48 h of transfections, NSC-34 cells from the 6-well plates were harvested for RNA and protein isolation, according to the protocol described in Chapter 2, Section 2.20. NSC-34 cells plated in 12-well plates were left to differentiate in DM_{NSC-34} until Day 11-12 post-transfections before being stained for imaging and assessment of phenotypic changes (Chapter 2, Section 2.22).

6.2.2 Image analysis of NSC-34 differentiated cells ($NSC-34_D$) following transfections with miR-128 and miR-133a

NSC-34 cells were immunostained with Anti-Beta-III Tubulin antibody and DAPI following successful differentiation, as described in Chapter 2, Section 2.22. Images of cells were acquired using a Nikon Ti Live cell imaging microscope under x20 magnification and the axonal length of differentiated NSC-34 cells was analysed using ImageJ software (Chapter 2, Section 2.23).

6.2.3 Plate assay for NSC-34 cell proliferation, viability and mitochondrial toxicity following transfections with miR-128 or miR-133a

NSC-34 cells were plated on 96-well plates (Costar) pre-coated with 5 µg/mL laminin and used for proliferation, viability and mitotoxicity assays. For proliferation and viability, NSC-34 cells were seeded according to the instruction in Chapter 2, Sections 2.27 (for proliferation assay) and Chapter 2, Section 2.28 (for cytotoxicity assay). Cells were left to incubate in GM_{NSC-34} for 24 h following plating and were subsequently transfected with scrambled sequence, miR-128 mimic, AM-128, miR-133a mimic and AM-133a, as previously described (Chapter 2, Section 2.21). Both proliferation and cytotoxicity assay were performed 48 h following transfections according to manufacturer's instructions. Data analysis was performed as indicated in the manufacturer's protocol. Mitotoxicity assay was conducted as described in Chapter 2, Section 2.19, following transfection of

NSC-34 cells with scrambled sequence, miR-128 mimic, AM-128. Data interpretation was performed according to manufacturer's instructions. The cytototoxic effect of miR-128 was assessed using the values recorded from the fluorescence absorbance. The mitotoxic effect of miR-128 was assessed using the values of LDH and ATP release recorded from luminescence measurement of NSC-34 cells. To determine whether miR-128 is a mitotoxic compound, fold-changes in mitotoxicity were assessed in comparison with the cytotoxicity values recorded.

6.2.4 Statistical Analysis

Statistical analysis was performed using Graphpad 5 (Graphpad Software, San Diego, USA). Data analyses of axonal length, proliferation and cytotoxicity assay were performed using a One-Way ANOVA, with Dunnet's post-hoc analysis, using Scr as the control group. Data from the mitotoxicity assay were analysed using a Two-Way ANOVA, with Bonferroni post-hoc analysis. Data from cytotoxicity and mitotoxicity assays were presented as fold-changes compared to the control (Scr) group. Data were represented as mean ± SEM. N Number represents wells used per transfection condition.

6.3 Results

6.3.1 Phenotype changes in NSC-34 cells following gain-of-function and loss-of-function of miR-128

NSC-34 cells transfected with miR-128 mimic (miR-128) and miR-128 inhibitor (AM-128) are shown in **Figure 6.3.1 A.** NSC-34 cells transfected with miR-128 mimic and imaged after 11 days of differentiation demonstrated distinct differences in the axonal length and confluency compared to the rest of the groups (**Figure 6.3.1 A**). Indeed, analysis revealed a significant decrease in the

axonal length of the NSC-34$_D$ cells transfected with miR-128 mimic in comparison with the control group (Scr) (**Figure 6.3.1 C**). The transfection process did not appear to have an impact on the axonal length of the cells, as seen from comparison between untreated cells (Control) and transfection control (Scr) (**Appendix, Figure A.14**).

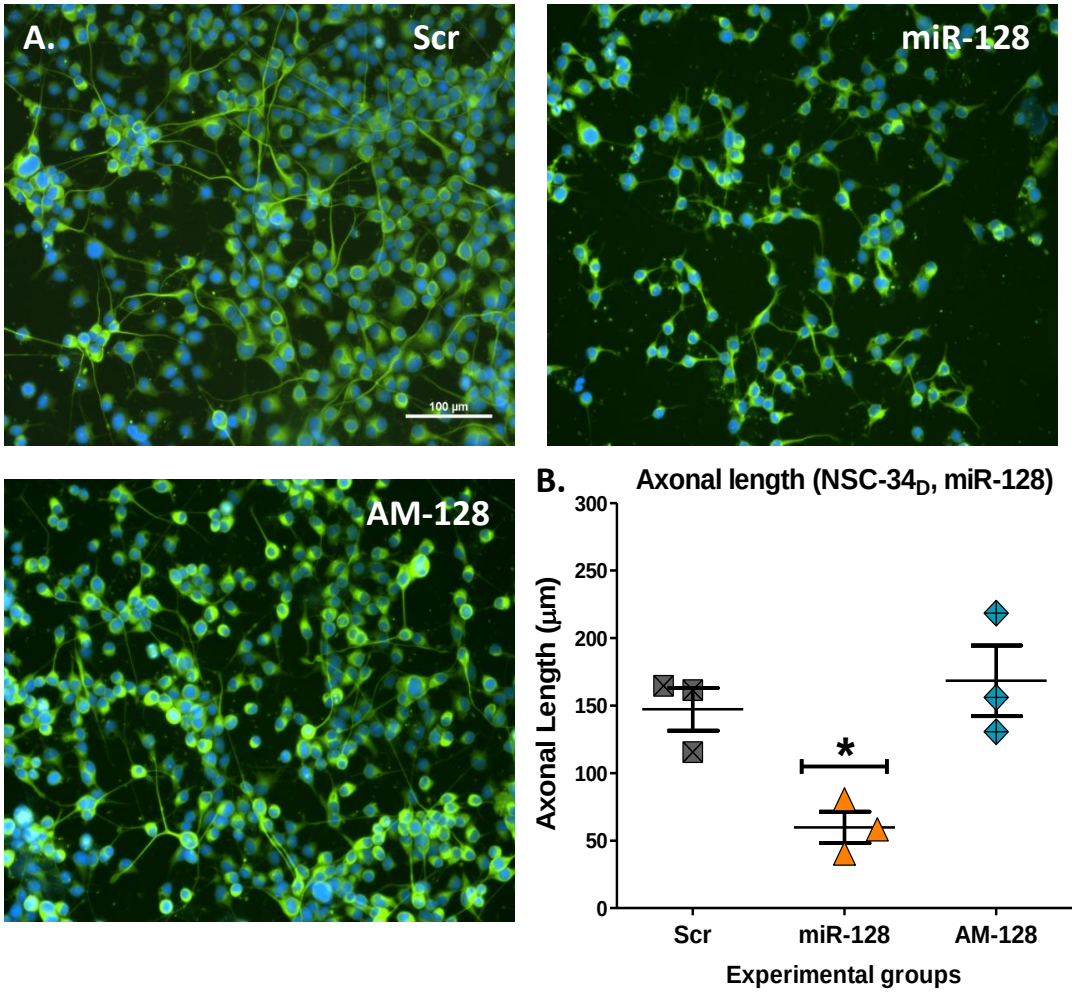

Figure 6.3.1 MicroRNA-128 gain- and loss-of-function in NSC-34$_D$ phenotype. **A)** Differentiated NSC-34 cells (NSC-34$_D$) transfected with Scr, miR-128 or AM-128 as indicated; NSC-34$_D$ cells were stained with Alexa Fluor 488 B-III Tubulin (Green) and DAPI (Blue) for the visualisation of the nuclei. **B)** Axonal length of NSC-34$_D$ after 11 days of differentiation. *represent significant differences compared with the Scr (control) group. *P≤0.05 (*mean ± SEM*; *n*=3*; One-Way ANOVA with Dunnett's post-hoc analysis*). Representative images show.

6.3.2 Phenotype changes in NSC-34 cells following gain-of-function and loss-of-function of miR-133a

NSC-34 cells transfected with miR-133a mimic (miR-133a) and miR-133a inhibitor (AM-133a) and differentiated for 11 days are shown in **Figure 6.3.2 A**. Overexpression or inhibition of miR-133a did not seem to have an apparent effect on the axonal length or number of NSC-34_D cells following 11 days of differentiation (**Figure 6.3.2 A**). Analysis of the axonal projections revealed a significant increase in the length of the axons of the NSC-34_D transfected with AM-133a compared to the control group (Scr) (**Figure 6.3.2 C**). Interestingly, axonal length of NSC-34_D treated with Scr showed a significant reduction when compared to non-transfected (Control) cells (**Appendix, Figure A.15**).

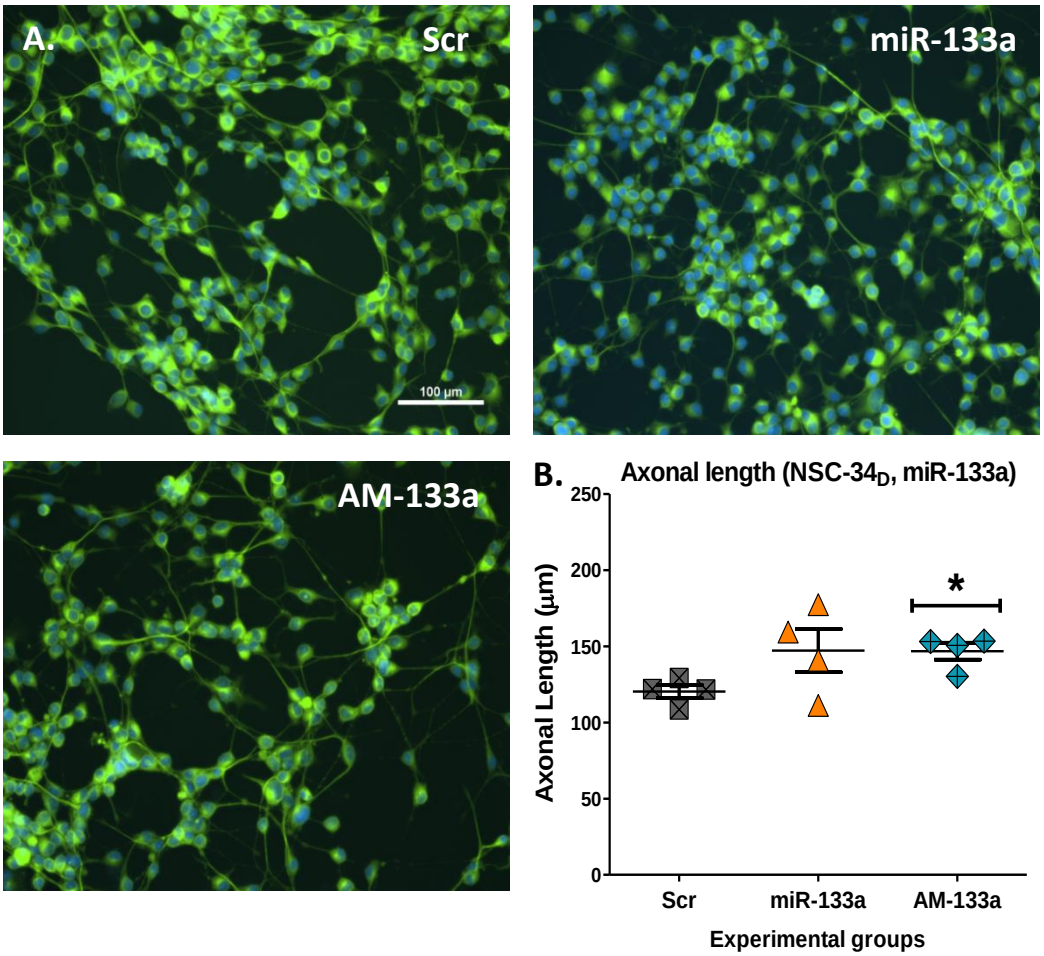

Figure 6.3.2 MicroRNA-133a gain- and loss-of-function in NSC-34_D phenotype. **A)** Differentiated NSC-34 (NSC-34_D) cells transfected with Scr, miR-133a or AM-133a

as indicated; NSC-34$_D$ cells were stained with Alexa Fluor 488 B-III Tubulin (Green) for and DAPI (Blue) for the visualisation of the nuclei. **B)** Axonal length of NSC-34$_D$ after 11 days of differentiation. *represent significant differences compared with the Scr (control) group. *P≤0.05 (*mean ± SEM*; *n*=3*; One-Way ANOVA with Dunnett's post-hoc analysis*). Representative images shown.

6.3.3 Proliferation rate of NSC-34 cells following gain-of-function and loss-of-function of miR-128 and miR-133a

Analysis of the CCK-8 proliferation assay on NSC-34 cells following manipulation of miR-128 or miR-133a expression are shown in **Figure 6.3.3**. Transfection of miR-128 and AM-128 had no effect on the proliferation of NSC-34 cells compared to the Scr-treated cells (**Figure 6.3.3 A**). Similar results were obtained from analysis of the proliferation rate of NSC-34 cells following miR-133a and AM-133a transfection, when compared to Scr-treated cells (**Figure 6.3.3 B**).

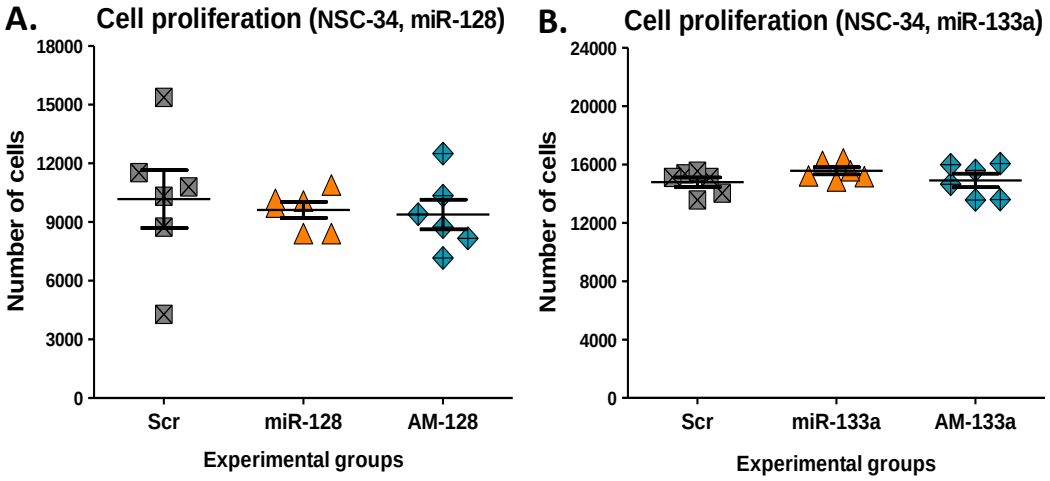

Figure 6.3.3 CCK-8 proliferation assay of NSC-34 cells following manipulation of miR-128 or miR-133a expression. **A)** NSC-34 number following transfection with miR-128 or AM-128. **B)** NSC-34 number following transfection with miR-133a or AM-133a. Scr served as control group for statistical comparison, (*mean ± SEM*; *n*=6*; One-way ANOVA with Dunnett's post-hoc analysis*).

6.3.4 The effect of miR-128 and miR-133a gain-of-function and loss-of-function on NSC-34 viability

The viability of NSC-34 cells was determined by a CytoTox96 cytotoxicity assay following manipulation of miR-128 and miR-133a expression as shown in **Figure 6.3.4.** NSC-34 cell viability was assessed based on the rate of cell death (expressed as fold-change in cytotoxicity). Transfection did not seem to affect the viability of NSC-34 cells, as no differences were observed in the cytotoxicity between Scr-treated cells and non-transfected (Control) cells (**Appendix, Figure A.16**). Overexpression of miR-128 led to a significant increase in cytotoxicity, compared to the control group (Scr) (**Figure 6.3.4 A**). However, miR-133a and AM-133a transfection had no impact on NSC-34 cell viability (**Figure 6.3.4 B**).

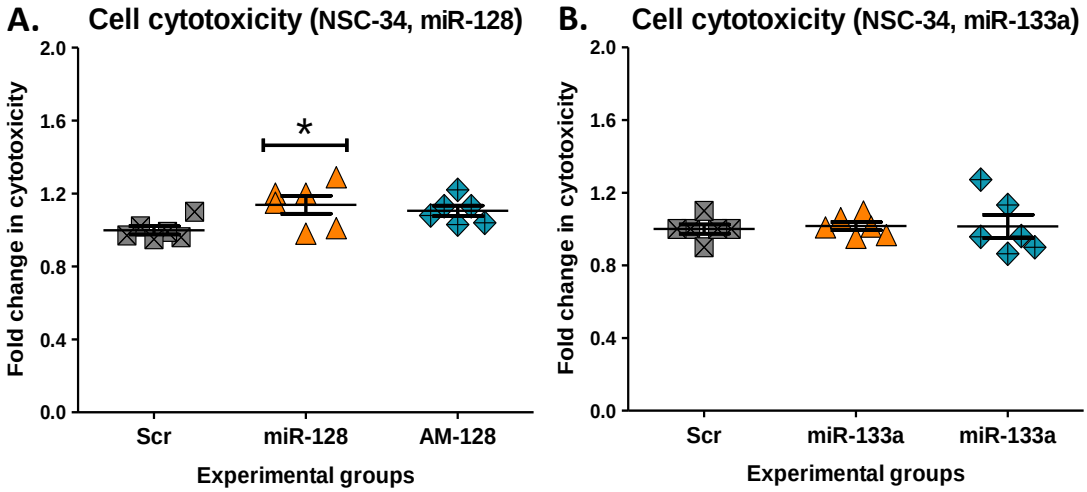

Figure 6.3.4 CytoTox96 cytotoxicity assay of miR-128 and miR-133a on NSC-34 cell for the determination of NSC-34 cell death. **A)** NSC-34 cell cytotoxicity following transfection with miR-128 or AM-128. **B)** NSC-34 cell cytotoxicity following transfection with miR-133a or AM-133a. *represent significant differences compared with the Scr (control) group. *P≤0.05. (*mean ± SEM*; *n*=6*; One-way ANOVA with Dunnett's post-hoc analysis*).

6.3.5 Mitochondrial toxicity following miR-128 and miR-133a gain-of-function and loss-of-function in NSC-34 cells

Results obtained from mitochondrial ToxGlo mitotoxicity assay analysis following transfections of NSC-34 cells with miR-128 are shown in **Figure 6.3.5.** Changes in cytotoxicity following overexpression or inhibition of miR-128 were not significantly higher compared to the control group. Similarly, fold-changes recorded in ATP release following overexpression or inhibition of miR-128 did not reveal a significant reduction compared to control group (Scr). These findings indicate that miR-128 does not act as a mitochondrial toxin.

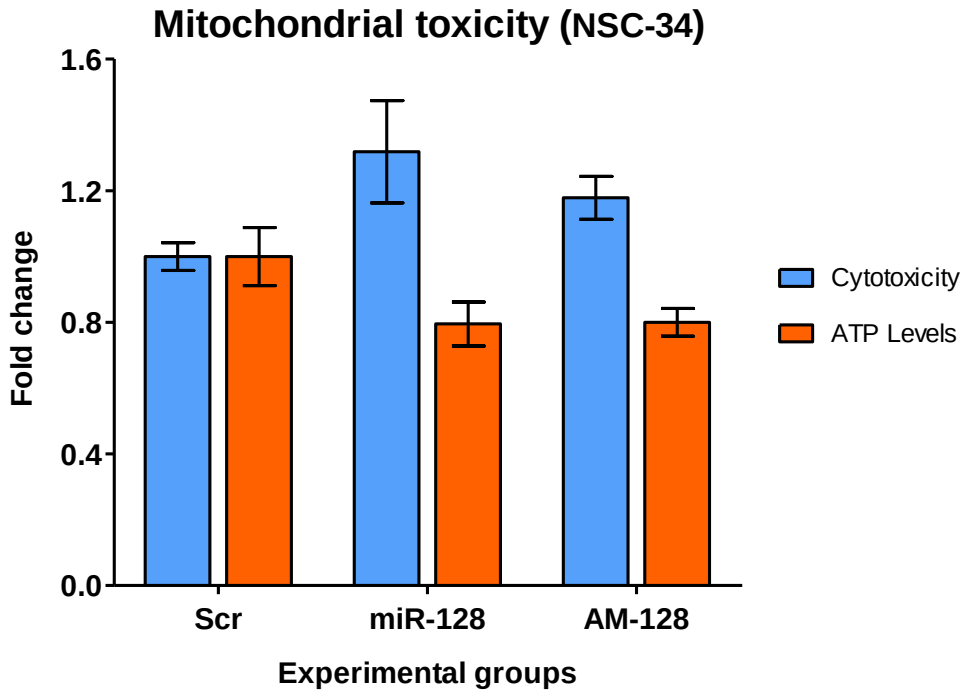

Figure 6.3.5 Mitochondrial ToxGlo two-stage mitotoxicity assay of NSC-34 neuronal cells following manipulation of miR-128 expression. The first step measures dying/dead cells, whilst the second step measures ATP produced. NSC-34 cell death (cytotoxicity) indicated as fold-change following transfection with Scr, miR-128 or AM-128. NSC-34 mitochondrial ATP release following transfection with Scr, miR-133a or AM-133a expressed as fold-change. Scr served

as the control group for statistical comparison (*mean ± SEM*; *n*=6*; Two-Way ANOVA with Bonferroni's post-hoc analysis*).

6.4 Discussion

In this chapter, gain- and loss-of-function of miR-128 and miR-133a were investigated in NSC-34 cells. The aim was to understand the mechanism affecting motoneuron cell behaviour following the dysregulation of miR-128 and miR-133a expression *in vivo* and *in vitro*. The main findings from this chapter are summarised in the table bellow:

Table 6.4 Summary of the main findings following miR-128 and miR-133a overexpression and inhibition in NSC-34 cells. ↑ indicates increase in the specific phenotype/function, ↓ indicates reduction in the specific phenotype/function, ─ indicates no change in the specific phenotype/function.

	miR-128	AM-128	miR-133a	AM-133a
Proliferation	─	─	─	─
Cell death	↑	─	─	─
Mitochondrial toxicity	─	─	N/A	N/A
Axonal Length	↓	─	─	↑

6.4.1 MicroRNA-128 gain- and loss-of-function effects on the phenotype of differentiated NSC-34 (NSC-34$_D$) cells

Image analysis of NSC-34 cells following 11 days of differentiation showed significant reduction in axonal length of NSC-34$_D$ following overexpression of

miR-128 (miR-128) (**Figure 6.3.1 C**). Overexpression of miR-128 appeared to have an impact on the overall cell number present per field of view suggesting a possible impact on either cell viability or proliferation. Unlike the rest of the groups, miR-128 transfected cells showed very little to no signs of "networking" with the neighbouring cells and lack of formation of "mesh-like" structure usually seen in untransfected differentiated cells (control) or scrambled-transfected cells.

MicroRNA-128 is known as a brain-enriched microRNA due to its high levels of expression in the brain and during development in mice (Franzoni *et al.* 2015). Previous studies have shown that a dysregulation of miR-128 can play a significant role in the development of neurological disorders (reviewed in Ching and Ahmad-Annuar, 2016). Specifically, inhibition of miR-128 expression has been associated with increased neuronal excitability and seizures in mice (McSweeney *et al.* 2016; Tan *et al.* 2013). Overexpression of miR-128 results in inhibition of neuronal responsiveness and suppression of motor activities in mice (Tan *et al.* 2013). This is in line with the phenotype recorded in our study following overexpression or inhibition of miR-128 in NSC-34 cells. The special and temporal versatility of miR-128 expression has been previously investigated *in vivo* (Franzoni *et al.* 2015). Both increased and decreased levels of miR-128 *in vivo* have been linked to the rise of diseases such as cancer and psychiatric disorders (reviewed in Ching and Ahmad-Annuar, 2016). Moreover, previously published data *in vitro* highlight the effect of inhibition and overexpression of miR-128 in regulating cell proliferation *via* two different mechanisms (Dai *et al.* 2016). Collectively, these data demonstrate the need for a tight regulation in the levels of miR-128 expression, as both up- and down-regulation of its expression levels may have a negative effect *in vivo* and *in vitro*. Furthermore, in order to assess whether the function of the NSC-34 cells is impaired during gain- or loss-of function of miR-128, further *in vivo* experiments are required.

6.4.2 MicroRNA-133a gain- and loss-of-function effects on the phenotype of differentiated NSC-34 (NSC-34$_D$) cells

Analysis of differentiated NSC-34 images following transfections with AM-133a revealed a significant increase in the axonal length of NSC-34 cells following 11 days of differentiation (**Figure 6.3.2 C**). Interestingly, miR-133a overexpression did not seem to have an impact in the axonal length of NSC-34 cells, compared to the control group (Scr). Unlike miR-128, miR-133a did not seem to cause such severe phenotype changes, since NSC-34 cells sprouted axons during overexpression and inhibition of miR-133a.

MiR-133a is a "myomiR", highly expressed in skeletal and cardiac muscle. Its involvement in neuronal behaviour and morphology has not been extensively studied. Previous studies have shown changes in miR-133a expression levels following spinal cord injury (reviewed in Li *et al.* 2016). Most importantly, miR-133a along with miR-218, a well-known "motomiR", has been associated with motoneuron fate determination postnatally. A study from Hoye *et al.* showed several target genes of miR-133a being downregulated specifically in motoneuron cells suggested a more distinctive functional role of miR-133a in motoneurons (Hoye *et al.* 2017). MicroRNA-133a has also been found to be elevated in human *in vitro* models during neuronal differentiation (Pallocca *et al.* 2014). Furthermore, overexpression of miR-133a *in vitro* has been shown to decrease the expression of neuronal marker genes during neuronal differentiation (Izarra *et al.* 2017). All things considered, miR-133a has been associated with neuronal cell function and behaviour, specifically motoneuron cells. However, there is limited evidence on the effect of miR-133a in motoneuron function and differentiation *in vitro* and *in vivo*. It is possible that miR-133a, may have a more significant role in cell function rather than the phenotype determination of the motoneurons, hence the effects we saw in the NSC-34 cells are not as profound as those seen with miR-128.

6.4.3 The effect of miR-128 overexpression and inhibition on NSC-34 proliferation rate, cell viability and mitochondrial function

Data analysis from proliferation assay of NSC-34 cells following transfections with miR-128 showed no significant differences in the cell number between the three groups (**Figure 6.3.3 A**). Although some studies are in support of the protective effect of miR-128 in neuronal cell proliferation (Zhou *et al.* 2018), other studies provide evidence of inhibition or reduction in the rate of cell proliferation with miR-128 overexpression (Zhang *et al.* 2016). Taken into consideration our data showing no difference in cell proliferation, it is possible that miR-128 could target different mechanisms in different neuronal cell types or act in a dose-dependent manner. Results obtained from the cytotoxicity assay measuring rate of cell death revealed a significant increase in NSC-34 cell death rate following overexpression of miR-128 (**Figure 6.3.4 A**), which could explain the lower number of cells seen during imaging. A study from Guidi *et al.* identified the downregulation of the TMSB10 gene, acting as an anti-apoptotic factor in chicken embryonic motoneurons, when miR-128 is overexpressed in neuronal cells (Guidi *et al.* 2010). In order to examine whether this increase in the cytotoxicity is due to an underlying mitochondrial dysfunction, a mitotoxicity assay was performed following manipulation of miR-128 expression in NSC-34 cells. This assay records cell death (cytotoxicity) and ATP release from cells, and a comparison of those two variables determine whether the microRNA under investigation acts as a mitochondrial toxin on the cells. Unlike in C2C12, neither the cytotoxicity nor the mitotoxicity data obtained from the assay revealed any significant differences in miR-128 transfected NSC-34 cells. It is noteworthy though that both cytotoxicity and mitotoxicity fold-changes show the same pattern as that seen in C2C12 (Chapter 5, Section 5.3.5). The lack of significant difference changes in cell death and ATP release as seen in this assay indicates that miR-128 does not act as a mitotoxin in NSC-34 cells. In order to identify the exact molecular mechanism resulting in increased cell death following overexpression of miR-128 in NSC-34 cells, further experiments need to be conducted specifically in motoneuron cells. Such experiments may include, but

not limited to, proteomics analysis in order to identify whether proteins involved in cell death may be overexpressed following transfections with miR-128 or AM-128.

6.4.4 The effect of miR-133a overexpression and inhibition on NSC-34 proliferation rate and cell viability

Analysis of data obtained from the proliferation assay showed no effects of miR-133a overexpression or inhibition on NSC-34 cell number (**Figure 6.3.3**). Similar results were also obtained from the cytotoxicity assay performed following overexpression or inhibition of miR-133a (**Figure 6.3.4**). Taken into consideration that miR-133a is predominantly a skeletal muscle microRNA and the levels of its expression are very low in neuronal cells, it is not surprising that the change of its expression has no impact on proliferation or viability of NSC-34 cells. Association of miR-133a with motoneuron cells has only been described by Hoye *et al.* supporting the role of miR-133a as functional in determining motoneuron cell fate (Hoye *et al.* 2017). Few other studies have associated miR-133a in neuronal cell differentiation. Members of the miR-133 family have been shown to play a role in NMJ formation and function (Valdez *et al.* 2014). However there is very limited evidence to support the exact role and mechanism of miR-133a in motoneuron cell phenotype and behaviour.

Analysis of the phenotype of NSC-34 cells following manipulation of miR-128 and miR-133a expression showed differences in the effect of the two microRNAs in NSC-34 cells. Therefore, the two microRNAs are likely affecting motoneuron cell behaviour *via* different mechanisms.

Chapter 7

Analysis of predicted target genes of miR-128 in muscle and nerve *in vitro* and *in vivo*

7.1 Introduction

MicroRNAs control gene expression *via* inhibition of translation and/or degradation of the mRNA transcript resulting in reduced protein expression (reviewed in Fazi and Nervi, 2008). Certain microRNAs have been proposed to induce upregulation of their mRNA targets and proteins under certain conditions (Orang *et al.* 2014). Some microRNAs may also control expression levels of their target genes indirectly *via* repression of mRNA degradation mechanisms. One such example is microRNA-128 which has been associated with repression of nonsense-mediated decay in neural cells, resulting in upregulation of certain mRNA transcripts (Bruno *et al.* 2011). MicroRNA-128, a brain-enriched microRNA, is highly expressed in CNS and skeletal muscle tissue (Lee *et al.* 2008). Previously published data and the bioinformatics analysis presented in Chapter 4 indicate that miR-128 may control the expression of several genes involved in key biochemical pathways in muscle and motoneurons. Specifically, predicted target genes of miR-128 are involved in neurotrophin signalling, MAPK and insulin signalling pathway (reviewed in Ching and Ahmed-Annuar, 2015).

A number of genes has been predicted to interact with miR-128 in muscle and nerve cells and tissues. Cytochrome c oxidase subunit I and IV genes (COX-I and COX-IV respectively) are major components of the mitochondrial electron transport chain and play a key role in energy production (reviewed in Gnaiger, 2009). NRF-1 is a transcription factor that has been associated with the regulation of the gene expression of all cytochrome c oxidase subunits, including COX-I and COX-IV (Dhar *et al.* 2008). Parkin-2 (Park-2) gene is linked to the removal of dysfunctioning mitochondria and regulation of mitochondrial activity (Narendra *et al.* 2008; Leduc-Gaudet *et al.* 2019). TOM-20 is localised in mitochondrial membrane and is a marker of mitochondrial content (Billing *et al.* 2010). PDGFRα has been associated with hypertrophy of skeletal muscle fibres *via* interaction with PI3K/AKT pathway (Sugg *et al.* 2017). PDGFRα expression is also necessary during embryonic stages and neuronal myelination (Oumesmar *et al.* 1997). GRB-2 and Gab-1 are essential for NMJ morphology and axonal myelination in peripheral nerve (Park *et al.* 2017; Gingras *et al.* 2016). SOS-1

forms a complex *via* binding with GRB-2 activation the RAS/ERK pathway following binding of growth factors to the upstream receptors (Findlay *et al.* 2013). SIRT-1 is capable of promoting de-acetylation of FoxO proteins, inhibiting the expression of atrophy-related genes (Lee and Goldberg, 2013).

The aim of this chapter was to assess the effects of miR-128 gain- and loss-of-function on the expression levels of predicted target genes associated with mitochondrial quality and quantity, skeletal muscle hypertrophy and neurotrophin signalling in C2C12 and NSC-34 cells. Furthermore, the levels of predicted target genes most likely directly regulated by miR-128, were assessed *in vivo*, in TA muscle and SN of 12-week old mice subjected to a low-protein diet pre- or postnatally.

7.2 Methods

7.2.1 First-strand cDNA synthesis and real-time qPCR analysis of miR-128 predicted target genes in cell and tissue lysates

For cell lysates:

C2C12 and NSC-34 cells were harvested as described in Chapter 2, Section 2.20 and stored in -20^{o}C until RNA isolation. Prior to RNA isolation, cell samples were retrieved from -20^{o}C and left at RT for 5 min. RNA isolation was performed as described in Chapter 2, Section 2.12. Following RNA isolation and determination of RNA concentration and integrity using the NanoDrop2000 (Thermofisher Scientific), RNA samples were used for first strand cDNA synthesis using SuperScript™ II Reverse Transcriptase (Chapter 2, Section 2.13). Following completion of cDNA synthesis, cDNA reaction volume was diluted 1:10 to a final volume of 200 µL and stored at -20^{o}C, until used for real-time qPCR.

For tissue lysates:

TA muscle and SN isolated from 12-week old mice were ground in a mortar using LN_2 and prepared for RNA isolation as described in Chapter 2, Section 2.12. RNA concentration and purity were recorded using NanoDrop2000 (Thermofisher Scientific). First Strand cDNA synthesis was performed using SuperScript™ IV VILO™ Master Mix, according to manufacturer's protocol (Cat# 11756050, Invitrogen, Paisley, UK). Following cDNA synthesis, each sample was diluted 1:10 to a final volume of 200 µL and stored at -20^{o}C until used for qPCR.

For real-time qPCR:

Real-time qPCR in cell and tissue samples was performed according to the protocol in Chapter 2, Section 2.15. Analysis of the data collected following completion of qPCR runs was performed according to the delta-delta Ct method (ddCt). For qPCR runs in cell samples, b2 microglobulin was used as the housekeeping gene and 18S was used as housekeeping gene for qPCR runs in tissue samples. Primer sequences were designed according to the instructions outlined in Chapter 2, Section 2.14 and shown in **Table 7.2.1** bellow:

Table 7.2.1 Primer sequences of miR-128 predicted target genes of interest.

Gene name	Primer sequences (5' – 3')	
	Forward	Reverse
Gab-1 (1)	CAGAGTCCCAGCGGAGC	TCTTCCACGCATAACGCTTC
Gab-1 (2)	GCGCACTGAAAGAAGGTCG	CTTCCACGCATAACGCTTCA
Pdgfrα-2	GGAACCTCAGAGAGAATCGGC	CATAGCTCCTGAGACCCGCTG
Cox-I	CACTAATAATCGGAGCCCCA	TTCATCCTGTTCCTGCTCCT
Cox-IV	TTCTTCCGGTCGCGAGCAC	GCTCTGGAAGCCAACATTCTGC
Grb-2	CGGAAGCTAGGTTGCTCTGT	ACACAATGCCACCCGTGA
Nrf-1	TTACTCTGCTGTGGCTGATGG	CCTCTGATGCTTGCGTCGTCT
Park-2	CAAGGACACGTCGGTAGCTT	ACAGGGCTCCTGACATCTG
Sirt-1	GATGACAGAACGTCACACGC	ACAAAAGTATATGGACCTATCCGC

Sos-1	CCGTGTGTGCCTTTCTTTGG	AGAACCTCTTGATGTCCGGC
Tomm-20	AGTCGAGCGAAGATGGTGG	GCCTTTTGCGGTCGAAGTAG
β2 microglobulin	TAAGCATGCCAGTATGGCCG	TGTCTCGATCCCAGTAGACG
18S	CGGCTACCACATCCAAGGAAGG	CCCGCTCCCAAGATCCAACTA

7.2.2 Quantification of the protein levels of miR-128 predicted target genes following manipulation of miR-128 levels in C2C12 and NSC-34 cells

Cell lysates from C2C12 and NSC-34 cells were used for protein extraction and determination of protein concentration using BCA assay (Chapter 2, Section 2.24 and Section 2.25). Protein expression was quantified using western blotting technique, as described in Chapter 2, Section 2.26. Data analysis for quantification of proteins of interest was performed according to instructions in Chapter 2, Section 2.26.5.

7.2.3 Statistical Analysis

Statistical analysis was performed using Graphpad 5 (Graphpad Software, San Diego, USA). Data analysis relative gene expression analysis and protein quantification analysis was performed using One-Way ANOVA with Dunnett's post-hoc analysis, using NNN as the control group for statistical comparisons. Data are represented as mean ± SEM. N number represents animals used per group for molecular analysis in tissue samples. N number represents wells used per transfection condition for molecular analysis in cell lysate samples.

7.3 Results

7.3.1 Changes in the expression profile of miR-128 predicted target genes following transfections of miR-128 in C2C12 cells

Relative gene expression of miR-128 predicted target genes of interest following transfections with miR-128 in C2C12 cells are shown in Figure 7.3.1.1 and Figure 7.3.1.2. Expression of Gab-1, isoforms 1 and 2, was not affected following overexpression or inhibition of miR-128 (**Figure 7.3.1.1 A, B**). Additionally, no differences in the expression levels were recorded for Tomm-20 (**Figure 7.3.1.1 E**), Sirt-1 (**Figure 7.3.1.2 B**) and Grb-2 (**Figure 7.3.1.2 C**) genes. Significant upregulation in the gene expression level was recorded in Cox-IV and Park-2 genes following overexpression of miR-128, when compared to Scr (**Figure 7.3.1.1 C, Figure 7.3.1.2 F**). Gene expression levels were significantly downregulated for Pdgfrα-2 following miR-128 overexpression (**Figure 7.3.1.1 D**) and Sos-1 and Nrf-1 only after inhibition of miR-128 (**Figure 7.3.1.2 A, F**). Interestingly, Cox-I expression levels were significantly downregulated following both overexpression and inhibition of miR-128 (**Figure 7.3.1.2 E**), consistent with the mitotoxicity data previously described (Chapter 5, Section 5.3.5).

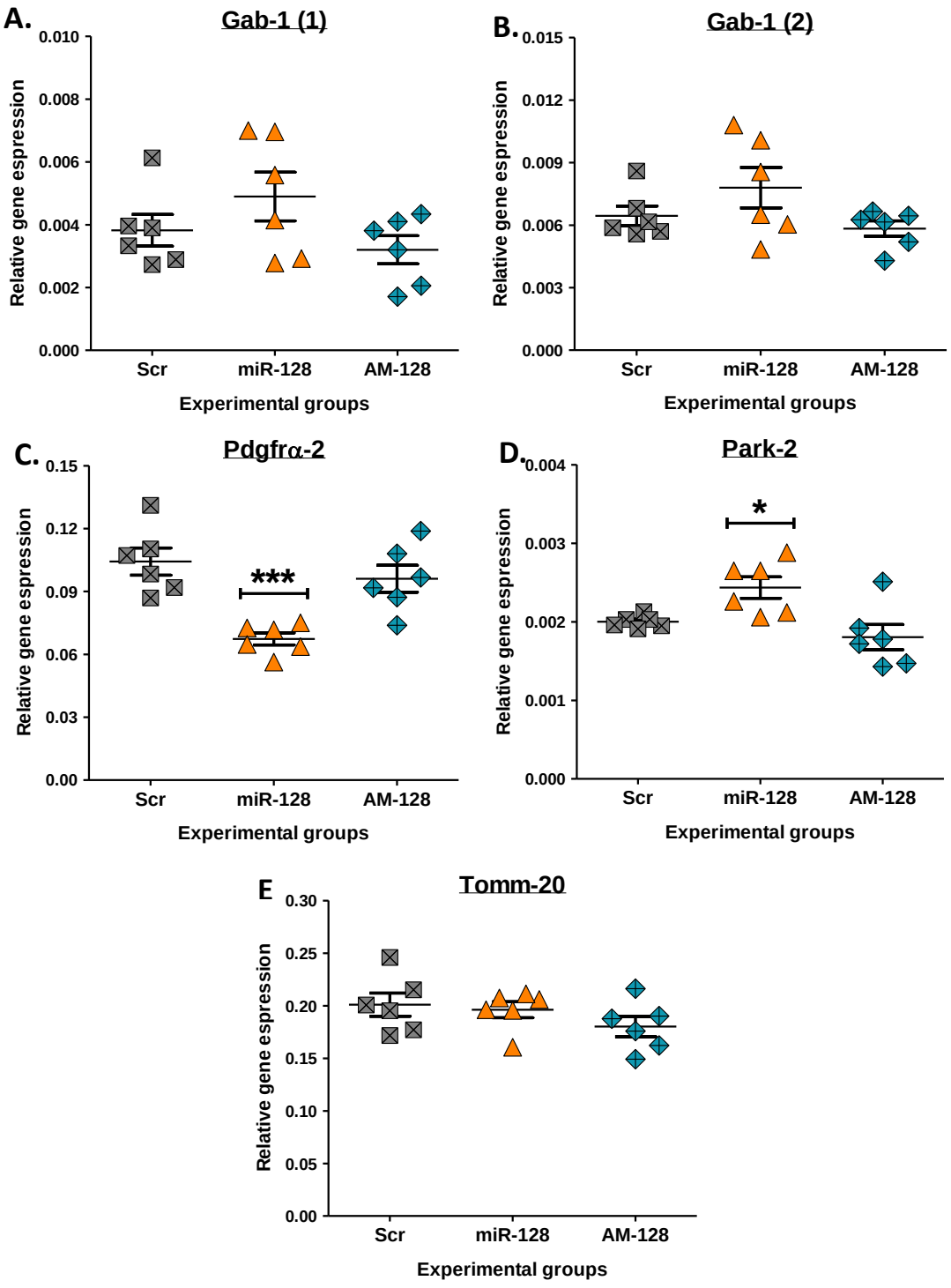

Figure 7.3.1.1 Relative expression of miR-128 predicted target genes following transfections with miR-128 in C2C12 cells. **A)** Gab-1, isoform 1, **B)** Gab-1, isoform 2, **C)** Park-2, **D)** Pdgfrα-2, **E)** Tomm-20 expression levels. *represent significant differences compared with the Scr (control) group. *P≤0.05, **P≤0.01, *** P≤0.001 (*mean ± SEM*; *n*=6*; One-Way ANOVA with Dunnett's post-hoc analysis*).

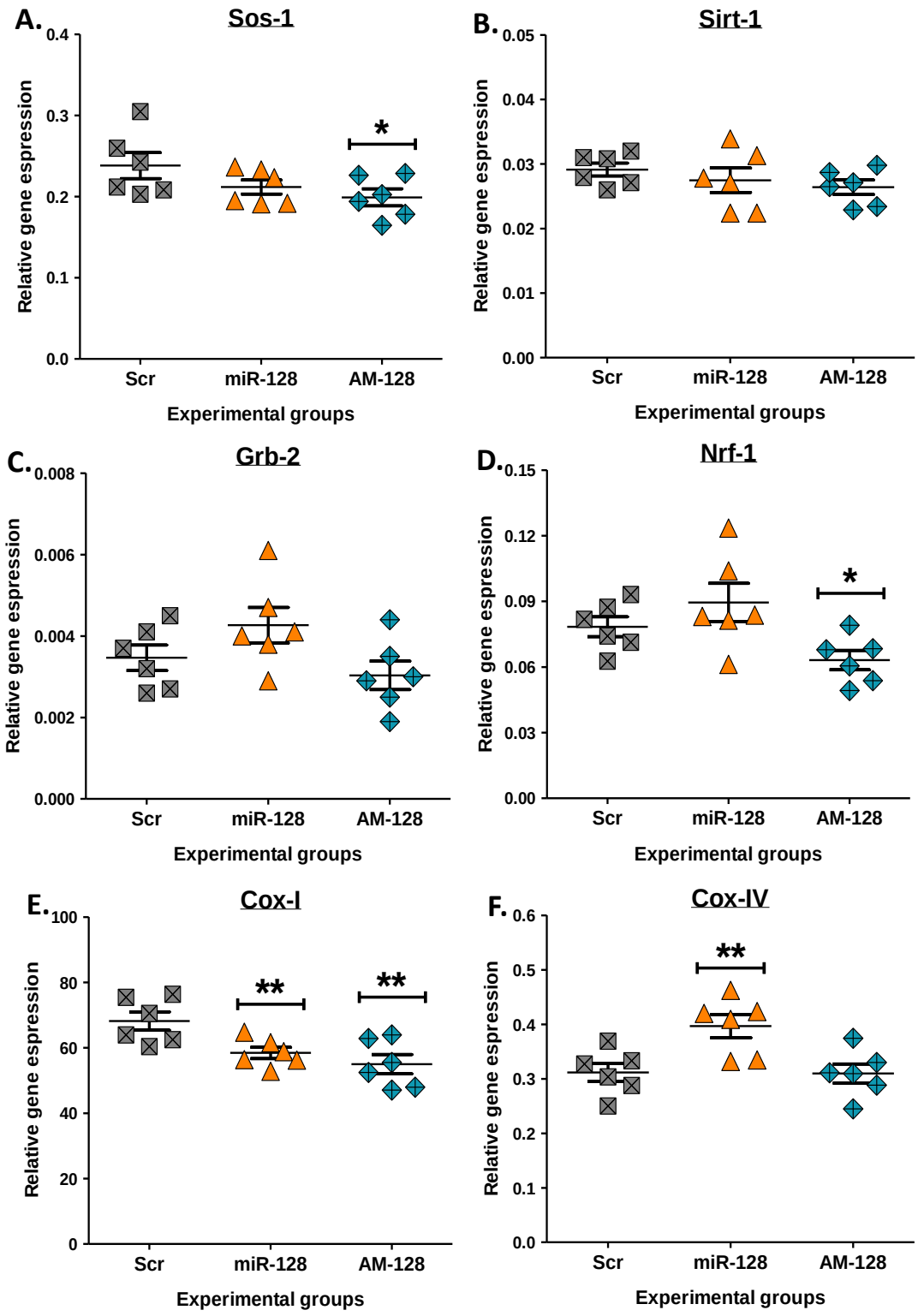

Figure 7.3.1.2 Relative expression of miR-128 predicted target genes following transfections with miR-128 in C2C12 cells. **A)** Sos-1, **B)** Sirt-1, **C)** Grb-2, **D)** Nrf-1, **E)** Cox-I and **F)** Cox-IV expression levels. *represent significant differences

compared with the Scr (control) group, *P≤0.05, **P≤0.01 (*mean ± SEM*; *n*=6*; One-Way ANOVA with Dunnett's post-hoc analysis*).

7.3.2 Changes in the expression levels of miR-128 predicted target genes following manipulation of miR-128 levels in NSC-34 cells

Analysis of the expression level of miR-128 predicted target genes of interest, following transfection of NSC-34 cells with miR-128, are shown in **Figure 7.3.2.1** and **7.3.2.2** Expression levels of Cox-I gene was significantly decreased in NSC-34 cells following overexpression of miR-128 (**Figure 7.3.2.2 A**). Moreover, expression levels of Nrf-1, Grb-2 and Pdgfrα-2 were significantly increased following inhibition of miR-128, when compared to control group (Scr) (**Figure 7.3.2.2 C-E**). Interestingly, Cox-IV expression levels were significantly increased following both overexpression and inhibition of miR-128 in NSC-34 cells (**Figure 7.3.2.2 B**). Sirt-1 and Tomm-20 expression levels were unaffected by miR-128 transfections (**Figure 7.3.2.1 A, B**).

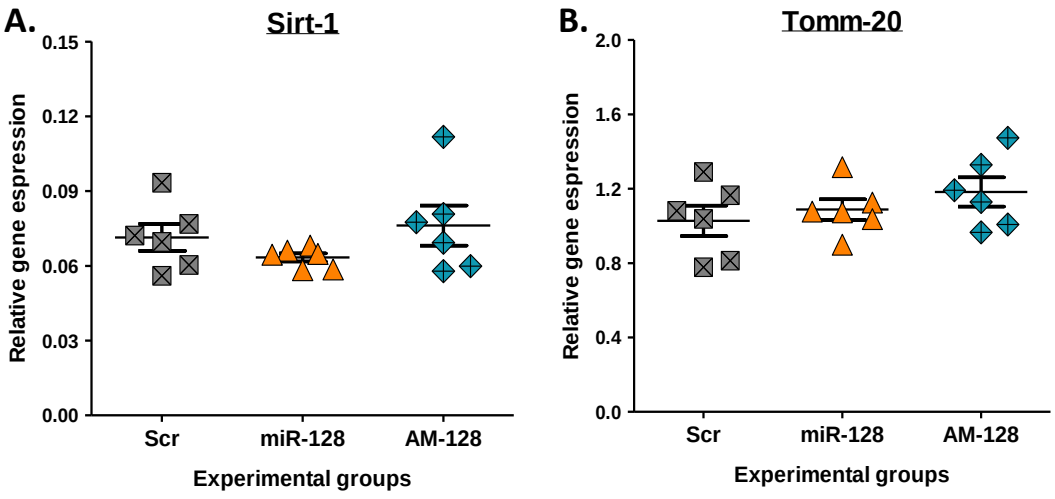

Figure 7.3.2.1 Relative expression of miR-128 predicted target genes following overexpression or inhibition of miR-128 in NSC-34 cells. **A)** Sirt-1 and **B)** Tomm-20 expression levels. Scr served as the control group for statistical comparison. (*mean ± SEM*; *n*=6*; One-Way ANOVA with Dunnett's post-hoc analysis*).

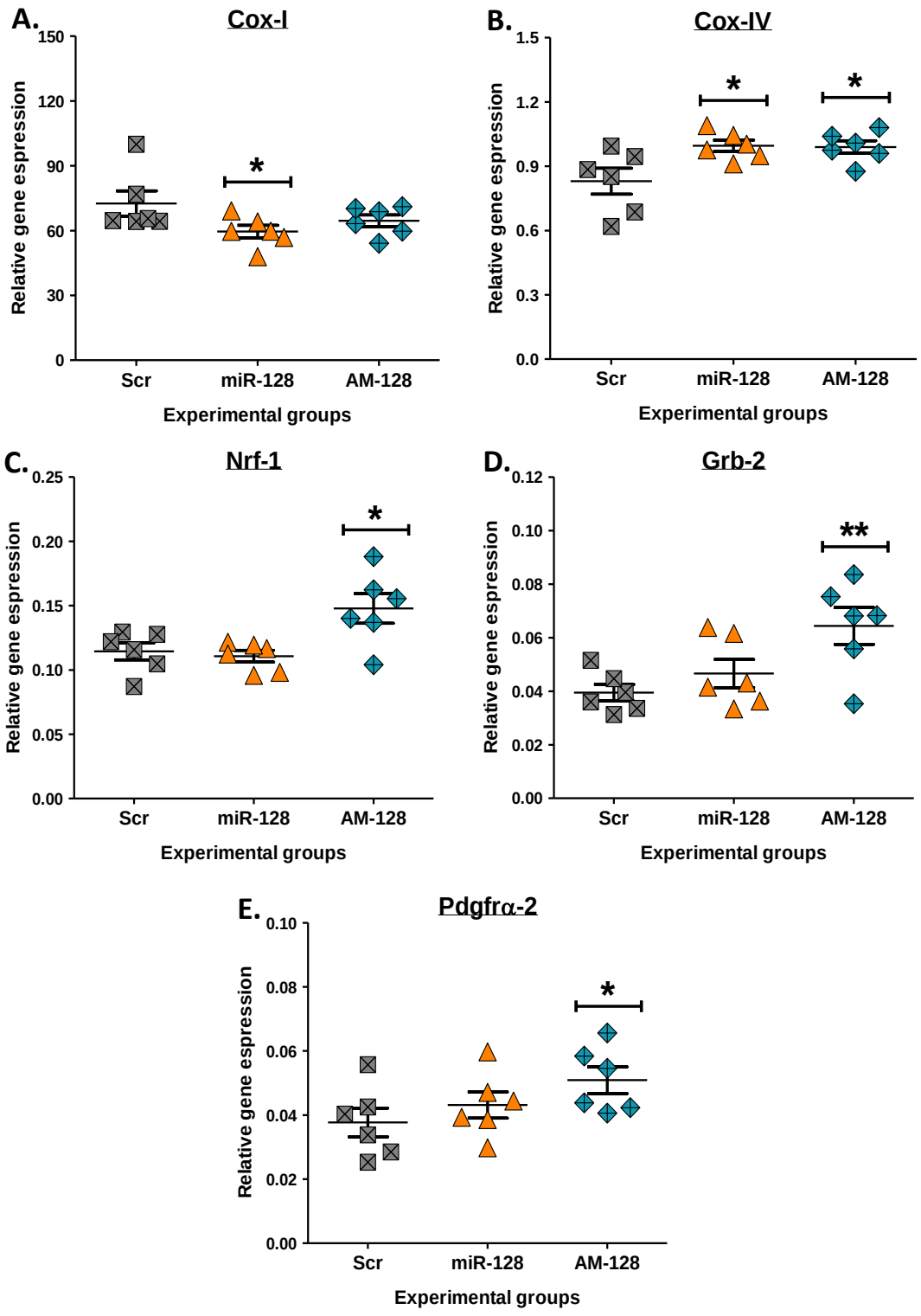

Figure 7.3.2.2 Relative expression of miR-128 predicted target genes following overexpression or inhibition of miR-128 in NSC-34 cells. **A)** Cox-I, **B)** Cox-IV, **C)** Nrf-1, **D)** Grb-2 and **E)** Pdgfrα-2 expression levels. *represent significant

differences compared with the Scr (control) group. *P≤0.05, **P≤0.01 (*mean ± SEM*; *n*=6*; One-Way ANOVA with Dunnett's post-hoc analysis*).

7.3.3 Protein expression levels in C2C12 and NSC-34 cells following overexpression or inhibition of miR-128

Data collected from analysis of protein expression in C2C12 cells following overexpression or inhibition of miR-128 are shown in **Figure 7.3.3.1 – 7.3.3.4**. Protein levels of LC-3 I and LC-3 II (recruited during autophagy/mitophagy process) were quantified using Ponceau S stain as an internal control (**Figure 7.3.3.1 A**). The ratio of LC-3 II/I protein expression revealed no significant differences following miR-128 transfections (**Figure 7.3.3.1 B**). Same results were obtained from analysis of LC-3 II/I ratio in NSC-34 cells following miR-128 transfections (**Figure 7.3.3.2**). Protein levels of NRF-1 were also unaffected by miR-128 transfections both in C2C12 and NSC-34 cells (**Figure 7.3.3.3, Figure 7.3.3.4 B**). Similar results were observed for protein expression levels of COX-IV in NSC-34 cells, which remained unaltered following overexpression and in inhibition of miR-128 (**Figure 7.3.3.4 C**).

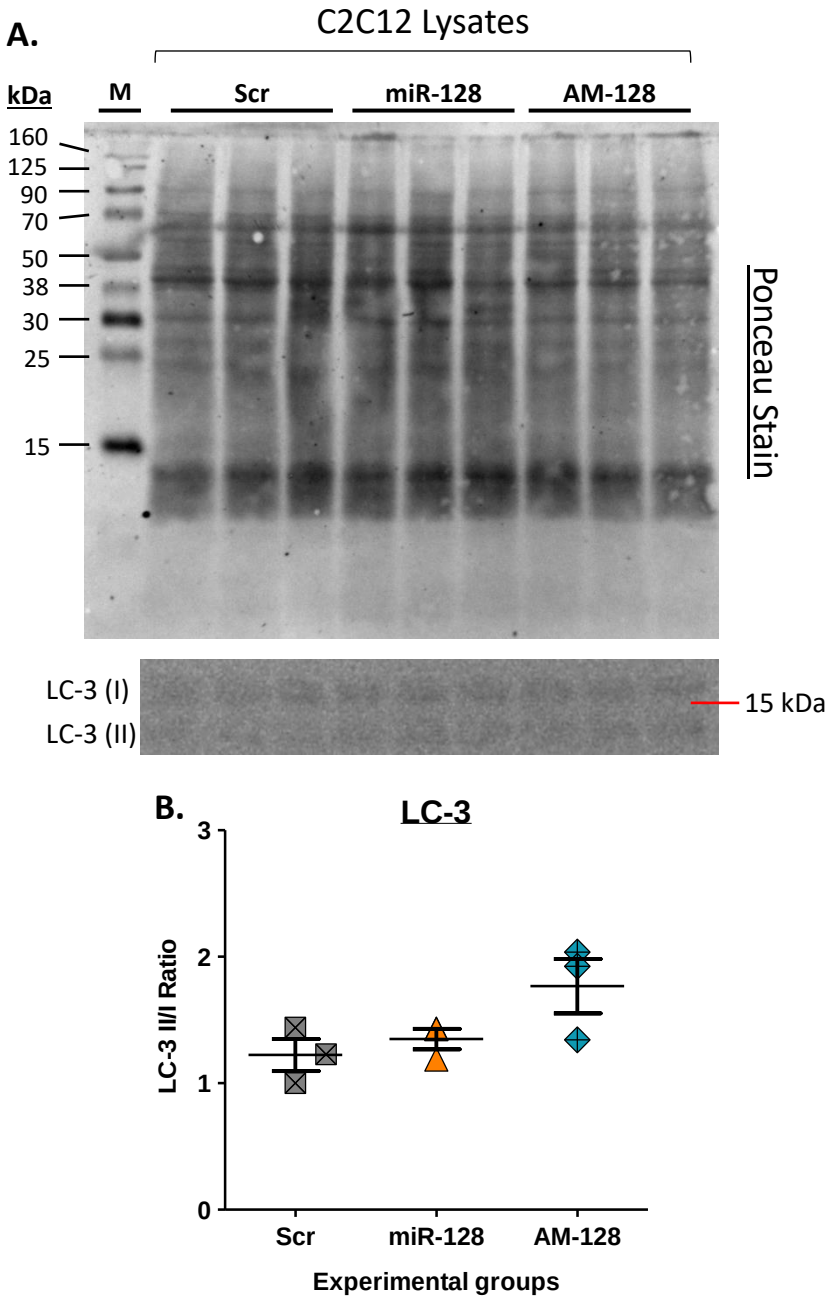

Figure 7.3.3.1 Quantification of protein levels of LC-3 following overexpression or inhibition of miR-128 in C2C12 cells. **A)** Blots LC-3 (I) and LC-3 (II), normalised to Ponceau S stain used as internal control for total protein concentration **B)** Ratio of LC-3 II/I, in order to determine the presence of autophagy/mitophagy in transfected cells. Scr served as the transfection control for statistical comparison. (*mean ± SEM*; *n*=3*; One-Way ANOVA with Dunnett's post-hoc analysis*).

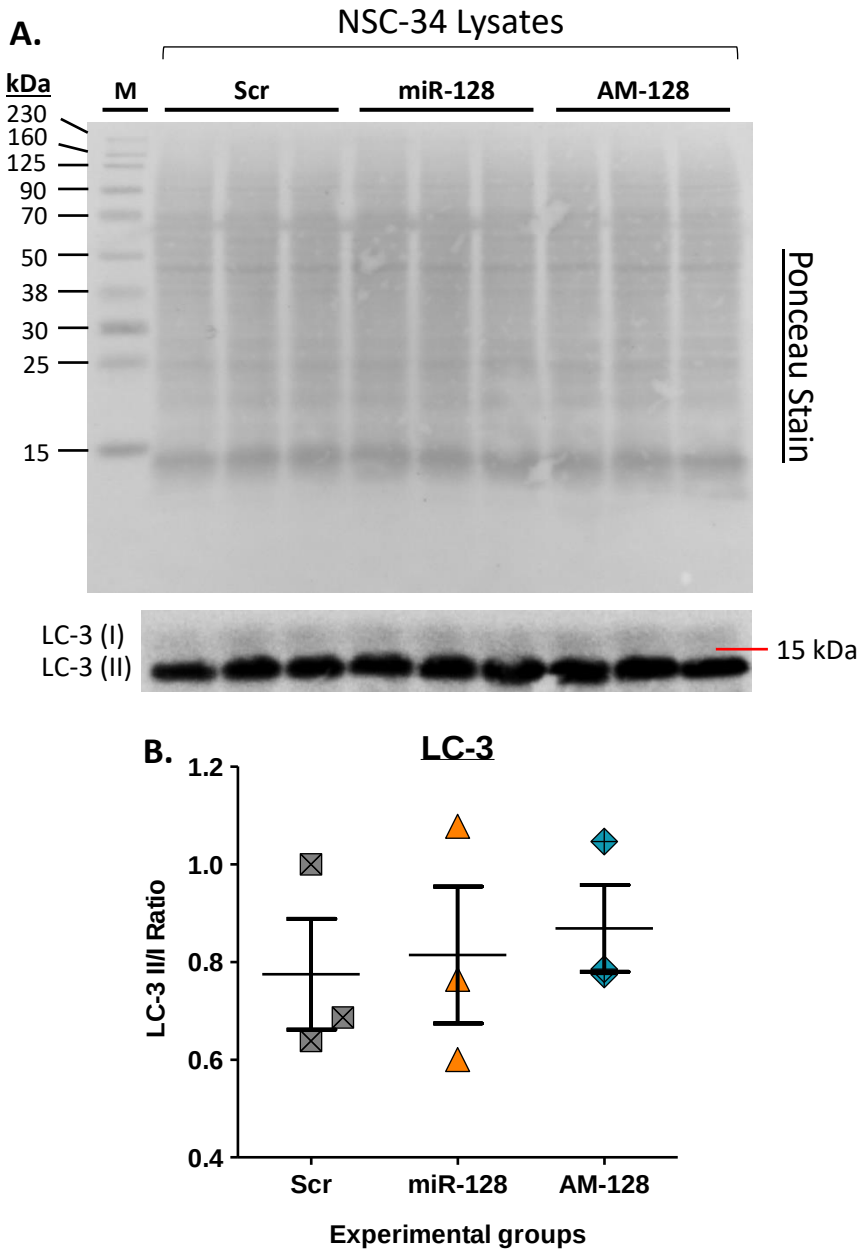

Figure 7.3.3.2 Quantification of protein levels of LC-3 following overexpression or inhibition of miR-128 in NSC-34 cells. **A)** Blots of LC-3 (I) and LC-3 (II) isoforms, normalised to Ponceau S stain used as internal control for total protein levels **B)** Ratio of LC-3 II/I, in order to determine the presence of autophagy/mitophagy in transfected cells. Scr served as the control group for statistical comparison. (*mean ± SEM*; *n*=3*; One-Way ANOVA with Dunnett's post-hoc analysis*).

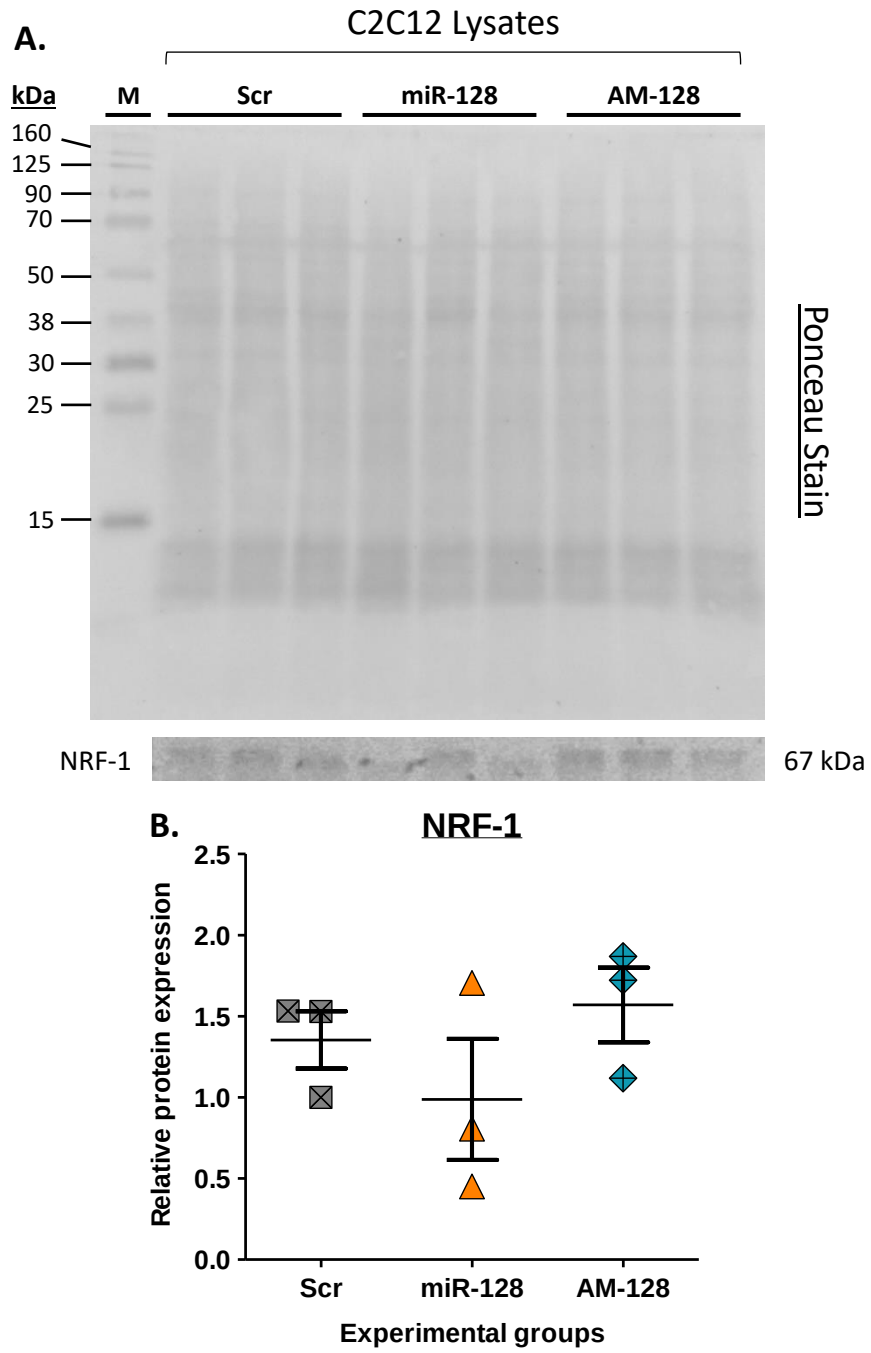

Figure 7.3.3.3 Quantification of protein levels of NRF-1 following inhibition or overexpression of miR-128 in C2C12 cells. **A)** NRF-1 protein blot, normalised to Ponceau S stain used as internal control for total protein concentration **B)** Protein levels of NRF-1. Scr served as the transfection control for statistical comparison. (*mean ± SEM*; *n*=3*; One-Way ANOVA with Dunnett's post-hoc analysis*).

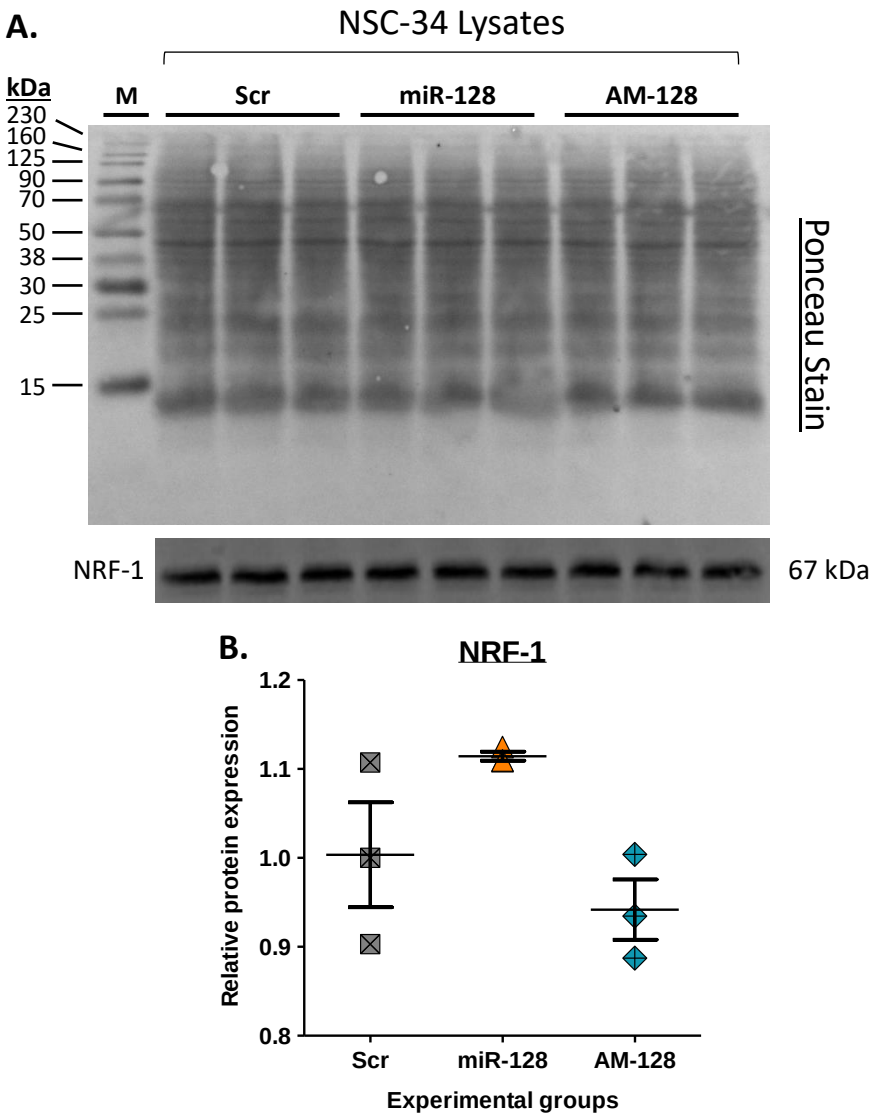

Figure 7.3.3.4 Quantification of protein levels of NRF-1 and COV-IV following overexpression or inhibition of miR-128 in NSC-34 cells. **A)** NRF-1 protein blot, normalised to Ponceau S stain used as internal control for total protein concentration **B)** Protein levels of NRF-1. Scr served as the control group for statistical comparison. (*mean ± SEM*; *n*=3*; One-Way ANOVA with Dunnett's post-hoc analysis*).

7.3.4 Expression levels of miR-128 predicted target genes in TA muscle and sciatic nerve of 12-week old mice

Relative gene expression analysis of miR-128 predicted target genes in TA muscle and SN of 12-week old mice are shown in **Figure 7.3.4**. Expression levels of NRF-1 and COX-IV in TA muscle showed no significant differences between the three groups (**Figure 7.3.4 A, B**). Expression of COX-IV in SN was also similar between the three groups, without significant changes being observed (**Figure 7.3.4 D**). However, relative expression levels of NRF-1 and GRB-2 were significantly increased in SN of NLL mice compared to the control group (NNN) (**Figure 7.3.4 C, E**).

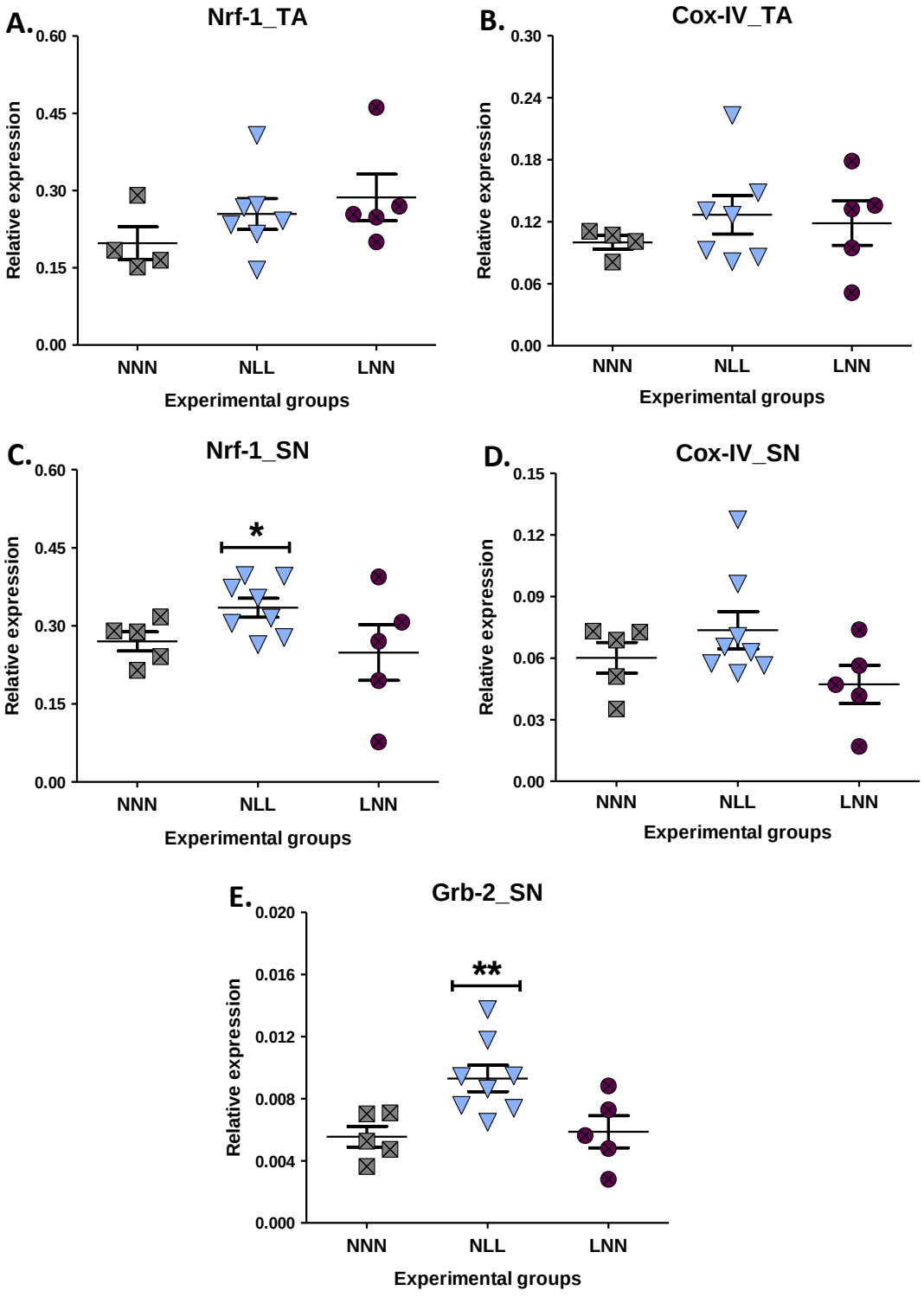

Figure 7.3.4 Relative expression levels of miR-128 predicted target genes in TA and SN of 12-week old mice. **A)** NRF-1 in TA, **B)** COX-IV in TA, **C)** NRF-1 in SN, **D)** COX-IV in SN, **E)** GRB-2 in SN. 18S was used as a housekeeping gene for normalisation of expression levels of the genes of interest. *represent significant differences compared with the NNN (control) group. *P≤0.05, **P≤0.01, ***

P≤0.001 (*mean ± SEM; n*=5-8*; One-Way ANOVA with Dunnett's post-hoc analysis*).

7.4 Discussion

This chapter focused on the expression patterns of miR-128 predicted target genes *in vitro* and *in vivo*. Analysis of the data obtained provided an insight into the molecular mechanisms affected by the deregulation of miR-128 expression on a post-transcriptional and post-translational level. Several predicted target genes showed differences in the expression patterns *in vitro* and *in vivo* in muscle and neurons, but no differences at a protein level were detected. Data suggested that changes in mitochondrial dynamics occurs, consistent with previous data on ATP production (Chapters 5 and 6), but the mechanisms causing these changes is not entirely clear.

7.4.1 The effects of miR-128 gain- and loss-of-function on the expression of predicted target genes in C2C12 and NSC-34 cells

Following the analyses of miR-128 gain- and loss-of-function in C2C12 and NSC-34 cells, we investigated whether changes in genes relevant for muscle and nerve function or development are affected by changes in miR-128 expression. It is important to note the unusual effects of miR-128 inhibition and overexpression on muscle cell phenotype with both overexpression and inhibition of miR having similar effects on proliferation, viability and myotube size of C2C12 cells. Quantitative PCR analysis of miR-128 predicted target gene expression in C2C12 cells showed significant downregulation of Pdgfrα-2 gene following overexpression of miR-128 (**Figure 7.3.1.1 D**). This observation may indicate that Pdgfrα-2 transcript might be a direct target of miR-128 in C2C12 cells. PGDFRα has been identified as a mediator of proliferation and survival of skeletal muscle during development (Fantauzzo and Soriano, 2018).

Downregulation of the Pdgfrα-2 gene could explain the reduction in cell proliferation and increase in cell death of C2C12 cells in Chapter 5, following overexpression of miR-128. PDGFR also plays an important role in regulating skeletal muscle hypertrophy *via* AKT/p70S6K pathway (Sugg *et al.* 2017). Interestingly, Pdgfrα-2 expression levels were significantly increased following inhibition of miR-128, while the opposite was not observed with overexpression of miR-128 in NSC-34 cells (**Figure 7.3.2.2 E**). PDGFRα is expressed in mouse motoneurons during embryonic stages and persists until adulthood (Oumesmar *et al.* 1997). PDGFRα knockout mice die at birth and exhibit defective myelination and tremor (reviewed in Funa and Sasahara, 2013). Therefore, upregulation of Pgdfrα-2 gene may have a neuroprotective role towards the NSC-34 cells, however the link between the expression of this gene with miR-128 remains to be established.

Overexpression of miR-128 in C2C12 cells was accompanied by upregulation of Cox-IV and Park-2 gene transcripts (**Figure 7.3.1.2 F, Figure 7.3.1.1 D**). Park-2, encoding parkin (PARK-2) protein, has been associated with removal of the dysfunctional mitochondria (Narendra *et al.* 2008). Overexpression of the Park-2 gene in skeletal muscle has been associated with muscle hypertrophy and improvement of mitochondrial enzyme activity (Leduc-Gaudet *et al.* 2019). COX-IV plays a central role in oxidative phosphorylation (OXPHOS) and mitochondria biogenesis (reviewed in Gnaiger, 2009). Specifically, COX-IV, like COX-I, is a subunit of cytochrome c oxidase, known as Complex IV, which is the terminal enzyme in the electron transport chain (Wong-Riley, 2013). Cox-IV is encoded by the nuclear DNA (Ze*via*ni *et al.* 1987), unlike Cox-I which is encoded by the mitochondrial DNA (Anderson *et al.* 1981). Reduction of COX-IV has been associated with the dysfunction of cytochrome c oxidase activity and therefore mitochondrial dysregulation in various cell types (reviewed in Arnold, 2012). Increased expression of Cox-IV gene transcript could be an indicator of increased mitochondrial activity during overexpression of miR-128. However, in NSC-34 cells, Cox-IV expression was upregulated following both overexpression and inhibition of miR-128 (**Figure 7.3.2.2 B**). This could either be due to expression of

different gene transcripts following overexpression or inhibition of miR-128 (reviewed in Arnold, 2012), or due to indirect regulation of Cox-IV transcripts. Upregulation of Park-2 and Cox-IV in C2C12 cells imply that their expression is unlikely to be directly mediated by miR-128 overexpression; it is possible that the expression levels of these two gene transcripts are controlled indirectly by miR-128. Another explanation is that miR-128 may regulate a different pool of target genes depending on its expression levels. A study from Shu et al. (2012) shows that miR-17-92 regulates a different subset of target genes in a dose-dependent manner, with implications for cell viability.

Interestingly, overexpression and inhibition of miR-128 resulted in downregulation of Cox-I gene expression in C2C12 cells (**Figure 7.3.1.2 E**), but Cox-I gene was downregulated following miR-128 overexpression in NSC-34 cells (**Figure 7.3.2.2 A**). COX-I, like COX-IV, plays a crucial role in OXPHOS and electron transport chain in the mitochondria (reviewed in Gnaiger, 2009). Cox-I gene is encoded by mitochondrial DNA (Anderson *et al.* 1981; reviewed in Taylor and Turnbull, 2005); therefore, alteration in the gene expression levels might be a marker of changes occurring in the mitochondria. Similar to Cox-IV, downregulation for Cox-I mRNA could be associated with deregulated oxidative phosphorylation and altered mitochondrial activity. Downregulation of Cox-I gene expression in NSC-34 cells following miR-128 overexpression make it a promising candidate target for direct binding by miR-128. Reduction in Cox-I expression levels following inhibition of miR-128 in C2C12 cells, might signify the regulation of Cox-I gene expression by multiple mechanisms. The downregulation of Cox-I mRNA following overexpression and inhibition of miR-128 in C2C12 is consistent with the reduction of ATP release seen in mitotoxicity assay in Chapter 5, Section 5.3.5. Therefore, it is possible that manipulation of miR-128 levels have a direct impact on the mitochondrial function, through control of genes encoding key enzymes of the mitochondrial electron transport chain. Increase in the levels of Cox-IV mRNA could also act as a compensation mechanism for the downregulation of Cox-I mRNA, as an attempt to restore or

maintain Complex IV integrity, during overexpression of miR-128 in C2C12 and NSC-34 cells.

In addition to these findings, miR-128 inhibition but not overexpression significantly reduced the expression levels of Nrf-1 and Sos-1 transcripts in C2C12 cells (**Figure 7.3.1.2 D, A**). The opposite was observed in NSC-34 cells, with Nrf-1 expression levels being increased following inhibition of miR-128 (**Figure 7.3.2.2 C**). Studies have shown that NRF-1 regulates the expression of all cytochrome c oxidase (Complex IV) subunits, including COX-I and COX-IV (Dhar *et al.* 2008). Although Cox-IV expression levels were not affected following inhibition of miR-128 in C2C12 cells, it is possible that the reduction in Nrf-1 expression is responsible for the reduction of Cox-I gene expression levels following miR-128 inhibition. Nrf-1 may have played a role in the increased expression of Cox-IV gene in NSC-34 cells, as both transcripts were upregulated following inhibition of miR-128. These data indicate the variable effect of miR-128 inhibition in C2C12 and NSC-34 cells. Both cell types have a high demand for mitochondrial respiration and OXPHOS activity in order to ensure proper mitochondrial function and metabolic activity. However, skeletal muscle and neuronal cells have shown distinct differences in mitochondrial bioenergetics during ageing. A study from Li *et al.* (2013) showed that skeletal muscle mitochondria were more susceptible to the presence for mitotoxins (e.g. FCCP). Mitochondrial respiration in skeletal muscle cells following treatment with FCCP declined earlier and the decline was more severe compared to the neuronal cells (Li *et al.* 2013). However, when ATP content was measured, the decline in total ATP produced was more severe in neuronal cells. Overall, mitochondrial deterioration occurred earlier and was more severe in skeletal muscle cells, compared to neuronal cells, which could be associated with the earlier decline in skeletal muscle mass and function during ageing, in comparison with the cognitive decline (Li *et al.* 2013).

SOS-1 forms a complex with GRB-2, activating RAS/ERK pathway following FGF or EGF signalling (Findlay *et al.* 2013). Downregulation of Sos-1 mRNA could have an impact on RAS/ERK signalling resulting in changes to downstream processes. Aside from forming a complex with SOS-1, GRB-2 is an essential

component of AChR cluster formation (Gingras *et al.* 2016). Although miR-128 overexpression had no impact on Grb-2 expression, inhibition of miR-128 resulted in increased expression of this transcript in NSC-34 cells (**Figure 7.3.2 E**). Upregulation of Grb-2 gene could promote upregulation of GRB-2 protein levels resulting in increased activation of downstream pathways such as PI3K and RAS signalling pathways (reviewed in Reichardt, 2006).

7.4.2 Changes in protein expression levels following miR-128 gain- and loss-of-function in C2C12 and NSC-34 cells

Protein levels of LC-3 and NRF-1 in C2C12 and NSC-34 cells showed no significant changes following overexpression or inhibition of miR-128 (**Figure 7.3.3.1-4**). Despite the significant changes seen in the levels NRF-1 transcripts in both C2C12 and NSC-34 transfected cells, there was no observed effect of miR-128 on NRF-1 protein levels. There are many parameters that could result in this difference between mRNA and protein expression. Protein levels depend on the rate of translation; therefore, abundance or inadequacy of mRNA transcript cannot automatically result in similar changes on a protein level. As a result, it is necessary to take into consideration any delays between transcription and translation process when comparing protein level changes with their respective mRNA transcript (reviewed in Liu *et al.* 2016). Another possibility is that despite the increase in the expression levels of Nrf-1 mRNA, there is no demand for new protein synthesis therefore the translation rate is not affected. Whether cell requirement for these protein increases, cells could undergo a "translation on demand" utilising the higher number of mRNA transcripts for increase of protein synthesis (reviewed in Liu *et al.* 2016). Absence of differences on a protein levels for NRF-1 and COX-IV could also be due to subtle changes seen on an mRNA detected *via* qPCR, which is a more sensitive method compared to protein quantification *via* Western Blot.

Protein expression levels also depend on the protein turnover rate, which is regulated by autophagy mechanism. LC3 proteins (LC3 I and LC3 II) play a crucial

role in autophagy and mitophagy process, as they are necessary for expansion and closure of autophagosomes (reviewed in Chen *et al.* 2018). During activation of autophagy, LC3 I is converted to LC3 II which is then recruited to autophagosome membrane (Tanida *et al.* 2008). LC3 proteins are also recruited during mitophagy, with dysfunctioning mitochondrial being discarded *via* phagocytosis (reviewed in Yoo and Jung, 2018). In order to measure activation of autophagy/mitophagy process, the ratio of LC3 II to LC3 I (LC3 II/I) was calculated following western blot analysis (Tanida *et al.* 2008). Western blot analysis of LC3 II/I ratio showed no significant changes following overexpression or inhibition of miR-128 in C2C12 and NSC-34 cells (**Figure 7.3.3.1-2**). Therefore, protein degradation rate *via* autophagy does not seem to be affected by alterations in miR-128 expression levels. As such, protein turnover rate could be either regulated *via* a different mechanism or remain stable in miR-128 transfected cells. Taken into consideration the cell viability and mitotoxicity data from Chapters 5 and 6 in C2C12 and NSC-34 cells, absence of differences in LC 3 ratio could indicate cell death in the presence of dysfunctioning mitochondria, but without the recruitment of autophagosomes (reviewed in Palikaras and Tavernarakis, 2014).

Despite the findings form the Western blot analysis, the low n number and the insufficient intensity of the band (potentially due to issues with the specific antibody binding or issues with sufficient protein loading) do not allow for solid conclusions to be drawn. Optimisation of antibody binding and protein loading or use of more sensitive techniques such as mass spectrometry or ELISA could provide more information about the levels of these proteins in C2C12 and NSC-34 cells following manipulation of miR-128 expression.

7.4.3 Expression of Nrf-1, Cox-IV and Grb-2 in TA muscle and SN tissue of 12-week old mice

Expression levels of Nrf-1 and Cox-IV mRNA levels showed no differences in the TA muscles of the three mouse groups (NNN, NLL, LNN) but Nrf-1 expression

was upregulated in SN of NLL mice (**Figure 7.3.4 C**). Significant upregulation of Grb-2 expression levels in SN of NLL mice was also recorded (**Figure 7.3.4 E**). MicroRNA-128 expression levels were significantly lower in NLL and LNN in TA muscle but no such differences were recorded in SN of those mice (Chapter 4, **Figure 4.3.2 A, C**). Together, these data indicate that Nrf-1 and Grb-2 are most likely not direct targets of miR-128, although this requires further investigation via 3'UTR reporter constructs. A possible scenario would be that Grb-2 and Nrf-1 expression might be regulated independently of miR-128 as a response to the low-protein diet postnatally. Considering the role of GRB-2 in the formation of AChR clusters at NMJs, it is possible that upregulation of its expression levels in NLL mice is a mechanism for repair of the defects at NMJ site or maturation of NMJ formation on a pre-synaptic level (discussed in detail in Chapter 3, Section 3.3.5). Increase in Nrf-1 expression could be associated with increased mitochondrial activity in SN of NLL mice. Mitochondria located in Schwann cells of myelinated axons are essential for their development and maintenance (reviewed in Ino and Lino, 2017). Therefore, increase in mitochondria biogenesis may signify the presence of an injury or damage caused by insufficient protein intake. In the case of delayed neuronal development due to low protein intake, increase in mitochondria activity could be necessary for the development and sufficient myelination of the axons. In order to answer these questions, further analysis of the morphology of the SN and quantification of mitochondrial content is required.

It is evident that miR-128 may control the expression of a number of transcripts differently in muscle and nerve *in vitro* and *in vivo*. Furthermore, miR-128 may also control a different pool of target genes in a dose-dependent manner, with implications for cell viability. However, further investigation is required, in order to identify the transcripts directly targeted by miR-128 and what would be the implications in metabolic processes *in vitro* and *in vivo*. A method commonly used in order to assess direct mRNA target/miR-128 interactions is *via* 3'UTR Luc/GFP reporter constructs.

Chapter 8

General discussion

8.1 Discussion

The present study examined the effect of low-protein diet at pre- and postnatal stages on the neuromuscular development and function in 12-week old mice. Furthermore, this study aimed to examine whether dietary protein restriction may alter the expression profile of microRNA molecules and therefore result in altered signalling of key metabolic pathways in skeletal muscle and motoneurons, using *in vivo* and *in vitro* approaches.

The main findings of this study are:

1. Pre- or postnatal protein restriction results in reduced muscle fibre number and increase of Atrogin-1 gene expression levels in 12-week old mice. Protein restriction only in postnatal stages resulted in reduced body weight and size, reduced weight of slow muscles or mixed muscles (but not in fast muscles), reduced maximum muscle forces without changes in specific force, and increase in morphological abnormalities of NMJs. Postnatal protein restriction was also accompanied by an increase in MyHC IIa expression levels in TA muscle.

2. Expression levels of miR-128 were downregulated in 12-week old mice on a low-protein diet pre- or postnatally, but expression levels of miR-133a were supressed only in 12-week old mice on a protein-deficient diet postnatally. *In silico* analysis of predicted target genes for miR-128 and miR-133a revealed a number of genes involved in key metabolic pathways including neurotrophin signalling pathway, FoxO signalling pathway, synaptic vesicle cycle and longevity regulating pathway. A number of predicted target genes were associated with mitochondrial function.

3. Gain- and loss-of-function of miR-128 in C2C12 cells resulted in increased fusion index, increased cell death, reduced myoblast proliferation and increased mitochondrial toxicity. miR-128 did not affect the diameter of terminally differentiated C2C12 myotubes following gain- and loss-of-

function experiments. Gain-of-function of miR-128 in NSC-34 cells resulted in reduction of axonal length and increase in cell death, but had no effect in cell proliferation.

4. Gain- and loss-of-function of miR-133a in C2C12 cells increased myoblast proliferation but had no impact on cell fusion. Overexpression of miR-133a reduced cell death, while inhibition of miR-133a increased myotube diameter and myotube area. Overexpression of miR-133a does not induce atrophy but possibly inhibits hypertrophy of C2C12 myotubes. miR-133a plays a role in regulation of myotube hypertrophy but not myogenesis. Inhibition of miR-133a in NSC-34 cells increased axonal length but had no impact in cell death and proliferation.

5. Gain-of-function of miR-128 resulted in increased expression of Park-2 and Cox-IV transcripts and reduced expression of Cox-I and Pdgfrα transcripts. Loss-of-function of miR-128 lead to reduction in Cox-I, Nrf-1 and Sos-1 transcripts in C2C12 myoblasts. Gain- and loss-of-function of miR-128 had no impact on NRF-1 and LC-3 protein content in C2C12 myoblasts. Findings suggest divergent mechanisms of miR-128 leading to cell death when miR-128 levels dysregulated (too high or low).

6. Gain- and loss-of-function of miR-128 resulted in increased expression of Cox-IV transcript in NSC-34 cells. Loss-of-function of miR-128 resulted in increased expression levels of Nrf-1, Grb-2 and Pdgfrα transcripts, while gain-of-function of miR-128 reduced the expression levels of Cox-I transcript in NSC-34 cells. Gain- and loss-of-function of miR-128 had no impact on NRF-1 and LC-3 protein content in NSC-34 cells. Nrf-1 and Grb-2 expression levels were upregulated in the SN of 12-week mice from the NLL group only.

In summary, dietary protein restriction postnatally has a negative impact in normal development, as seen in 12-week old mice, in line with previously

published data (Chen *et al*. 2009). Although 12-week old mice on a protein restricted diet pre-or postnatally seem to have similar muscle phenotype, muscle function and NMJ integrity is affected only by postnatal protein restriction. Furthermore, protein restriction appeared to have an impact on muscle weight of slow-twitch (SOL) or mixed-fibre-type (Quad, GTN) muscles, but no reduction in muscle weight was recorded in fast-twitch muscles (EDL, TA). Histological examination of the EDL muscle showed no apparent differences in the fibre crossectional area but a reduction if fibre number in both NLL and LNN groups of mice, indicating the role of dietary protein intake in muscle fibre number determination during development. Although the reduction in fibre number without accompanying differences in fibre sizes would be expected to have an impact on the muscle weight, such difference was not observed in the EDL muscle. One possible explanation for this phenomenon is that the protein-deficient diet at pre- or postnatal stages of development may have resulted in water retention in fast-twitch muscles, such as the EDL and TA muscle, which could explain the absence of significant differences in the muscle weight between the three groups of mice. Previous studies have highlighted the effect of a protein-deficient diet early in life on the water retention and abnormal water and electrolyte distribution, resulting in growth abnormalities (Fiorotto *et al.* 1987). However, water retention has been reported to affect differently the fast-twitch and the slow-twitch muscles due to their different osmolality sensitivity (Farhat *et al.* 2018). However, due to the lack of evidence supporting water imbalances in our study, the role of water in the muscle weight and fibre number differences in fast-twitch muscles (EDL, TA) in comparison with the slow-twitch or mixed fibre-type muscles (SOL, GTN, Quad) can only be speculated. In order to exclude the possibility that the reduction in fibre number in NLL and LNN groups is due to unintended selection of muscles belonging to a specific subgroup (muscles with lower weight), analysis of the body weight and muscle weight of the mice selected for histological examination were compared to the rest of the mice in each group (Appendix Section A7, **Figure A19**). Body weight and EDL muscle weight analysis confirm that the samples chosen for histological analysis did not present significant differences with the rest of the population in

each group. Therefore, we are confident that findings on body and muscle weight as well as muscle fibre number and size are real and not an unintended consequence of subgroup analyses. Furthermore, the differences recorded in the muscle force of the EDL muscle do not seem to be consistent with the differences in EDL fibre number analysis, which could indicate that reduction in muscle fibre number alone may not be sufficient to induce changes in the muscle strength. The reduction in the EDL muscle force may also be attributed to significant morphological changes seen at the NMJ site. Whether these morphological changes could also be due to or result in functional changes of the NMJ, remains currently unknown and requires further investigation with electrophysiology techniques. All things considered, the physiological differences observed between the NLL and LNN groups of mice highlight the possibility that protein restriction may modulate development *via* different mechanisms depending on the developmental stage it is introduced. Protein restriction seems to regulate the expression level of two microRNAs expressed in muscle, miR-128 and miR-133a. These findings are supported by a recent study from Sharma *et al*. showing regulation of small RNA fragments following parental dietary protein restriction and their influence in embryonic development of the offspring (Sharma *et al*. 2015). *In vitro* analysis focusing on the manipulation of miR-128 expression in skeletal muscle (C2C12) and motoneuron (NSC-34) cells indicates potential involvement of miR-128 in mitochondrial homeostasis and function, which may subsequently modulate cell survival and/or proliferation.

Previously published data on miR-128 directly targeting transcripts of components of IGF-1 signalling pathway, Sirt-1 and Pdgfrα, along with the data from gene expression analysis on Grb-2, Nrf-1, Cox-I and Cox-IV, we propose the following:

i) Regulation of skeletal muscle function occurs indirectly of miR-128 expression *via* genes involved in NMJ formation (Grb-2) and potentially mitochondrial function (Nrf-1, Cox-I, Cox-IV) in 12-week old mice.

ii) miR-133a may have a role in regulation of genes involved in neurotransmission and axonal sprouting in neuronal cells while inhibition of miR-133a may induce hypertrophy in myotubes *in vitro.* The role of miR-133a in neuromuscular transmission *in vivo* needs further exploration.

Downregulation of miR-128 expression levels in mice from both NLL and LNN groups are in line with upregulation of Atrogin-1 expression levels and reduction in EDL muscle fibre number of 12-week old mice. Despite the fibre loss, downregulation of miR-128 in 12-week old mice should increase the levels of its direct targets, Igf1, Igf1r, Sirt-1 and Pdgfrα, which would cause hypertrophy of the remaining EDL muscle fibres in NLL and LNN mice. Despite the potential effect of miR-128 following a low-protein diet pre- or postnatally, skeletal muscle function could be regulated indirectly of miR-128 *via* a different mechanism. Immature NMJ morphology (small area of synaptic site, limited branching and fragmentation) might be the result of slow growth of mice in the NLL group. This would be in line with the data from Chen *et al*. (2009) showing that mice on a normal diet pre-natally, but subjected to a protein-restricted diet postnatally displayed slow growth but increased lifespan. It is possible that slow growth may be attributed to decrease in ATP production from the mitochondria affecting both muscle function and neurotransmission, although this would need further investigation. Furthermore, the differences seen in the phenotype of mice of the NLL and LNN groups along with the reduction in miR-128 expression levels support the possibility that miR-128 may be regulated by a feedback mechanism involving different subset of genes controlling different aspects of cell behaviour and survival. Collectively, despite the significant reduction seen in miR-128 and miR-133a expression levels in skeletal muscle *in vivo* and taking into consideration the phenotype and gene expression changes seen in muscle and motoneuron cells *in vitro*, it remains unclear whether the difference in miR-128 and miR-133a expression in the skeletal muscle of mice is a direct consequence of the protein-deficient diet. Furthermore, the reduction in miR-128 and miR-133a levels may be the result of deregulation of molecular mechanisms directly

affected by the protein-deficient diet, which may differ depending on the developmental stage in which this diet was introduced. Therefore, the mechanisms affecting miR-128 and/or miR133a expression or the mechanisms affected by the downregulation of miR-128 and/or miR-133a expression might be different between the NLL and LNN groups of mice.

8.2 Limitation

Muscle and SN tissue samples from 12-week old mice used for molecular work in this study had been previously fixed with 10% NBF for 24 h. Fixation of this samples was a significant limitation towards investigating components of signalling pathways, such as FoxO, whose activity depends on post-translational modifications (acetylation, phosphorylation). Therefore, the exact effect of protein-restricted diet on these signalling pathways remains unknown. Tissue fixation was a limitation for detection of miR-128 and miR-133a in α-motoneurons on the spinal cord *via in situ* hybridisation. Tissue fixation was an important factor for the absence of MyHC isoform assessment, as the staining for the different MyHC isoforms requires unfixed tissue samples. Despite the absence of experimental analysis of the protein expression levels, the gene expression levels of many these proteins was performed via qPCR, which is a more sensitive technique for the detection of even subtle changes in their expression level.

Due to time restrictions, it was not possible to access the morphology of the SN and determine the degree of myelination and the number and size of axons. Although the morphology of the SN does not reflect the morphology and function of the motoneuron, it would provide important data on the efficiency of neurotransmission and/or motor unit number following dietary protein restriction.

Analysis of miR-133a following gain- and loss-of function experiments was limited, due to challenges achieving sufficient inhibition of miR-133a in C2C12

and NSC-34 cells. Additionally, design of primers for miR-133a predicted target genes of interest proved challenging. Therefore, investigation of predicted target genes was mainly focused on miR-128. Optimisation of *in vitro* miR-133a inhibition and primer design for predicted target genes of interest is of future interest.

Fixation of tissues in combination with limited financial support and time did not allow the investigation of the expression levels of specific proteins and their gene transcripts *in vivo* and *in vitro*. Transcriptomics and sequence analysis *in vivo* (in muscle and nerve) and *in vitro* (in C2C12 and NSC-34 cells following transfection experiments with miR-128 and miR-133a) could aid our understanding of the potential role of miR-128 and miR-133a following a low-protein diet pre- or postnatally. Specifically, identification of potentially common genes showing similar expression patterns *in vivo* and *in vitro* could refine potential molecular mechanisms most likely being affected by a protein-deficient diet and whether they are directly associated with or controlled by miR-128 and/or miR-133a. Additionally, proteomic analysis could reveal potential changes in the protein expression levels *in vivo* and *in vitro*, and whether these changes are in line the bioinformatics data, confirming the involvement of miR-128 and miR-133a in certain signalling pathways both *in vivo* and *in vitro*. Furthermore, protein expression changes in muscle and nerve both *in vivo* and *in vitro* would provide further explanation of the signalling pathways implicated in the physiological and functional changes seen in mice subjected to a low-protein diet pre- or postnatally.

8.3 Future directions

This study has provided some novel data on the effect of low-protein diet at pre- or postnatal stages of development on the neuromuscular physiology and function of adult mice and the potential molecular mechanisms involved.

In order to access whether reduction in skeletal muscle function is also attributed to fibre type distribution, immunofluorescent staining and analysis for different MyHC isoforms (type I, IIa, IIb, IIx/d) is necessary in both fast muscles (EDL, TA) and slow muscles (SOL).

To understand the exact mechanism of neuromuscular regulation by miR-128, assessment of direct binding of the predicted target genes by miR-128 should be conducted using 3'UTR luciferase assay in C2C12 and NSC-34 cells, following by western blotting to access protein content changes following manipulation of miR-128 expression levels. Similar protocol should be followed for miR-133a as well, in both *in vitro* models. Whether a successful muscle:nerve co-culture model is available, gain- and loss-of-function of miR-128 and miR-133a should be tested, to examine the effect of the two microRNAs at the early stages of synaptic formation. This experiment would determine whether delayed development indeed occurs following protein-restriction prenatally. Motoneuron function could also be assessed using electrophysiology techniques, in order to determine whether manipulation of miR-128 and miR-133a expression has any effect on neurotransmission. These data could provide an additional explanation on the mechanism causing reduced muscle function in mice of the NLL group. Assessment of miR-128 and miR-133a levels in skeletal muscle and α-motoneurons and their impact on signalling pathways in mice on a low-protein diet could also be investigated using high-throughput methods, including proteomics and RNA sequencing.

In vivo assessment of α-motoneuron and SN integrity should be assessed following appropriate histochemistry techniques. As mentioned in Section 8.2, histological examination of the SN would provide valuable data on the myelination, axonal size and axon number. These data would indicate whether reduced muscle function in mice of the NLL group might also be attributed to defective neurotransmission due to disruption ion myelination and/or reduced motor unit number. Transverse section of the lumbar region of the spinal cord would allow the direct assessment of the size and number of motoneurons, as well as assessment of miR-128 and miR-133a levels *via in situ* hybridisation.

Expression of neurotrophic factors and mitochondrial markers could also be assessed by immunofluorescent techniques.

In order to determine the quality and number of mitochondria, assessment of mitochondria respiration using muscle or neuronal tissue could be evaluated. Mitochondrial respiration can be measured using a Seahorse platform or an Oroboros O2k Oxygraph, using both cell and tissue samples. This instrument would allow the determination of mitochondrial respiration from both *in vivo* and *in vitro* models following miR-128 and miR-133a manipulation or tissues from mice on a protein restricted diet. This technique would allow the determination the determination of mitochondrial function and direct correlation of these data with data from mitochondrial marker assessment.

Importantly, to investigate the impact of miR-128 and/or miR-133a in neuromuscular maintenance of 12-week old mice on a low-protein diet pre- or postnatally, *in vivo* gain- and loss-of-function experiments would be crucial. These experiments would determine whether miR-128 and/or miR-133a could be used as therapeutic targets for any defects occurring in muscle and nerve, following dietary protein restriction.

In order to determine whether dietary protein restriction can contribute to premature ageing phenotype in muscle and nerve, maintenance of mice on a low-protein protocol until 22-24 months of age and assessment of their phenotype and neuromuscular function would be essential. Gain- and loss-of-function of miR-128 and/or miR-133a in ageing mice would provide evidence on whether this approach could rescue neuromuscular phenotype only early in life or whether it could be used as a therapeutic tool for improvement of neuromuscular ageing.

References

Acakpo-Satchivi, L. J., Edelmann, W., Sartorius, C., Lu, B. D., Wahr, P. A., Watkins, S. C., … Kucherlapati, R. (1997). Growth and muscle defects in mice lacking adult myosin heavy chain genes. *The Journal of Cell Biology*, *139*(5), 1219–1229.

Adlakha, Y K, Khanna, S., Singh, R., Singh, V. P., Agrawal, A., & Saini, N. (2013). Pro-apoptotic miRNA-128-2 modulates ABCA1, ABCG1 and RXRalpha expression and cholesterol homeostasis. *Cell Death & Disease*, *4*, e780.

Adlakha, Yogita K, & Saini, N. (2011). MicroRNA-128 downregulates Bax and induces apoptosis in human embryonic kidney cells. *Cellular and Molecular Life Sciences : CMLS*, *68*(8), 1415–1428.

Adlakha, Yogita K, & Saini, N. (2016). MicroRNA: a connecting road between apoptosis and cholesterol metabolism. *Tumour Biology : The Journal of the International Society for Oncodevelopmental Biology and Medicine*, *37*(7), 8529–8554.

Agbulut, O., Noirez, P., Beaumont, F., & Butler-Browne, G. (2003). Myosin heavy chain isoforms in postnatal muscle development of mice. *Biology of the Cell*, *95*(6), 399–406.

Aldridge, G. M., Podrebarac, D. M., Greenough, W. T., & Weiler, I. J. (2008). The use of total protein stains as loading controls: an alternative to high-abundance single-protein controls in semi-quantitative immunoblotting. *Journal of Neuroscience Methods*, *172*(2), 250–254.

Alexander, M. S., Kawahara, G., Motohashi, N., Casar, J. C., Eisenberg, I., Myers, J. A., … Kunkel, L. M. (2013). MicroRNA-199a is induced in dystrophic muscle and affects WNT signaling, cell proliferation, and myogenic differentiation. *Cell Death and Differentiation*, *20*(9), 1194–1208.

Alnaqeeb, M. A., & Goldspink, G. (1987). Changes in fibre type, number and diameter in developing and ageing skeletal muscle. *Journal of Anatomy*, *153*, 31–45.

Ambros, V. (2001). microRNAs: tiny regulators with great potential. *Cell*, *107*(7), 823–826.

Ambros, Victor. (2004). The functions of animal microRNAs. *Nature*, *431*(7006), 350–355.

Anderson, M. J., & Cohen, M. W. (1977). Nerve-induced and spontaneous redistribution of acetylcholine receptors on cultured muscle cells. *The Journal of Physiology*, *268*(3), 757–773.

Anderson, S., Bankier, A. T., Barrell, B. G., de Bruijn, M. H. L., Coulson, A. R., Drouin, J., … Young, I. G. (1981). Sequence and organization of the human mitochondrial genome. *Nature*, *290*(5806), 457–465.

Apel, P. J., Alton, T., Northam, C., Ma, J., Callahan, M., Sonntag, W. E., & Li, Z. (2009). How age impairs the response of the neuromuscular junction to nerve transection and repair: An experimental study in rats. *Journal of Orthopaedic Research : Official Publication of the Orthopaedic Research Society*, *27*(3), 385–393.

Arnold, A.-S., Christe, M., & Handschin, C. (2012). A functional motor unit in the

culture dish: co-culture of spinal cord explants and muscle cells. *Journal of Visualized Experiments : JoVE*, (62).

Arnold, S. (2012). The power of life--cytochrome c oxidase takes center stage in metabolic control, cell signalling and survival. *Mitochondrion*, *12*(1), 46–56.

Ashley, C. C., & Ridgway, E. B. (1968). Simultaneous recording of membrane potential, calcium transient and tension in single muscle fibers. *Nature*, *219*(5159), 1168–1169.

Augusto, V., Padovani, C. R., & Rocha Campos, G. E. (2004). Skeletal muscle fiber types in C57Bl6J mice. In *Braz. J. morphol. Sci* (Vol. 21).

Baker, K., Gordon, S. L., Melland, H., Bumbak, F., Scott, D. J., Jiang, T. J., … Raymond, F. L. (2018). SYT1-associated neurodevelopmental disorder: a case series. *Brain : A Journal of Neurology*, *141*(9), 2576–2591.

Balice-Gordon, R. J., & Lichtman, J. W. (1993). In vivo observations of pre- and postsynaptic changes during the transition from multiple to single innervation at developing neuromuscular junctions. *The Journal of Neuroscience : The Official Journal of the Society for Neuroscience*, *13*(2), 834–855.

Baloh, R. H., Rakowicz, W., Gardner, R., & Pestronk, A. (2007). Frequent atrophic groups with mixed-type myofibers is distinctive to motor neuron syndromes. *Muscle & Nerve*, *36*(1), 107–110.

Barany, M. (1967). ATPase activity of myosin correlated with speed of muscle shortening. *The Journal of General Physiology*, *50*(6), Suppl:197-218.

Baumann, H., Jaggi, M., Soland, F., Howald, H., & Schaub, M. C. (1987). Exercise training induces transitions of myosin isoform subunits within histochemically typed human muscle fibres. *Pflugers Archiv : European Journal of Physiology*, *409*(4–5), 349–360.

Bee, G. (2004). Effect of early gestation feeding, birth weight, and gender of progeny on muscle fiber characteristics of pigs at slaughter1. *Journal of Animal Science*, *82*(3), 826–836.

Beermann, D. H. (1983). Effects of Maternal Dietary Restriction during Gestation and Lactation, Muscle, Sex and Age on Various Indices of Skeletal Muscle Growth in the Rat. *Journal of Animal Science*, *57*(2), 328–337.

Bernstein, E., Caudy, A. A., Hammond, S. M., & Hannon, G. J. (2001). Role for a bidentate ribonuclease in the initiation step of RNA interference. *Nature*, *409*(6818), 363–366.

Billing, O., Kao, G., & Naredi, P. (2011). Mitochondrial function is required for secretion of DAF-28/insulin in C. elegans. *PloS One*, *6*(1), e14507.

Blattler, S. M., Verdeguer, F., Liesa, M., Cunningham, J. T., Vogel, R. O., Chim, H., … Puigserver, P. (2012). Defective mitochondrial morphology and bioenergetic function in mice lacking the transcription factor Yin Yang 1 in skeletal muscle. *Molecular and Cellular Biology*, *32*(16), 3333–3346.

Boggio, E. M., Pancrazi, L., Gennaro, M., Lo Rizzo, C., Mari, F., Meloni, I., … Costa, M. (2016). Visual impairment in FOXG1-mutated individuals and mice. *Neuroscience*, *324*, 496–508.

Bolliger, M. F., Zurlinden, A., Luscher, D., Butikofer, L., Shakhova, O., Francolini, M., … Sonderegger, P. (2010). Specific proteolytic cleavage of agrin regulates maturation of the neuromuscular junction. *Journal of Cell Science*,

123(Pt 22), 3944–3955.

Bruno, I. G., Karam, R., Huang, L., Bhardwaj, A., Lou, C. H., Shum, E. Y., … Wilkinson, M. F. (2011). Identification of a microRNA that activates gene expression by repressing nonsense-mediated RNA decay. *Molecular Cell*, *42*(4), 500–510.

Burke, R. E., Levine, D. N., Tsairis, P., & Zajac, F. E. 3rd. (1973). Physiological types and histochemical profiles in motor units of the cat gastrocnemius. *The Journal of Physiology*, *234*(3), 723–748.

Burke, R. E., Levine, D. N., & Zajac, F. E. 3rd. (1971). Mammalian motor units: physiological-histochemical correlation in three types in cat gastrocnemius. *Science (New York, N.Y.)*, *174*(4010), 709–712.

Butikofer, L., Zurlinden, A., Bolliger, M. F., Kunz, B., & Sonderegger, P. (2011). Destabilization of the neuromuscular junction by proteolytic cleavage of agrin results in precocious sarcopenia. *FASEB Journal : Official Publication of the Federation of American Societies for Experimental Biology*, *25*(12), 4378–4393.

Caggiano, R., Cattaneo, F., Moltedo, O., Esposito, G., Perrino, C., Trimarco, B., … Faraonio, R. (2017). miR-128 Is Implicated in Stress Responses by Targeting MAFG in Skeletal Muscle Cells. *Oxidative Medicine and Cellular Longevity*, *2017*, 9308310.

Campbell, M., & Ganetzky, B. (2012). Extensive morphological divergence and rapid evolution of the larval neuromuscular junction in Drosophila. *Proceedings of the National Academy of Sciences of the United States of America*, *109*(11), E648-55.

Cashman, N. R., Durham, H. D., Blusztajn, J. K., Oda, K., Tabira, T., Shaw, I. T., … Antel, J. P. (1992). Neuroblastoma x spinal cord (NSC) hybrid cell lines resemble developing motor neurons. *Developmental Dynamics : An Official Publication of the American Association of Anatomists*, *194*(3), 209–221.

Chaban, Y., Boekema, E. J., & Dudkina, N. V. (2014). Structures of mitochondrial oxidative phosphorylation supercomplexes and mechanisms for their stabilisation. *Biochimica et Biophysica Acta*, *1837*(4), 418–426.

Chai, R. J., Vukovic, J., Dunlop, S., Grounds, M. D., & Shavlakadze, T. (2011). Striking Denervation of Neuromuscular Junctions without Lumbar Motoneuron Loss in Geriatric Mouse Muscle. *PLOS ONE*, *6*(12), 1–11.

Chao, M. V. (2003). Neurotrophins and their receptors: a convergence point for many signalling pathways. *Nature Reviews. Neuroscience*, *4*(4), 299–309.

Chen, J.-F., Mandel, E. M., Thomson, J. M., Wu, Q., Callis, T. E., Hammond, S. M., … Wang, D.-Z. (2006). The role of microRNA-1 and microRNA-133 in skeletal muscle proliferation and differentiation. *Nature Genetics*, *38*(2), 228–233.

Chen, J.-H., Martin-Gronert, M. S., Tarry-Adkins, J., & Ozanne, S. E. (2009). Maternal protein restriction affects postnatal growth and the expression of key proteins involved in lifespan regulation in mice. *PloS One*, *4*(3), e4950.

Chen, Q., Kang, J., & Fu, C. (2018). The independence of and associations among apoptosis, autophagy, and necrosis. *Signal Transduction and Targeted Therapy*, *3*(1), 18.

Chen, X., Wang, K., Chen, J., Guo, J., Yin, Y., Cai, X., … Zhang, C.-Y. (2009). In vitro evidence suggests that miR-133a-mediated regulation of uncoupling protein

2 (UCP2) is an indispensable step in myogenic differentiation. *The Journal of Biological Chemistry*, *284*(8), 5362–5369.

Chen, Y., Zeng, J., Cen, L., Chen, Y., Wang, X., Yao, G., … Kong, K. (2009). Multiple roles of the p75 neurotrophin receptor in the nervous system. *The Journal of International Medical Research*, *37*(2), 281–288.

Chendrimada, T. P., Finn, K. J., Ji, X., Baillat, D., Gregory, R. I., Liebhaber, S. A., … Shiekhattar, R. (2007). MicroRNA silencing through RISC recruitment of eIF6. *Nature*, *447*(7146), 823–828.

Ching, A.-S., & Ahmad-Annuar, A. (2015). A Perspective on the Role of microRNA-128 Regulation in Mental and Behavioral Disorders. *Frontiers in Cellular Neuroscience*, *9*, 465.

Choi, S. J. (2014). Differential susceptibility on myosin heavy chain isoform following eccentric-induced muscle damage. *Journal of Exercise Rehabilitation*, *10*(6), 344–348.

Clark, P., Dunn, G. A., Knibbs, A., & Peckham, M. (2002). Alignment of myoblasts on ultrafine gratings inhibits fusion in vitro. *The International Journal of Biochemistry & Cell Biology*, *34*(7), 816–825.

Costello, P. M., Hollis, L. J., Cripps, R. L., Bearpark, N., Patel, H. P., Sayer, A. A., … Green, L. R. (2013). Lower maternal body condition during pregnancy affects skeletal muscle structure and glut-4 protein levels but not glucose tolerance in mature adult sheep. *Reproductive Sciences (Thousand Oaks, Calif.)*, *20*(10), 1144–1155.

Costello, P. M., Rowlerson, A., Astaman, N. A., Anthony, F. E. W., Sayer, A. A., Cooper, C., … Green, L. R. (2008). Peri-implantation and late gestation maternal undernutrition differentially affect fetal sheep skeletal muscle development. *The Journal of Physiology*, *586*(9), 2371–2379.

Cunningham, J. T., Rodgers, J. T., Arlow, D. H., Vazquez, F., Mootha, V. K., & Puigserver, P. (2007). mTOR controls mitochondrial oxidative function through a YY1-PGC-1alpha transcriptional complex. *Nature*, *450*(7170), 736–740.

d'Albis, A., Chanoine, C., Janmot, C., Mira, J. C., & Couteaux, R. (1990). Muscle-specific response to thyroid hormone of myosin isoform transitions during rat postnatal development. *European Journal of Biochemistry*, *193*(1), 155–161.

da Silva Aragao, R., Guzman-Quevedo, O., Perez-Garcia, G., Manhaes-de-Castro, R., & Bolanos-Jimenez, F. (2014). Maternal protein restriction impairs the transcriptional metabolic flexibility of skeletal muscle in adult rat offspring. *The British Journal of Nutrition*, *112*(3), 328–337.

Dai, Y., Zhang, W. R., Wang, Y. M., Liu, X. F., Li, X., Ding, X. Bin, & Guo, H. (2016). MicroRNA-128 regulates the proliferation and differentiation of bovine skeletal muscle satellite cells by repressing Sp1. *Molecular and Cellular Biochemistry*, *414*(1–2), 37–46.

Davies, K. M., Blum, T. B., & Kühlbrandt, W. (2018). Conserved in situ arrangement of complex I and III₂ in mitochondrial respiratory chain supercomplexes of mammals, yeast, and plants. *Proceedings of the National Academy of Sciences*, *115*(12), 3024 LP – 3029.

DeNardi, C., Ausoni, S., Moretti, P., Gorza, L., Velleca, M., Buckingham, M., &

Schiaffino, S. (1993). Type 2X-myosin heavy chain is coded by a muscle fiber type-specific and developmentally regulated gene. *The Journal of Cell Biology*, *123*(4), 823–835.

Deng, Z., Chen, J.-F., & Wang, D.-Z. (2011). Transgenic overexpression of miR-133a in skeletal muscle. *BMC Musculoskeletal Disorders*, *12*, 115.

Deretic, V. (2008). Autophagosome and phagosome. *Methods in Molecular Biology (Clifton, N.J.)*, *445*, 1–10.

Dhar, S. S., Ongwijitwat, S., & Wong-Riley, M. T. T. (2008). Nuclear respiratory factor 1 regulates all ten nuclear-encoded subunits of cytochrome c oxidase in neurons. *The Journal of Biological Chemistry*, *283*(6), 3120–3129.

Dodge, J. C., Haidet, A. M., Yang, W., Passini, M. A., Hester, M., Clarke, J., … Kaspar, B. K. (2008). Delivery of AAV-IGF-1 to the CNS extends survival in ALS mice through modification of aberrant glial cell activity. *Molecular Therapy : The Journal of the American Society of Gene Therapy*, *16*(6), 1056–1064.

Doench, J. G., & Sharp, P. A. (2004). Specificity of microRNA target selection in translational repression. *Genes & Development*, *18*(5), 504–511.

Doherty, T. J. (2003). Invited review: Aging and sarcopenia. *Journal of Applied Physiology (Bethesda, Md. : 1985)*, *95*(4), 1717–1727.

Eaton, S. L., Roche, S. L., Llavero Hurtado, M., Oldknow, K. J., Farquharson, C., Gillingwater, T. H., & Wishart, T. M. (2013). Total protein analysis as a reliable loading control for quantitative fluorescent Western blotting. *PloS One*, *8*(8), e72457.

ECCLES, J. C., ECCLES, R. M., IGGO, A., & LUNDBERG, A. (1960). Electrophysiological studies on gamma motoneurones. *Acta Physiologica Scandinavica*, *50*, 32–40.

Efremov, R. G., Baradaran, R., & Sazanov, L. A. (2010). The architecture of respiratory complex I. *Nature*, *465*(7297), 441–445.

Egan, D. F., Shackelford, D. B., Mihaylova, M. M., Gelino, S., Kohnz, R. A., Mair, W., … Shaw, R. J. (2011). Phosphorylation of ULK1 (hATG1) by AMP-activated protein kinase connects energy sensing to mitophagy. *Science (New York, N.Y.)*, *331*(6016), 456–461.

Eggett, C. J., Crosier, S., Manning, P., Cookson, M. R., Menzies, F. M., McNeil, C. J., & Shaw, P. J. (2000). Development and characterisation of a glutamate-sensitive motor neurone cell line. *Journal of Neurochemistry*, *74*(5), 1895–1902.

Ennion, S., Sant'ana Pereira, J., Sargeant, A. J., Young, A., & Goldspink, G. (1995). Characterization of human skeletal muscle fibres according to the myosin heavy chains they express. *Journal of Muscle Research and Cell Motility*, *16*(1), 35–43.

Eshima, H., Tamura, Y., Kakehi, S., Kurebayashi, N., Murayama, T., Nakamura, K., … Watada, H. (2017). Long-term, but not short-term high-fat diet induces fiber composition changes and impaired contractile force in mouse fast-twitch skeletal muscle. *Physiological Reports*, *5*(7).

Eulalio, A., Behm-Ansmant, I., Schweizer, D., & Izaurralde, E. (2007). P-body formation is a consequence, not the cause, of RNA-mediated gene silencing. *Molecular and Cellular Biology*, *27*(11), 3970–3981.

Fagman, H., Andersson, L., & Nilsson, M. (2006). The developing mouse thyroid: embryonic vessel contacts and parenchymal growth pattern during specification, budding, migration, and lobulation. *Developmental Dynamics : An Official Publication of the American Association of Anatomists*, *235*(2), 444–455.

Faitg, J., Leduc-Gaudet, J.-P., Reynaud, O., Ferland, G., Gaudreau, P., & Gouspillou, G. (2019). Effects of Aging and Caloric Restriction on Fiber Type Composition, Mitochondrial Morphology and Dynamics in Rat Oxidative and Glycolytic Muscles. *Frontiers in Physiology*, *10*, 420.

Fan, S., Ung, B., Parrott, E. P. J., & Pickwell-MacPherson, E. (2015). Gelatin embedding: a novel way to preserve biological samples for terahertz imaging and spectroscopy. *Physics in Medicine and Biology*, *60*(7), 2703–2713.

Fantauzzo, K. A., & Soriano, P. (2014). PI3K-mediated PDGFRalpha signaling regulates survival and proliferation in skeletal development through p53-dependent intracellular pathways. *Genes & Development*, *28*(9), 1005–1017.

Farhat, F., Grosset, J. F., & Canon, F. (2018). Water deprivation decreases strength in fast twitch muscle in contrast to slow twitch muscle in rat. *Acta Physiologica (Oxford, England)*, *224*(1), e13072.

Faulkner, J. A., Larkin, L. M., Claflin, D. R., & Brooks, S. V. (2007). Age-related changes in the structure and function of skeletal muscles. *Clinical and Experimental Pharmacology and Physiology*, *34*(11), 1091–1096.

Fazi, F., & Nervi, C. (2008). MicroRNA: basic mechanisms and transcriptional regulatory networks for cell fate determination. *Cardiovascular Research*, *79*(4), 553–561.

Feliciano, A., Sánchez-Sendra, B., Kondoh, H., & Lleonart, M. E. (2011). MicroRNAs Regulate Key Effector Pathways of Senescence. *Journal of Aging Research*, *2011*, 205378.

Feng, Y., Niu, L.-L., Wei, W., Zhang, W.-Y., Li, X.-Y., Cao, J.-H., & Zhao, S.-H. (2013). A feedback circuit between miR-133 and the ERK1/2 pathway involving an exquisite mechanism for regulating myoblast proliferation and differentiation. *Cell Death & Disease*, *4*, e934.

Fernandez-Marcos, P. J., & Auwerx, J. (2011). Regulation of PGC-1alpha, a nodal regulator of mitochondrial biogenesis. *The American Journal of Clinical Nutrition*, *93*(4), 884S – 90.

Feuers, R. J. (1998). The effects of dietary restriction on mitochondrial dysfunction in aging. *Annals of the New York Academy of Sciences*, *854*, 192–201.

Filipowicz, W., Bhattacharyya, S. N., & Sonenberg, N. (2008). Mechanisms of post-transcriptional regulation by microRNAs: are the answers in sight? *Nature Reviews. Genetics*, *9*(2), 102–114.

Findlay, G. M., Smith, M. J., Lanner, F., Hsiung, M. S., Gish, G. D., Petsalaki, E., … Pawson, T. (2013). Interaction domains of Sos1/Grb2 are finely tuned for cooperative control of embryonic stem cell fate. *Cell*, *152*(5), 1008–1020.

Fiorotto, M. L., Sheng, H. P., Evans, H. J., Leblanc, A. D., Johnson, P. C., & Nichols, B. L. (1987). Specific effects of weight loss, protein deficiency and energy deprivation on the water and electrolyte composition of young rats. *The*

Journal of Nutrition, *117*(5), 933–940.

Fischer, L. R., Igoudjil, A., Magrane, J., Li, Y., Hansen, J. M., Manfredi, G., & Glass, J. D. (2011). SOD1 targeted to the mitochondrial intermembrane space prevents motor neuropathy in the Sod1 knockout mouse. *Brain : A Journal of Neurology*, *134*(Pt 1), 196–209.

Fowden, A L, Mundy, L., & Silver, M. (1998). Developmental regulation of glucogenesis in the sheep fetus during late gestation. *The Journal of Physiology*, *508 (Pt 3*(Pt 3), 937–947.

Fowden, A L, Sibley, C., Reik, W., & Constancia, M. (2006). Imprinted genes, placental development and fetal growth. *Hormone Research*, *65 Suppl 3*(Suppl. 3), 50–58.

Fowden, Abigail L, & Forhead, A. J. (2009). Hormones as epigenetic signals in developmental programming. *Experimental Physiology*, *94*(6), 607–625.

Fox, M. A. (2009). Development of the Vertebrate Neuromuscular Junction. In H. Umemori & M. Hortsch (Eds.), *The Sticky Synapse: Cell Adhesion Molecules and Their Role in Synapse Formation and Maintenance* (pp. 39–84). New York, NY: Springer New York.

Franzoni, E., Booker, S. A., Parthasarathy, S., Rehfeld, F., Grosser, S., Srivatsa, S., … Wulczyn, F. G. (2015). miR-128 regulates neuronal migration, outgrowth and intrinsic excitability via the intellectual disability gene Phf6. *ELife*, *4*.

Frontera, W. R., & Ochala, J. (2015). Skeletal muscle: a brief review of structure and function. *Calcified Tissue International*, *96*(3), 183–195.

Funa, K., & Sasahara, M. (2014). The roles of PDGF in development and during neurogenesis in the normal and diseased nervous system. *Journal of Neuroimmune Pharmacology : The Official Journal of the Society on NeuroImmune Pharmacology*, *9*(2), 168–181.

Funston, R. N., Larson, D. M., & Vonnahme, K. A. (2010). Effects of maternal nutrition on conceptus growth and offspring performance: implications for beef cattle production. *Journal of Animal Science*, *88*(13 Suppl), E205-15.

Gabisonia, K., Prosdocimo, G., Aquaro, G. D., Carlucci, L., Zentilin, L., Secco, I., … Giacca, M. (2019). MicroRNA therapy stimulates uncontrolled cardiac repair after myocardial infarction in pigs. *Nature*, *569*(7756), 418–422.

Gagan, J., Dey, B. K., Layer, R., Yan, Z., & Dutta, A. (2011). MicroRNA-378 targets the myogenic repressor MyoR during myoblast differentiation. *The Journal of Biological Chemistry*, *286*(22), 19431–19438.

Gallagher, E. A. L., Newman, J. P., Green, L. R., & Hanson, M. A. (2005). The effect of low protein diet in pregnancy on the development of brain metabolism in rat offspring. *The Journal of Physiology*, *568*(Pt 2), 553–558.

Ge, Y., & Chen, J. (2011). MicroRNAs in skeletal myogenesis. *Cell Cycle (Georgetown, Tex.)*, *10*(3), 441–448.

Gill, E. L., Yost, R. A., Vedam-Mai, V., & Garrett, T. J. (2017). Precast Gelatin-Based Molds for Tissue Embedding Compatible with Mass Spectrometry Imaging. *Analytical Chemistry*, *89*(1), 576–580.

Gingras, J., Gawor, M., Bernadzki, K. M., Grady, R. M., Hallock, P., Glass, D. J., … Proszynski, T. J. (2016). Alpha-Dystrobrevin-1 recruits Grb2 and alpha-catulin to organize neurotransmitter receptors at the neuromuscular junction. *Journal of Cell Science*, *129*(5), 898–911.

Glaser, J., & Suzuki, M. (2018). Skeletal Muscle Fiber Types in Neuromuscular Diseases. In K. Sakuma (Ed.), *Muscle Cell and Tissue*. Rijeka: IntechOpen.

Glynn, D., Bortnick, R. A., & Morton, A. J. (2003). Complexin II is essential for normal neurological function in mice. *Human Molecular Genetics*, *12*(19), 2431–2448.

Gokhin, D. S., Ward, S. R., Bremner, S. N., & Lieber, R. L. (2008). Quantitative analysis of neonatal skeletal muscle functional improvement in the mouse. *The Journal of Experimental Biology*, *211*(Pt 6), 837–843.

Gold, S. M., Schulz, K.-H., Hartmann, S., Mladek, M., Lang, U. E., Hellweg, R., … Heesen, C. (2003). Basal serum levels and reactivity of nerve growth factor and brain-derived neurotrophic factor to standardized acute exercise in multiple sclerosis and controls. *Journal of Neuroimmunology*, *138*(1–2), 99–105.

Goljanek-Whysall, K., Mok, G. F., Fahad Alrefaei, A., Kennerley, N., Wheeler, G. N., & Munsterberg, A. (2014). myomiR-dependent switching of BAF60 variant incorporation into Brg1 chromatin remodeling complexes during embryo myogenesis. *Development (Cambridge, England)*, *141*(17), 3378–3387.

Goljanek-Whysall, K., Pais, H., Rathjen, T., Sweetman, D., Dalmay, T., & Munsterberg, A. (2012). Regulation of multiple target genes by miR-1 and miR-206 is pivotal for C2C12 myoblast differentiation. *Journal of Cell Science*, *125*(Pt 15), 3590–3600.

Goljanek-Whysall, K., Sweetman, D., Abu-Elmagd, M., Chapnik, E., Dalmay, T., Hornstein, E., & Munsterberg, A. (2011). MicroRNA regulation of the paired-box transcription factor Pax3 confers robustness to developmental timing of myogenesis. *Proceedings of the National Academy of Sciences of the United States of America*, *108*(29), 11936–11941.

Gomes, M. D., Lecker, S. H., Jagoe, R. T., Navon, A., & Goldberg, A. L. (2001). Atrogin-1, a muscle-specific F-box protein highly expressed during muscle atrophy. *Proceedings of the National Academy of Sciences of the United States of America*, *98*(25), 14440–14445.

Gong, J., Gu, H., Zhao, L., Wang, L., Liu, P., Wang, F., … Zhao, T. (2018). Phosphorylation of ULK1 by AMPK is essential for mouse embryonic stem cell self-renewal and pluripotency. *Cell Death & Disease*, *9*(2), 38.

Gonzalez, P. N., Gasperowicz, M., Barbeito-Andrés, J., Klenin, N., Cross, J. C., & Hallgrímsson, B. (2016). Chronic Protein Restriction in Mice Impacts Placental Function and Maternal Body Weight before Fetal Growth. *PLOS ONE*, *11*(3), 1–18.

Gould, J. M., Smith, P. J., Airey, C. J., Mort, E. J., Airey, L. E., Warricker, F. D. M., … Willaime-Morawek, S. (2018). Mouse maternal protein restriction during preimplantation alone permanently alters brain neuron proportion and adult short-term memory. *Proceedings of the National Academy of Sciences*, *115*(31), E7398 LP-E7407.

Green, H. J., Klug, G. A., Reichmann, H., Seedorf, U., Wiehrer, W., & Pette, D. (1984). Exercise-induced fibre type transitions with regard to myosin, parvalbumin, and sarcoplasmic reticulum in muscles of the rat. *Pflugers Archiv : European Journal of Physiology*, *400*(4), 432–438.

Grefte, S., Wagenaars, J. A. L., Jansen, R., Willems, P. H. G. M., & Koopman, W. J. H. (2015). Rotenone inhibits primary murine myotube formation via Raf-1 and ROCK2. *Biochimica et Biophysica Acta*, *1853*(7), 1606–1614.

Greising, S. M., Gransee, H. M., Mantilla, C. B., & Sieck, G. C. (2012). Systems biology of skeletal muscle: fiber type as an organizing principle. *Wiley Interdisciplinary Reviews. Systems Biology and Medicine*, *4*(5), 457–473.

Guidi, M., Muinos-Gimeno, M., Kagerbauer, B., Marti, E., Estivill, X., & Espinosa-Parrilla, Y. (2010). Overexpression of miR-128 specifically inhibits the truncated isoform of NTRK3 and upregulates BCL2 in SH-SY5Y neuroblastoma cells. *BMC Molecular Biology*, *11*, 95.

Guo, H., Ingolia, N. T., Weissman, J. S., & Bartel, D. P. (2010). Mammalian microRNAs predominantly act to decrease target mRNA levels. *Nature*, *466*(7308), 835–840.

Hather, B. M., Tesch, P. A., Buchanan, P., & Dudley, G. A. (1991). Influence of eccentric actions on skeletal muscle adaptations to resistance training. *Acta Physiologica Scandinavica*, *143*(2), 177–185.

He, M., Liu, Y., Wang, X., Zhang, M. Q., Hannon, G. J., & Huang, Z. J. (2012). Cell-type-based analysis of microRNA profiles in the mouse brain. *Neuron*, *73*(1), 35–48.

Hering, T., Braubach, P., Landwehrmeyer, G. B., Lindenberg, K. S., & Melzer, W. (2016). Fast-to-Slow Transition of Skeletal Muscle Contractile Function and Corresponding Changes in Myosin Heavy and Light Chain Formation in the R6/2 Mouse Model of Huntington's Disease. *PloS One*, *11*(11), e0166106.

Hirsch, N. P. (2007). Neuromuscular junction in health and disease. *British Journal of Anaesthesia*, *99*(1), 132–138.

Hitachi, K., & Tsuchida, K. (2013). Role of microRNAs in skeletal muscle hypertrophy. *Frontiers in Physiology*, *4*, 408.

Horak, M., Novak, J., & Bienertova-Vasku, J. (2016). Muscle-specific microRNAs in skeletal muscle development. *Developmental Biology*, *410*(1), 1–13.

Hortsch, M., & Umemori, H. (2009). *The Sticky Synapse: Cell Adhesion Molecules and Their Role in Synapse Formation and Maintenance*. Springer New York.

Hosokawa, N., Hara, T., Kaizuka, T., Kishi, C., Takamura, A., Miura, Y., … Mizushima, N. (2009). Nutrient-dependent mTORC1 association with the ULK1-Atg13-FIP200 complex required for autophagy. *Molecular Biology of the Cell*, *20*(7), 1981–1991.

Hoye, M. L., Koval, E. D., Wegener, A. J., Hyman, T. S., Yang, C., O'Brien, D. R., … Miller, T. M. (2017). MicroRNA Profiling Reveals Marker of Motor Neuron Disease in ALS Models. *The Journal of Neuroscience : The Official Journal of the Society for Neuroscience*, *37*(22), 5574–5586.

Huang, M.-B., Xu, H., Xie, S.-J., Zhou, H., & Qu, L.-H. (2011). Insulin-like growth factor-1 receptor is regulated by microRNA-133 during skeletal myogenesis. *PloS One*, *6*(12), e29173.

Huang, W., Feng, Y., Liang, J., Yu, H., Wang, C., Wang, B., … Wang, Y. (2018). Loss of microRNA-128 promotes cardiomyocyte proliferation and heart regeneration. *Nature Communications*, *9*(1), 700.

Humphreys, D. T., Westman, B. J., Martin, D. I. K., & Preiss, T. (2005). MicroRNAs control translation initiation by inhibiting eukaryotic initiation factor 4E/cap

and poly(A) tail function. *Proceedings of the National Academy of Sciences of the United States of America*, *102*(47), 16961–16966.

Huntley, R. P., Sitnikov, D., Orlic-Milacic, M., Balakrishnan, R., D'Eustachio, P., Gillespie, M. E., … Lovering, R. C. (2016). Guidelines for the functional annotation of microRNAs using the Gene Ontology. *RNA (New York, N.Y.)*, *22*(5), 667–676.

Hutvagner, G., McLachlan, J., Pasquinelli, A. E., Balint, E., Tuschl, T., & Zamore, P. D. (2001). A cellular function for the RNA-interference enzyme Dicer in the maturation of the let-7 small temporal RNA. *Science (New York, N.Y.)*, *293*(5531), 834–838.

HUXLEY, A. F., & NIEDERGERKE, R. (1954). Structural changes in muscle during contraction; interference microscopy of living muscle fibres. *Nature*, *173*(4412), 971–973.

Hyatt, J.-P. K., Nguyen, L., Hall, A. E., Huber, A. M., Kocan, J. C., Mattison, J. A., … Talmadge, R. J. (2016). Muscle-Specific Myosin Heavy Chain Shifts in Response to a Long-Term High Fat/High Sugar Diet and Resveratrol Treatment in Nonhuman Primates. *Frontiers in Physiology*, *7*, 77.

Ino, D., & Iino, M. (2017). Schwann cell mitochondria as key regulators in the development and maintenance of peripheral nerve axons. *Cellular and Molecular Life Sciences : CMLS*, *74*(5), 827–835.

Itakura, M., Misawa, H., Sekiguchi, M., Takahashi, S., & Takahashi, M. (1999). Transfection analysis of functional roles of complexin I and II in the exocytosis of two different types of secretory vesicles. *Biochemical and Biophysical Research Communications*, *265*(3), 691–696.

Ivey, K. N., Muth, A., Arnold, J., King, F. W., Yeh, R.-F., Fish, J. E., … Srivastava, D. (2008). MicroRNA regulation of cell lineages in mouse and human embryonic stem cells. *Cell Stem Cell*, *2*(3), 219–229.

Izarra, A., Moscoso, I., Canon, S., Carreiro, C., Fondevila, D., Martin-Caballero, J., … Bernad, A. (2017). miRNA-1 and miRNA-133a are involved in early commitment of pluripotent stem cells and demonstrate antagonistic roles in the regulation of cardiac differentiation. *Journal of Tissue Engineering and Regenerative Medicine*, *11*(3), 787–799.

Jackman, R. W., & Kandarian, S. C. (2004). The molecular basis of skeletal muscle atrophy. *American Journal of Physiology. Cell Physiology*, *287*(4), C834-43.

Jahn, R., & Fasshauer, D. (2012). Molecular machines governing exocytosis of synaptic vesicles. *Nature*, *490*(7419), 201–207.

Jing, L., Gordon, L. R., Shtibin, E., & Granato, M. (2010). Temporal and spatial requirements of unplugged/MuSK function during zebrafish neuromuscular development. *PloS One*, *5*(1), e8843.

Jonckheere, A. I., Smeitink, J. A. M., & Rodenburg, R. J. T. (2012). Mitochondrial ATP synthase: architecture, function and pathology. *Journal of Inherited Metabolic Disease*, *35*(2), 211–225.

Jones, R. A., Harrison, C., Eaton, S. L., Llavero Hurtado, M., Graham, L. C., Alkhammash, L., … Gillingwater, T. H. (2017). Cellular and Molecular Anatomy of the Human Neuromuscular Junction. *Cell Reports*, *21*(9), 2348–2356.

Joseph, A.-M., Malamo, A. G., Silvestre, J., Wawrzyniak, N., Carey-Love, S.,

Nguyen, L. M.-D., … Adhihetty, P. J. (2013). Short-term caloric restriction, resveratrol, or combined treatment regimens initiated in late-life alter mitochondrial protein expression profiles in a fiber-type specific manner in aged animals. *Experimental Gerontology*, *48*(9), 858–868.

Kaeser, P. S., Deng, L., Fan, M., & Sudhof, T. C. (2012). RIM genes differentially contribute to organizing presynaptic release sites. *Proceedings of the National Academy of Sciences of the United States of America*, *109*(29), 11830–11835.

Kaeser, P. S., Kwon, H.-B., Chiu, C. Q., Deng, L., Castillo, P. E., & Sudhof, T. C. (2008). RIM1alpha and RIM1beta are synthesized from distinct promoters of the RIM1 gene to mediate differential but overlapping synaptic functions. *The Journal of Neuroscience : The Official Journal of the Society for Neuroscience*, *28*(50), 13435–13447.

Kanda, K., & Hashizume, K. (1989). Changes in properties of the medial gastrocnemius motor units in aging rats. *Journal of Neurophysiology*, *61*(4), 737–746.

Kanning, K. C., Kaplan, A., & Henderson, C. E. (2010). Motor neuron diversity in development and disease. *Annual Review of Neuroscience*, *33*, 409–440.

Kim, H.-E., Rhee, J., Park, S., Yang, J., & Chun, J.-S. (2017). Upregulation of Atrogin-1/FBXO32 is not necessary for cartilage destruction in mouse models of osteoarthritis. *Osteoarthritis and Cartilage*, *25*(3), 397–400.

Kim, H. K., Lee, Y. S., Sivaprasad, U., Malhotra, A., & Dutta, A. (2006). Muscle-specific microRNA miR-206 promotes muscle differentiation. *The Journal of Cell Biology*, *174*(5), 677–687.

Kim, J., Kundu, M., Viollet, B., & Guan, K.-L. (2011). AMPK and mTOR regulate autophagy through direct phosphorylation of Ulk1. *Nature Cell Biology*, *13*(2), 132–141.

Kong, L., Wang, X., Choe, D. W., Polley, M., Burnett, B. G., Bosch-Marce, M., … Sumner, C. J. (2009). Impaired synaptic vesicle release and immaturity of neuromuscular junctions in spinal muscular atrophy mice. *The Journal of Neuroscience : The Official Journal of the Society for Neuroscience*, *29*(3), 842–851.

Koo, S. J., Kochlamazashvili, G., Rost, B., Puchkov, D., Gimber, N., Lehmann, M., … Maritzen, T. (2015). Vesicular Synaptobrevin/VAMP2 Levels Guarded by AP180 Control Efficient Neurotransmission. *Neuron*, *88*(2), 330–344.

Kummer, T. T., Misgeld, T., Lichtman, J. W., & Sanes, J. R. (2004). Nerve-independent formation of a topologically complex postsynaptic apparatus. *The Journal of Cell Biology*, *164*(7), 1077–1087.

Kummer, T. T., Misgeld, T., & Sanes, J. R. (2006). Assembly of the postsynaptic membrane at the neuromuscular junction: paradigm lost. *Current Opinion in Neurobiology*, *16*(1), 74–82.

Kuromi, H., Brass, B., & Kidokoro, Y. (1985). Formation of acetylcholine receptor clusters at neuromuscular junction in Xenopus cultures. *Developmental Biology*, *109*(1), 165–176.

Lagos-Quintana, M, Rauhut, R., Lendeckel, W., & Tuschl, T. (2001). Identification of novel genes coding for small expressed RNAs. *Science (New York, N.Y.)*, *294*(5543), 853–858.

Lagos-Quintana, Mariana, Rauhut, R., Yalcin, A., Meyer, J., Lendeckel, W., & Tuschl, T. (2002). Identification of tissue-specific microRNAs from mouse. *Current Biology : CB*, *12*(9), 735–739.

Landmesser, L. (1978). The distribution of motoneurones supplying chick hind limb muscles. *The Journal of Physiology*, *284*, 371–389.

Lapuente-Brun, E., Moreno-Loshuertos, R., Acin-Perez, R., Latorre-Pellicer, A., Colas, C., Balsa, E., … Enriquez, J. A. (2013). Supercomplex assembly determines electron flux in the mitochondrial electron transport chain. *Science (New York, N.Y.)*, *340*(6140), 1567–1570.

Larsson, L, Biral, D., Campione, M., & Schiaffino, S. (1993). An age-related type IIB to IIX myosin heavy chain switching in rat skeletal muscle. *Acta Physiologica Scandinavica*, *147*(2), 227–234.

Larsson, L, Muller, U., Li, X., & Schiaffino, S. (1995). Thyroid hormone regulation of myosin heavy chain isoform composition in young and old rats, with special reference to IIX myosin. *Acta Physiologica Scandinavica*, *153*(2), 109–116.

Larsson, Lars, Degens, H., Li, M., Salviati, L., Lee, Y. Il, Thompson, W., … Sandri, M. (2019). Sarcopenia: Aging-Related Loss of Muscle Mass and Function. *Physiological Reviews*, *99*(1), 427–511.

Lavasani, M., Lu, A., Peng, H., Cummins, J., & Huard, J. (2006). Nerve growth factor improves the muscle regeneration capacity of muscle stem cells in dystrophic muscle. *Human Gene Therapy*, *17*(2), 180–192.

Lawlor, M. A., Mora, A., Ashby, P. R., Williams, M. R., Murray-Tait, V., Malone, L., … Alessi, D. R. (2002). Essential role of PDK1 in regulating cell size and development in mice. *The EMBO Journal*, *21*(14), 3728–3738.

Leduc-Gaudet, J.-P., Reynaud, O., Hussain, S. N., & Gouspillou, G. (2019). Parkin overexpression protects from ageing-related loss of muscle mass and strength. *The Journal of Physiology*, *597*(7), 1975–1991.

Lee, D., & Goldberg, A. L. (2013). SIRT1 protein, by blocking the activities of transcription factors FoxO1 and FoxO3, inhibits muscle atrophy and promotes muscle growth. *The Journal of Biological Chemistry*, *288*(42), 30515–30526.

Lee, E.-J., & Tournier, C. (2011). The requirement of uncoordinated 51-like kinase 1 (ULK1) and ULK2 in the regulation of autophagy. *Autophagy*, *7*(7), 689–695.

Lee, J.-W., Kim, N.-H., & Milanesi, A. (2014). Thyroid Hormone Signaling in Muscle Development, Repair and Metabolism. *Journal of Endocrinology, Diabetes & Obesity*, *2*(3), 1046.

Lee, R. C., Feinbaum, R. L., & Ambros, V. (1993). The C. elegans heterochronic gene lin-4 encodes small RNAs with antisense complementarity to lin-14. *Cell*, *75*(5), 843–854.

Lee, Y., Ahn, C., Han, J., Choi, H., Kim, J., Yim, J., … Kim, V. N. (2003). The nuclear RNase III Drosha initiates microRNA processing. *Nature*, *425*(6956), 415–419.

Lexell, J., & Downham, D. Y. (1991). The occurrence of fibre-type grouping in healthy human muscle: a quantitative study of cross-sections of whole vastus lateralis from men between 15 and 83 years. *Acta Neuropathologica*,

81(4), 377–381.

Lexell, J., Taylor, C. C., & Sjostrom, M. (1988). What is the cause of the ageing atrophy? Total number, size and proportion of different fiber types studied in whole vastus lateralis muscle from 15- to 83-year-old men. *Journal of the Neurological Sciences*, *84*(2–3), 275–294.

Li, H., Kumar Sharma, L., Li, Y., Hu, P., Idowu, A., Liu, D., … Bai, Y. (2013). Comparative bioenergetic study of neuronal and muscle mitochondria during aging. *Free Radical Biology & Medicine*, *63*, 30–40.

Li, J., Kinoshita, T., Pandey, S., Ng, C. K.-Y., Gygi, S. P., Shimazaki, K., & Assmann, S. M. (2002). Modulation of an RNA-binding protein by abscisic-acid-activated protein kinase. *Nature*, *418*(6899), 793–797.

Li, L., Xiong, W.-C., & Mei, L. (2018). Neuromuscular Junction Formation, Aging, and Disorders. *Annual Review of Physiology*, *80*, 159–188.

Li, M., Fu, W., Wo, L., Shu, X., Liu, F., & Li, C. (2013). miR-128 and its target genes in tumorigenesis and metastasis. *Experimental Cell Research*, *319*(20), 3059–3064.

Li, P., Teng, Z.-Q., & Liu, C.-M. (2016). Extrinsic and Intrinsic Regulation of Axon Regeneration by MicroRNAs after Spinal Cord Injury. *Neural Plasticity*, *2016*, 1279051.

Li, Yan, Jiang, J., Liu, W., Wang, H., Zhao, L., Liu, S., … Ying, H. (2018). microRNA-378 promotes autophagy and inhibits apoptosis in skeletal muscle. *Proceedings of the National Academy of Sciences of the United States of America*, *115*(46), E10849–E10858.

Li, Yinghui, Li, F., Wu, L., Wei, H., Liu, Y., Li, T., … Yin, Y. (2016). Effects of dietary protein restriction on muscle fiber characteristics and mTORC1 pathway in the skeletal muscle of growing-finishing pigs. *Journal of Animal Science and Biotechnology*, *7*(1), 47.

Li, Youfen, Park, J.-S., Deng, J.-H., & Bai, Y. (2006). Cytochrome c oxidase subunit IV is essential for assembly and respiratory function of the enzyme complex. *Journal of Bioenergetics and Biomembranes*, *38*(5–6), 283–291.

Lian, B., Yang, D., Liu, Y., Shi, G., Li, J., Yan, X., … Zhang, R. (2018). miR-128 Targets the SIRT1/ROS/DR5 Pathway to Sensitize Colorectal Cancer to TRAIL-Induced Apoptosis. *Cellular Physiology and Biochemistry : International Journal of Experimental Cellular Physiology, Biochemistry, and Pharmacology*, *49*(6), 2151–2162.

Lichtman, J. W., & Sanes, J. R. (2003). Watching the neuromuscular junction. *Journal of Neurocytology*, *32*(5–8), 767–775.

Lindstrom, J. (1997). Nicotinic acetylcholine receptors in health and disease. *Molecular Neurobiology*, *15*(2), 193–222.

Liu, N., Bezprozvannaya, S., Shelton, J. M., Frisard, M. I., Hulver, M. W., McMillan, R. P., … Olson, E. N. (2011). Mice lacking microRNA 133a develop dynamin 2-dependent centronuclear myopathy. *The Journal of Clinical Investigation*, *121*(8), 3258–3268.

Liu, N., Williams, A. H., Kim, Y., McAnally, J., Bezprozvannaya, S., Sutherland, L. B., … Olson, E. N. (2007). An intragenic MEF2-dependent enhancer directs muscle-specific expression of microRNAs 1 and 133. *Proceedings of the National Academy of Sciences of the United States of America*, *104*(52),

20844–20849.
Liu, Yansheng, Beyer, A., & Aebersold, R. (2016). On the Dependency of Cellular Protein Levels on mRNA Abundance. *Cell*, *165*(3), 535–550.
Liu, Yun, Li, H., Sugiura, Y., Han, W., Gallardo, G., Khvotchev, M., … Lin, W. (2015). Ubiquitin-Synaptobrevin Fusion Protein Causes Degeneration of Presynaptic Motor Terminals in Mice. *The Journal of Neuroscience : The Official Journal of the Society for Neuroscience*, *35*(33), 11514–11531.
Liu, Yun, Padgett, D., Takahashi, M., Li, H., Sayeed, A., Teichert, R. W., … Lin, W. (2008). Essential roles of the acetylcholine receptor gamma-subunit in neuromuscular synaptic patterning. *Development (Cambridge, England)*, *135*(11), 1957–1967.
Livak, K. J., & Schmittgen, T. D. (2001). Analysis of relative gene expression data using real-time quantitative PCR and the 2(-Delta Delta C(T)) Method. *Methods (San Diego, Calif.)*, *25*(4), 402–408.
Long, A. A., Mahapatra, C. T., Woodruff, E. A. 3rd, Rohrbough, J., Leung, H.-T., Shino, S., … Broadie, K. (2010). The nonsense-mediated decay pathway maintains synapse architecture and synaptic vesicle cycle efficacy. *Journal of Cell Science*, *123*(Pt 19), 3303–3315.
Louicharoen, C., Patin, E., Paul, R., Nuchprayoon, I., Witoonpanich, B., Peerapittayamongkol, C., … Sakuntabhai, A. (2009). Positively selected G6PD-Mahidol mutation reduces Plasmodium vivax density in Southeast Asians. *Science (New York, N.Y.)*, *326*(5959), 1546–1549.
Luo, Y., Wu, X., Ling, Z., Yuan, L., Cheng, Y., Chen, J., & Xiang, C. (2015). microRNA133a targets Foxl2 and promotes differentiation of C2C12 into myogenic progenitor cells. *DNA and Cell Biology*, *34*(1), 29–36.
Lynch, G. S., Hinkle, R. T., Chamberlain, J. S., Brooks, S. V, & Faulkner, J. A. (2001). Force and power output of fast and slow skeletal muscles from mdx mice 6-28 months old. *The Journal of Physiology*, *535*(Pt 2), 591–600.
Lyons, P. R., & Slater, C. R. (1991). Structure and function of the neuromuscular junction in young adult mdx mice. *Journal of Neurocytology*, *20*(12), 969–981.
MacRae, I. J., Zhou, K., & Doudna, J. A. (2007). Structural determinants of RNA recognition and cleavage by Dicer. *Nature Structural & Molecular Biology*, *14*(10), 934–940.
Majdan, M., & Miller, F. D. (1999). Neuronal life and death decisions functional antagonism between the Trk and p75 neurotrophin receptors. *International Journal of Developmental Neuroscience : The Official Journal of the International Society for Developmental Neuroscience*, *17*(3), 153–161.
Marabita, M., Baraldo, M., Solagna, F., Ceelen, J. J. M., Sartori, R., Nolte, H., … Blaauw, B. (2016). S6K1 Is Required for Increasing Skeletal Muscle Force during Hypertrophy. *Cell Reports*, *17*(2), 501–513.
Mariani, J., Coppola, G., Zhang, P., Abyzov, A., Provini, L., Tomasini, L., … Vaccarino, F. M. (2015). FOXG1-Dependent Dysregulation of GABA/Glutamate Neuron Differentiation in Autism Spectrum Disorders. *Cell*, *162*(2), 375–390.
Marieb, E. N., & Hoehn, K. (2010). *Human Anatomy & Physiology* (8th ed.). Benjamin Cummings.

Marques, M. J., Conchello, J. A., & Lichtman, J. W. (2000). From plaque to pretzel: fold formation and acetylcholine receptor loss at the developing neuromuscular junction. *The Journal of Neuroscience : The Official Journal of the Society for Neuroscience*, *20*(10), 3663–3675.

Martinez-Hernandez, R., Bernal, S., Alias, L., & Tizzano, E. F. (2014). Abnormalities in early markers of muscle involvement support a delay in myogenesis in spinal muscular atrophy. *Journal of Neuropathology and Experimental Neurology*, *73*(6), 559–567.

Martini, F. H., Welch, K., & Ober, W. C. (2006). *Fundamentals of Anatomy & Physiology* (7th ed.). Prentice Hall.

Marwarha, G., Claycombe-Larson, K., Schommer, J., & Ghribi, O. (2017). Maternal low-protein diet decreases brain-derived neurotrophic factor expression in the brains of the neonatal rat offspring. *The Journal of Nutritional Biochemistry*, *45*, 54–66.

Marzetti, E., Lees, H. A., Wohlgemuth, S. E., & Leeuwenburgh, C. (2009). Sarcopenia of aging: underlying cellular mechanisms and protection by calorie restriction. *BioFactors (Oxford, England)*, *35*(1), 28–35.

Mastroeni, D., Khdour, O. M., Delvaux, E., Nolz, J., Olsen, G., Berchtold, N., … Coleman, P. D. (2017). Nuclear but not mitochondrial-encoded oxidative phosphorylation genes are altered in aging, mild cognitive impairment, and Alzheimer's disease. *Alzheimer's & Dementia : The Journal of the Alzheimer's Association*, *13*(5), 510–519.

Matusica, D., Fenech, M. P., Rogers, M.-L., & Rush, R. A. (2008). Characterization and use of the NSC-34 cell line for study of neurotrophin receptor trafficking. *Journal of Neuroscience Research*, *86*(3), 553–565.

MAURO, A. (1961). Satellite cell of skeletal muscle fibers. *The Journal of Biophysical and Biochemical Cytology*, *9*, 493–495.

Mazzon, C., Anselmo, A., Soldani, C., Cibella, J., Ploia, C., Moalli, F., … Viola, A. (2012). Agrin is required for survival and function of monocytic cells. *Blood*, *119*(23), 5502–5511.

McCarthy, J. J. (2011). The MyomiR network in skeletal muscle plasticity. *Exercise and Sport Sciences Reviews*, *39*(3), 150–154.

McCarthy, J. J., Mula, J., Miyazaki, M., Erfani, R., Garrison, K., Farooqui, A. B., … Peterson, C. A. (2011). Effective fiber hypertrophy in satellite cell-depleted skeletal muscle. *Development (Cambridge, England)*, *138*(17), 3657–3666.

McKiernan, S. H., Bua, E., McGorray, J., & Aiken, J. (2004). Early-onset calorie restriction conserves fiber number in aging rat skeletal muscle. *FASEB Journal : Official Publication of the Federation of American Societies for Experimental Biology*, *18*(3), 580–581.

McMahon, H. T., Missler, M., Li, C., & Sudhof, T. C. (1995). Complexins: cytosolic proteins that regulate SNAP receptor function. *Cell*, *83*(1), 111–119.

McSweeney, K. M., Gussow, A. B., Bradrick, S. S., Dugger, S. A., Gelfman, S., Wang, Q., … Goldstein, D. B. (2016). Inhibition of microRNA 128 promotes excitability of cultured cortical neuronal networks. *Genome Research*, *26*(10), 1411–1416.

Megraw, M., Sethupathy, P., Gumireddy, K., Jensen, S. T., Huang, Q., & Hatzigeorgiou, A. G. (2010). Isoform specific gene auto-regulation via

miRNAs: a case study on miR-128b and ARPP-21. *Theoretical Chemistry Accounts*, *125*(3), 593–598.

Meister, G., Landthaler, M., Patkaniowska, A., Dorsett, Y., Teng, G., & Tuschl, T. (2004). Human Argonaute2 mediates RNA cleavage targeted by miRNAs and siRNAs. *Molecular Cell*, *15*(2), 185–197.

Mishina, M., Takai, T., Imoto, K., Noda, M., Takahashi, T., Numa, S., … Sakmann, B. (1986). Molecular distinction between fetal and adult forms of muscle acetylcholine receptor. *Nature*, *321*(6068), 406–411.

Missias, A. C., Chu, G. C., Klocke, B. J., Sanes, J. R., & Merlie, J. P. (1996). Maturation of the acetylcholine receptor in skeletal muscle: regulation of the AChR gamma-to-epsilon switch. *Developmental Biology*, *179*(1), 223–238.

Mok, G. F., Lozano-Velasco, E., Maniou, E., Viaut, C., Moxon, S., Wheeler, G., & Munsterberg, A. (2018). miR-133-mediated regulation of the Hedgehog pathway orchestrates embryo myogenesis. *Development (Cambridge, England)*, *145*(12).

Motohashi, N., Alexander, M. S., Casar, J. C., & Kunkel, L. M. (2012). Identification of a novel microRNA that regulates the proliferation and differentiation in muscle side population cells. *Stem Cells and Development*, *21*(16), 3031–3043.

Motohashi, N., Alexander, M. S., Shimizu-Motohashi, Y., Myers, J. A., Kawahara, G., & Kunkel, L. M. (2013). Regulation of IRS1/Akt insulin signaling by microRNA-128a during myogenesis. *Journal of Cell Science*, *126*(Pt 12), 2678–2691.

Mousavi, K., & Jasmin, B. J. (2006). BDNF is expressed in skeletal muscle satellite cells and inhibits myogenic differentiation. *The Journal of Neuroscience : The Official Journal of the Society for Neuroscience*, *26*(21), 5739–5749.

Mukai, J., Shoji, S., Kimura, M. T., Okubo, S., Sano, H., Suvanto, P., … Sato, T.-A. (2002). Structure-function analysis of NADE: identification of regions that mediate nerve growth factor-induced apoptosis. *The Journal of Biological Chemistry*, *277*(16), 13973–13982.

Naguibneva, I., Ameyar-Zazoua, M., Polesskaya, A., Ait-Si-Ali, S., Groisman, R., Souidi, M., … Harel-Bellan, A. (2006). The microRNA miR-181 targets the homeobox protein Hox-A11 during mammalian myoblast differentiation. *Nature Cell Biology*, *8*(3), 278–284.

Nait Oumesmar, B., Vignais, L., & Baron-Van Evercooren, A. (1997). Developmental expression of platelet-derived growth factor alpha-receptor in neurons and glial cells of the mouse CNS. *The Journal of Neuroscience : The Official Journal of the Society for Neuroscience*, *17*(1), 125–139.

Nakanishi, K., Nakasa, T., Tanaka, N., Ishikawa, M., Yamada, K., Yamasaki, K., … Ochi, M. (2010). Responses of microRNAs 124a and 223 following spinal cord injury in mice. *Spinal Cord*, *48*(3), 192–196.

Nakazato, K., & Song, H. (2008). Increased oxidative properties of gastrocnemius in rats fed on a high-protein diet. *The Journal of Nutritional Biochemistry*, *19*(1), 26–32.

Narendra, D., Tanaka, A., Suen, D.-F., & Youle, R. J. (2008). Parkin is recruited selectively to impaired mitochondria and promotes their autophagy. *The*

Journal of Cell Biology, *183*(5), 795–803.

Nguyen, Q. T., Parsadanian, A. S., Snider, W. D., & Lichtman, J. W. (1998). Hyperinnervation of neuromuscular junctions caused by GDNF overexpression in muscle. *Science (New York, N.Y.)*, *279*(5357), 1725–1729.

Nilsen, T. W. (2007). Mechanisms of microRNA-mediated gene regulation in animal cells. *Trends in Genetics : TIG*, *23*(5), 243–249.

Nurcombe, V., Hill, M. A., Eagleson, K. L., & Bennett, M. R. (1984). Motor neuron survival and neuritic extension from spinal cord explants induced by factors released from denervated muscle. *Brain Research*, *291*(1), 19–28.

Olguin, H. C., & Pisconti, A. (2012). Marking the tempo for myogenesis: Pax7 and the regulation of muscle stem cell fate decisions. *Journal of Cellular and Molecular Medicine*, *16*(5), 1013–1025.

Olson, E. N. (1992). Interplay between proliferation and differentiation within the myogenic lineage. *Developmental Biology*, *154*(2), 261–272.

Oster, M., Murani, E., Metges, C. C., Ponsuksili, S., & Wimmers, K. (2012). A gestational high protein diet affects the abundance of muscle transcripts related to cell cycle regulation throughout development in porcine progeny. *PloS One*, *7*(4), e34519.

Owen, D. J., Collins, B. M., & Evans, P. R. (2004). Adaptors for clathrin coats: structure and function. *Annual Review of Cell and Developmental Biology*, *20*, 153–191.

Paik, J., Ding, Z., Narurkar, R., Ramkissoon, S., Muller, F., Kamoun, W. S., … DePinho, R. A. (2009). FoxOs cooperatively regulate diverse pathways governing neural stem cell homeostasis. *Cell Stem Cell*, *5*(5), 540–553.

Pallocca, G., Fabbri, M., Nerini-Molteni, S., Pistollato, F., Zagoura, D., Sacco, G. M., … Bal-Price, A. (2014). Changes in miRNA Expression Profiling during Neuronal Differentiation and Methyl Mercury-Induced Toxicity in Human in Vitro Models. *Toxics*, Vol. 2, pp. 443–463.

Pancrazi, L., Di Benedetto, G., Colombaioni, L., Della Sala, G., Testa, G., Olimpico, F., … Costa, M. (2015). Foxg1 localizes to mitochondria and coordinates cell differentiation and bioenergetics. *Proceedings of the National Academy of Sciences of the United States of America*, *112*(45), 13910–13915.

Papagiannakopoulos, T., Friedmann-Morvinski, D., Neveu, P., Dugas, J. C., Gill, R. M., Huillard, E., … Kosik, K. S. (2012). Pro-neural miR-128 is a glioma tumor suppressor that targets mitogenic kinases. *Oncogene*, *31*(15), 1884–1895.

Park, S. Y., Jang, S. Y., Shin, Y. K., Jung, D. K., Yoon, B. A., Kim, J. K., … Park, H. T. (2017). The Scaffolding Protein, Grb2-associated Binder-1, in Skeletal Muscles and Terminal Schwann Cells Regulates Postnatal Neuromuscular Synapse Maturation. *Experimental Neurobiology*, *26*(3), 141–150.

Pasquinelli, A. E., Reinhart, B. J., Slack, F., Martindale, M. Q., Kuroda, M. I., Maller, B., … Ruvkun, G. (2000). Conservation of the sequence and temporal expression of let-7 heterochronic regulatory RNA. *Nature*, *408*(6808), 86–89.

Pearn, J. (1980). CLASSIFICATION OF SPINAL MUSCULAR ATROPHIES. *The Lancet*, *315*(8174), 919–922.

Peter, J. B., Barnard, R. J., Edgerton, V. R., Gillespie, C. A., & Stempel, K. E. (1972). Metabolic profiles of three fiber types of skeletal muscle in guinea pigs and

rabbits. *Biochemistry*, *11*(14), 2627–2633.
Peters, L., & Meister, G. (2007). Argonaute proteins: mediators of RNA silencing. *Molecular Cell*, *26*(5), 611–623.
Petersen, C. P., Bordeleau, M.-E., Pelletier, J., & Sharp, P. A. (2006). Short RNAs repress translation after initiation in mammalian cells. *Molecular Cell*, *21*(4), 533–542.
Pette, D., & Staron, R. S. (2000). Myosin isoforms, muscle fiber types, and transitions. *Microscopy Research and Technique*, *50*(6), 500–509.
Piasecki, M., Ireland, A., Piasecki, J., Stashuk, D. W., Swiecicka, A., Rutter, M. K., … McPhee, J. S. (2018). Failure to expand the motor unit size to compensate for declining motor unit numbers distinguishes sarcopenic from non-sarcopenic older men. *The Journal of Physiology*, *596*(9), 1627–1637.
Pillai, R. S., Bhattacharyya, S. N., Artus, C. G., Zoller, T., Cougot, N., Basyuk, E., … Filipowicz, W. (2005). Inhibition of translational initiation by Let-7 MicroRNA in human cells. *Science (New York, N.Y.)*, *309*(5740), 1573–1576.
Porporato, P. E., Filigheddu, N., Reano, S., Ferrara, M., Angelino, E., Gnocchi, V. F., … Graziani, A. (2013). Acylated and unacylated ghrelin impair skeletal muscle atrophy in mice. *The Journal of Clinical Investigation*, *123*(2), 611–622.
Poskanzer, K. E., Marek, K. W., Sweeney, S. T., & Davis, G. W. (2003). Synaptotagmin I is necessary for compensatory synaptic vesicle endocytosis in vivo. *Nature*, *426*(6966), 559–563.
Pratt, S. J. P., Shah, S. B., Ward, C. W., Inacio, M. P., Stains, J. P., & Lovering, R. M. (2013). Effects of in vivo injury on the neuromuscular junction in healthy and dystrophic muscles. *The Journal of Physiology*, *591*(2), 559–570.
Pratt, S. J. P., Valencia, A. P., Le, G. K., Shah, S. B., & Lovering, R. M. (2015). Pre- and postsynaptic changes in the neuromuscular junction in dystrophic mice. *Frontiers in Physiology*, *6*, 252.
Quintens, R., Singh, S., Lemaire, K., De Bock, K., Granvik, M., Schraenen, A., … Schuit, F. (2013). Mice deficient in the respiratory chain gene Cox6a2 are protected against high-fat diet-induced obesity and insulin resistance. *PloS One*, *8*(2), e56719.
Rao, P. K., Kumar, R. M., Farkhondeh, M., Baskerville, S., & Lodish, H. F. (2006). Myogenic factors that regulate expression of muscle-specific microRNAs. *Proceedings of the National Academy of Sciences of the United States of America*, *103*(23), 8721–8726.
Redenbach, D. M., Ovalle, W. K., & Bressler, B. H. (1988). Effect of neonatal denervation on the distribution of fiber types in a mouse fast-twitch skeletal muscle. *Histochemistry*, *89*(4), 333–342.
Rehfeldt, C., Te Pas, M. F. W., Wimmers, K., Brameld, J. M., Nissen, P. M., Berri, C., … Oksbjerg, N. (2011). Advances in research on the prenatal development of skeletal muscle in animals in relation to the quality of muscle-based food. I. Regulation of myogenesis and environmental impact. *Animal : An International Journal of Animal Bioscience*, *5*(5), 703–717.
Reichardt, L. F. (2006). Neurotrophin-regulated signalling pathways. *Philosophical Transactions of the Royal Society of London. Series B, Biological Sciences*, *361*(1473), 1545–1564.

Reinhart, B. J., Slack, F. J., Basson, M., Pasquinelli, A. E., Bettinger, J. C., Rougvie, A. E., … Ruvkun, G. (2000). The 21-nucleotide let-7 RNA regulates developmental timing in Caenorhabditis elegans. *Nature*, *403*(6772), 901–906.

Ribchester, R. R., Thomson, D., Haddow, L. J., & Ushkaryov, Y. A. (1998). Enhancement of spontaneous transmitter release at neonatal mouse neuromuscular junctions by the glial cell line-derived neurotrophic factor (GDNF). *The Journal of Physiology*, *512 (Pt 3*, 635–641.

Risson, V., Mazelin, L., Roceri, M., Sanchez, H., Moncollin, V., Corneloup, C., … Gangloff, Y.-G. (2009). Muscle inactivation of mTOR causes metabolic and dystrophin defects leading to severe myopathy. *The Journal of Cell Biology*, *187*(6), 859–874.

Ruberti, F., Capsoni, S., Comparini, A., Di Daniel, E., Franzot, J., Gonfloni, S., … Cattaneo, A. (2000). Phenotypic knockout of nerve growth factor in adult transgenic mice reveals severe deficits in basal forebrain cholinergic neurons, cell death in the spleen, and skeletal muscle dystrophy. *The Journal of Neuroscience : The Official Journal of the Society for Neuroscience*, *20*(7), 2589–2601.

Ruby, J. G., Jan, C. H., & Bartel, D. P. (2007). Intronic microRNA precursors that bypass Drosha processing. *Nature*, *448*(7149), 83–86.

Rudolf, R., Khan, M. M., Labeit, S., & Deschenes, M. R. (2014). Degeneration of neuromuscular junction in age and dystrophy. *Frontiers in Aging Neuroscience*, *6*, 99.

Ruegg, M. A., & Bixby, J. L. (1998). Agrin orchestrates synaptic differentiation at the vertebrate neuromuscular junction. *Trends in Neurosciences*, *21*(1), 22–27.

Russell, S. D., Cambon, N., Nadal-Ginard, B., & Whalen, R. G. (1988). Thyroid hormone induces a nerve-independent precocious expression of fast myosin heavy chain mRNA in rat hindlimb skeletal muscle. *The Journal of Biological Chemistry*, *263*(13), 6370–6374.

Rutter, J., Winge, D. R., & Schiffman, J. D. (2010). Succinate dehydrogenase - Assembly, regulation and role in human disease. *Mitochondrion*, *10*(4), 393–401.

Sakellariou, G. K., Pearson, T., Lightfoot, A. P., Nye, G. A., Wells, N., Giakoumaki, I. I., … Jackson, M. J. (2016). Long-term administration of the mitochondria-targeted antioxidant mitoquinone mesylate fails to attenuate age-related oxidative damage or rescue the loss of muscle mass and function associated with aging of skeletal muscle. *FASEB Journal : Official Publication of the Federation of American Societies for Experimental Biology*, *30*(11), 3771–3785.

Sakellariou, G. K., Pearson, T., Lightfoot, A. P., Nye, G. A., Wells, N., Giakoumaki, I. I., … McArdle, A. (2016). Mitochondrial ROS regulate oxidative damage and mitophagy but not age-related muscle fiber atrophy. *Scientific Reports*, *6*, 33944.

Sakuma, K., & Yamaguchi, A. (2011). The recent understanding of the neurotrophin's role in skeletal muscle adaptation. *Journal of Biomedicine & Biotechnology*, *2011*, 201696.

Salpeter, M. M., Marchaterre, M., & Harris, R. (1988). Distribution of extrajunctional acetylcholine receptors on a vertebrate muscle: evaluated by using a scanning electron microscope autoradiographic procedure. *The Journal of Cell Biology*, *106*(6), 2087–2093.

Sander, A., Hesser, B. A., & Witzemann, V. (2001). MuSK induces in vivo acetylcholine receptor clusters in a ligand-independent manner. *The Journal of Cell Biology*, *155*(7), 1287–1296.

Sandri, M., Lin, J., Handschin, C., Yang, W., Arany, Z. P., Lecker, S. H., … Spiegelman, B. M. (2006). PGC-1alpha protects skeletal muscle from atrophy by suppressing FoxO3 action and atrophy-specific gene transcription. *Proceedings of the National Academy of Sciences of the United States of America*, *103*(44), 16260–16265.

Satoh, A., & Imai, S. (2014). Systemic regulation of mammalian ageing and longevity by brain sirtuins. *Nature Communications*, *5*, 4211.

Savtchenko, L. P., & Rusakov, D. A. (2007). The optimal height of the synaptic cleft. *Proceedings of the National Academy of Sciences of the United States of America*, *104*(6), 1823–1828.

Sayer, A. A., Syddall, H. E., Gilbody, H. J., Dennison, E. M., & Cooper, C. (2004). Does sarcopenia originate in early life? Findings from the Hertfordshire cohort study. *The Journals of Gerontology. Series A, Biological Sciences and Medical Sciences*, *59*(9), M930-4.

Schiaffino, S, Gorza, L., Sartore, S., Saggin, L., Ausoni, S., Vianello, M., … Lomo, T. (1989). Three myosin heavy chain isoforms in type 2 skeletal muscle fibres. *Journal of Muscle Research and Cell Motility*, *10*(3), 197–205.

Schiaffino, S, & Reggiani, C. (1994). Myosin isoforms in mammalian skeletal muscle. *Journal of Applied Physiology (Bethesda, Md. : 1985)*, *77*(2), 493–501.

Schiaffino, Stefano, Dyar, K. A., Ciciliot, S., Blaauw, B., & Sandri, M. (2013). Mechanisms regulating skeletal muscle growth and atrophy. *The FEBS Journal*, *280*(17), 4294–4314.

Schiaffino, Stefano, & Reggiani, C. (2011). Fiber types in mammalian skeletal muscles. *Physiological Reviews*, *91*(4), 1447–1531.

Schoch, S., Deak, F., Konigstorfer, A., Mozhayeva, M., Sara, Y., Sudhof, T. C., & Kavalali, E. T. (2001). SNARE function analyzed in synaptobrevin/VAMP knockout mice. *Science (New York, N.Y.)*, *294*(5544), 1117–1122.

Schoneich, C., Dremina, E., Galeva, N., & Sharov, V. (2014). Apoptosis in differentiating C2C12 muscle cells selectively targets Bcl-2-deficient myotubes. *Apoptosis : An International Journal on Programmed Cell Death*, *19*(1), 42–57.

Schwarz, D. S., Hutvagner, G., Du, T., Xu, Z., Aronin, N., & Zamore, P. D. (2003). Asymmetry in the assembly of the RNAi enzyme complex. *Cell*, *115*(2), 199–208.

Selman, C., Tullet, J. M. A., Wieser, D., Irvine, E., Lingard, S. J., Choudhury, A. I., … Withers, D. J. (2009). Ribosomal protein S6 kinase 1 signaling regulates mammalian life span. *Science (New York, N.Y.)*, *326*(5949), 140–144.

Sharma, U., Conine, C. C., Shea, J. M., Boskovic, A., Derr, A. G., Bing, X. Y., … Rando, O. J. (2016). Biogenesis and function of tRNA fragments during

sperm maturation and fertilization in mammals. *Science (New York, N.Y.)*, *351*(6271), 391–396.

Sheard, P. W., & Anderson, R. D. (2012). Age-related loss of muscle fibres is highly variable amongst mouse skeletal muscles. *Biogerontology*, *13*(2), 157–167.

Shi, L., Fu, A. K. Y., & Ip, N. Y. (2012). Molecular mechanisms underlying maturation and maintenance of the vertebrate neuromuscular junction. *Trends in Neurosciences*, *35*(7), 441–453.

Shi, L., Zhou, B., Li, P., Schinckel, A. P., Liang, T., Wang, H., … Huang, R. (2015). MicroRNA-128 targets myostatin at coding domain sequence to regulate myoblasts in skeletal muscle development. *Cellular Signalling*, *27*(9), 1895–1904.

Shima, H., Pende, M., Chen, Y., Fumagalli, S., Thomas, G., & Kozma, S. C. (1998). Disruption of the p70(s6k)/p85(s6k) gene reveals a small mouse phenotype and a new functional S6 kinase. *The EMBO Journal*, *17*(22), 6649–6659.

Short, K. R., Bigelow, M. L., Kahl, J., Singh, R., Coenen-Schimke, J., Raghavakaimal, S., & Nair, K. S. (2005). Decline in skeletal muscle mitochondrial function with aging in humans. *Proceedings of the National Academy of Sciences of the United States of America*, *102*(15), 5618–5623.

Shu, J., Xia, Z., Li, L., Liang, E. T., Slipek, N., Shen, D., … Steer, C. J. (2012). Dose-dependent differential mRNA target selection and regulation by let-7a-7f and miR-17-92 cluster microRNAs. *RNA Biology*, *9*(10), 1275–1287.

Siengdee, P., Trakooljul, N., Murani, E., Schwerin, M., Wimmers, K., & Ponsuksili, S. (2015). MicroRNAs Regulate Cellular ATP Levels by Targeting Mitochondrial Energy Metabolism Genes during C2C12 Myoblast Differentiation. *PLOS ONE*, *10*(5), 1–20.

Simon, M., Terenghi, G., Green, C. J., & Coulton, G. R. (2000). Differential effects of NT-3 on reinnervation of the fast extensor digitorum longus (EDL) and the slow soleus muscle of rat. *The European Journal of Neuroscience*, *12*(3), 863–871.

Slater, C. R. (1982). Postnatal maturation of nerve-muscle junctions in hindlimb muscles of the mouse. *Developmental Biology*, *94*(1), 11–22.

Smerdu, V., Karsch-Mizrachi, I., Campione, M., Leinwand, L., & Schiaffino, S. (1994). Type IIx myosin heavy chain transcripts are expressed in type IIb fibers of human skeletal muscle. *The American Journal of Physiology*, *267*(6 Pt 1), C1723-8.

Soliman, A., De Sanctis, V., & Elalaily, R. (2014). Nutrition and pubertal development. *Indian Journal of Endocrinology and Metabolism*, *18*(Suppl 1), S39-47.

Soriano-Arroquia, A., House, L., Tregilgas, L., Canty-Laird, E., & Goljanek-Whysall, K. (2016). The functional consequences of age-related changes in microRNA expression in skeletal muscle. *Biogerontology*, *17*(3), 641–654.

Soriano-Arroquia, A., McCormick, R., Molloy, A. P., McArdle, A., & Goljanek-Whysall, K. (2016). Age-related changes in miR-143-3p:Igfbp5 interactions affect muscle regeneration. *Aging Cell*, *15*(2), 361–369.

Starega-Roslan, J., Koscianska, E., Kozlowski, P., & Krzyzosiak, W. J. (2011). The role of the precursor structure in the biogenesis of microRNA. *Cellular and*

Molecular Life Sciences : CMLS, *68*(17), 2859–2871.

Staron, R. S., Malicky, E. S., Leonardi, M. J., Falkel, J. E., Hagerman, F. C., & Dudley, G. A. (1990). Muscle hypertrophy and fast fiber type conversions in heavy resistance-trained women. *European Journal of Applied Physiology and Occupational Physiology*, *60*(1), 71–79.

Stifani, N. (2014). Motor neurons and the generation of spinal motor neuron diversity. *Frontiers in Cellular Neuroscience*, *8*, 293.

Stroynowska-Czerwinska, A., Fiszer, A., & Krzyzosiak, W. J. (2014). The panorama of miRNA-mediated mechanisms in mammalian cells. *Cellular and Molecular Life Sciences : CMLS*, *71*(12), 2253–2270.

Südhof, T. C., & Rizo, J. (2011). Synaptic vesicle exocytosis. *Cold Spring Harbor Perspectives in Biology*, *3*(12).

Sugg, K. B., Korn, M. A., Sarver, D. C., Markworth, J. F., & Mendias, C. L. (2017, March). Inhibition of platelet-derived growth factor signaling prevents muscle fiber growth during skeletal muscle hypertrophy. *FEBS Letters*, Vol. 591, pp. 801–809. England.

Suh, N. (2018, October). MicroRNA controls of cellular senescence. *BMB Reports*, Vol. 51, pp. 493–499.

Suzuki, H., Hase, A., Miyata, Y., Arahata, K., & Akazawa, C. (1998). Prominent expression of glial cell line-derived neurotrophic factor in human skeletal muscle. *The Journal of Comparative Neurology*, *402*(3), 303–312.

Suzuki, T., Maruyama, A., Sugiura, T., Machida, S., & Miyata, H. (2009). Age-related changes in two- and three-dimensional morphology of type-identified endplates in the rat diaphragm. *The Journal of Physiological Sciences : JPS*, *59*(1), 57–62.

Sweetman, D., Goljanek, K., Rathjen, T., Oustanina, S., Braun, T., Dalmay, T., & Munsterberg, A. (2008). Specific requirements of MRFs for the expression of muscle specific microRNAs, miR-1, miR-206 and miR-133. *Developmental Biology*, *321*(2), 491–499.

Swiecicka, A., Piasecki, M., Stashuk, D. W., Ireland, A., Jones, D. A., Rutter, M. K., & McPhee, J. S. (2019). Frailty phenotype and frailty index are associated with distinct neuromuscular electrophysiological characteristics in men. *Experimental Physiology*, *104*(8), 1154–1161.

Szeto, H. H. (2017). Pharmacologic Approaches to Improve Mitochondrial Function in AKI and CKD. *Journal of the American Society of Nephrology : JASN*, *28*(10), 2856–2865.

Tan, C. L., Plotkin, J. L., Veno, M. T., von Schimmelmann, M., Feinberg, P., Mann, S., … Schaefer, A. (2013). MicroRNA-128 governs neuronal excitability and motor behavior in mice. *Science (New York, N.Y.)*, *342*(6163), 1254–1258.

Taylor, S. C., & Posch, A. (2014). The design of a quantitative western blot experiment. *BioMed Research International*, *2014*, 361590.

Tintignac, L. A., Brenner, H.-R., & Ruegg, M. A. (2015). Mechanisms Regulating Neuromuscular Junction Development and Function and Causes of Muscle Wasting. *Physiological Reviews*, *95*(3), 809–852.

Toscano, A. E., Manhães-de-Castro, R., & Canon, F. (2008). Effect of a low-protein diet during pregnancy on skeletal muscle mechanical properties of offspring rats. *Nutrition (Burbank, Los Angeles County, Calif.)*, *24*(3), 270–278.

Tsujimura, K., Irie, K., Nakashima, H., Egashira, Y., Fukao, Y., Fujiwara, M., … Nakashima, K. (2015). miR-199a Links MeCP2 with mTOR Signaling and Its Dysregulation Leads to Rett Syndrome Phenotypes. *Cell Reports*, *12*(11), 1887–1901.

Tu, H., Zhang, D., Corrick, R. M., Muelleman, R. L., Wadman, M. C., & Li, Y.-L. (2017). Morphological Regeneration and Functional Recovery of Neuromuscular Junctions after Tourniquet-Induced Injuries in Mouse Hindlimb. *Frontiers in Physiology*, *8*, 207.

Tuppen, H. A. L., Blakely, E. L., Turnbull, D. M., & Taylor, R. W. (2010). Mitochondrial DNA mutations and human disease. *Biochimica et Biophysica Acta*, *1797*(2), 113–128.

Uriguen, L., Gil-Pisa, I., Munarriz-Cuezva, E., Berrocoso, E., Pascau, J., Soto-Montenegro, M. L., … Meana, J. J. (2013). Behavioral, neurochemical and morphological changes induced by the overexpression of munc18-1a in brain of mice: relevance to schizophrenia. *Translational Psychiatry*, *3*, e221.

Valdez, G., Heyer, M. P., Feng, G., & Sanes, J. R. (2014). The role of muscle microRNAs in repairing the neuromuscular junction. *PloS One*, *9*(3), e93140.

Valdez, G., Tapia, J. C., Kang, H., Clemenson, G. D. J., Gage, F. H., Lichtman, J. W., & Sanes, J. R. (2010). Attenuation of age-related changes in mouse neuromuscular synapses by caloric restriction and exercise. *Proceedings of the National Academy of Sciences of the United States of America*, *107*(33), 14863–14868.

Valinezhad Orang, A., Safaralizadeh, R., & Kazemzadeh-Bavili, M. (2014). Mechanisms of miRNA-Mediated Gene Regulation from Common Downregulation to mRNA-Specific Upregulation. *International Journal of Genomics*, *2014*, 970607.

Van Remmen, H., & Richardson, A. (2001). Oxidative damage to mitochondria and aging. *Experimental Gerontology*, *36*(7), 957–968.

van Rooij, E., Liu, N., & Olson, E. N. (2008). MicroRNAs flex their muscles. *Trends in Genetics : TIG*, *24*(4), 159–166.

Varoqueaux, F., Sons, M. S., Plomp, J. J., & Brose, N. (2005). Aberrant morphology and residual transmitter release at the Munc13-deficient mouse neuromuscular synapse. *Molecular and Cellular Biology*, *25*(14), 5973–5984.

Vasilaki, A., Pollock, N., Giakoumaki, I., Goljanek-Whysall, K., Sakellariou, G. K., Pearson, T., … McArdle, A. (2016). The effect of lengthening contractions on neuromuscular junction structure in adult and old mice. *Age (Dordrecht, Netherlands)*, *38*(4), 259–272.

Vasudevan, S., Tong, Y., & Steitz, J. A. (2007). Switching from repression to activation: microRNAs can up-regulate translation. *Science (New York, N.Y.)*, *318*(5858), 1931–1934.

Vega, R. B., Huss, J. M., & Kelly, D. P. (2000). The coactivator PGC-1 cooperates with peroxisome proliferator-activated receptor alpha in transcriptional control of nuclear genes encoding mitochondrial fatty acid oxidation enzymes. *Molecular and Cellular Biology*, *20*(5), 1868–1876.

Venkataraman, S., Alimova, I., Fan, R., Harris, P., Foreman, N., & Vibhakar, R. (2010). MicroRNA 128a Increases Intracellular ROS Level by Targeting Bmi-1

and Inhibits Medulloblastoma Cancer Cell Growth by Promoting Senescence. *PLOS ONE*, *5*(6), 1–10.

Verschuuren, J., Strijbos, E., & Vincent, A. (2016). Neuromuscular junction disorders. *Handbook of Clinical Neurology*, *133*, 447–466.

Victora, C. G., Adair, L., Fall, C., Hallal, P. C., Martorell, R., Richter, L., & Sachdev, H. S. (2008). Maternal and child undernutrition: consequences for adult health and human capital. *Lancet (London, England)*, *371*(9609), 340–357.

Wahl, D., Solon-Biet, S. M., Wang, Q.-P., Wali, J. A., Pulpitel, T., Clark, X., … Le Couteur, D. G. (2018). Comparing the Effects of Low-Protein and High-Carbohydrate Diets and Caloric Restriction on Brain Aging in Mice. *Cell Reports*, *25*(8), 2234-2243.e6.

Wallace, D. C. (1999). Mitochondrial Diseases in Man and Mouse. *Science*, *283*(5407), 1482 LP – 1488.

Wan, J.-J., Qin, Z., Wang, P.-Y., Sun, Y., & Liu, X. (2017). Muscle fatigue: general understanding and treatment. *Experimental & Molecular Medicine*, *49*(10), e384.

Wang, B., Pan, L., Wei, M., Wang, Q., Liu, W.-W., Wang, N., … Bao, L. (2015). FMRP-Mediated Axonal Delivery of miR-181d Regulates Axon Elongation by Locally Targeting Map1b and Calm1. *Cell Reports*, *13*(12), 2794–2807.

Wang, D. Z., Hammond, V. E., Abud, H. E., Bertoncello, I., McAvoy, J. W., & Bowtell, D. D. (1997). Mutation in Sos1 dominantly enhances a weak allele of the EGFR, demonstrating a requirement for Sos1 in EGFR signaling and development. *Genes & Development*, *11*(3), 309–320.

Washbourne, P., Thompson, P. M., Carta, M., Costa, E. T., Mathews, J. R., Lopez-Bendito, G., … Wilson, M. C. (2002). Genetic ablation of the t-SNARE SNAP-25 distinguishes mechanisms of neuroexocytosis. *Nature Neuroscience*, *5*(1), 19–26.

Webster, R. G. (2018). Animal Models of the Neuromuscular Junction, Vitally Informative for Understanding Function and the Molecular Mechanisms of Congenital Myasthenic Syndromes. *International Journal of Molecular Sciences*, *19*(5).

Wells, D. G., McKechnie, B. A., Kelkar, S., & Fallon, J. R. (1999). Neurotrophins regulate agrin-induced postsynaptic differentiation. *Proceedings of the National Academy of Sciences of the United States of America*, *96*(3), 1112–1117.

Westholm, J. O., & Lai, E. C. (2011). Mirtrons: microRNA biogenesis via splicing. *Biochimie*, *93*(11), 1897–1904.

Wilborn, C. D., & Willoughby, D. S. (2004). The Role of Dietary Protein Intake and Resistance Training on Myosin Heavy Chain Expression. *Journal of the International Society of Sports Nutrition*, *1*(2), 27.

Wilczynska, A., & Bushell, M. (2015). The complexity of miRNA-mediated repression. *Cell Death and Differentiation*, *22*(1), 22–33.

Willadt, S., Nash, M., & Slater, C. R. (2016). Age-related fragmentation of the motor endplate is not associated with impaired neuromuscular transmission in the mouse diaphragm. *Scientific Reports*, *6*, 24849.

Wong-Riley, M. T. T. (2012). Bigenomic regulation of cytochrome c oxidase in neurons and the tight coupling between neuronal activity and energy

metabolism. *Advances in Experimental Medicine and Biology*, *748*, 283–304.
Woo, M., Isganaitis, E., Cerletti, M., Fitzpatrick, C., Wagers, A. J., Jimenez-Chillaron, J., & Patti, M. E. (2011). Early Life Nutrition Modulates Muscle Stem Cell Number: Implications for Muscle Mass and Repair. *Stem Cells and Development*, *20*(10), 1763–1769.
Wu, L., Fan, J., & Belasco, J. G. (2006). MicroRNAs direct rapid deadenylation of mRNA. *Proceedings of the National Academy of Sciences of the United States of America*, *103*(11), 4034–4039.
Xu, M., Chen, X., Chen, D., Yu, B., & Huang, Z. (2017). FoxO1: a novel insight into its molecular mechanisms in the regulation of skeletal muscle differentiation and fiber type specification. *Oncotarget*, *8*(6), 10662–10674.
YAFFE, D., & SAXEL, O. R. A. (1977). Serial passaging and differentiation of myogenic cells isolated from dystrophic mouse muscle. *Nature*, *270*(5639), 725–727.
Yang, K.-F., Shen, X.-H., & Cai, W. (2012). Prenatal and early postnatal exposure to high-saturated-fat diet represses Wnt signaling and myogenic genes in offspring rats. *Experimental Biology and Medicine (Maywood, N.J.)*, *237*(8), 912–918.
Yang, Q., & Guan, K.-L. (2007). Expanding mTOR signaling. *Cell Research*, *17*(8), 666–681.
Yao, J., Kwon, S. E., Gaffaney, J. D., Dunning, F. M., & Chapman, E. R. (2011). Uncoupling the roles of synaptotagmin I during endo- and exocytosis of synaptic vesicles. *Nature Neuroscience*, *15*(2), 243–249.
Yi, R., Qin, Y., Macara, I. G., & Cullen, B. R. (2003). Exportin-5 mediates the nuclear export of pre-microRNAs and short hairpin RNAs. *Genes & Development*, *17*(24), 3011–3016.
Yoo, S.-M., & Jung, Y.-K. (2018). A Molecular Approach to Mitophagy and Mitochondrial Dynamics. *Molecules and Cells*, *41*(1), 18–26.
Yu, F., Degens, H., Li, X., & Larsson, L. (1998). Gender- and age-related differences in the regulatory influence of thyroid hormone on the contractility and myosin composition of single rat soleus muscle fibres. *Pflugers Archiv : European Journal of Physiology*, *437*(1), 21–30.
Yu, W.-W., Jiang, H., Zhang, C.-T., & Peng, Y. (2017). The SNAIL/miR-128 axis regulated growth, invasion, metastasis, and epithelial-to-mesenchymal transition of gastric cancer. *Oncotarget*, *8*(24), 39280–39295.
Yu, Y.-M., Gibbs, K. M., Davila, J., Campbell, N., Sung, S., Todorova, T. I., … Schachner, M. (2011). MicroRNA miR-133b is essential for functional recovery after spinal cord injury in adult zebrafish. *The European Journal of Neuroscience*, *33*(9), 1587–1597.
Yunta, M., Nieto-Diaz, M., Esteban, F. J., Caballero-Lopez, M., Navarro-Ruiz, R., Reigada, D., … Maza, R. M. (2012). MicroRNA dysregulation in the spinal cord following traumatic injury. *PloS One*, *7*(4), e34534.
Zeviani, M., Nakagawa, M., Herbert, J., Lomax, M. I., Grossman, L. I., Sherbany, A. A., … Schon, E. A. (1987). Isolation of a cDNA clone encoding subunit IV of human cytochrome c oxidase. *Gene*, *55*(2–3), 205–217.
Zhang, D., Li, X., Chen, C., Li, Y., Zhao, L., Jing, Y., … Ying, H. (2012). Attenuation of p38-Mediated miR-1/133 Expression Facilitates Myoblast Proliferation

during the Early Stage of Muscle Regeneration. *PLOS ONE*, *7*(7), 1–13.

Zhang, D., Wang, X., Li, Y., Zhao, L., Lu, M., Yao, X., … Ying, H. (2014). Thyroid hormone regulates muscle fiber type conversion via miR-133a1. *The Journal of Cell Biology*, *207*(6), 753–766.

Zhang, J., Gao, Z., & Ye, J. (2013). Phosphorylation and degradation of S6K1 (p70S6K1) in response to persistent JNK1 Activation. *Biochimica et Biophysica Acta*, *1832*(12), 1980–1988.

Zhang, W., Kim, P. J., Chen, Z., Lokman, H., Qiu, L., Zhang, K., … Zeng, L. (2016). MiRNA-128 regulates the proliferation and neurogenesis of neural precursors by targeting PCM1 in the developing cortex. *ELife*, *5*.

Zhou, H.-J., Wang, L.-Q., Xu, Q.-S., Fan, Z.-X., Zhu, Y., Jiang, H., … Zhan, R.-Y. (2016). Downregulation of miR-199b promotes the acute spinal cord injury through IKKbeta-NF-kappaB signaling pathway activating microglial cells. *Experimental Cell Research*, *349*(1), 60–67.

Zhou, L., Yang, L., Li, Y.-J., Mei, R., Yu, H.-L., Gong, Y., … Wang, F. (2018). MicroRNA-128 Protects Dopamine Neurons from Apoptosis and Upregulates the Expression of Excitatory Amino Acid Transporter 4 in Parkinson's Disease by Binding to AXIN1. *Cellular Physiology and Biochemistry : International Journal of Experimental Cellular Physiology, Biochemistry, and Pharmacology*, *51*(5), 2275–2289.

Zhu, Y.-D., Wang, L., Sun, C., Fan, L., Zhu, D.-X., Fang, C., … Xu, W. (2012). Distinctive microRNA signature is associated with the diagnosis and prognosis of acute leukemia. *Medical Oncology (Northwood, London, England)*, *29*(4), 2323–2331.

Appendix

A.1 Amplification curves and melt peaks of qPCR on TA muscle and SN in 12-week old mice

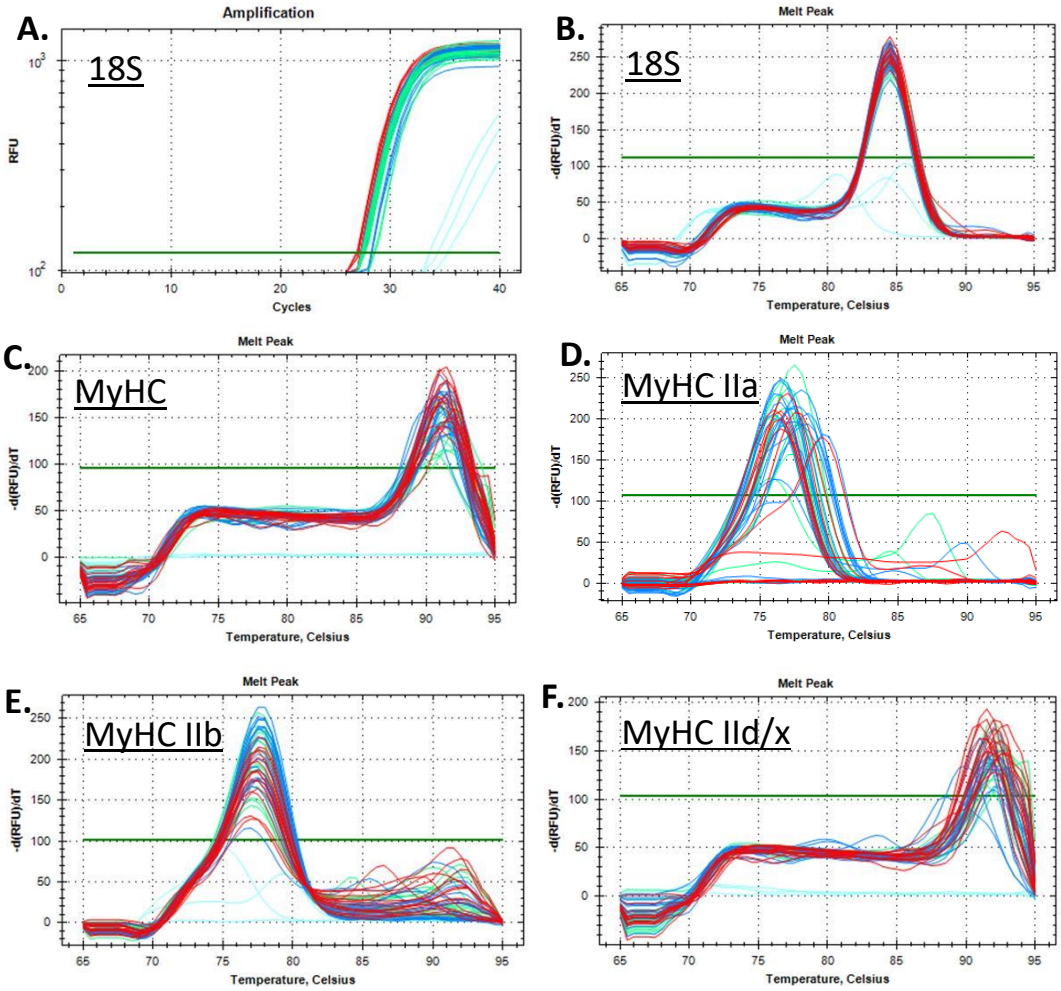

Figure A.1 Melt peaks of 18S and MyHC isoforms (I, IIa, IIb, and IId/x) qPCR in TA muscle of 12-week old mice. **A)** Amplification peak and **B)** melt peak of 18S gene, **C)** MyHC I, D**)** MyHC IIa, **E)** MyHC IIb and **F)** MyHC IId/x.

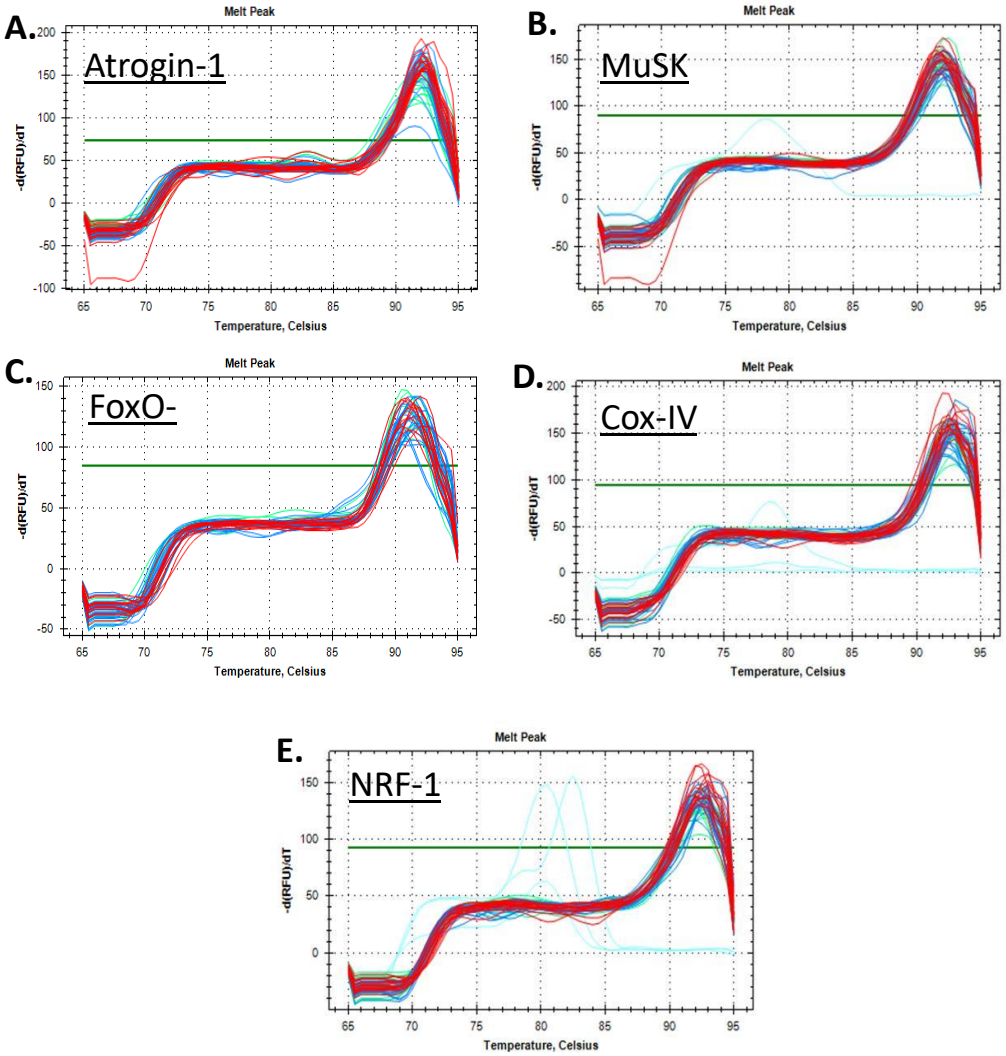

Figure A.2 Melt peaks of Atrogin-1, MuSK and FoxO-3 qPCR in TA muscle of 12-week old mice. Melt peaks of **A)** Atrogin-1, **B)** MuSK and **C)** FoxO-3.

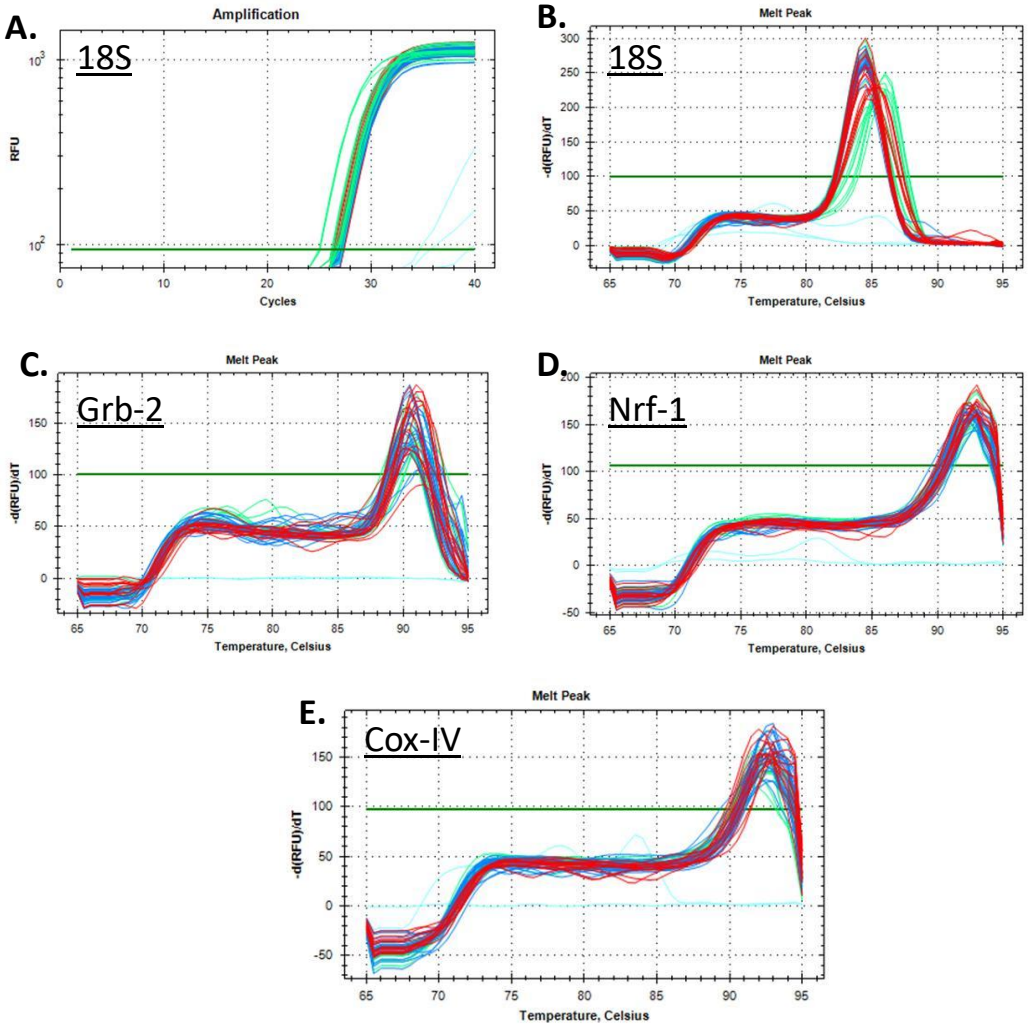

Figure A.3 Melt peaks of 18S and Grb-2, Nrf-1 and Cox-IV qPCR in SN of 12-week old mice. **A)** Amplification peak and **B)** melt peak of 18S gene, **C)** Grb-2, D**)** Nrf-1 and **E)** Cox-IV.

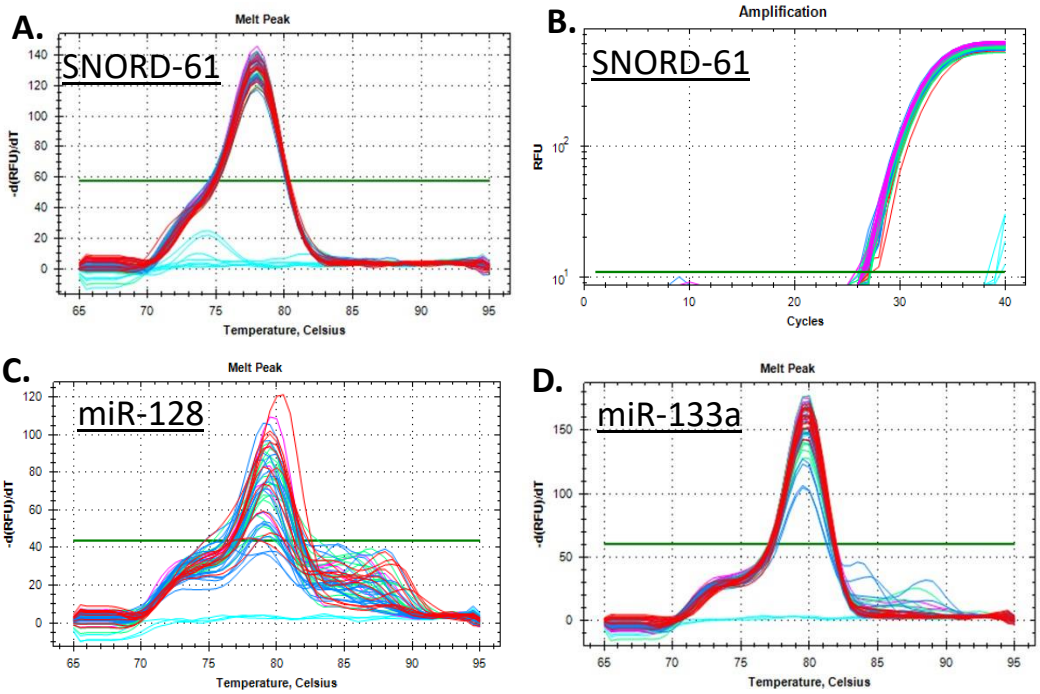

Figure A.4 Amplification curve and melt peaks of SNORD-61, miR-128 and miR-133a qPCR in TA muscle of 12-week old mice. **A)** Amplification curve of SNORD-61 and melt peaks of **B)** SNORD-61, **C)** miR-128 and **D)** miR-133a.

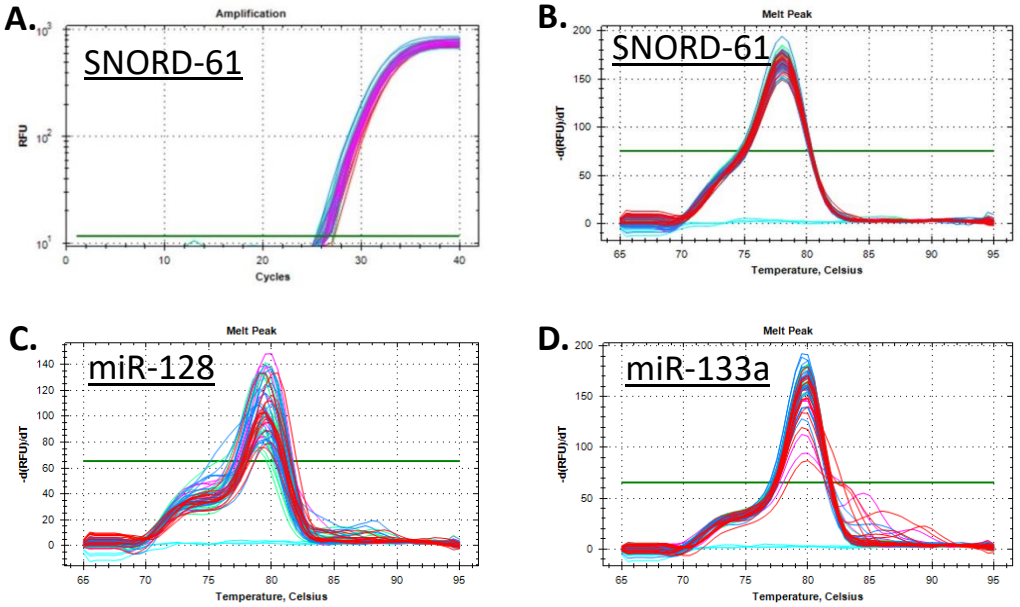

Figure A.5 Amplification curve and melt peaks of SNORD-61, miR-128 and miR-133a qPCR in SN of 12-week old mice. **A)** Amplification curve of SNORD-61 and melt peaks of **B)** SNORD-61, **C)** miR-128 and **D)** miR-133a.

A.2 Predicted target genes of miR-128 and miR-133a with seed regions for binding of alternative miRs

A.2.1 Predicted target genes of miR-128 with seed regions for miR-133a binding

Table A.1 List of the selected miR-128 predicted target with seed regions targeted by miR-133a, recorded using TargetScanMouse 7.1. Ensembl ID and seed region in 3'UTR are shown.

miR-128 predicted target genes (TargetScan)			
		miR-133a seed region (in the 3'-UTR)	
Gene	Ensembl ID	Conserved	Poorly conserved
Ngfr	ENSMUST00000000122.6	N/A	925-932, 1404-1410
Insr	ENSMUST00000091291.4	1063-1069	N/A
Fbxo32	ENSMUST00000022986.6	N/A	1195-1201, 3735-3741
Foxo1	ENSMUST00000053764.5	N/A	1788-1794, 1812-1818
Sirt1	ENSMUST00000120239.2	344-350	N/A
Syt1	ENSMUST00000105276.2	1606-1612, 2246-2252	N/A
Nrf1	ENSMUST00000115212.2	N/A	457-463

A.2.2 Predicted target genes of miR-133a with seed regions for miR-128 binding

Table A.2 List of the selected miR-133a predicted target with seed regions targeted by miR-128, recorded using TargetScanMouse 7.1. Ensembl ID and seed region in 3'UTR are shown.

miR-133a predicted target genes (TargetScan)			
		miR-128 seed region (in the 3'-UTR)	
Gene	Ensembl ID	Conserved	Poorly conserved
Syt1	ENSMUST00000105276.2	1460-1467, 1692-1698	N/A
Rims1	ENSMUST00000115273.3	N/A	1844-1850
Cplx2	ENSMUST00000026985.8	N/A	5493-5500, 5584-5590
Braf	ENSMUST00000002487.9	N/A	4044-4051
Insr	ENSMUST00000091291.4	207-213	3851-3858
Fgf1	ENSMUST00000117566.2	N/A	1016-1022, 1121-1127, 1593-1599, 1749-1755, 3116-3122
Pax7	ENSMUST00000030508.8	N/A	755-761
Myo9b	ENSMUST00000168839.2	N/A	870-876, 2893-2900
Myh1	ENSMUST00000124516.2	N/A	763-769
Nrf1	ENSMUST00000115212.2	N/A	1232-1239, 1603-1609

A.3 Assessment of transfection efficiency of C2C12 and NSC-34 cells following manipulation of miR-128 or miR-133a expression

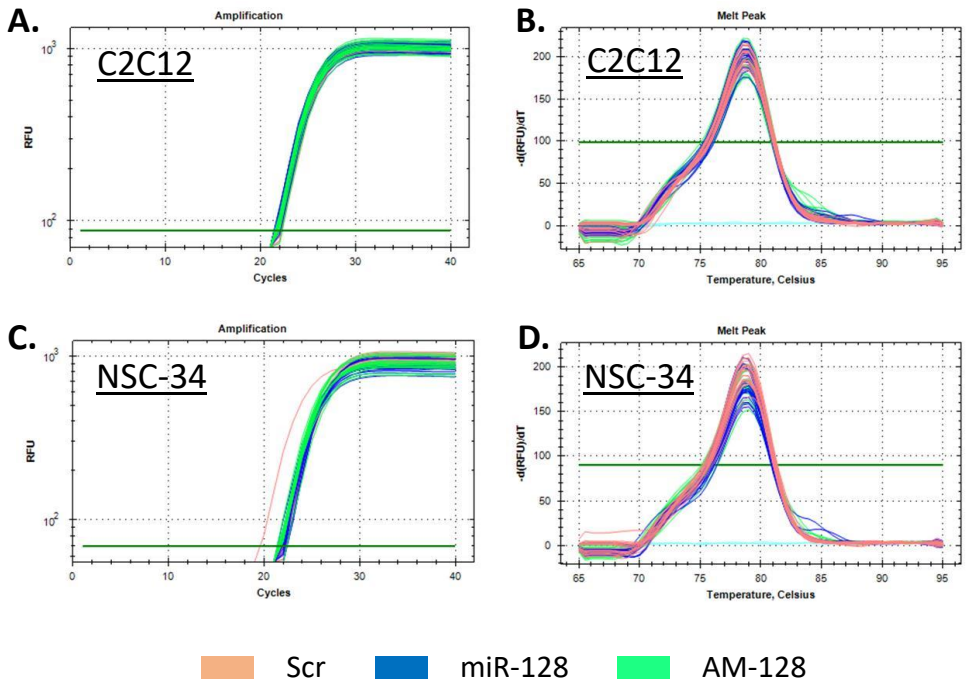

Figure A.6 Amplification curve and melt peak of SNORD-61 in C2C12 and NSC-34 cells following transfections with either Scr, miR-128 or AM-128. **A)** Amplification

curve and **B)** melt peak of SNORD-61 in C2C12 cells. **C)** Amplification curve and **D)** melt peak of SNORD-61 in NSC-34 cells.

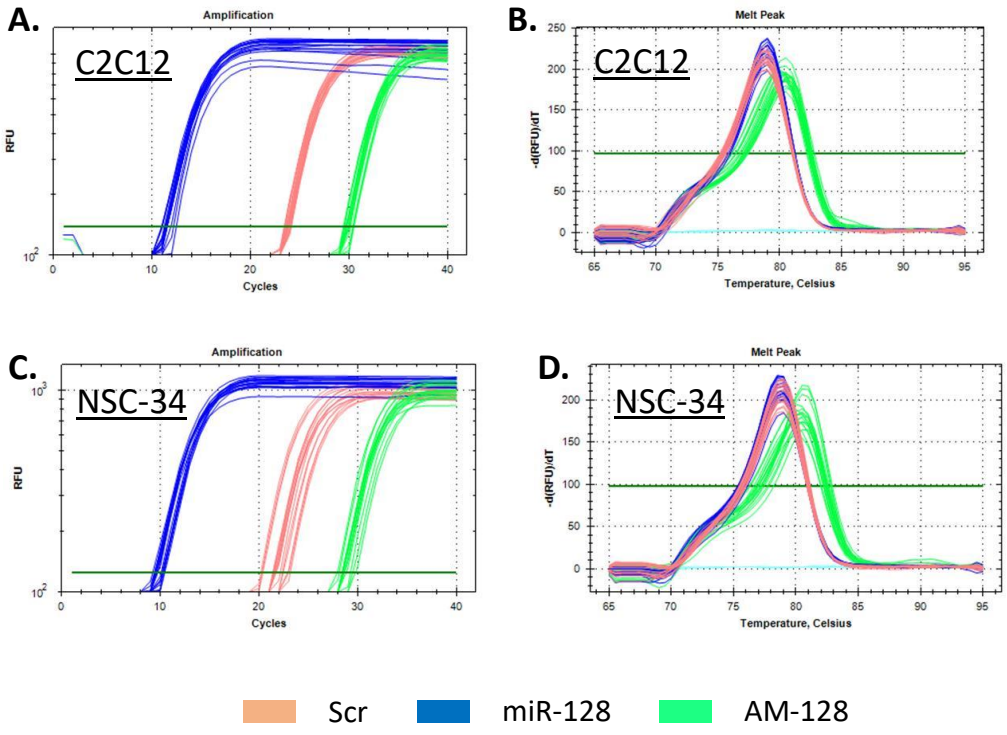

Figure A.7 Amplification curve and melt peak of miR-128 qPCR in C2C12 and NSC-34 cells following transfections with either Scr, miR-128 or AM-128. **A)** Amplification curve and **B)** melt peak of miR-128 in C2C12 cells. **C)** Amplification curve and **D)** melt peak of miR-128 in NSC-34 cells.

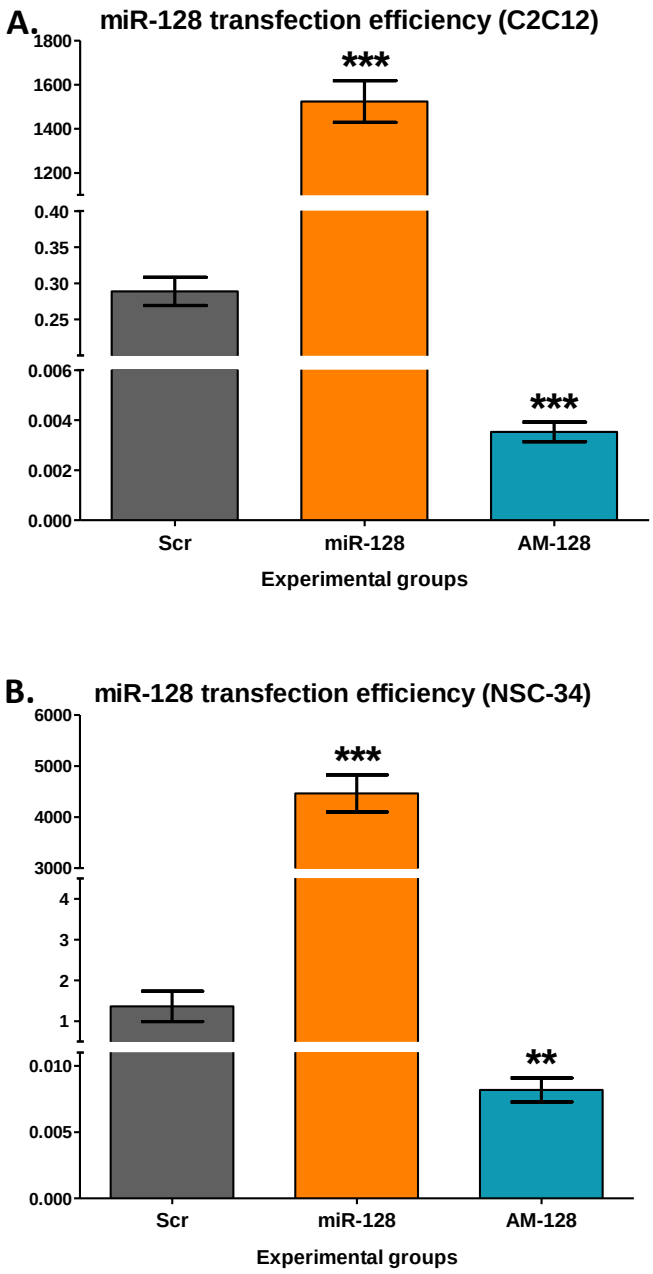

Figure A.8 Transfection efficiency of miR-128 and AM-128 in C2C12 and NSC-34 cells. Scr serves as the control for statistical comparison, **P≤0.01, ***P≤0.001 (*mean ± SEM*; *n*=6*; One-Way ANOVA with Dunnett's post-hoc analysis*).

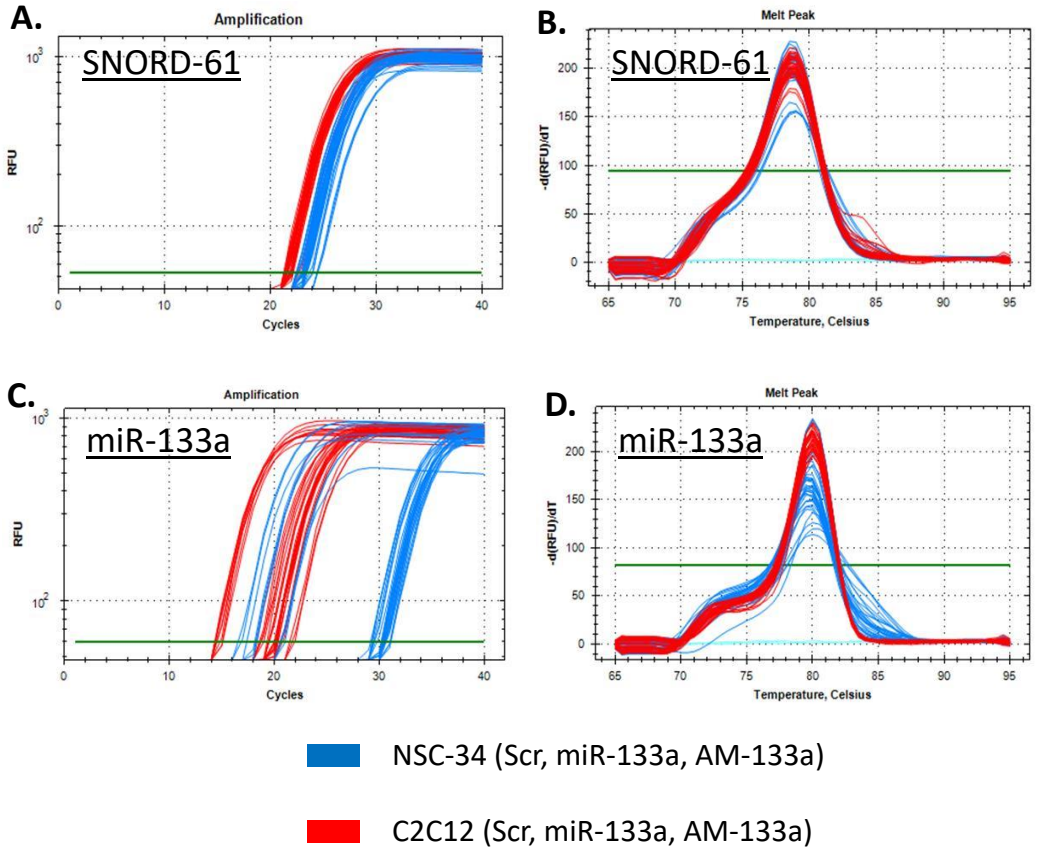

Figure A.9 Amplification curve and melt peak of SNORD-61 and miR-133a in C2C12 (red) and NSC-34 (blue) cells following transfections with either Scr, miR-133a or AM-133a. **A)** Amplification curve and **B)** melt peak of SNORD-61. **C)** Amplification curve and **D)** melt peak of miR-133a.

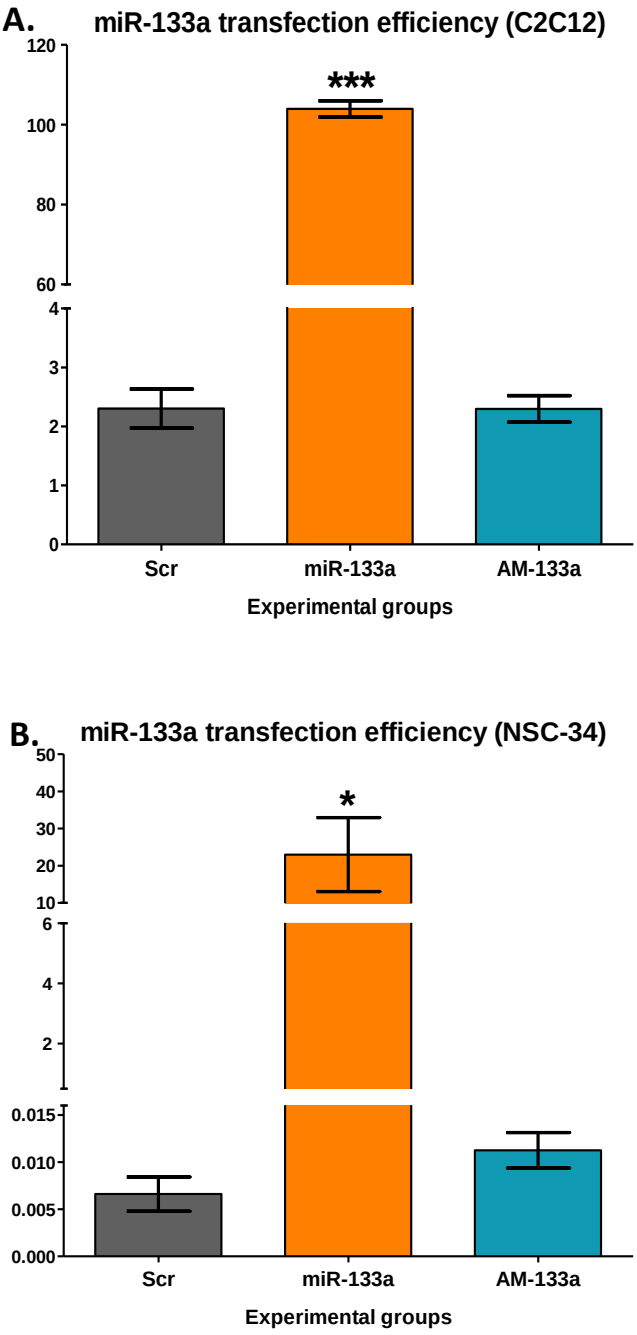

Figure A.10 Transfection efficiency of miR-133a and AM-133a in C2C12 and NSC-34 cells. Scr serves as the control for statistical comparison, *P≤0.05, *** P≤0.001 (*mean ± SEM*; *n=3; One-Way ANOVA with Dunnett's post-hoc analysis*).

A.4 Phenotypic analysis and comparison of C2C12 and NSC-34 untransfected cells in comparison with scrambled-treated cells, following manipulation of miR-128 and miR-133a expression experiments

A.4.1 Analysis of C2C12 untransfected and scr-treated cells

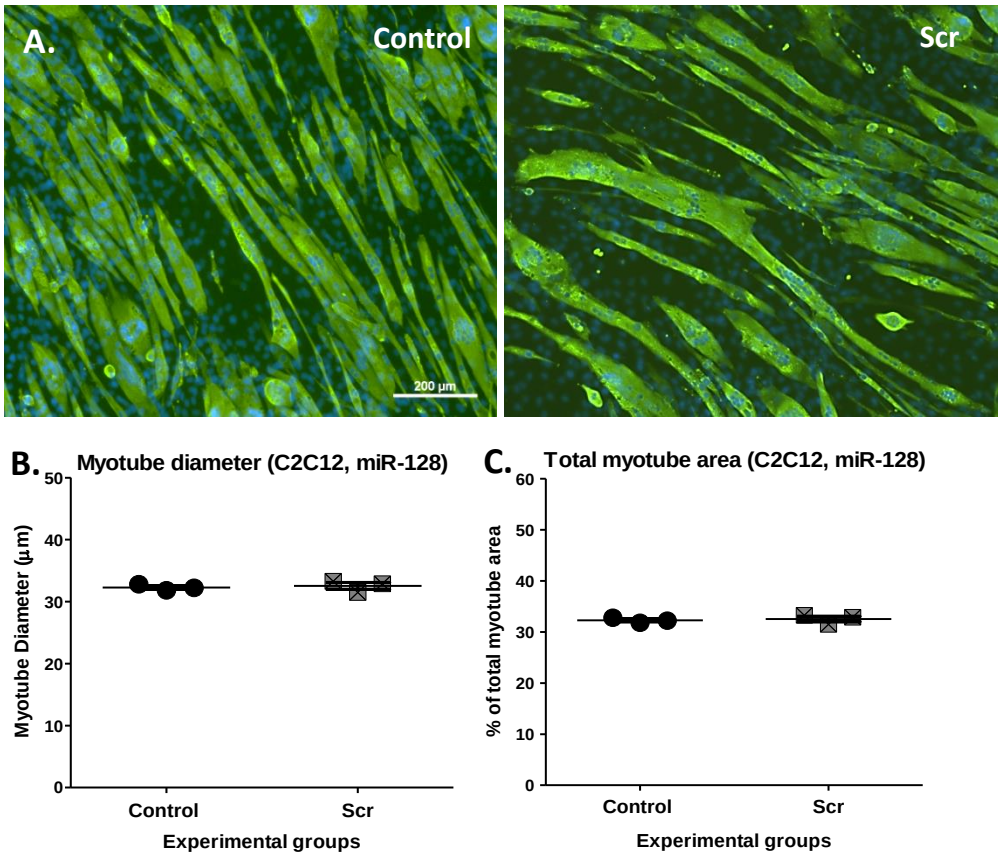

Figure A.11 Phenotype analysis of untransfected (control) and scrambled-transfected (Scr) C2C12 myotubes, following manipulation of miR-128 expression experiments. **A)** Untransfected (control) and Scr C2C12 myotubes; myotube formation was established with myosin heavy chain and nuclei immunostaining (MF20=Green; DAPI=Blue). **B)** Myotube diameter of untransfected and Scr C2C12 myotubes with ≥2 nuclei. **C)** Quantification of total C2C12 myotube area expressed as a percentage of total area per field of view, of untransfected (control) and Scr C2C12 myotubes. (*mean ± SEM*; *n*=3-4*; Unpaired two-tailed t-test with Welsh correction*). Representative images shown.

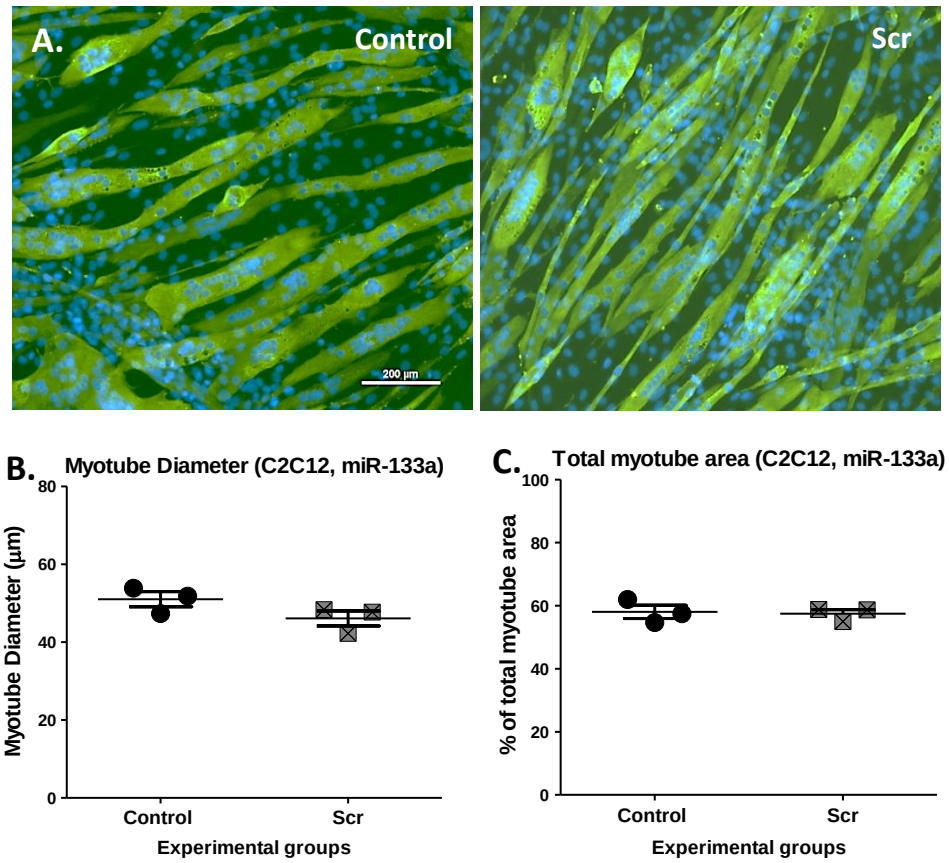

Figure A.12 Phenotype analysis of untransfected (control) and scrambled-transfected (Scr) C2C12 myotubes, following manipulation of miR-133a expression experiments. **A)** Untransfected (control) and Scr C2C12 myotubes; myotube formation was established with myosin heavy chain and nuclei immunostaining (MF20=Green; DAPI=Blue). **B)** Myotube diameter of untransfected and Scr C2C12 myotubes with ≥2 nuclei. **C)** Quantification of total C2C12 myotube area expressed as a percentage of total area per field of view, of untransfected (control) and Scr C2C12 myotubes. (*mean ± SEM*; *n*=3-4*; Unpaired two-tailed t-test with Welsh correction*). Representative images shown.

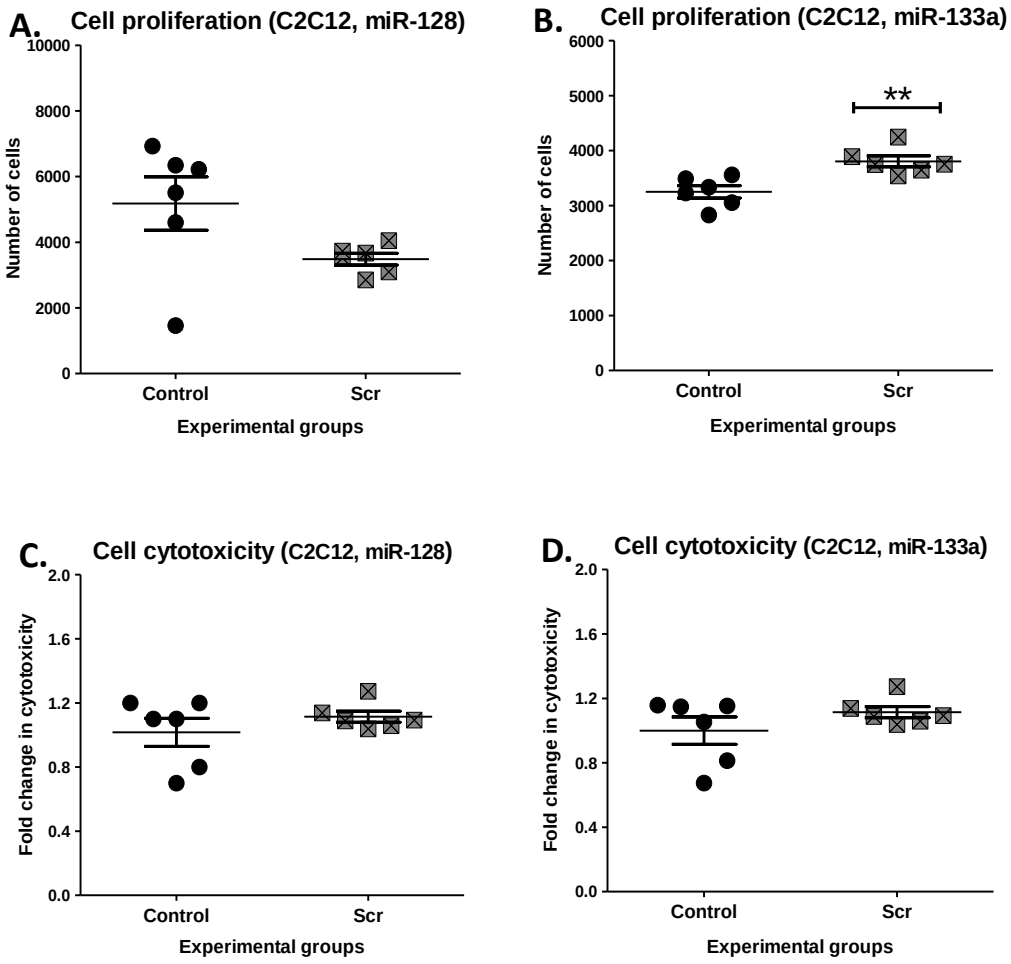

Figure A.13 CCK-8 proliferation and CytoTox96 cytotoxicity assay of untransfected (control) C2C12 myoblasts and C2C12 myoblasts transfected with scrambled negative control (Scr). C2C12 myoblast number in control group and scrambled-transfected group for **A)** miR-128 and **B)** miR-133a. C2C12 cell death expressed as fold-change in cytotoxicity in control group and scrambled-transfected group for **C)** miR-128 and **D)** miR-133a. **P≤0.01 (*mean ± SEM*; *n*=6*; Unpaired two-tailed t-test with Welsh correction*).

A.4.2 Analysis of NSC-34 untransfected and scr-treated cells

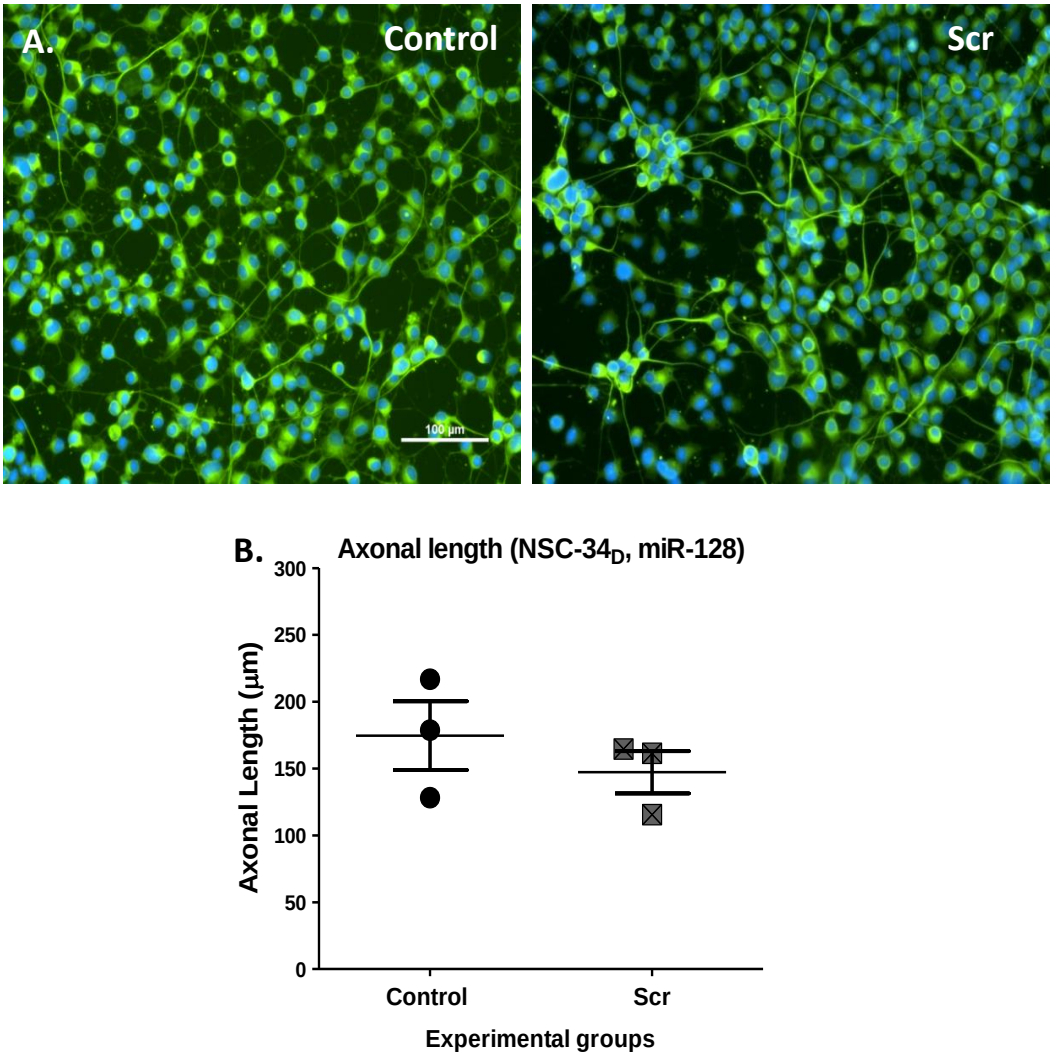

Figure A.14 Phenotype analysis of untransfected (control) and scrambled-transfected (Scr) differentiated NSC-34 (NSC-34_D) cells, following manipulation of miR-128 expression experiments. **A)** Untransfected (control) and Scr NSC-34_D cells stained with Alexa Fluor 488 B-III Tubulin (green) for and DAPI (blue) and **B)** Axonal length of untransfected (control) and Scr NSC-34_D after 11 days of differentiation. (*mean ± SEM*; *n*=3*; Unpaired two-tailed t-test with Welsh correction*). Representative images shown.

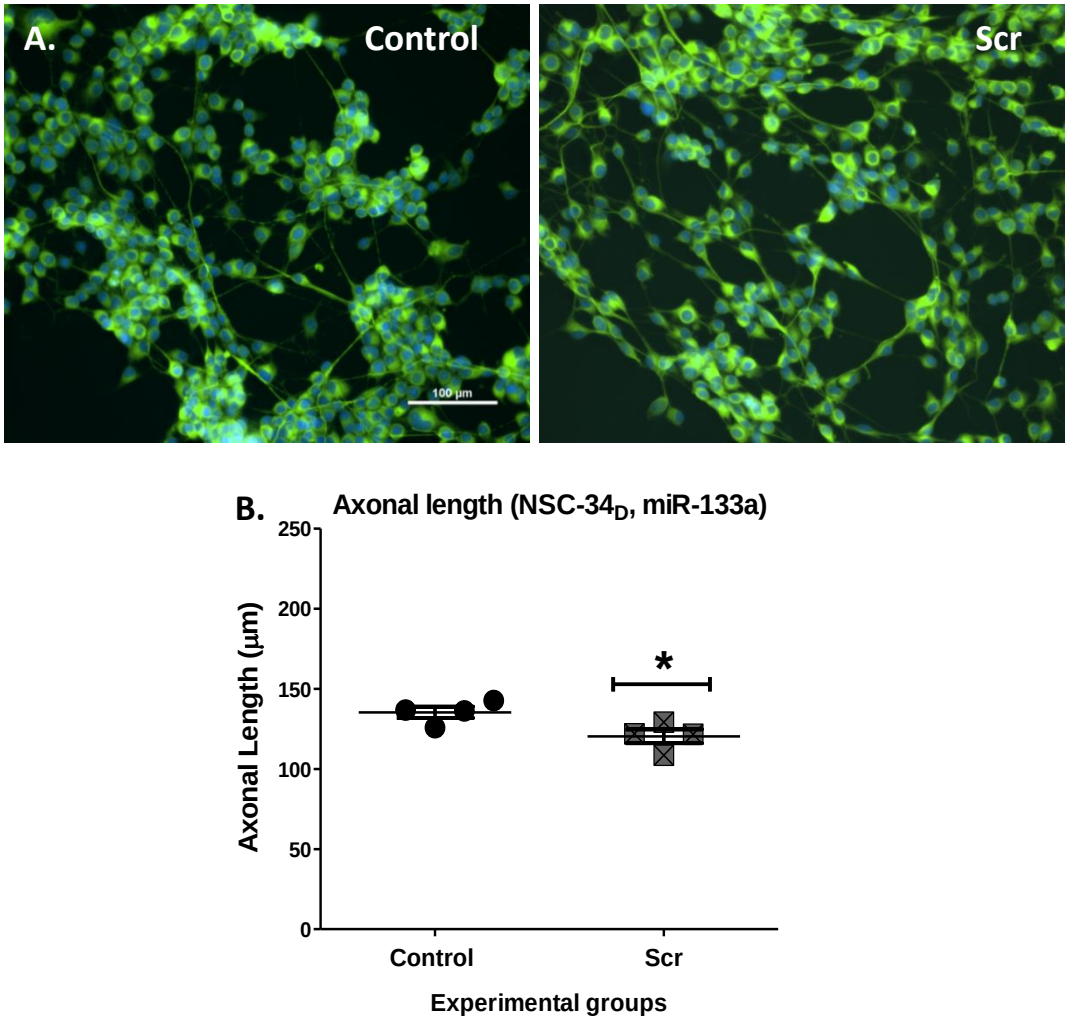

Figure A.15 Phenotype analysis of untransfected (control) and scrambled-transfected (Scr) differentiated NSC-34 (NSC-34$_D$) cells, following manipulation of miR-133a expression experiments. **A)** Untransfected (control) and Scr NSC-34$_D$ cells stained with Alexa Fluor 488 B-III Tubulin (green) for and DAPI (blue) and **B)** Axonal length of untransfected (control) and Scr NSC-34$_D$ after 11 days of differentiation. (*mean ± SEM*; *n*=3*; Unpaired two-tailed t-test with Welsh correction*). Representative images shown.

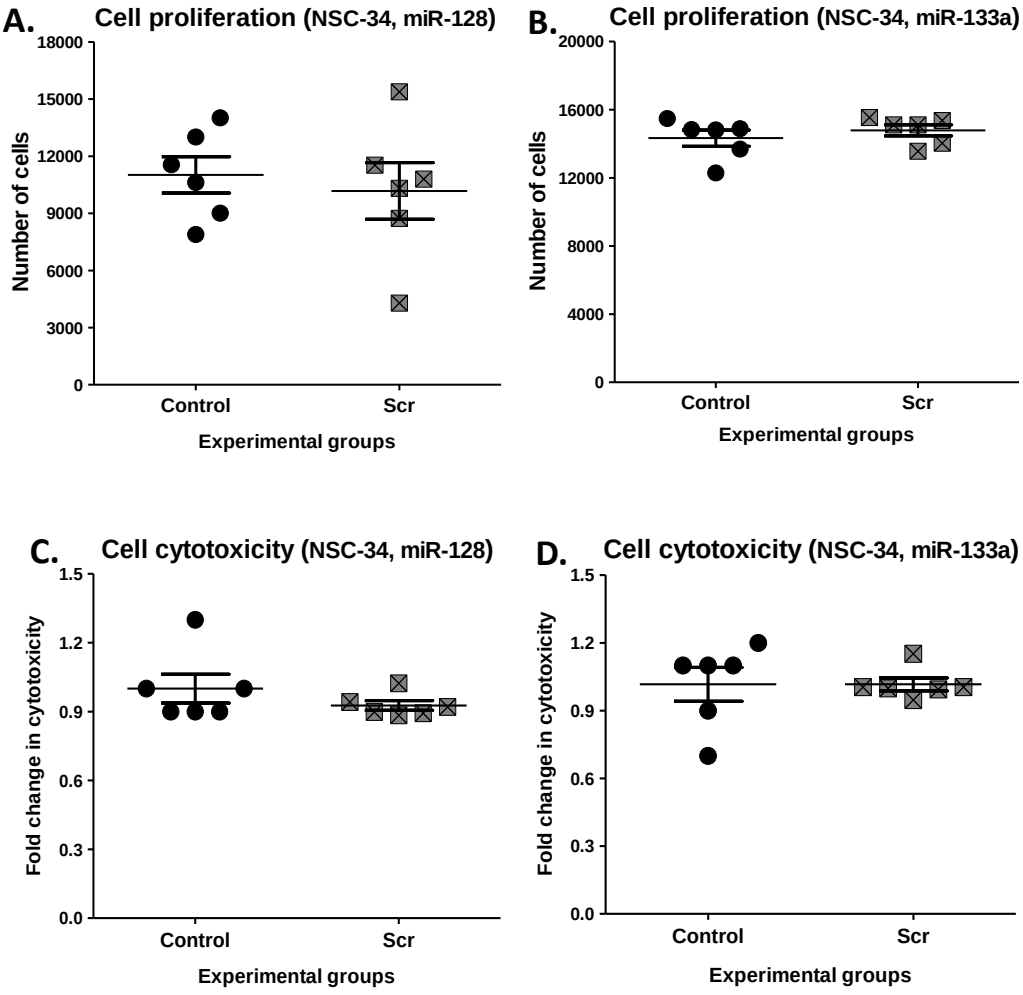

Figure A.16 CCK-8 proliferation and CytoTox96 cytotoxicity assay of untransfected (control) C2C12 myoblasts and NSC-34 cells transfected with scrambled negative control. NSC-34 cell number in control group and scrambled-transfected group for **A)** miR-128 and **B)** miR-133a. NSC-34 cell death expressed as fold-change in cytotoxicity in control group and scrambled-transfected group for **C)** miR-128 and **D)** miR-133a. (*mean ± SEM*; *n*=6*; Unpaired two-tailed t-test with Welsh correction*).

A.5 Amplification curves and melt peaks of qPCR of predicted target genes following manipulation of miR-128 expression experiments *in vitro*

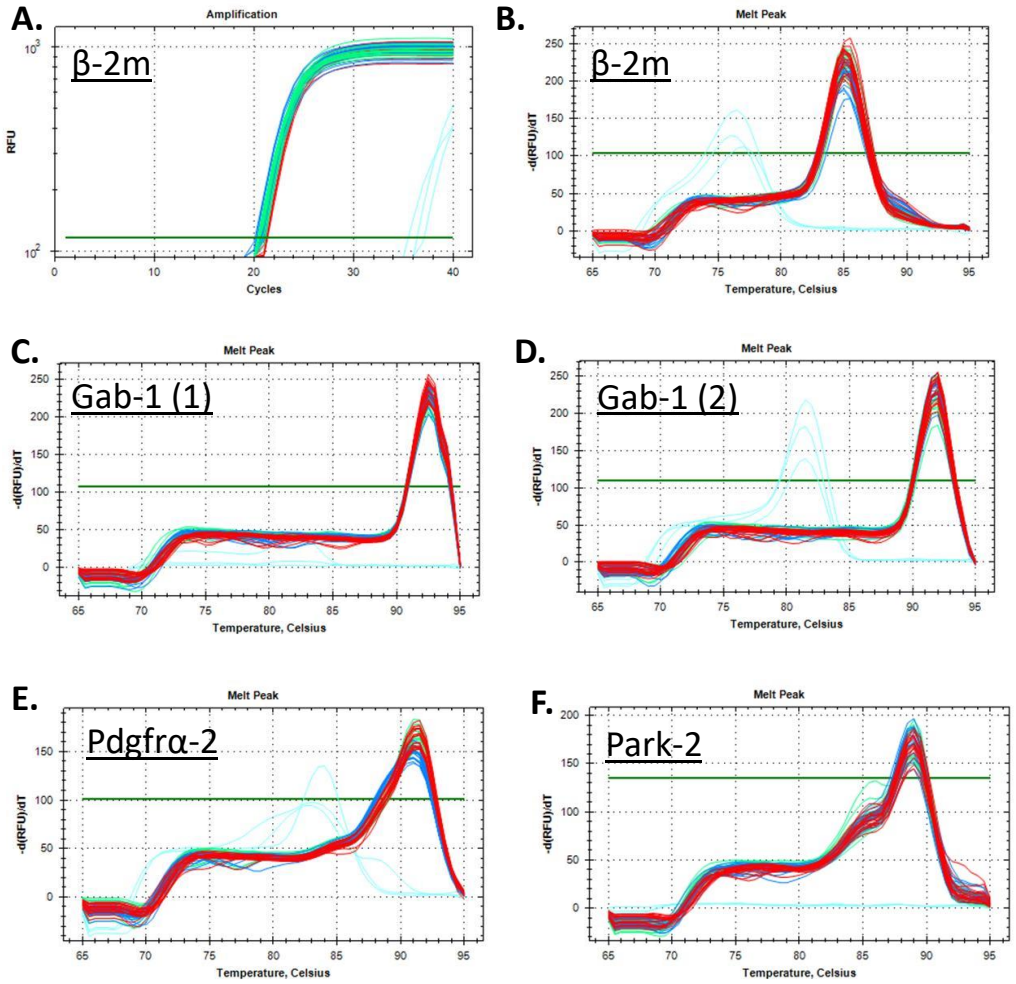

Figure A.17 Melt peaks from qPCR analysis following manipulation of miR-128 expression experiments.

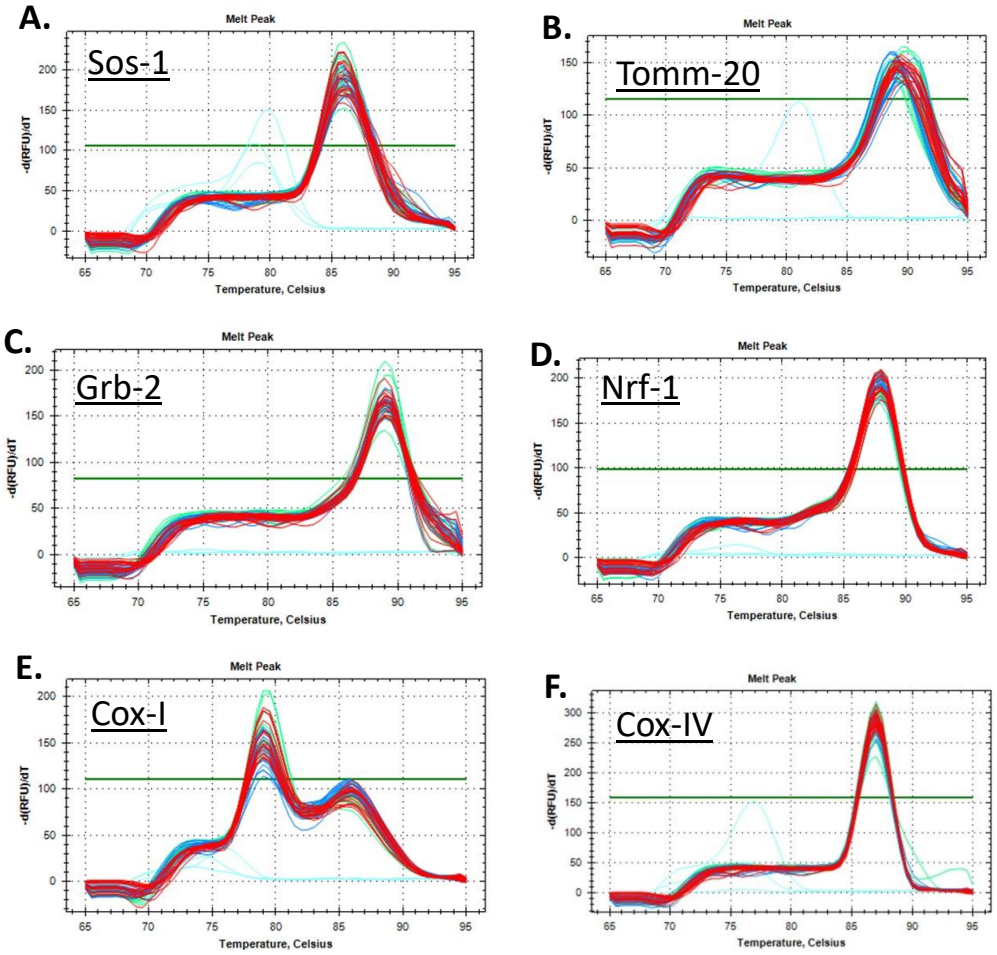

Figure A.18 Melt peaks from qPCR analysis following manipulation of miR-128 expression experiments.

A.6 Dietary information of normal and protein-restricted diet used for *in vivo* experiments

Table A.3 Nutrient composition of 20% and 5% protein diet used for *in vivo* experiments

	20% protein	5% protein
MAIZE STARCH	37.31 %	51.47 %
MALTODEXTRIN	13.20 %	13.20 %
SUCROSE	9.39 %	12.95 %
SOYA OIL	7.00 %	7.00 %
CASEIN (88 g protein/100 g)	23.00 %	5.55 %
CELLULOSE	5.00 %	5.00 %
MINERAL MIX	3.50 %	3.50 %
VITAMIN MIX	1.00 %	1.00 %
CHOLINE BITARTRATE	0.25 %	0.25 %
L-CYSTINE	0.35 %	0.08 %

A.7 Comparison of muscle and body weight of muscles used for experimental analysis

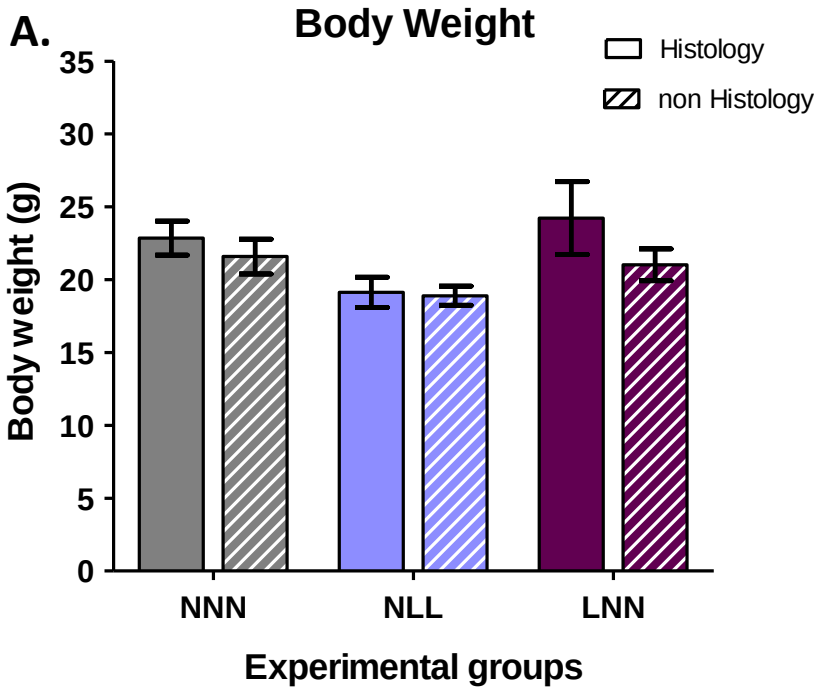

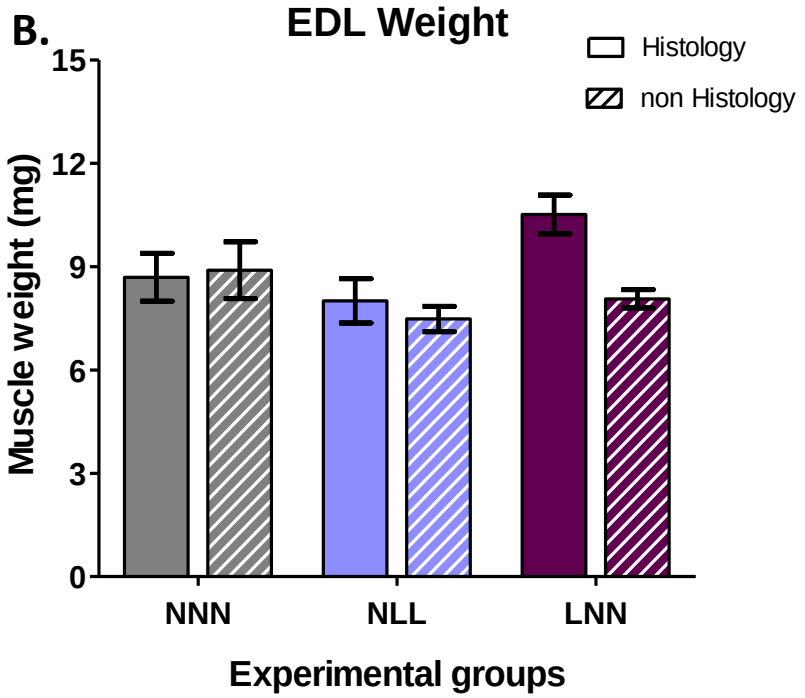

Figure A.19 Total body weight and EDL muscle of 12-week old mice used for histological analysis in comparison with those not selected for experimental analysis. **A)** Total body weight (g) and **B)** EDL muscle weight (mg) used in histological analysis compared to those that were not selected for experimental analysis. (*mean ± SEM*; *n*=3-9*; Two-Way ANOVA with Bonferroni post-hoc analysis*).